

# On the Combustion Chemistry of Biofuels and The Activist Engineer

by

Darshan Mukesh Karwat

A dissertation submitted in partial fulfillment  
of the requirements for the degree of  
Doctor of Philosophy  
(Aerospace Engineering)  
in The University of Michigan  
2012

Doctoral Committee:

Professor Margaret S. Wooldridge, Chair  
Professor Iain D. Boyd  
Associate Professor Thomas E. Princen  
Adjunct Professor Elaine S. Oran



by Ander Erickson

© Darshan Mukesh Karwat

---

All rights reserved  
2012



to those things that sustain, nourish, and enrich  
to those people who imagine radical possibilities

## Gratefulness

Just as it takes (or should take) a village to take to raise a child, it has taken the support, guidance, and positive energy of a whole host of people to put this dissertation together. Having been in Ann Arbor for exactly nine years now, there are many people that I am deeply indebted to and grateful to know. The scope of this dissertation has been fed by doctoral students, bloggers, student leaders and activists, staff members and professors from all across the University and this great town. This work has been influenced as much by occurrences outside the laboratory as it has by those inside.

First, I am grateful for my family's constant love, even though at times I could tell that they had no idea what I was working on. My parents have let me do whatever I have wanted to in life, and I am grateful for the trust they have put in me.

The Graham Doctoral Fellowship Program has given me the liberty to engage in experiential and service learning and teaching, in Ann Arbor and the bizarrely charismatic city of Detroit. To Laura Sherman, Laura Smith, Krista Badiane, Paul Coseo, and Professor Larissa Larsen I give thanks. I thank the staff at the Graham Environmental Sustainability Institute, the Graham Doctoral Fellows, and particularly Dr. Michael Shriberg for his enthusiasm and active engagement of students of all ages and levels.

Along those lines, I am thankful to be surrounded by such amazing student activists and leaders. The Student Sustainability Initiative has grown deep roots and branched healthily to significantly influence university policy over the past four years, and I am grateful for Dr. Melissa Forbes' hard work in helping get SSI off the ground. To Merry Walker, Dana Arnold, Zakiyah Sayyed, Aaron James, Greg Buzzell, Matthew Gacioch, Graham Brown, Ryan Smith, Devi Glick, Poonam Dagli, Lydia McMullen-Laird, Sam Schiebold, Phel Meyer, Megan Pfeiffer and Pete Chirawongwiroj, I thank you for service and dedication.

Soccerfever always provided temporary cures for my footballitis over the past nine years, for which I am grateful. The High House housemates—Dr. Arnab Nandi, Dr. Kaushik Veeraraghavan, Dr. Benji Wester, Dr. Dan Peek, Tim Whittemore, Dr. Alex Gray, Meg Allison, Rob Cohn, Johannes Strom, Jessie Olpere, Kristen Anderson—and the Enigmatic House on Division housemates—Dr. Sean Munson, Aston Gonzalez, Kaitlin Barancik, and others—always provided me the comfort of a safe space to work in.

I thank the Department of Mechanical Engineering office staff—Amanda Gaytan, Tracie Straub, Laura Vespaziani, Kelly Chantelois, Yan Wang, Paul Gorny, Mindy LaRocca, Sarah Flynn, Karen Raab, Merlis Nolan, Barb Behm, Debbie Hemmeter, Carol Girata and the rest of the Sweet Friday clan—for their constant smiles and letting The Tea Party swarm the office every two hours to make tea from first principles. I thank Matt Navarre, Sally Smith, Charlie Weger, Charlie Wiykovics, Mike Lazarz and Lance Dicken for their constant readiness to help out in the lab. I also want to point out and appreciate the good work done by Kent Pruss, Bill Kirkpatrick, John Myers, and Marv Cressey in the machine shop. Denise Phelps and Linda Weiss in the Department of Aerospace Engineering have difficult jobs, and I thank them for what they do. I especially thank Denise for making the bureaucracies of graduate education and the department effortless to navigate.

I thank Matt Spears of the Environmental Protection Agency for constantly giving me the inside scoop on the politics of international aviation and climate change. Brian Bennett of Perkin Elmer was always available for help with the gas chromatography systems, and I thank him for his advice and stories.

My labmates have made coming to North Campus fun and something to look forward to...really. I thank Dr. Brad Zigler, Dr. Smitesh Bakrania, Dr. James Wiswall, Dr. Paul Teini, and Dr. Stephen Walton for making the lab a welcoming place to someone much younger than them. I sincerely thank the at times overlapping The Tea Party and Optical Research in Combustion Association members—Peter Keros, Andrew Mansfield, Steve Morris, Dimitris Assanis, Scott Wagnon, Mohammad Fatouraie, Eric Bumbalough, Dr. Siamak Riahi, and Dr. W. Ethan Eagle—for the variegated discussions on religion, spirituality, politics, philosophy, ethics, morality, science and technology over the years. That said, I would also like to thank the people whose good work brought us good radio to listen

to. *The Story, On Being*, and *This American Life* turned the lab space into one in which everything could be questioned and debated and imagined. Marco Ceze is one cool dude in the aerospace engineering department, and Jason Lai has always been available for help with chemical kinetic mechanisms and supercomputers.

To those that have constantly engaged me with my blog, I thank you for challenging my remarks, thoughts, and assumptions. Much of that writing has influenced this dissertation. I thank Professor Victoria Johnson and Rebecca Sunde in particular.

I thank my committee—Dr. Elaine Oran, Professor Iain Boyd, and Professor Thomas Princen—for their support in allowing me to write a thesis that tries to break the norm. Professor Princen’s insights, and critiques of my writing and arguments have made me try to constantly choose the better word and active sentence construction, lending more force to the dissertation. Dr. Charles Westbrook deserves special recognition for I have learned a lot about combustion chemistry from his many contributions to the field and this dissertation. I would like to thank Professor Gabrielle Hecht, Professor Paul Edwards, and the students of the last class I took at the University for making it the most impactful on my thinking. The later chapters of this dissertation would not have been possible without what I learned from them. I am grateful to know Lia Wolock, who has helped me think about issues of power, oppression, and agency. I thank Robyn d’Avignon for her insights into technology, politics, colonialism, and activist theory, and Ethan Schoolman and Dr. Cynthia Finelli for helping think about how to frame sociological questions.

Scott “Mr. PID” (I’m sorry!) Wagnon I would like to thank especially. I could not have asked for a more thorough, engaging, and hardworking labmate to collaborate with. Much of the work in the laboratory would have been impossible without his skills and dedication.

And most importantly, I would like to thank Professor Margaret Wooldridge for being my mentor and friend over these past years. She has encouraged me to constantly push my own boundaries. Her openness to discussing issues of the environment, gender, inequity, the scientific process, and university politics has allowed me to explore diverse areas of thought that have in ways intangible shaped this dissertation. She gave me the freedom to spend my time as I thought necessary,

whether for going back to India, helping develop and teach a class in urban planning, or working with other professors in other areas of study. She is the best advisor I could have asked for, and I am eternally grateful to be her student. I eagerly look forward to collaborating and engaging with her in the years to come.



## Table of Contents

<b>Dedication</b> .....	<b>ii</b>
<b>Gratefulness</b> .....	<b>iii</b>
<b>List of Figures</b> .....	<b>ix</b>
<b>List of Tables</b> .....	<b>xv</b>
<b>Abstract</b> .....	<b>xvi</b>
<b>Chapter 1 Introduction</b> .....	<b>1</b>
<b>Chapter 2 A speciation study of the chemical kinetics of <i>n</i>-heptane</b> .....	<b>6</b>
Introduction .....	6
Experimental Setup .....	8
<i>The University of Michigan Rapid Compression Facility</i> .....	8
<i>High-speed gas sampling and gas chromatography</i> .....	12
Mechanism Description .....	14
Experimental Results and Discussion .....	16
<i>Ignition experiments</i> .....	16
<i>High-speed gas sampling experiments</i> .....	22
Conclusions .....	33
<b>Chapter 3 Ignition and speciation studies of the chemical kinetics of <i>n</i>-butanol</b> <b>36</b>	
Introduction .....	36
Experimental Setup .....	39
<i>The University of Michigan Rapid Compression Facility</i> .....	39
<i>High-speed gas sampling and gas chromatography</i> .....	40
Experimental Results and Discussion .....	42
<i>Ignition experiments</i> .....	42
<i>High-speed gas sampling experiments</i> .....	49
Conclusions .....	64
<b>Chapter 4 On the combustion chemistry of <i>n</i>-heptane and <i>n</i>-butanol blends</b> .....	<b>68</b>
Introduction .....	68
Experimental Setup .....	70
Model Description .....	70

Results and Discussion .....	70
<i>Ignition experiments and modeling</i> .....	70
<i>High-speed gas sampling experiments</i> .....	80
Conclusions .....	98
Thoughts on future work .....	100
<b>Chapter 5 “We’ve generated a lot of knowledge...but we’ve gained very little wisdom.”</b> .....	<b>102</b>
<b>Chapter 6 Is there an ecological problem that technology cannot solve?.....</b>	<b>106</b>
Not wasting a drop—“conservation” through use .....	109
Hindsight is not 20/20.....	118
“You know, I don’t have any data. I can’t advise a decision now.”.....	121
The existential pleasures of engineering.....	123
Biofuels, aviation, and climate change .....	126
“It’s all fuckin’ ridiculous. You should just all ride bicycles.” .....	129
Concluding thoughts .....	135
<b>Chapter 7 The activist engineer .....</b>	<b>139</b>
<b>Technical references .....</b>	<b>152</b>

## List of Figures

Figure 2.1 Shown are a representation of the UM RCF (top panel) with key dimensions, the configuration for end-view imaging (middle panel), and the configuration for high-speed gas sampling (bottom panel).....	10
Figure 2.2 Results from a typical UM RCF $n$ -C <sub>7</sub> H <sub>16</sub> ignition experiment. The lower panel depicts the pressure time-history in the test section, along with the rate of pressure rise, which allows definition of $\tau_{\text{ign}}$ and consequently effective pressure and temperature conditions. The upper panel shows still images taken at 30,000 fps via end-view imaging. Note the homogeneity of the ignition event. The color of these images has been adjusted for clarity. ....	18
Figure 2.3 Ignition characteristics of $n$ -C <sub>7</sub> H <sub>16</sub> over a wide range of temperatures (650-1400 K) and pressures (3-42 atm), including results of the current work. Error bars representing the standard deviation of $\tau_{\text{ign}}$ (0.63 ms) for UM RCF data do not show up on plot. ....	19
Figure 2.4 A comparison of ignition delay times from a typical UM RCF ignition experiment, the current mechanism, the LLNL mechanism <sup>24</sup> and the mechanism from PdM. <sup>23</sup> Constant volume, adiabatic simulations were performed with $P_0 = 9$ atm, $T_0 = 700$ K. The expansion simulation was performed by using a volume profile generated from the pressure trace of an inert experiment. ....	21
Figure 2.5 An Arrhenius plot of ignition data from the UM RCF and other rapid compression machine studies. ....	22
Figure 2.6 Typical results from a sampling experiment conducted on the UM RCF. Notice the agreement, until the first stage of ignition, between a non-reacting, inert pressure trace and the reacting pressure trace, which signifies that the heat transfer physics of the sampling experiments remain unaffected by the sampling event.....	23
Figure 2.7 The unnormalized experimental pressure traces of the thirteen sampling experiments. Although unnormalized, note the level of repeatability of the compression process, as well as the first and second stages of ignition and heat release. ....	25
Figure 2.8 The normalized experimental pressure traces of the thirteen sampling experiments. 0 represents EOC, 1 represents the first stage of ignition, and 2 represents the second stage of ignition. Shown also are the normalized sampling times at which samples were pulled from the test section. ....	25
Figure 2.9 An example of gas chromatography signals output by the three gas chromatographs. These particular signals are for the experiment depicted in Figure 7. ....	26

Figure 2.10 Species concentration time-histories for UM RCF sampling experiments (filled black circles), along with Minetti <i>et al.</i> <sup>12</sup> data (open red squares), and current mechanism predictions corresponding to these two sets of experimental data, with the black solid line corresponding to predictions of UM RCF data and the red dashed line to predictions of the Minetti <i>et al.</i> <sup>12</sup> data. Also shown with dotted black lines are PdM mechanism <sup>23</sup> predictions for the UM RCF data. ....	30
Figure 2.11 Predictions of radical concentrations at the first and second stage of ignition. ....	33
Figure 3.1 Results for a typical <i>n</i> -C <sub>4</sub> H <sub>9</sub> OH ignition experiment with $P_{\text{eff}} = 3.35$ atm, $T_{\text{eff}} = 1031$ K, $\phi = 1$ , inert/O <sub>2</sub> = 5.64 and $\tau_{\text{ign}} = 6.6$ ms. The lower panel shows the pressure ( $P$ ) and the rate of pressure rise ( $dP/dt$ ) in the test section. End of compression is set as time $t = 0$ ms. The upper panel shows the corresponding still images (end view), acquired at 26,000 fps, of the chemiluminescence during ignition (no color adjustment). ....	43
Figure 3.2 Comparison of experimental results for <i>n</i> -C <sub>4</sub> H <sub>9</sub> OH ignition delay time measured in the current work with model predictions ( $P = 3.25$ atm) based on the reaction mechanisms developed by Black <i>et al.</i> <sup>50</sup> (solid line) and Veloo <i>et al.</i> <sup>46</sup> (dotted line). All results presented are for $\phi = 1$ , inert/O <sub>2</sub> = 5.64. ○—Current work, $P = 2.9$ -3.4 atm, ■—Current work, gas-sampling experiments, $P = 3.22$ -3.34 atm.....	45
Figure 3.3 CHEMKIN™ simulation representing the compression stroke of the UM RCF for the targeted EOC conditions of $T = 975$ K and $P = 3.25$ atm using the Black <i>et al.</i> <sup>50</sup> reaction mechanism, with initial mole fractions of $\chi(n\text{-but}) = 0.025$ , $\chi(\text{O}_2) = 0.147$ , $\chi(\text{N}_2) = 0.541$ , and $\chi(\text{Ar}) = 0.288$ . ....	47
Figure 3.4 CHEMKIN™ simulation representing the compression stroke of the UM RCF for the targeted EOC conditions of $T = 1025$ K and $P = 3.25$ atm using the Black <i>et al.</i> <sup>50</sup> reaction mechanism, with initial mole fractions of $\chi(n\text{-but}) = 0.025$ , $\chi(\text{O}_2) = 0.147$ , $\chi(\text{N}_2) = 0.429$ , and $\chi(\text{Ar}) = 0.399$ . ....	47
Figure 3.5 Results for OH sensitivity analysis using the mechanism of Black <i>et al.</i> <sup>50</sup> for the target gas sampling conditions of $\phi = 1.0$ , $T = 975$ K, $P = 3.25$ atm, inert/O <sub>2</sub> = 5.64. ....	48
Figure 3.6 Comparison of the <i>n</i> -C <sub>4</sub> H <sub>9</sub> OH ignition delay times measured in the current work with the experimental results for shock tube studies of <i>n</i> -C <sub>4</sub> H <sub>9</sub> OH ignition by Moss <i>et al.</i> <sup>49</sup> and Black <i>et al.</i> <sup>50</sup> where $\phi = 1$ for all data. ○—Current work, $P = 2.9$ -3.4 atm, inert/O <sub>2</sub> = 5.64, ■—Current work, gas-sampling experiments, $P = 3.22$ -3.34 atm, inert/O <sub>2</sub> = 5.64, △—Moss <i>et al.</i> <sup>49</sup> , $P = 1$ atm, inert/O <sub>2</sub> = 15.5, ▲—Moss <i>et al.</i> <sup>49</sup> , $P = 1.3$ atm, inert/O <sub>2</sub> = 32, ▽—Moss <i>et al.</i> <sup>49</sup> , $P = 4$ atm, inert/O <sub>2</sub> = 65.7, ★—Black <i>et al.</i> <sup>50</sup> , $P = 1$ atm, inert/O <sub>2</sub> = 21, ×—Black <i>et al.</i> <sup>50</sup> , $P = 2.5$ -3.1 atm, inert/O <sub>2</sub> = 26.6, □—Noorani <i>et al.</i> <sup>53</sup> , $P = 1.8$ -2.5 atm, inert/O <sub>2</sub> = 10, ◇—Noorani <i>et al.</i> <sup>53</sup> , $P = 1.8$ -2.5 atm, inert/O <sub>2</sub> = 10. Model predictions based on the Black <i>et al.</i> <sup>50</sup> mechanism are presented for conditions of $P = 1$ atm, inert/O <sub>2</sub> = 21 (dashed line) and $P = 3.25$ atm, inert/O <sub>2</sub> = 5.64 (solid line). ....	49
Figure 3.7 Results for a typical <i>n</i> -C <sub>4</sub> H <sub>9</sub> OH ignition experiment with gas-sampling during the ignition delay period. The pressure and pressure derivative time histories in the test section and in the two sampling chambers are presented. The	

triggering signals for the rapid gas sampling valves are also provided. The pressure time-history for a non-igniting (i.e. inert) experiment is included for comparison. ...	50
Figure 3.8 Comparison of the pressure time-histories for the high-speed gas-sampling experiments of $n$ -C <sub>4</sub> H <sub>9</sub> OH ignition. Note the nearly identical compression processes for all experiments.....	51
Figure 3.9 Comparison of the pressure time-histories of the sampling experiments on a time scale normalized to $\tau_{\text{ign}}$ for each experiment. The normalized time for each gas-sample measurement is labeled in the figure.....	52
Figure 3.10 Typical GC-FID chromatogram results of a gas sample acquired at $t = 7.2$ ms, $t/\tau_{\text{ign}} = 0.45$ , for experimental conditions of $P_{\text{eff}} = 3.27$ atm, $T_{\text{eff}} = 974$ K, $\tau_{\text{ign}} = 16.0$ ms. ....	53
Figure 3.11 Comparison between measured intermediate species and model predictions using the reaction mechanism of Black <i>et al.</i> <sup>50</sup> and the initial conditions of $P = 3.25$ atm, $T = 975$ K, inert/O <sub>2</sub> = 5.64, and $n$ -C <sub>4</sub> H <sub>9</sub> OH = 2.45% ( $\tau_{\text{ign, predicted}} = 18.6$ ms). The unmodified mechanism predictions are shown with solid lines, and the modified mechanism predictions are shown with dotted black lines. The average experimental conditions are $P_{\text{eff}} = 3.29$ atm, $T_{\text{eff}} = 975$ K, inert/O <sub>2</sub> = 5.63, and $n$ -C <sub>4</sub> H <sub>9</sub> OH = 2.44% ( $\tau_{\text{ign, average}} = 15.7$ ms). The error bars represent the experimental uncertainties. The time domain has been normalized from $t = 0$ (end of compression) to the time of ignition, $t/\tau_{\text{ign}} = 1$ . ....	54
Figure 3.12 Species time histories of radicals predicted using the reaction mechanism of Black <i>et al.</i> <sup>50</sup> for initial conditions of $P = 3.25$ atm, $T = 975$ K, inert/O <sub>2</sub> = 5.64, and $n$ -C <sub>4</sub> H <sub>9</sub> OH = 2.45%.....	56
Figure 3.13 Reaction path diagram of the primary decomposition reactions for $n$ -C <sub>4</sub> H <sub>9</sub> OH for $t/\tau_{\text{ign}} = 0.75$ and the initial conditions of $P = 3.25$ atm, $T = 975$ K, inert/O <sub>2</sub> = 5.64, and $n$ -C <sub>4</sub> H <sub>9</sub> OH = 2.45%.....	57
Figure 3.14 Reaction path diagram of the primary formation pathways for carbon monoxide. Same model conditions as Figure 14.....	58
Figure 3.15 Reaction path diagram of the primary formation and removal pathways for ethene and methane. Same model conditions as Figure 14. ....	58
Figure 3.16 Reaction path diagram of the primary formation and removal pathways for propene. Same model conditions as Figure 14.....	59
Figure 3.17 Reaction path diagram of the primary formation and removal pathways for 1-butene. Same model conditions as Figure 14. ....	59
Figure 3.18 Reaction path diagram of the primary formation and removal pathways for acetaldehyde. Same model conditions as Figure 14. ....	60
Figure 3.19 Reaction path diagram of the primary formation and removal pathways for $n$ -butyraldehyde. Same model conditions as Figure 14.....	61
Figure 3.20 Rate constants for the overall $n$ -C <sub>4</sub> H <sub>9</sub> OH+OH reaction from Vasu <i>et al.</i> , <sup>57</sup> Zhou <i>et al.</i> , <sup>58</sup> and Black <i>et al.</i> <sup>50</sup> .....	62
Figure 3.21 Branching fractions for the five H-atom abstraction channels by OH from the $\alpha$ , $\beta$ , $\gamma$ , and $\delta$ carbon sites and from the alcohol group of $n$ -C <sub>4</sub> H <sub>9</sub> OH. The	

legend includes the site of the H-atom abstraction and the designation of the corresponding C <sub>4</sub> H <sub>8</sub> OH isomer produced. The solid lines are the values used in the Black <i>et al.</i> <sup>50</sup> mechanism, and the dashed lines are the values recommended by Zhou <i>et al.</i> <sup>58</sup> based on their G3 calculations. ....	64
Figure 4.1 Results from a typical UM RCF 80-20 ignition experiment. The lower panel depicts the pressure time-history in the test section and the rate of pressure rise, which are used to define $\tau_{\text{ign}}$ and the effective pressure and temperature conditions. The upper panel shows still images taken at 30,000 fps via end-view imaging. Note the homogeneity of the ignition event. The color of the images has been adjusted for clarity. ....	72
Figure 4.2 Results from a typical UM RCF 50-50 ignition experiment. Additional details described in the caption of Figure 4.1.....	73
Figure 4.3 Comparison of experimental (solid lines) and modeling (dashed lines) pressure time-histories for the 100-0, 80-20, and 50-50 blend cases. While the model and the experimental data agree adequately for the 100-0 case, differences increase with increasing concentrations of <i>n</i> -C <sub>4</sub> H <sub>9</sub> OH in the mixture. Shown also are time-histories for simulations in which <i>n</i> -C <sub>4</sub> H <sub>9</sub> OH was removed from the 80-20 and 50-50 mixtures, thus simulating lean 80-0 (dark cyan) and 50-0 (pink) <i>n</i> -C <sub>7</sub> H <sub>16</sub> mixtures.	74
Figure 4.4 Comparison of experimental and modeling pressure time-histories for the 100-0, 80-20, and 50-50 blend cases using a normalized time domain, where 0 corresponds to EOC, 1 corresponds to the first stage of ignition, and 2 corresponds to overall ignition. ....	75
Figure 4.5 Ignition delay times as a function of blend ratio, and a comparison of the current model and a model developed by Saisirirat <i>et al.</i> <sup>64</sup> .....	76
Figure 4.6 Comparison of <i>n</i> -C <sub>4</sub> H <sub>9</sub> OH submechanism performance against previous UM RCF data from Karwat <i>et al.</i> <sup>34</sup> Simulations performed with zero-dimensional, constant volume, adiabatic assumptions.....	77
Figure 4.7 Simulation predictions of key intermediate and radical species using the current mechanism and that of Saisirirat <i>et al.</i> <sup>64</sup> for the 100-0, 80-20, and 50-50 cases. ....	80
Figure 4.8 Typical results for the pressure time-histories in the test section and the sampling volume for an 80-20 sampling experiment (solid lines). The pressure time-history from a non-igniting (labeled inert) experiment is presented as the dashed line. The agreement until the first stage of ignition between the non-igniting pressure trace and the igniting pressure trace indicates the heat transfer physics of the sampling experiments are unaffected by the sampling event. ....	81
Figure 4.9 The left panel depicts the unnormalized experimental pressure time-histories of the sampling experiments for the 80-20 blend; note the level of repeatability of the compression process, as well as the first and second stages of ignition and heat release. The right panel presents the normalized data where 0 represents EOC, 1 represents the first stage of ignition, and 2 represents the second stage of ignition. Shown also are the normalized times when samples were taken from the test section.....	82

Figure 4.10 The left panel depicts the unnormalized experimental pressure time-histories of the sampling experiments for the 80-20 blend; note the level of repeatability of the compression process, as well as the first and second stages of ignition and heat release. The right panel presents the normalized data where 0 represents EOC, 1 represents the first stage of ignition, and 2 represents the second stage of ignition. Shown also are the normalized times when samples were taken from the test section.....83

Figure 4.11 Typical gas chromatograms obtained from the three gas chromatographs. The particular data are for the experiment depicted in Figure 4.8, which was an 80-20 blend experiment with a normalized sampling time of 1.69.....84

Figure 4.12 Experimental  $n\text{-C}_7\text{H}_{16}$  concentration time-histories for stoichiometric 100-0 (black circles), 80-20 (green squares), and 50-50 (red triangles) blends obtained from the UM RCF at nominal conditions of 700 K and 9 atm. Also shown are zero-dimensional, constant volume, adiabatic mechanism predictions using the current mechanism and the Saisirirat *et al.*<sup>64</sup> mechanism. ....86

Figure 4.13 Experimental  $n\text{-C}_4\text{H}_9\text{OH}$  concentration time-histories for stoichiometric 80-20 (green squares), and 50-50 (red triangles) blends obtained from the UM RCF. Also shown are mechanism predictions using the current mechanism and the Saisirirat *et al.*<sup>64</sup> mechanism. Experimental and simulation conditions are the same as in Figure 4.12. ....87

Figure 4.14 Experimental  $\text{CH}_4$  time-histories for stoichiometric 100-0 (black circles) 80-20 (green squares), and 50-50 (red triangles) blends. Also shown are predictions using the current mechanism. Experimental and simulation conditions are the same as in Figure 4.12. ....88

Figure 4.15 Experimental  $\text{C}_2\text{H}_6$  time-histories for stoichiometric 100-0 (black circles) 80-20 (green squares), and 50-50 (red triangles) blends. Also shown are predictions using the current mechanism. Experimental and simulation conditions are the same as in Figure 4.12. ....88

Figure 4.16 Experimental  $\text{C}_2\text{H}_4$  time-histories for stoichiometric 100-0 (black circles) 80-20 (green squares), and 50-50 (red triangles) blends. Also shown are predictions using the current mechanism. Experimental and simulation conditions are the same as in Figure 4.12. ....88

Figure 4.17 Experimental  $\text{C}_3\text{H}_8$  time-histories for stoichiometric 100-0 (black circles) 80-20 (green squares), and 50-50 (red triangles) blends. Also shown are predictions using the current mechanism. Experimental and simulation conditions are the same as in Figure 4.12. ....89

Figure 4.18 Experimental  $\text{C}_3\text{H}_6$  time-histories for stoichiometric 100-0 (black circles) 80-20 (green squares), and 50-50 (red triangles) blends. Also shown are predictions using the current mechanism, as well as mechanism predictions where the  $n\text{-C}_4\text{H}_9\text{OH}$  has been removed from the initial reactant mixture (i.e. 80-20  $\rightarrow$  80-0 and 50-50  $\rightarrow$  50-0). Experimental conditions are the same as in Figure 4.12. ....90

Figure 4.19 Experimental  $1\text{-C}_4\text{H}_8$  time-histories for stoichiometric 100-0 (black circles) 80-20 (green squares), and 50-50 (red triangles) blends. Also shown are predictions using the current mechanism, as well as mechanism predictions where the  $n\text{-C}_4\text{H}_9\text{OH}$  has been removed from the initial reactant mixture (i.e. 80-20  $\rightarrow$  80-0 and 50-50  $\rightarrow$  50-0). Experimental conditions are the same as in Figure 4.12. ....91

Figure 4.20 Experimental 1,3-C <sub>4</sub> H <sub>6</sub> time-histories for stoichiometric 100-0 (black circles) 80-20 (green squares), and 50-50 (red triangles) blends. Also shown are predictions using the current mechanism. Experimental and simulation conditions are the same as in Figure 4.12. ....	91
Figure 4.21 Experimental CH <sub>3</sub> CHO time-histories for stoichiometric 100-0 (black circles) 80-20 (green squares), and 50-50 (red triangles) blends. Also shown are predictions using the current mechanism, as well as mechanism predictions where the <i>n</i> -C <sub>4</sub> H <sub>9</sub> OH has been removed from the initial reactant mixture (i.e. 80-20 → 80-0 and 50-50 → 50-0). Experimental conditions are the same as in Figure 4.12. ....	92
Figure 4.22 Experimental CH <sub>3</sub> OH time-histories for stoichiometric 100-0 (black circles) 80-20 (green squares), and 50-50 (red triangles) blends. Also shown are predictions using the current mechanism. Experimental and simulation conditions are the same as in Figure 4.12 .....	92
Figure 4.23 Experimental <i>n</i> -C <sub>3</sub> H <sub>7</sub> CHO time-histories for stoichiometric 100-0 (black circles) 80-20 (green squares), and 50-50 (red triangles) blends. Also shown are predictions using the current mechanism, as well as mechanism predictions where the <i>n</i> -C <sub>4</sub> H <sub>9</sub> OH has been removed from the initial reactant mixture (i.e. 80-20 → 80-0 and 50-50 → 50-0). Experimental conditions are the same as in Figure 4.12. ....	93
Figure 4.24 Experimental CO time-histories for stoichiometric 100-0 (black circles) 80-20 (green squares), and 50-50 (red triangles) blends. Also shown are predictions using the current mechanism. Experimental and simulation conditions are the same as in Figure 4.12.....	94
Figure 4.25 Experimental 1-C <sub>5</sub> H <sub>10</sub> time-histories for stoichiometric 100-0 (black circles) 80-20 (green squares), and 50-50 (red triangles) blends. See caption of Figure 4.23 for further details. ....	95
Figure 4.26 Experimental 1-C <sub>6</sub> H <sub>12</sub> time-histories for stoichiometric 100-0 (black circles) 80-20 (green squares), and 50-50 (red triangles) blends. See caption of Figure 4.23 for further details. ....	96
Figure 4.27 Experimental 2-C <sub>7</sub> H <sub>14</sub> time-histories for stoichiometric 100-0 (black circles) 80-20 (green squares), and 50-50 (red triangles) blends. See caption of Figure 4.23 for further details.....	96
Figure 4.28 Experimental 3-C <sub>7</sub> H <sub>14</sub> time-histories for stoichiometric 100-0 (black circles) 80-20 (green squares), and 50-50 (red triangles) blends. See caption of Figure 4.23 for further details. ....	97
Figure 4.29 Small radical concentration predictions using the current mechanism at $T_0 = 700$ K, $P_0 = 9$ atm, $\phi = 1$ , at a dilution of $\sim 5.64$ .....	97



## List of Tables

Table 2.1 Summary of experimental conditions and results. The top panel provides a summary of sampling experiments, depicted in Figure 2.3 with green triangles, and the bottom panel provides a summary of ignition experiments, depicted in Figure 2.3 as magenta pentagons.....	35
Table 3.1 A summary of ignition and sampling (in italics) experiments for <i>n</i> -butanol. Predicted ignition delay times from Black <i>et al.</i> <sup>50</sup> mechanism. ....	66
Table 3.2 A summary of sampling experiments for <i>n</i> -butanol.....	67
Table 4.1 A comparison of experimental and predicted ignition results based on the current mechanism for first stage ignition and autoignition features. ....	76
Table 4.2 A summary of sampling experiment conditions for the 80-20 and 50-50 blend ratios. Table 2.1 provides the same summary for the 100-0 blend. The first row of italics for each blend ratio is the standard deviation of the column, and the second row of italics represents the standard deviation of the column.....	101

## Abstract

On the Combustion Chemistry of Biofuels and The Activist Engineer

by

Darshan Mukesh Karwat

Chair: Margaret S. Wooldridge

This dissertation presents detailed work on the chemical kinetics of biofuel/fossil fuel blends through experimental combustion studies, and explores whether or not issues of the environment have changed the way engineers think about what they do by drawing on literature in history, ethics, philosophy, science and technology studies, and activist theories, as well as interviews conducted with practicing engineers.

Biofuels are being promoted to combat aviation's impact on climate change. Yet, there is a lack of understanding of how biofuels change the combustion chemistry of traditional fuels when blended together, and it is unclear whether chemical kinetic mechanisms capture this chemistry. This work focuses on two important molecules—*n*-heptane, a chemical surrogate of complex fuel mixtures such as kerosene; and *n*-butanol, an alternative, bio-derived fuel that is of particular interest in aviation applications. Presented are experimental ignition and speciation studies, at conditions relevant to modern combustion applications, of *n*-heptane/*n*-butanol blends. The presence of *n*-butanol slows the global reactivity of *n*-heptane, decreases the emission of species that lead to particulate formation, and fundamentally changes the branching pathways of *n*-heptane combustion.

That said, what are the underlying ethical, political, and philosophical principles that engineers draw upon to legitimize biofuel development efforts? And are these

principles any different from those that were drawn upon in past technological development? This work investigates these questions by comparing thinking between engineers that were involved in the damming of rivers to open the American West, and interviews of contemporary engineers that are involved in biofuel development for aviation. Broadly, biofuels may have the capacity to limit climate change given their potential to be made from waste streams and plants. Yet, even though understanding of the sociotechnical causes of ecological problems has increased greatly, biofuels are being developed and promoted using the same thinking and paradigms as a century ago, and are not being complemented with broader socioeconomic transformation; they may thus merely substitute one ecological problem for another bigger ecological problem. The role of the activist engineer is to consider how technologies transform the socioecological environments they are deployed in through praxis—critical thinking and reflective action.

# Chapter 1

## Introduction

We have heard about the problems of climate change, ecological degradation, and unsustainability for decades now; long enough for those entities that have a vested interest in *not* changing—oil corporations, defense contractors, Wall Street, consumer brands, and consumers—to have usurped language that was meant to open a new way of thinking; we now have “sustainable growth” and “green consumerism”. Yet these problems are not like problems of old that were local in character and bounded in time. These problems span political, cultural, emotional and ecological scales; from the personal to the collective, from the local to the global, from now unto who knows when, from the Rust Belt of Middle America to the rainforests of Indonesia. In every way, large problems such as climate change transcend the current ways of thinking and doing. They transcend disciplinary focus, traditional time scales (beyond quarters and years, beyond even lifetimes) and national securities and corporate profits. Mustn’t the work we do to address these problems appreciate those scales, respect the spectrum of needs and impact, and be more holistic in its framing? With this work, I have tried to overcome boundaries between disciplines. Some might think of this dissertation work as “interdisciplinary”. I prefer to think of it as trying to tear down disciplinary boundaries and bridge divides between pedagogies. In this dissertation, ethics are no longer “out there” or siloed off in engineering contexts. Instead they are explored and questioned given they are intrinsic to defining the need and direction of engineering; engineering does not operate in a vacuum. The political motives of technological developers have been put front and center in technological development.

Engineering as a profession must evolve. Technological optimism is not the cure for our ecological malaises. It is short-sighted and myopic to think of engineering

work, or any work for that matter, only within the disciplinary contexts—a mundane engineering project like a road actually *changes* the way people behave, it changes economic and social patterns, and the road affects the relationship between people and the ecology that surrounds them. Often the impact of engineering projects is obvious, and often not. While we have developed many methods to assess impact, such as life-cycle analysis and environment impact statements, engineers often distance themselves from the more intangible outcomes, including social and ecological considerations. Conversely, society places impossible demands on engineers to invent problem-solving technologies (miracle cures), rather than altering destructive behaviors. I take these impacts and this sociotechnical (i.e., the confluence of the “social” and the “technical”) dynamic as given, and build this dissertation from there.

I came to combustion chemistry to understand how air pollutants and greenhouse gases are formed, to understand the local and global impacts of combustion, and to understand the ways in which we ought to use combustion (if we choose to do so, given its significant contributions to climate change). I wish to emphasize that this dissertation does not focus on climate change in a standard manner (e.g. methods for carbon sequestration or how to achieve zero emissions vehicles), but rather on how and why a problem like climate change comes to be and how engineers have historically responded to such challenges. Of combustion, I have learned much, and this dissertation contributes to the understanding of how biofuels, in particular alcohols such as ethanol and butanol, affect the combustion chemistry of traditional fuel mixtures such as gasoline, kerosene, and diesel. Much of the dissertation is highly technical, and rests on physical chemistry theory, with data collected by pressure sensors and gas chromatographs and high-speed cameras. The contexts of the work are, however, decidedly non-technical for it is important to remember that biofuels are a *technological* solution to climate change, which is a *sociotechnically* created ecological problem. I therefore try to contextualize biofuels in technological thinking. There are splashes of sociology, history, philosophy, ethics, politics, science and technology studies, activist theory, and liberative pedagogy, forming a dissertational stew. This dissertation contributes to the understanding of how paradigms of technological development are perpetuated in engineering culture, and provides guidance to and tries to empower individual

engineers to radically re-envision these paradigms. What has brought us here will not take us there.

Given that this dissertation is a collection of manuscripts, each chapter has a separate introduction. This introduction provides a summary of the content of the individual chapters: from physical chemistry, to a more detailed historical and contemporary view of why we are investing so much in biofuels in the first place.

From a combustion chemistry standpoint, this work focuses on two important molecules—*n*-heptane, a chemical surrogate of complex fuel mixtures such as kerosene; and *n*-butanol, an alternative, bio-derived fuel that is of particular interest in aviation applications. Chapter 2\* presents ignition and speciation studies of *n*-heptane, an important reference compound for traditional fossil fuels. A part of primary reference fuel along with *iso*-octane, *n*-heptane has been studied extensively given its favorable thermophysical properties. It is an *n*-alkane that is small enough to have a high vapor pressure at room temperature, thereby allowing gas phase kinetic studies of it, and it is large enough to exhibit the array of chemical features of larger *n*-alkanes, including important low-temperature chemistry pathways that result in engine knocking and negative temperature coefficient behavior. Yet, there remains a dearth of detailed speciation data that shed light on whether chemical kinetic models adequately capture this chemistry. Studies were performed at conditions relevant to modern combustion applications, such as jet engines that fly you across the world and internal combustion engines that drive you to work. Chapter 3† follows the same trajectory as does Chapter 2, where *n*-butanol is the focus. *n*-Butanol is an alcohol that has garnered significant interest as a potential biofuel. The thermophysical properties of *n*-butanol, including a *low* vapor pressure, make it a prime candidate for use in aviation fuel. Many industrialists, government agencies and military branches hope for such biofuels to be produced in large quantities, to address national energy security and climate change concerns.

If employed widely, it is likely that biofuels will be blended with traditional fuels. These blends, when burned, may exhibit different chemical kinetic features than when individual components are burned separately; one component of the blend has

---

\* This chapter has been submitted for publication in the *Journal of Physical Chemistry A*.

† This chapter has been published in the *Journal of Physical Chemistry A*.

the capacity to affect what happens to the other both macroscopically in terms of overall ignition behavior, and also microscopically in terms of toxic pollutant, particulate, and greenhouse gas formation. Building on Chapters 2 and 3, Chapter 4<sup>‡</sup> explores these potentialities by presenting novel ignition and speciation work on blends of *n*-heptane and *n*-butanol to provide understanding of how *n*-butanol affects the chemistry of *n*-heptane.

What does the understanding of this chemistry mean more broadly? Why are biofuels being developed in the first place? Given the nature of climate change, and given all the knowledge of ecological issues available today, do engineers think differently about what they do? What are the underlying ethical, political, and philosophical principles that engineers draw upon to legitimize biofuel development efforts? And are these foundational principles any different from those that were drawn upon in past technological development and engineering? In Chapter 6 (Chapter 5 provides a short bridge between the technical and the non-technical), I tackle these questions by comparing engineering thinking between engineers that were involved in the damming of one of America's most storied rivers—the Colorado—to open the American West, and contemporary engineers that are involved in biofuel development for aviation. I rely on historical texts, interviews I conducted in Montréal at the International Civil Aviation Organisation, and theoretical guidance provided through case studies in the history of science and technology to analyze what I found. I chose these two case studies given the century or so of technical development and ecological awareness that has been gained between them. Furthermore, there are significant differences between the organizational hierarchies of engineers in these two cases; during the Progressive Era when rivers were being dammed, engineers were intimately involved in policy formulation, whereas most contemporary engineers work in corporate contexts.

Chapter 7 concludes the dissertation with reflections based on experience as well as diverse literature on what *individual* engineers can do given these large, complex issues of technological development, ethics, politics, and the environment. I build on the work of Karl Marx, Paolo Friere, Thomas Kuhn, and Donna Riley to propose how traditional paradigms of engineering can be replaced by an activist paradigm

---

<sup>‡</sup> This chapter has been submitted for publication in the *Journal of the American Chemical Society*.

through *praxis*. I intend this chapter (and hopefully the bulk of the dissertation) to be accessible to engineers and non-engineers alike. I hope to provide a small footing upon which to envision and enact a paradigmatically new technological development given the massive challenges we face as a global society. The goal of this work is to start a culture of activist engineering—engineering that transcends the current paradigms that bind us to ecologically degrading and socially unjust outcomes.

The crux of the dissertation is this: From a combustion system standpoint, the operating thermodynamic conditions at which *n*-butanol and fossil fuel blends can be burned might change current engine design, given the slower reactivity of *n*-butanol. The presence of *n*-butanol decreases the emission of chemical species that lead to particulate formation, while not significantly affecting small toxic emissions. However, *n*-butanol fundamentally changes the reaction kinetics of *n*-heptane as observed through measurements of key intermediate species formed during the oxidation of *n*-heptane. Broadly, biofuels may have the capacity to limit anthropogenic climate change and ecological degradation given their potential to be made from various waste streams and plants. Yet, even though our understanding of ecological issues and their sociotechnical causes has increased greatly over time, biofuels are being developed and promoted using decidedly traditional thinking and paradigms; the mentality of the engineers and technocrats such as corporate managers and lawyers involved in technological development has changed minimally over the past century. Biofuel development is not being complemented with broader economic and social transformation that fundamentally changes the way we use energy itself, and may thus merely substitute one ecological problem for another bigger ecological problem. Engineers, as powerful players in developing new technologies, must become leaders in achieving these transformations through engagement in broader conversations of how technologies interact with society and the environment.

It is my hope that this work informs not only combustion engineers and chemical kineticists. I hope that the broader contexts of technological development, engineering thinking and decision-making in response to ecological problems will be thought-provoking, especially to engineers who leave academic institutions and assume positions elsewhere in the community. If so, I will have accomplished what I have aimed to do.



## Chapter 2

### A speciation study of the chemical kinetics of *n*-heptane

*This chapter has been submitted to the Journal of Physical Chemistry A as, Karwat, D. M. A.; Wagnon, S. W.; Wooldridge, M. S.; Westbrook, C. K. "A speciation study of the chemical kinetics of n-heptane".*

#### Introduction

*n*-Heptane (*n*-C<sub>7</sub>H<sub>16</sub>) represents an important reference compound to study the chemical kinetics of large *n*-alkanes, which comprise significant fractions of complex commercial fuel blends such as gasoline, kerosene, and diesel. Its size allows *n*-C<sub>7</sub>H<sub>16</sub> to have both a high vapor pressure allowing gas-phase studies of its chemistry, as well as to exhibit chemical kinetic features that distinguish large-chain *n*-alkanes from other hydrocarbons (specifically its negative-temperature coefficient behavior). As a component of gasoline primary reference fuel (in which *n*-C<sub>7</sub>H<sub>16</sub> is blended with *iso*-octane), the global reactivity of *n*-C<sub>7</sub>H<sub>16</sub> has been extensively studied in shock tubes,<sup>1-7</sup> jet-stirred reactors,<sup>8</sup> rapid compression machines (RCMs),<sup>9-13</sup> and premixed laminar flames.<sup>14-18</sup> There have been a handful of studies<sup>8,12,14</sup> in which the products of *n*-C<sub>7</sub>H<sub>16</sub> oxidation—intermediate and final—have been measured experimentally.

Dagaut *et al.*<sup>8</sup> studied the oxidation of highly diluted stoichiometric *n*-C<sub>7</sub>H<sub>16</sub> mixtures in a jet-stirred reactor at residence times between 0.1 and 2 seconds, between pressures of 1-40 atm and temperatures of 550-1150 K, and with an inert/O<sub>2</sub> ratio between 90 and 180. Using gas chromatography and gas chromatography coupled with mass spectrometry, the authors were able to measure 44 different chemical species. They noted that increasing the pressure from 10 to 40 atm increased CO and CO<sub>2</sub> formation, while cyclic ethers such as *cis*-2-methyl-5-ethyltetrahydrofuran became more prevalent at higher temperatures as the

pressure increased. This shift in cyclic ether production they attributed to QOOH formation, which increases with increasing pressure. While the rate of  $n\text{-C}_7\text{H}_{16}$  consumption with increasing pressure was expected, Dagaut *et al.*<sup>8</sup> noted that in contrast to the experiments at 10 atm, at 40 atm, the reactivity of  $n\text{-C}_7\text{H}_{16}$  did not decrease significantly when the temperature was below 650 K.

While they did not measure product compositions, the intention of the Cox *et al.*<sup>13</sup> study was to explore the extent of reaction during compression in an RCM. The authors used gas chromatography to measure the amount of  $n$ -pentane and  $n\text{-C}_7\text{H}_{16}$  that reacted during the 22 ms stroke of their RCM as a function of temperature. They supplemented these data with chemiluminescence measurements of the first stage of ignition and found significant amounts of fuel consumption during the compression stroke when the targeted top-dead center (TDC) temperature exceeded 800 K.

Minetti *et al.*<sup>12</sup> remains the only study presented with extensive sampling of the intermediates of  $n\text{-C}_7\text{H}_{16}$  consumption in an RCM. In this study, the authors performed their sampling experiments of stoichiometric  $n\text{-C}_7\text{H}_{16}$  mixtures with a dilution of 3.76 at a temperature of 667 K and a pressure of 3.4 bar, i.e.,  $\chi(n\text{-C}_7\text{H}_{16}) = 0.0187$ ,  $\chi(\text{O}_2) = 0.2061$ ,  $\chi(\text{N}_2) = 0.7$ , and  $\chi(\text{CO}_2) = 0.0752$ , where  $\chi$  represents mole fractions. Using gas chromatography/mass spectrometry, they were able to identify 36 distinct compounds formed during an ignition delay time of 41 ms, with the first stage of ignition occurring at 30 ms after TDC in their RCM. They compared their experiments with a chemical mechanism presented by Warnatz *et al.*,<sup>19</sup> a mechanism that adequately reproduced ignition delay times, but did not perform well at predicting intermediate species profiles. Most importantly, the Warnatz *et al.* mechanism<sup>19</sup> predicted significant consumption of  $n\text{-C}_7\text{H}_{16}$  at the first stage of ignition (80%), while experimental measurements put this number closer to 20%. This discrepancy raised the question about how extensive chemical mechanisms need to be to adequately represent decomposition kinetics.

While recent modeling efforts have focused on  $n$ -alkanes with more than ten carbon atoms, there have been several chemical kinetic mechanisms developed to describe  $n\text{-C}_7\text{H}_{16}$  chemistry. Chemistry at temperatures higher than the negative temperature coefficient regime of large hydrocarbons was the first to be tackled<sup>20,21</sup>

and descriptions of low-temperature chemistry were later added to chemical kinetic mechanisms. The mechanism developed by Curran *et al.*<sup>22</sup> remains the most widely cited chemical kinetic mechanism, which included 25 reaction classes that included low-temperature chemistry. A paper published by Côme *et al.*<sup>20</sup> detailed a high-temperature mechanism for  $n\text{-C}_7\text{H}_{16}$  that has been modified recently. A recent mechanism<sup>23</sup> developed at Politecnico di Milano (PdM) includes low-temperature chemistry, building on a previously developed mechanism,<sup>21</sup> and contains more than 13,000 reactions and 400 chemical species to describe the kinetics of alkanes with up to sixteen carbon atoms. In order to study gasoline surrogate mixtures, Mehl *et al.*<sup>24</sup> updated the Curran *et al.*<sup>22</sup> mechanism by incorporating improved kinetic rates for linear alkenes.

The work presented in this chapter builds on these previous studies and complements them by presenting new experimental data on and analysis of speciation during the ignition delay of  $n\text{-C}_7\text{H}_{16}$  at high pressure and low temperatures. Chemical kinetic mechanism computations are compared to the experimental data presented. This work improves understanding of  $n\text{-C}_7\text{H}_{16}$  reaction chemistry, and provides a strong baseline against which to compare oxygenated and other alternative fuels. The thermodynamic conditions  $n$ -heptane was studied at were chosen given their importance to modern combustion applications; for example, the pressures achieved by the compressor stages of jet engines are routinely on the order of  $\sim 10$  atmospheres at cruise.

## Experimental Setup

### *The University of Michigan Rapid Compression Facility*

As a unique and powerful apparatus for studying fuel chemistry over a broad range of thermodynamic conditions, the University of Michigan Rapid Compression Facility (UM RCF) has been used to study the ignition of reference hydrocarbon fuel compounds such as *iso*-octane,<sup>25,26</sup> simulated syngas mixtures of hydrogen and carbon monoxide,<sup>27</sup> and oxygenated hydrocarbons,<sup>28</sup> as well as to study soot formation and morphology.<sup>29,30</sup> The UM RCF has allowed time-resolved measurements of hydroxyl radical formation during *iso*-octane/air mixtures,<sup>31</sup> as well as quantitative measurements of the intermediate species of *iso*-octane,<sup>32</sup> methyl

butanoate,<sup>33</sup> and *n*-butanol<sup>34</sup> oxidation by gas chromatography using rapid gas sampling.

The UM RCF uses a free-piston/cylinder compression process to create a chemical reactor for combustion chemistry studies. The key characteristics of the combustion kinetics are interrogated using the optical and physical access provided by the test section of the facility. The UM RCF consists of five major components as shown in the top panel of Figure 2.1—the driver section, the driven section, the test section (or test manifold), the sabot (a free piston with a tapered nosecone that forms an interference fit with the test section) and the hydraulic globe valve system. At the start of an experiment, the sabot is located at the upstream end of the driven section. The driven section (2.74 m long, 101.2 mm inner diameter) is evacuated and then filled with a pre-prepared fuel/oxidizer/diluent mixture. The driver section (with an inner diameter of 154 mm) is charged with high pressure gas. The driver and driven sections are separated by the fast-acting globe valve. When the valve is opened (with a typical cycle time of 100 ms), the sabot is launched down the length of the driven section compressing the test gas mixture. At the end of compression (EOC), the nose cone of the sabot seals the fuel/oxidizer/diluent mixture in the test section at specifically targeted temperatures and pressures, with the majority of the rise in temperature and pressure occurring during the last 10 ms of the stroke. Targeted temperatures and pressures are achieved by varying the compression ratio of the test section, as well as the composition of inert gases in the test mixture. At a given pressure and temperature after EOC, the fuel/oxidizer/diluent mixture in the test section autoignites after a period of time that is designated the ignition delay time ( $\tau_{\text{gn}}$ ).

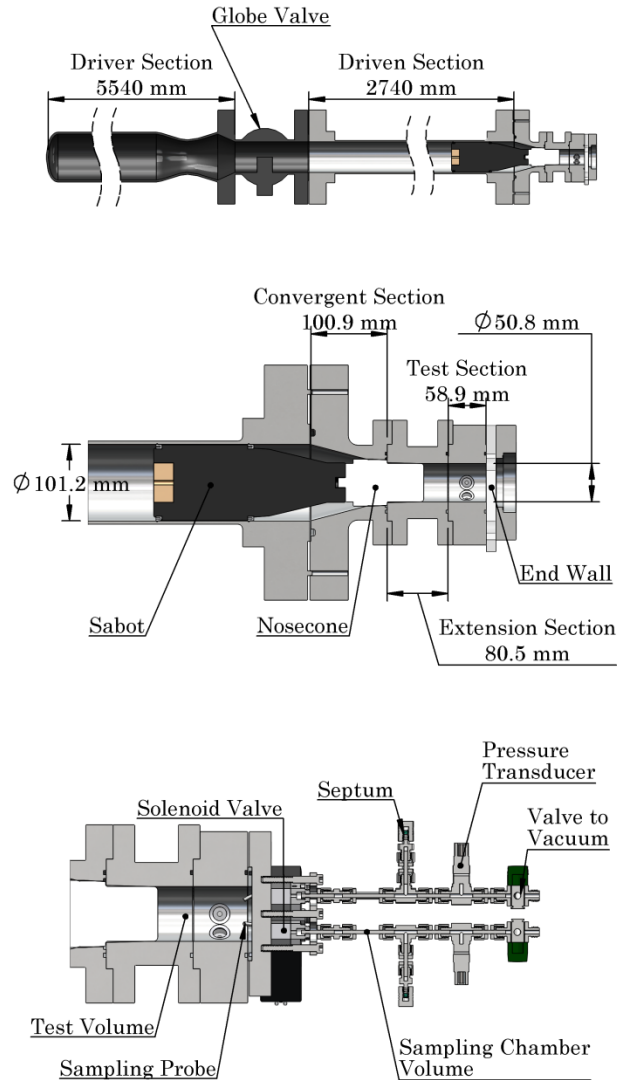


Figure 2.1 Shown are a representation of the UM RCF (top panel) with key dimensions, the configuration for end-view imaging (middle panel), and the configuration for high-speed gas sampling (bottom panel).

The UM RCF is designed to create uniform conditions at EOC in order to isolate reaction chemistry during the experiments and to minimize other interfering effects. Two important features include the geometry of the convergent section and the mixing manifold. The convergent section, the test section and the nose cone of the sabot are designed to trap the cold boundary layer outside the test section. The middle panel of Figure 2.1 shows a schematic of these RCF components with key dimensions. The unique shape of the sabot and the geometry of the convergent

section cause the core region of the test gases to be compressed into the test section, trapping the cold boundary layer gases in the shoulder region created by the body of the sabot and the convergent section. The compression of the core gases is therefore well described as an isentropic process, and characterization studies show less than 5% difference in measured and predicted isentropic conditions in the core region of the test section.<sup>35</sup> The characterization studies further show the isentropic core region extends across 70% of the diameter of the test section, and that the bulk of the pressure rise (~80%) and half of the temperature rise (~50%) occur during the last 10 ms of the compression process, where the total stroke lasts approximately 145 ms. An additional important outcome of trapping the cold boundary layers outside the test section is that heat losses from the gases in the core region are minimized, which maximizes the amount of time the test gases are at uniform state conditions. Consequently, conditions can be maintained for long test times on the order of 50 ms, with pressure >75% of EOC pressure and temperature >80% of EOC temperature, depending on the test gas mixtures.

For this study, stoichiometric  $n\text{-C}_7\text{H}_{16}/\text{O}_2$  mixtures, with an inert/ $\text{O}_2$  diluent ratio of 5.64, were prepared manometrically in a magnetically-stirred mixing tank external to the UM RCF using a mixing manifold ( $n\text{-C}_7\text{H}_{16}$ —Sigma-Aldrich, puriss. p.a.,  $\geq 99.5\%$ , GC grade;  $\text{O}_2$ —Cryogenic Gases, Purity Plus 4.3, 99.993%, <40 ppm Ar, <3 ppm moisture, <10 ppm  $\text{N}_2$ , <0.5 ppm hydrocarbons; inert diluents:  $\text{CO}_2$ —Cryogenic Gases, Laser Grade, 99.995%, <1 ppm of  $\text{O}_2$ , moisture and hydrocarbons, <0.2 ppm CO; and  $\text{N}_2$ —Cryogenic Gases, Purity Plus 5.0, 99.999%, <2 ppm  $\text{O}_2$ , <3 ppm moisture, <0.5 ppm hydrocarbons). Mixture compositions were determined using partial pressures measured with a capacitance diaphragm gauge (Varian CeramiCel VCMT12TFA, with an accuracy of  $\pm 0.01$  torr). The partial pressure of  $n\text{-C}_7\text{H}_{16}$  was maintained well below its saturation vapor pressure at room temperature ( $5.9 \times 10^{-2}$  atm or 45 torr at  $25^\circ\text{C}$ ) in order to avoid concerns of fuel condensation. Total mixture pressures in the mixing tank were 0.5-0.8 atm, with initial fill pressures ( $P_0$ ) in the RCF being approximately  $1.3 \times 10^{-1}$  atm.

The pressure in the test section is monitored using a piezoelectric transducer (Kistler 6041AX4) and charge amplifier (Kistler 5010B) with a combined accuracy of 0.01 atm and 0.015 ms. A National Instruments (NI) cDAQ 9172 chassis coupled

with NI 9215 cards recorded all electronic signals at 100 kHz. For ignition experiments, a transparent end wall (configuration seen in the middle panel of Figure 2.1) coupled with a high-speed Vision Research Phantom v711 camera with a widescreen CMOS array (maximum resolution of 1280×800 pixels, capable of 1.4 million frames per second at reduced resolution, 20  $\mu\text{m}$  pixels with 0.34  $\mu\text{m}$  spacing) with a fast 50 mm lens ( $f/0.95$ , Navitar) and c-mount extension tube recorded the ignition events in the test section by viewing along the axis of the test section. Imaging data provide qualitative and quantitative indications of the ignition homogeneity. Imaging data were acquired at 30,000 frames per second (fps) at a spatial resolution of 256×256 pixels, with an image exposure time of 34  $\mu\text{s}$ .

### ***High-speed gas sampling and gas chromatography***

Instead of the transparent end wall, an endwall with a high-speed gas sampling system was used for gas sampling experiments. The gas sampling system removes a very small portion (quantified below) of the test gas mixture (as shown in the bottom panel of Figure 2.1) at targeted times during the ignition delay period. The samples are then analyzed using gas chromatographic techniques to identify and quantify the intermediate species present in the sample. A series of samples pulled from experiments conducted at the same targeted EOC conditions allows a compilation of overall species time-histories for the intermediates identified. Several previous studies, including on fuels such as *iso*-octane,<sup>32</sup> and methyl butanoate<sup>33</sup> have proved the validity of this experimental technique.

The sampling system used for these experiments was comprised of sample chambers ( $\sim 4.5 \pm 0.5$  mL) equipped with a piezoresistive pressure transducer (Kistler 4045A2), charge amplifiers (Kistler 4618A0), low-bleed septa (VICI Valco), fast-acting sampling valves (modified Festo MHE3 valves with a stock response time of 3 ms, 3 mm orifice), and vacuum isolation valves (Swagelok). Independent control of each sampling valve using two digital delay/pulse generators (Stanford Research Systems Model DG535) allows the collection of up to four samples per experiment. The four samples are acquired through probes located on a square spacing (26×26 mm) on the end wall, 19 mm (radially) from the center of the test section. (Recall the test section inner diameter is 50.8 mm.) For the sampling data presented here,

one gas sample was collected in each experiment by triggering the fast-acting valve located at the northeast position of the sampling end wall. Significant care was taken to ensure that the samples were pulled from the volume of the test section well beyond the cold thermal boundary layer of the test section end wall. During the sampling event, the reacting gases removed from the test section gases are quenched in less than 0.3 ms as they expand into the vacuum of the sample chamber ( $P_{\text{test section}}/P_{\text{sample chamber}} \sim 11$ ,  $V_{\text{test section}}/V_{\text{sample chamber}} \sim 39$ ). Once the samples are acquired, the gases are drawn into a syringe (Hamilton Gastight #1010, 10 mL) through the syringe port on the sampling chamber for delivery to the gas chromatographs. As will be shown later, the sampling of very small volumes of test gas mixture samples left the reactive mixture in the test section unaffected; the ignition delay times ( $\tau_{\text{ign}}$ , defined below) values determined from the gas-sampling experiments were in excellent agreement with experiments where gas sampling was not used.

The dilution of the sample by unreacted gases trapped in the “dead” volume of the sampling system of the sampling probe ( $\pm 16\%$ , as determined in Chapter 3) along with the gas chromatography calibration uncertainties for each species are the chief contributors to uncertainty of the gas sampling measurements. For the data presented in this paper, the temporal uncertainties resulting from the triggering of the fast-acting valves on the sampling end wall  $\pm 0.75$  ms centered on the falling edge of the sampling pulse sent to the fast-acting valves. The gas-sampling results therefore represent the average value of the species during the sampling time.

Three gas chromatographs (GCs) equipped with four different columns, with each connected to a separate detector, were calibrated for quantitative measurements of species of interest. A temperature-controlled 10-port gas sampling valve injected the samples into the columns in the GCs. Ultra high purity helium (Cryogenic Gases, Purity Plus, 99.999%) was the carrier gas for all of the GCs. The first GC, a Perkin Elmer Autosystem GC with a Varian CP-PoraBOND Q (25 m $\times$ 0.53 mm $\times$ 0.7  $\mu$ m) column was connected to a flame ionization detector (FID) to detect *n*-C<sub>7</sub>H<sub>16</sub>, methanol (CH<sub>3</sub>OH), acetaldehyde (CH<sub>3</sub>CHO), and propionaldehyde (C<sub>2</sub>H<sub>5</sub>CHO). (The temperature program for this GC was: 30°C for 4.5 minutes  $\rightarrow$  45°C/minute  $\rightarrow$  110°C for 9 minutes  $\rightarrow$  45°C/minute  $\rightarrow$  150°C for 20 minutes.) A second GC, a Perkin Elmer Autosystem GC with a Varian CP-Al<sub>2</sub>O<sub>3</sub>/Na<sub>2</sub>SO<sub>4</sub> (25



m $\times$ 0.53 mm $\times$ 0.7  $\mu$ m) column was connected to an FID to detect methane (CH<sub>4</sub>), ethane (C<sub>2</sub>H<sub>6</sub>), ethene (C<sub>2</sub>H<sub>4</sub>), ethyne (C<sub>2</sub>H<sub>2</sub>), propane (C<sub>3</sub>H<sub>8</sub>), propene (C<sub>3</sub>H<sub>6</sub>), 1-butene (1-C<sub>4</sub>H<sub>8</sub>), 1-pentene (1-C<sub>5</sub>H<sub>10</sub>), 1-hexene (1-C<sub>6</sub>H<sub>12</sub>), 1,3-butadiene (1,3-C<sub>4</sub>H<sub>6</sub>), and 3-heptene (3-C<sub>7</sub>H<sub>14</sub>). (The temperature program for this GC was: 30°C for 4 minutes  $\rightarrow$  25°C/minute  $\rightarrow$  150°C for 7 minutes  $\rightarrow$  45°C/minute  $\rightarrow$  200°C for 2 minutes.) The third GC, a Perkin Elmer Clarus 500, used a Agilent DB-Wax (30 m $\times$ 0.25 mm $\times$ 0.25  $\mu$ m) column connected to an FID to detect 2-heptene (2-C<sub>7</sub>H<sub>14</sub>) and *n*-butyraldehyde (*n*-C<sub>3</sub>H<sub>7</sub>CHO), and a Restek ShinCarbon ST packed (2 m $\times$ 1 mm, silica steel) column connected to a thermal conductivity detector (TCD) to detect carbon monoxide (CO). (The temperature program for this GC was: 25°C for 5 minutes  $\rightarrow$  45°C/minute  $\rightarrow$  200°C for 5 minutes.) Each of the FIDs used a hydrogen/air flame, were maintained at 300°C, and were set with a range and attenuation of 1. The TCD was maintained at 100°C with an attenuation of 1 and current of  $\pm$ 160 mA. The helium, air, and hydrogen were further purified before use in the GC using adsorbents to remove water, hydrocarbons, and oxygen. High-purity reference chemicals (either gaseous or vapors of liquid) were characterized and calibrated for the GC temperature programs used in the study, and the chromatograms were used to establish the calibrations for absolute concentration. Calibration mixtures were made in the magnetically-stirred mixing tank with the upper limit of concentrations calibrated for being greater than the maximum concentrations predicted by the reaction mechanism discussed below for the ignition delay of a mixture with  $\chi(n\text{-C}_7\text{H}_{16}) = 0.0135$ ,  $\chi(\text{O}_2) = 0.1486$ ,  $\chi(\text{N}_2) = 0.2179$ ,  $\chi(\text{CO}_2) = 0.62$  at  $P = 9$  atm and  $T = 700$  K. Calibration curves were linear in all cases. Voltage signals from the GC detectors were recorded using an NI PXI 4472 data acquisition system with a sampling rate of 8 Hz.

## Mechanism Description

Kinetic modeling calculations were carried out using the CHEMKIN Release 10101 (x64).<sup>36</sup> The detailed chemical kinetic mechanism for *n*-C<sub>7</sub>H<sub>16</sub> was taken from an updated version of Mehl *et al.*<sup>24</sup> based on the original mechanism of Curran *et al.*<sup>22</sup> The core mechanism for hydrocarbons from C<sub>1</sub> to C<sub>4</sub> species was taken from a recently refined mechanism from Metcalfe *et al.*<sup>37</sup>

Preliminary calculations with this composite mechanism produced two-stage ignitions over the entire range of post-compression stroke temperatures, and included predictions of ignition delay times that were shorter than those measured by nearly a factor of two. In particular, the extents of reaction during the first stage ignition, and specifically the amounts of  $n$ -C<sub>7</sub>H<sub>16</sub> fuel consumed, were larger than observed in the experimental sampling. This directed our attention to the equilibria in the addition reactions of heptyl and hydroperoxyheptyl radicals with O<sub>2</sub>.



The first stage ignition proceeds until the temperature has increased enough to make the reverse, dissociation reactions of Reactions 2.1 and 2.2 faster than the forward, addition reactions. If the rates of the dissociation reactions are too slow, too much first stage ignition will be predicted. The predicted ignition delay times showed considerable sensitivity to the rates of these dissociation reactions.

The reaction classes corresponding to Reaction 2.1 (alkyl peroxy formation) and Reaction 2.2 (addition of molecular oxygen to hydroperoxyalkyl radicals) have been the subject of recent *ab initio* studies by Villano *et al.*,<sup>38,39</sup> in which the authors systematically studied the first two steps of low-temperature chemistry exhibited by alkanes using the CBS-QB3 level of theory. In the original  $n$ -C<sub>7</sub>H<sub>16</sub> mechanism of Curran *et al.*<sup>22</sup>, both the addition and decomposition reaction rates for the classes of reactions corresponding to Reaction 2.1 and Reaction 2.2 were specified explicitly, so these reactions were not guaranteed to produce the reverse reaction rates required by the equilibrium constants of these reactions. In more recent kinetic mechanisms,<sup>40</sup> these reaction rates have been written in the addition direction, and the dissociation rates are determined from the relevant equilibrium constants. However, this approach had not yet been implemented in the much older  $n$ -C<sub>7</sub>H<sub>16</sub> mechanism. Therefore, the reaction rates for Reactions 2.1 and 2.2 above were corrected to specify the rates in the addition direction and use equilibrium constants for the dissociation rates. This modification reduced the extents of reaction in the first stage ignition, and the predicted ignition delay times much closer to the experimental results, as will be shown below. No other mechanism changes were

made for the present study; the key to detecting this problem with the mechanism was the availability of the time-resolved  $n\text{-C}_7\text{H}_{16}$  concentrations and experimental measurements of the pressure increase caused by the first stage ignition.

## Experimental Results and Discussion

### *Ignition experiments*

While this chapter focuses primarily on speciation studies of  $n\text{-C}_7\text{H}_{16}$ , ignition experiments with end-view imaging were performed not only to measure the ignition delay time ( $\tau_{\text{ign}}$ ) as a function of temperature, but also to identify the appropriate temperature and pressure conditions at which to conduct sampling experiments. Given that each sampling event lasts approximately 1.5 ms, we targeted a  $\tau_{\text{ign}}$  of approximately 15 ms for sampling experiments. This time would comfortably allow for at least ten discrete sampling times during the ignition delay period. For each experiment, the effective test conditions corresponding to a  $\tau_{\text{ign}}$  value are determined based on the pressure time-history (an example of which is seen in Figure 2.2 below).  $n\text{-C}_7\text{H}_{16}$  exhibited two-stage ignition for all of the experimental data presented here; therefore, a modified method compared to previous studies<sup>33,34</sup> was used to determine the experimental conditions. Equation 2.1 was used to determine the effective pressure ( $P_{\text{eff}}$ ), which is the time-integrated average pressure from the maximum pressure ( $P_{\text{max}}$ ) at EOC to the maximum of rate of pressure rise at the *1st stage of ignition* ( $dP/dt_{\text{max, 1st stage}}$ ),

$$P_{\text{eff}} = \frac{1}{t_{dP/dt_{\text{max}}} - t_{P_{\text{max}}}} \int_{t_{P_{\text{max}}}}^{t_{dP/dt_{\text{max, 1st stage}}}} P \cdot dt . \quad (2.1)$$

The effective temperature ( $T_{\text{eff}}$ ) for each experiment was determined using  $P_{\text{eff}}$  and numerical integration of the isentropic relation (Equation 2.2),

$$\int_{T_0}^{T_{\text{eff}}} \frac{\gamma}{\gamma-1} d \ln T = \ln \left( \frac{P_{\text{eff}}}{P_0} \right) , \quad (2.2)$$

where  $P_0$  is the initial charge pressure,  $T_0$  is the initial temperature, and  $\gamma$  is the temperature-dependent ratio of the specific heats of the unreacted test gas mixture

(determined using the NASA thermodynamic data base<sup>41</sup>).  $\tau_{\text{ign}}$  for each experiment was defined as the time between EOC ( $t = 0$  ms, defined by the first maximum in  $P$ ) and the maximum rate of pressure rise corresponding to autoignition ( $dP/dt_{\text{max, 2nd stage}}$ ). Ignition experiments were performed in the narrow temperature range of 660-707 K at an effective pressure between 8.92-9.53 atm. The low end of the temperature window was dictated by the compression ratio of the UM RCF; the diluent was solely  $\text{CO}_2$  for these experiments. The high end of the temperature window was chosen to avoid reaction during compression, thereby avoiding complications in defining the experimental state conditions and the interpretation of the resulting  $\tau_{\text{ign}}$  and gas sampling results. All mixtures had an equivalence ratio ( $\phi = [\chi(n\text{-C}_7\text{H}_{16})/\chi(\text{O}_2)]_{\text{actual}}/[\chi(n\text{-C}_7\text{H}_{16})/\chi(\text{O}_2)]_{\text{stoichiometric}}$ ) of 1, and a dilution of inert/ $\text{O}_2 = 5.62\text{-}5.64$ , with  $\text{N}_2$  and  $\text{CO}_2$  being the sole diluents used in the experiments. The  $n\text{-C}_7\text{H}_{16}$  concentration for the experiments was 1.34-1.35%. Table 2.1 found at the end of this chapter provides a summary of the experimental conditions and results for  $\tau_{\text{ign}}$  for all of the UM RCF data presented.

Figure 2.2 presents typical results from a UM RCF  $n\text{-C}_7\text{H}_{16}$  ignition experiment in which imaging data were acquired. The lower panel depicts the time-histories of the pressure ( $P$ ) and rate of pressure rise ( $dP/dt$ ) in the test section. A fast Fourier transform has been applied to filter high-frequency disturbances greater than 2.5 kHz generated by the impact of the sabot near EOC. A smooth compression process due to the motion of the sabot brings the pressure to the first maximum, and the EOC is set as time  $t = 0$ , after which the volume in the test section is constant. The first stage of ignition ( $\tau_1$ ) occurs at 7.13 ms, corresponding to a local maximum in  $dP/dt$  (circled in Figure 2.2), and  $P_{\text{eff}}$  and  $T_{\text{eff}}$  are 9.32 atm and 707 K, respectively. After the first stage of ignition, the pressure rises abruptly again to the maximum value corresponding to the autoignition of the test mixture— $\tau_{\text{ign}} = 12.73$  ms.

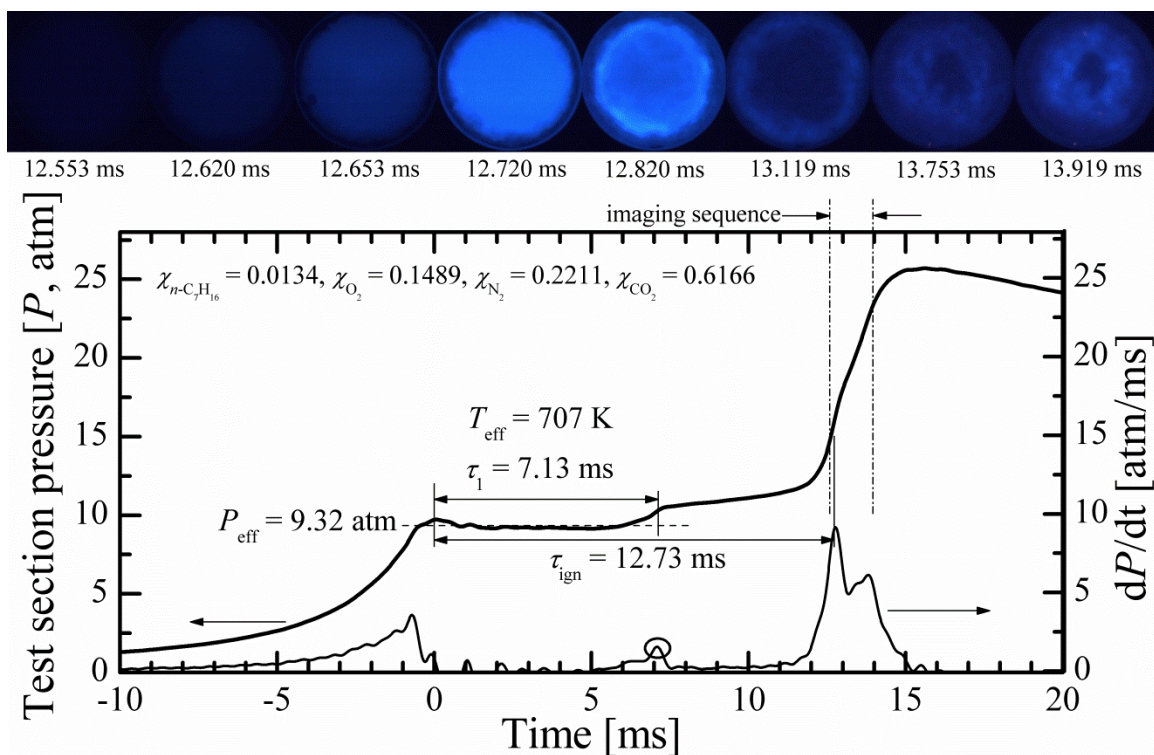


Figure 2.2 Results from a typical UM RCF  $n$ -C<sub>7</sub>H<sub>16</sub> ignition experiment. The lower panel depicts the pressure time-history in the test section, along with the rate of pressure rise, which allows definition of  $\tau_{\text{ign}}$  and consequently effective pressure and temperature conditions. The upper panel shows still images taken at 30,000 fps via end-view imaging. Note the homogeneity of the ignition event. The color of these images has been adjusted for clarity.

The upper panel of Figure 2.2 shows stills from the image sequence of the chemiluminescence that occurs during ignition. This emission is attributed to CH and C<sub>2</sub> radicals, which have strong spectroscopic features in the blue part of the visible spectrum (CH: 431.2 nm; C<sub>2</sub>: 473.7 nm, 516.5 nm, 563.5 nm) and are generated only through the decomposition of intermediate hydrocarbons present in the test mixture. That the intense blue emission occurs simultaneously throughout the test section with uniform intensity attests to the high degree of homogeneity of the reactant mixture and the state conditions in the test section. Such uniformity gives confidence in the application of localized sampling.

An Arrhenius diagram presenting the results of UM RCF ignition and sampling experiments, along with  $n$ -C<sub>7</sub>H<sub>16</sub> ignition data from other studies, namely, Minetti *et al.*,<sup>12</sup> Shen *et al.*,<sup>2</sup> and Ciezki and Adomeit<sup>1</sup> is seen in Figure 2.3. Given the plethora

of  $n\text{-C}_7\text{H}_{16}$  ignition data available in the literature, data for this plot have been selected to show the influence of pressure of pressure on  $\tau_{\text{ign}}$ . As seen in Figure 2.3,  $n\text{-C}_7\text{H}_{16}$  exhibits significant negative temperature coefficient (NTC) behavior between 720 K and 950 K, and the NTC region shifts to higher temperatures as pressure increases. Reasons for this shift are well known; NTC behavior is governed by the ratio of  $\text{RO}_2$  to R, and since at higher pressures the concentrations of  $\text{O}_2$  are higher, the equilibrium is shifted towards  $\text{RO}_2$ , consequently moving the NTC region to higher temperatures.<sup>38</sup> The degree of NTC behavior also decreases with increasing pressure. Also observed is the quickening of  $\tau_1$  with increasing temperature, even in the NTC region, particularly in the Minetti *et al.*<sup>12</sup> data. Detailed explanations of the chemistry that leads to this behavior, in which  $\tau_{\text{ign}}$  increases with increasing temperature, can be found elsewhere.<sup>2,22</sup> The filled and open blue triangles represent zero-dimensional, constant volume, adiabatic CHEMKIN<sup>TM</sup> simulations for the UM RCF sampling conditions, and shown with lines are constant volume, adiabatic mechanism predictions of the PdM mechanism<sup>23</sup>.

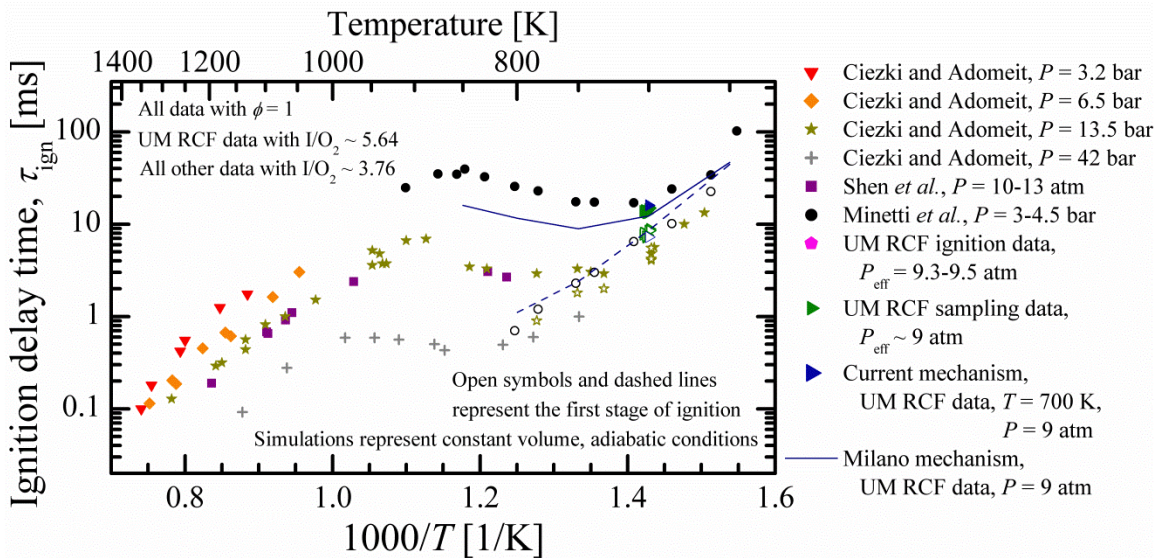


Figure 2.3 Ignition characteristics of  $n\text{-C}_7\text{H}_{16}$  over a wide range of temperatures (650-1400 K) and pressures (3-42 atm), including results of the current work. Error bars representing the standard deviation of  $\tau_{\text{ign}}$  (0.63 ms) for UM RCF data do not show up on plot.

Given that the compression process of the UM RCF takes a finite amount of time, there is the potential that the  $n$ -C<sub>7</sub>H<sub>16</sub> spends a non-negligible amount of time at low temperatures where the reactivity of  $n$ -C<sub>7</sub>H<sub>16</sub> is higher than at the EOC conditions. As is noticed in Figure 2.3 above, the experiments conducted in the UM RCF were performed at temperatures before the beginning of the NTC region to avoid complications of reaction during compression. These temperatures are coincidentally very relevant to modern combustion applications such as pilot injections of fuel into high pressure environments.

There is always a question of how best to conduct simulation experiments and represent them on Arrhenius diagrams. Several simulations were conducted using a constant volume, adiabatic approach as well as an expanding volume profile representing the heat losses inherent in the UM RCF. Shown in Figure 2.4 is a comparison of various CHEMKIN™ simulations with a typical UM RCF experiment. All the simulations and the experiment were conducted with  $\chi(n\text{-C}_7\text{H}_{16}) = 0.01343$ ,  $\chi(\text{O}_2) = 0.149$ ,  $\chi(\text{N}_2) = 0.2334$ , and  $\chi(\text{CO}_2) = 0.60417$ . Taking the pressure time-history as an indicator of heat loss, the experimental pressure trace shows very little heat loss between EOC and the first stage of ignition (pressure drops <3%, temperature drops correspondingly by <1%) given the very high volume-to-surface area ratio of the test section. Constant volume, adiabatic simulations at  $P_0 = 9$  atm,  $T_0 = 700$  K using the current mechanism (black dashed line), the Curran *et al.*<sup>22</sup> mechanism updated by Mehl *et al.*<sup>24</sup> (blue short dashed line) and the PdM mechanism<sup>23</sup> (red dotted line) follow the experimental pressure trace very closely. A simulation using an expansion volume profile (green dot-dash line) generated from an inert experiment (shown later in Figure 2.6) was also conducted. As is seen clearly in the inset, the simulation captures the peak EOC pressure in the UM RCF and the small heat losses that occur quickly after EOC. It is observed that the results of such simulations are very close to the constant volume, adiabatic simulations, showing that heat losses in the UM RCF minimally affect the test gas mixture. Furthermore, the use of the effective pressure and temperature (which are always lower than the EOC pressure and temperature) in defining the thermodynamic parameters of each experiment adequately capture any potential



heat losses. We are therefore confident in presenting constant volume, adiabatic simulations on Arrhenius diagrams.

In Figure 2.4, we observe that the experiment shows a slightly more prolonged first stage of ignition compared to mechanism predictions. This may be due to the presence of a boundary layer in the test section that acts as a compressible wall that absorbs the energy released by the first stage of ignition, or it may be due to deficiencies in the kinetic mechanism. Also, the ceiling pressure reached by the first stage of ignition is lower experimentally than is predicted computationally. Both of these issues will require further analysis with additional experiments and kinetic mechanism development.

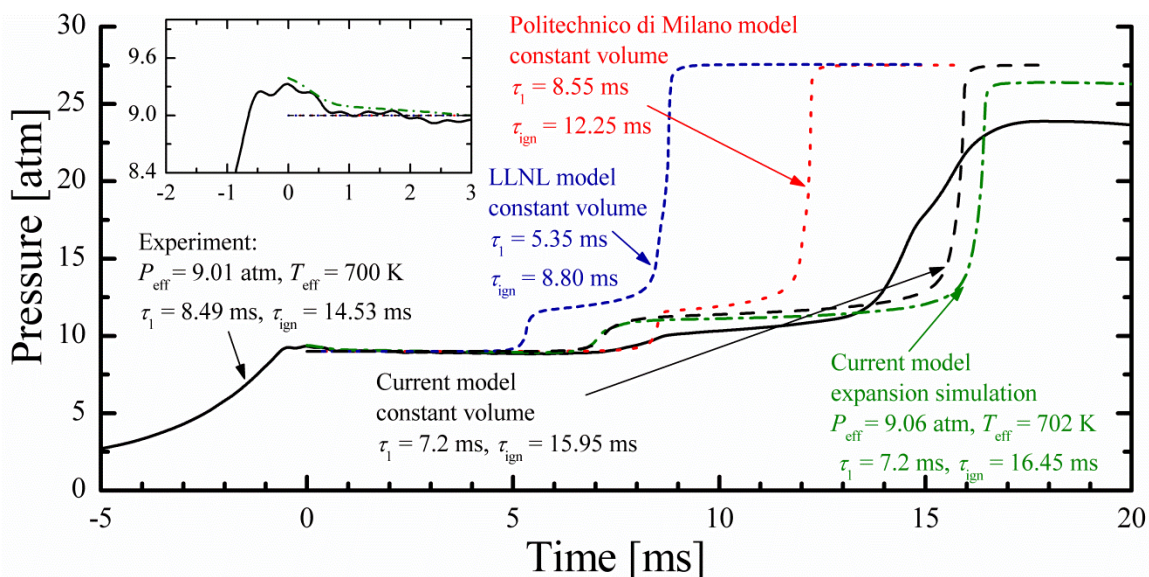


Figure 2.4 A comparison of ignition delay times from a typical UM RCF ignition experiment, the current mechanism, the LLNL mechanism<sup>24</sup> and the mechanism from PdM.<sup>23</sup> Constant volume, adiabatic simulations were performed with  $P_0 = 9 \text{ atm}$ ,  $T_0 = 700 \text{ K}$ . The expansion simulation was performed by using a volume profile generated from the pressure trace of an inert experiment.

Figure 2.5 is an Arrhenius diagram that summarizes the vast amount of  $n\text{-C}_7\text{H}_{16}$  ignition data taken using rapid compression machines. Plotted specifically, in addition to the UM RCF data (obtained using an inert/ $\text{O}_2$  molar dilution of  $\sim 5.64$ ), are data from Griffiths *et al.*,<sup>11</sup> Silke *et al.*,<sup>9</sup> and Minetti *et al.*,<sup>12</sup> all of which were obtained using an inert/ $\text{O}_2$  molar dilution of 3.76. The Minetti *et al.*<sup>12</sup> data, obtained at pressures of 3-4.5 bar, when scaled to 9 atm, fall smoothly in line with the 8-10



atm data of Griffiths *et al.*<sup>11</sup> at temperatures below 725 K. Differences in the reactivity between the combination of these data sets and the UM RCF data are due largely to the different levels of dilution between studied mixtures. It is important to note that interpretation of many rapid compression machine datasets, especially for highly reactive fuels such as  $n$ -C<sub>7</sub>H<sub>16</sub>, must take account of potential reaction during compression, given that the test mixtures may spend non-negligible amounts of time at low temperatures where the reactivity of the fuel may be significant. As already noted, we have tried to avoid entering regimes with significant reactivity before EOC by using higher dilution levels than the previous studies presented in Figure 2.5.

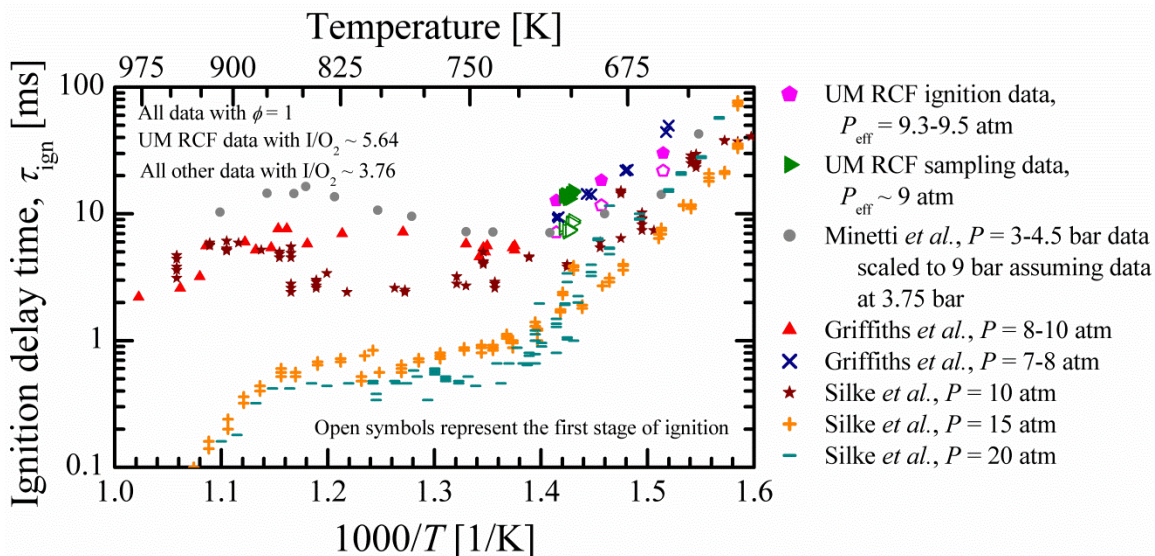


Figure 2.5 An Arrhenius plot of ignition data from the UM RCF and other rapid compression machine studies.

### ***High-speed gas sampling experiments***

While the ignition studies provide an understanding of the global kinetics of  $n$ -C<sub>7</sub>H<sub>16</sub> ignition, speciation measurements provide more detailed understandings of the dominant chemical pathways in the reacting test gas mixture. We therefore performed sampling experiments to speciate the intermediates formed during the ignition delay time. Figure 2.6 presents results from a typical sampling experiment, in which  $P_{\text{eff}} = 9.01$  atm,  $T_{\text{eff}} = 700$  K,  $\tau_1 = 8.49$  ms and  $\tau_{\text{ign}} = 14.53$  ms. Seen are the pressure time-history in the test section, the sampling pulse sent to the high-speed gas sampling system, and the pressure in the sampling chamber. As mentioned

previously, since only a very small amount of sample is removed from the reacting mixture in the test section, the pressure in the test section remains unaffected by the sampling process; the pressure features seen in Figure 2.2 are thus identical to those seen in Figure 2.6, which depicts an ignition experiment in which sampling was not performed. The pressure rise in the sampling volume occurs less than 2 ms after the fall of the sampling signal. Also shown is the time-history of a non-igniting inert experiment, in which the  $O_2$  of an igniting experiment is replaced with  $N_2$ . Given the almost identical thermal characteristics of  $O_2$  and  $N_2$ , the mixture compressed in a non-igniting experiment provides a baseline for comparison, including an understanding of the effects of heat transfer during the experiments. The pressure time-history of the non-igniting experiment is almost indistinguishable from the igniting experiment ( $P_{\text{eff}}$  and  $T_{\text{eff}}$  differ by less 0.1% and 0.3%, respectively) until the first stage of ignition, and the heat transfer physics of the experiments remain unaffected by both the ignition events in the test section and the sampling events. Also, since the bulk of compression process in the UM RCF occurs over approximately ten milliseconds, there is always a concern about possible reaction of the test gas mixture during compression, which affects the assumptions used to define the effective thermodynamic conditions (Equations 2.1 and 2.2) of the experiment. As seen in Figure 2.6, however, the non-igniting experiment shows a nearly identical compression process to the igniting experiment.

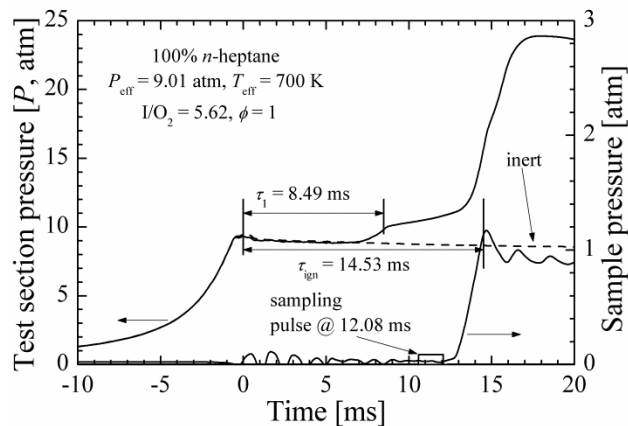


Figure 2.6 Typical results from a sampling experiment conducted on the UM RCF. Notice the agreement, until the first stage of ignition, between a non-reacting, inert pressure trace and the reacting pressure trace, which signifies that the heat transfer physics of the sampling experiments remain unaffected by the sampling event.

A summary of the gas-sampling experiments, including mixture compositions, can be found in Table 2.1 at the end of the chapter. Figure 2.7 shows the pressure time-histories for the thirteen experiments, all of which show nearly identical, smooth compression processes, and very similar pressure time-histories after EOC. The average  $P_{\text{eff}}$ ,  $T_{\text{eff}}$ ,  $\tau_1$ , and  $\tau_{\text{ign}}$  for all of the gas-sampling experiments were 9.02 atm, 701 K, 7.94 ms, and 14.09 ms, respectively, with the corresponding standard deviations of 0.07 atm, 1.5 K, 0.52 ms, and 0.63 ms, respectively, which demonstrate the excellent level of repeatability of these experiments. Furthermore, since for the current experimental setup end-view imaging cannot be conducted simultaneously with gas-sampling through the end wall, an experiment to ensure spatial homogeneity of the reacting mixture in the test section was performed by rotating the high-speed gas sampling system by  $180^\circ$  to pull a sample from the southwest corner of the test section at almost the same time during the ignition delay period as a sample pulled from the northeast corner. Within measurement uncertainties, the sample yielded species concentrations that were consistent with the overall species time-histories. For comparison with mechanism predictions, the pressure time-histories and sampling times were converted to normalized times. The period of time between EOC and first stage of ignition of each experiment was normalized by  $\tau_1$  (resulting in a normalized time domain of 0 to 1), and the period of time between the first stage of ignition and autoignition ( $\tau_{\text{ign}} - \tau_1$ ) was normalized by  $\tau_{\text{ign}} - \tau_1$  and added on to the first normalized time domain. The result, seen in Figure 2.8, is an overall normalized time domain in which 0 to 1 represents the first stage of ignition, and 1 to 2 represents the second stage of ignition.

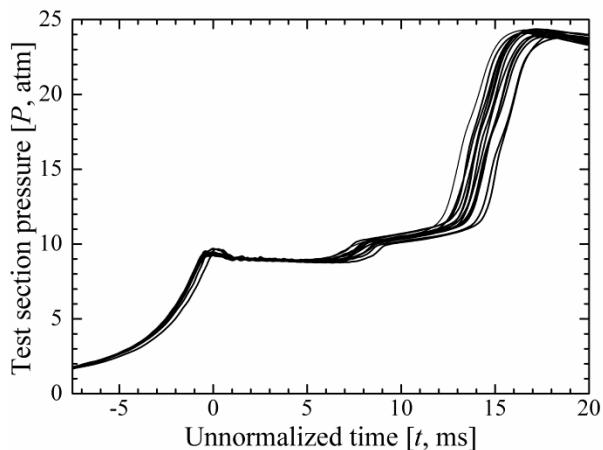


Figure 2.7 The unnormalized experimental pressure traces of the thirteen sampling experiments. Although unnormalized, note the level of repeatability of the compression process, as well as the first and second stages of ignition and heat release.

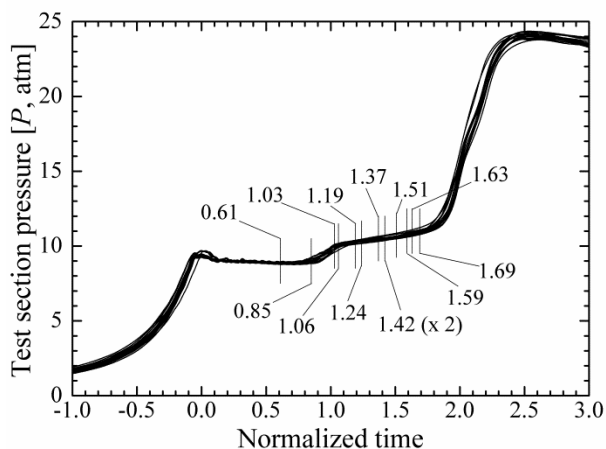


Figure 2.8 The normalized experimental pressure traces of the thirteen sampling experiments. 0 represents EOC, 1 represents the first stage of ignition, and 2 represents the second stage of ignition. Shown also are the normalized sampling times at which samples were pulled from the test section.

Comparing Figure 2.7 and Figure 2.8, we see that the pressure traces in the normalized time domain fall squarely on top of each other, thus allowing meaningful comparisons between UM RCF experiments. The use of a normalized time domain also allows for adequate comparison between the speciation data obtained by the UM RCF and the Minetti *et al.*<sup>12</sup> data, which were obtained for much different experimental conditions—at an EOC temperature of 667K and an EOC pressure of 3.4 bar resulting in  $\tau_1 = 30$  ms, and  $\tau_{\text{ign}} = 41$  ms.

Figure 2.9 provides typical chromatograms obtained from the GCs from a sampling experiment. These particular chromatograms were obtained from the experiment depicted in Figure 2.6, and all identified species except CO are shown.  $C_2H_2$  was not observed in any experiment, while several peaks remained unidentified. Yet the carbon balance was  $90\pm 12\%$  for sampling at early times during the ignition delay period and  $65\pm 9\%$  for sampling closer to autoignition. The peaks identified in the chromatograms were converted into discrete measurements of intermediate species for each normalized sampling time using the calibrations for each species.

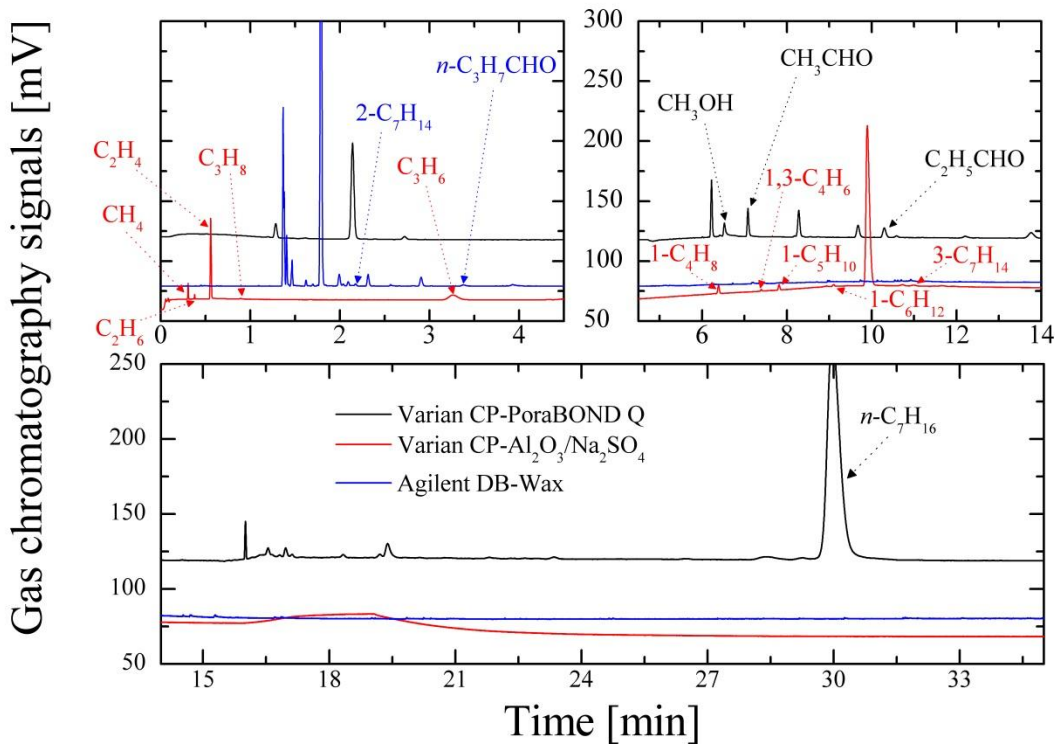
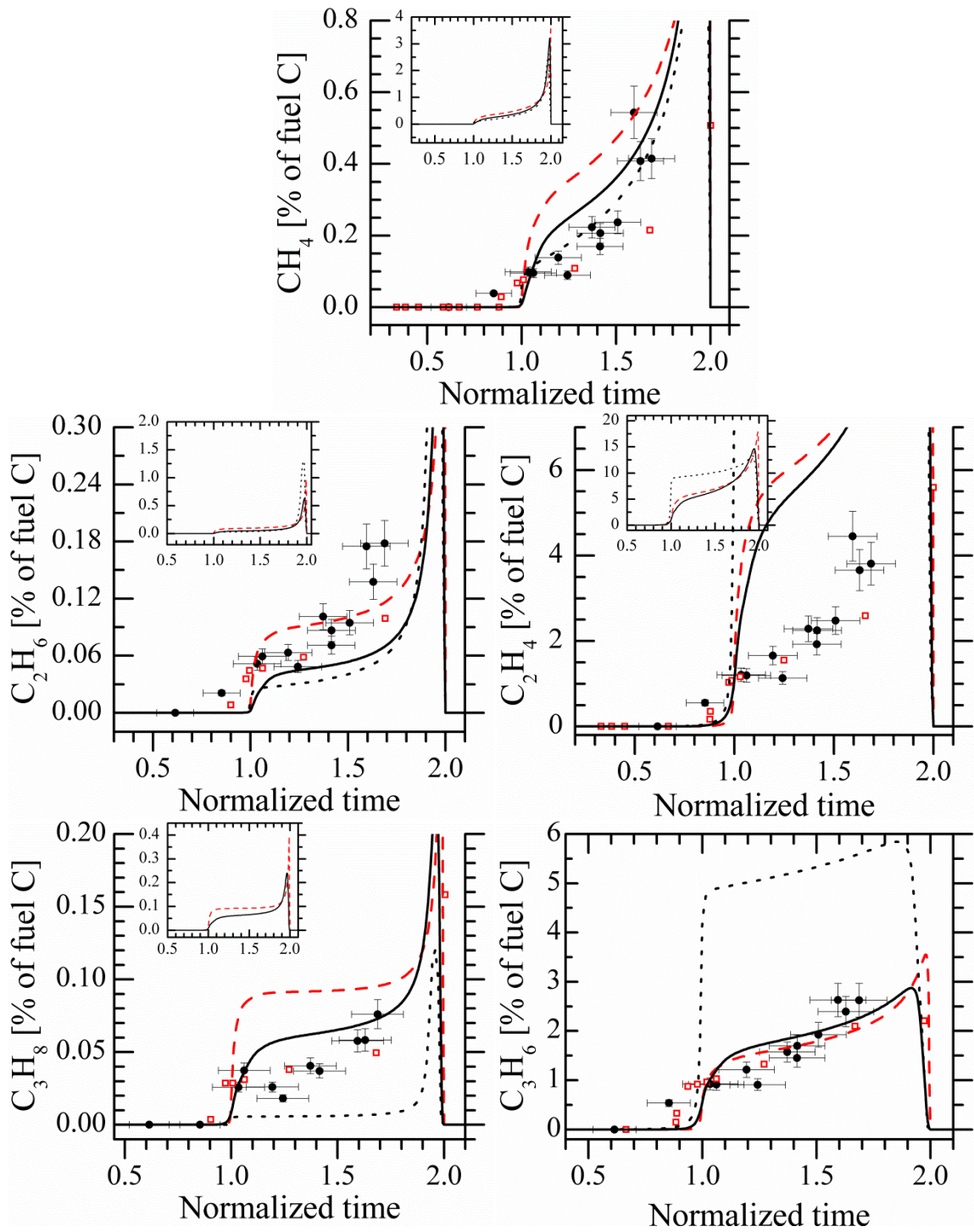


Figure 2.9 An example of gas chromatography signals output by the three gas chromatographs. These particular signals are for the experiment depicted in Figure 2.6.

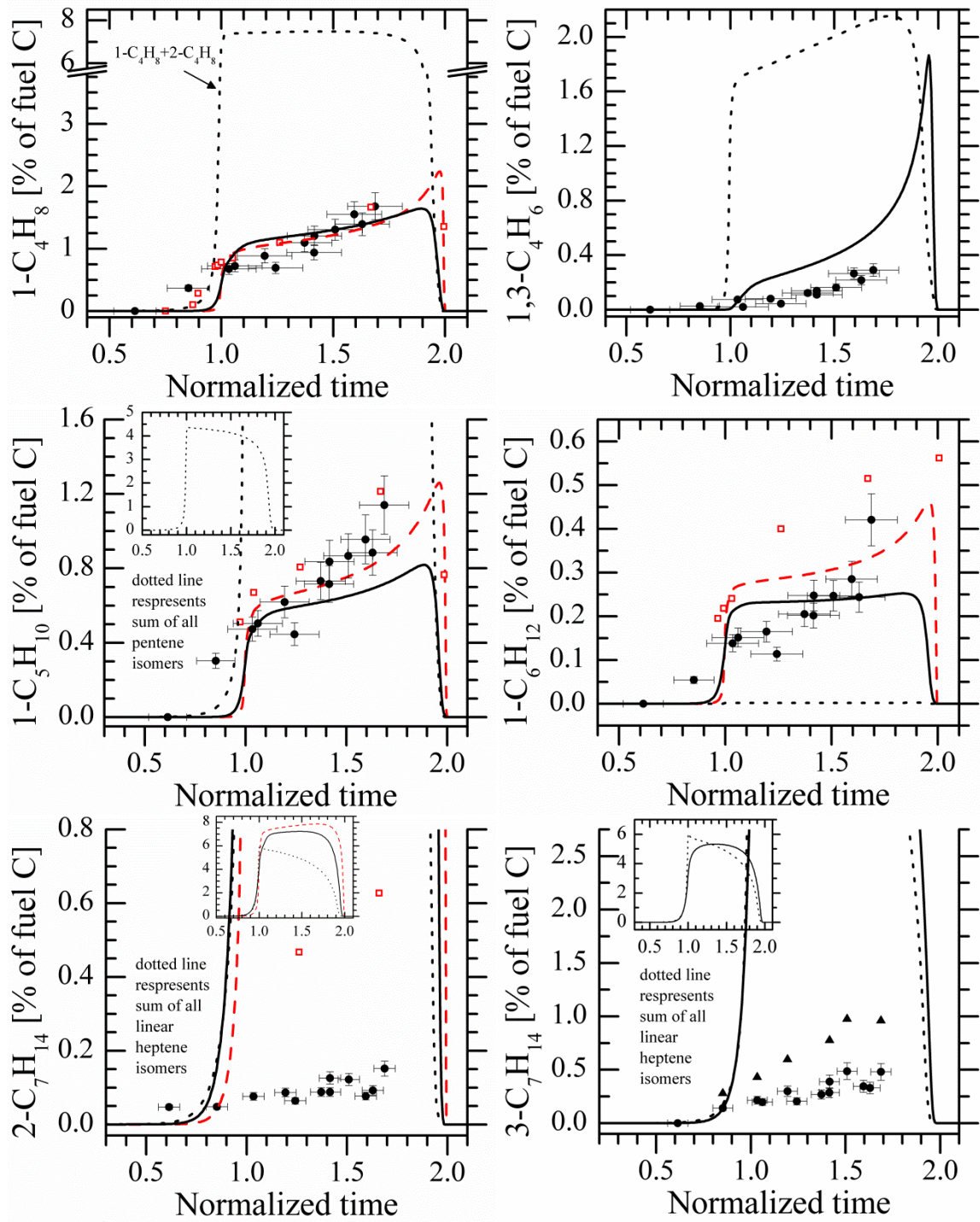
Figure 2.10 a-q (in reading order) presents the species measurements (in filled black circles) during the ignition delay time of  $n-C_7H_{16}$  for the average experimental conditions of  $P_{\text{eff}} = 9.02$  atm,  $T_{\text{eff}} = 701$  K,  $\chi(n-C_7H_{16}) = 0.0134$ ,  $\chi(O_2) = 0.1490$ ,  $\chi(N_2) = 0.2336$ , and  $\chi(CO_2) = 0.6040$ , resulting in  $\tau_1 = 7.94$  ms and  $\tau_{\text{ign}} = 14.09$  ms with standard deviations of 0.52 ms and 0.63 ms, respectively. The uncertainties are

represented by error bars in Figure 2.10. The  $\pm 0.75$  ms uncertainty in the sampling times, when normalized by the average  $\tau_{\text{ign}}$ , corresponds to approximately  $\pm 0.053$ . The uncertainty in species calibrations (varying for each species) and the uncertainty due to pressure measurements in the sampling volume ( $\pm 10\%$ ) were considered as independent sources of uncertainty on the species concentrations, and were therefore combined by using the square root of the sum of the squares. Plotted with solid black lines are the constant volume, adiabatic mechanism predictions of species concentration time-histories for the average experimental conditions mentioned above. At these conditions, the mechanism predicts  $\tau_1 = 7.35$  ms and  $\tau_{\text{ign}} = 16.05$  ms. The dotted black lines represent constant volume, adiabatic PdM mechanism<sup>23</sup> predictions of species concentration time-histories. For an initial pressure of 9.02 atm and initial temperature of 701 K, the mechanism predicts  $\tau_1 = 8.55$  ms and  $\tau_{\text{ign}} = 12.25$  ms





(caption at end of figure)



(caption on next page)



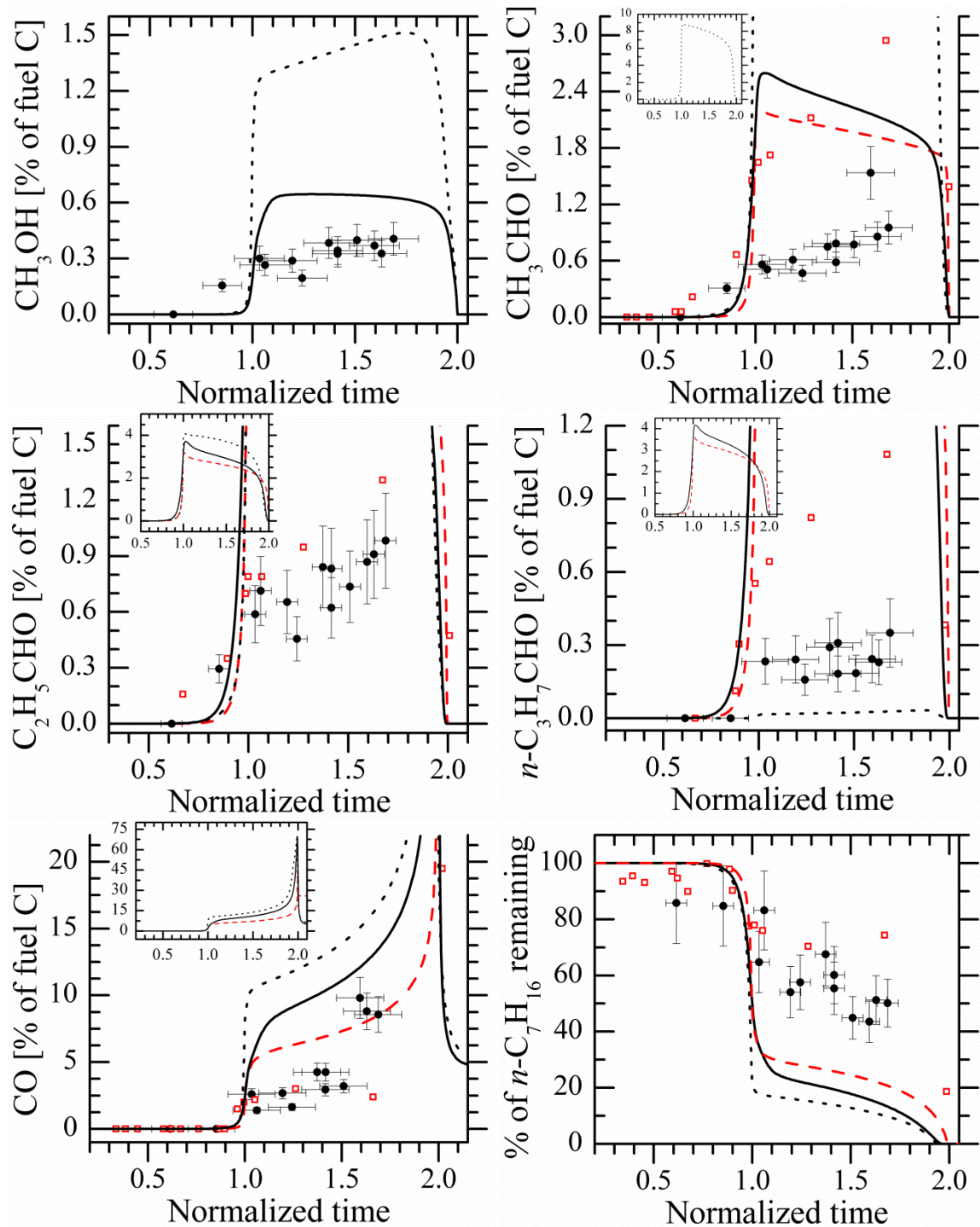


Figure 2.10 Species concentration time-histories for UM RCF sampling experiments (filled black circles), along with Minetti *et al.*<sup>12</sup> data (open red squares), and current mechanism predictions corresponding to these two sets of experimental data, with the black solid line corresponding to predictions of UM RCF data and the red dashed line to predictions of the Minetti *et al.*<sup>12</sup> data. Also shown with dotted black lines are PdM mechanism<sup>23</sup> predictions for the UM RCF data.

Seen also in these figures are measurements of species time-histories (open red squares) reported by Minetti *et al.*<sup>12</sup> in their ignition and speciation study. Their experiments were conducted at an end of compression pressure and temperature of 3.4 bar and 667 K, for a stoichiometric mixture of *n*-C<sub>7</sub>H<sub>16</sub> and O<sub>2</sub>, and a dilution of 3.76, resulting in an average  $\tau_{ign}$  of 41 ms, with the  $\tau_1$  around 30 ms. The red dashed lines represent the current mechanism predictions— $\tau_1 = 16.7$  ms and  $\tau_{ign} = 28.5$  ms—for the experimental conditions of Minetti *et al.*<sup>12</sup>

The current mechanism predicts many species very accurately. (While concentrations were experimentally measured to be non-zero right before and right after the first stage of ignition for many species, the abruptness of the rise in concentrations was not captured experimentally. As mentioned previously, this is likely due to the averaging of the concentration measurements over the finite amount of time over which the sampling valves open and shut.) In particular, alkanes for both the UM RCF and Minetti *et al.*<sup>12</sup> data are well represented, as are alkenes such as C<sub>3</sub>H<sub>6</sub>, 1-C<sub>4</sub>H<sub>8</sub>, 1-C<sub>5</sub>H<sub>10</sub> and 1-C<sub>6</sub>H<sub>12</sub>. However, the current mechanism overpredicts key species such as C<sub>2</sub>H<sub>4</sub> (by a factor of two) and the larger aldehydes C<sub>2</sub>H<sub>5</sub>CHO (by a factor of four) and *n*-C<sub>3</sub>H<sub>7</sub>CHO (by an order of magnitude). Smaller oxygenates such as CH<sub>3</sub>OH and CH<sub>3</sub>CHO are captured well by the current mechanism. CO was predicted within a factor of two to three of the experimentally measured values. The two heptene isomers we were able to quantify were measured in much smaller quantities than predicted. 2-C<sub>7</sub>H<sub>14</sub> was measured in very small amounts, and 3-C<sub>7</sub>H<sub>14</sub> was overpredicted by a factor of 3. (Given that the 3-C<sub>7</sub>H<sub>14</sub> calibration standard was an uncertain mixture of *cis*-3-C<sub>7</sub>H<sub>14</sub> and *trans*-3-C<sub>7</sub>H<sub>14</sub> and that the measured areas of these two isomers were approximately equal in the chromatograms, 3-C<sub>7</sub>H<sub>14</sub> was quantified within a factor of two. The solid triangles in Figure 2.10k represent this upper bound.) The overprediction of the heptenes suggests that the current mechanism does not accurately represent the branching fractions from *n*-C<sub>7</sub>H<sub>16</sub>. That being said, the current mechanism overpredicts the amount of *n*-C<sub>7</sub>H<sub>16</sub> consumed at the first stage of ignition even though it accurately predicts  $\tau_1$  and  $\tau_{ign}$ ; while we measured approximately 30-40% consumption of *n*-C<sub>7</sub>H<sub>16</sub> at the first stage, the mechanism predicts approximately 80% consumption. The PdM mechanism<sup>23</sup> also makes a similar overprediction.

Apart from 1,3-C<sub>4</sub>H<sub>6</sub>, the PdM mechanism<sup>23</sup> predicts similar trends for the species time-histories as does the current mechanism. Also, most of the concentrations predicted by the PdM mechanism<sup>23</sup> are on the same order of magnitude as the current mechanism—only CH<sub>3</sub>CHO, 1-C<sub>5</sub>H<sub>10</sub> are overpredicted by a factor of three compared to the current mechanism, and C<sub>3</sub>H<sub>8</sub>, 1-C<sub>6</sub>H<sub>12</sub>, and *n*-C<sub>3</sub>H<sub>7</sub>CHO are significantly underrepresented in the PdM mechanism.<sup>23</sup>

While the sampling experiments conducted by Minetti *et al.*<sup>12</sup> were at a pressure of 3.4 bar, they were conducted at a similar temperature to the UM RCF experiments, and the species measurements are very similar to those from the current work, particularly when accounting for the differences in dilution for the two data sets—dilution for the UM RCF experiments was 5.64, versus 3.76 for the Minetti *et al.*<sup>12</sup> experiments. As can be seen from the *n*-C<sub>7</sub>H<sub>16</sub> consumption in the Minetti *et al.*<sup>12</sup> work in Figure 2.10q, the first stage of ignition consumes 20-25% of the initial amount of *n*-C<sub>7</sub>H<sub>16</sub>. The current mechanism, however, predicts approximately 80% consumption at the first stage of ignition for the Minetti *et al.*<sup>12</sup> experimental conditions, almost identical to the predictions for the current work. Minetti *et al.*<sup>12</sup>, in 1995, had compared their experimental results with a reduced mechanism published by Westbrook, Warnatz and Pitz,<sup>42</sup> which also predicted approximately 80% consumption at the first stage.

The kinetics of large olefins have only recently been added to chemical kinetic mechanisms, and the major reaction pathways and their reaction rates are still relatively untested. Since the current mechanism and the PdM mechanism<sup>23</sup> show more fuel consumption and higher intermediate heptene production than observed in the experimental speciation measurements, the consumption of heptenes should be faster than the mechanisms currently prediction. The heat release associated with heptene conversion would also lead to a more rapid end to the low-temperature reactions.

The quenching of reactions that occurs when gases from the test section are sampled can lead radicals such as O, H, OH, and CH<sub>3</sub> to recombine to form water vapor and small hydrocarbons, which may interfere with concentration measurements of stable species. However, predicted radical concentrations, seen in Figure 2.11, are very low (< 40 ppm) until very close to autoignition. Radicals are

thus not expected to be a source of error in the species concentration measurements presented in this work.

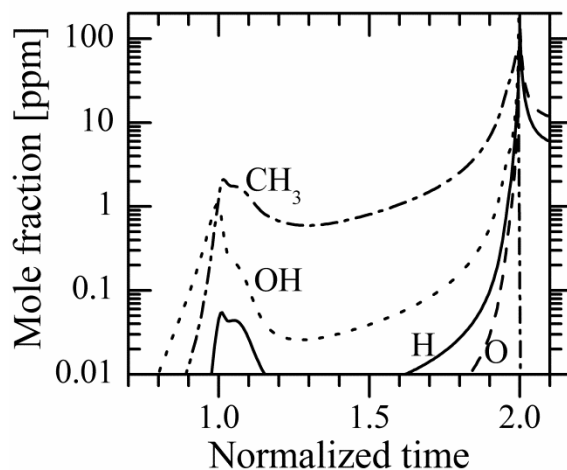


Figure 2.11 Predictions of radical concentrations at the first and second stage of ignition.

## Conclusions

This chapter presents a detailed investigation of low-temperature chemical kinetics of a key reference *n*-alkane, *n*-heptane ( $n\text{-C}_7\text{H}_{16}$ ). Ignition data collected at approximately 9 atm over the temperature range 660-710 K using the University of Michigan Rapid Compression Facility agree with the trends of previous  $n\text{-C}_7\text{H}_{16}$  ignition data obtained using shock tubes and rapid compression machines. The mechanism developed in this work predicts higher heat release and fuel consumption at the first stage of ignition than measured experimentally at the speciation conditions of 9 atm and 700 K.

While  $n\text{-C}_7\text{H}_{16}$  ignition studies have given an understanding of the influences of temperature and pressure on ignition delay times, very few experimental studies have interrogated the validity of reaction pathways represented in chemical kinetic mechanisms. The speciation work presented thus provides important insights into concentrations of various intermediates formed during the ignition delay of  $n\text{-C}_7\text{H}_{16}$ . Speciation data from the current work obtained at a pressure of 9 atm and a temperature of 700 K show very good agreement when compared against previous speciation work done by Minetti *et al.*<sup>12</sup> obtained at a pressure of 3.4 bar and a temperature of 667 K. The current mechanism predicts much higher consumption of

$n\text{-C}_7\text{H}_{16}$  at the first stage of ignition for both the current work as well as the Minetti *et al.*<sup>12</sup> data. A mechanism developed at the PdM,<sup>23</sup> while predicting ignition delay times in agreement with the current work, predicts the same amount of  $n\text{-C}_7\text{H}_{16}$  consumption at the first stage of ignition as the current mechanism does. Future experimental and modeling studies should focus on the combustion of large olefins formed during the consumption of  $n\text{-C}_7\text{H}_{16}$ .

Table 2.1 Summary of experimental conditions and results. The top panel provides a summary of sampling experiments, depicted in Figure 2.3 with green triangles, and the bottom panel provides a summary of ignition experiments, depicted in Figure 2.3 as magenta pentagons.

$P_{\text{eff}}$ (atm)	$T_{\text{eff}}$ (K)	$1000/T_{\text{eff}}$ (1/K)	$I/O_2$	$\chi(n\text{-C}_7\text{H}_{16})$	$\chi(O_2)$	$\chi(N_2)$	$\chi(CO_2)$	$\tau_1$ (ms)	$\tau_{\text{ign}}$ (ms)	sample time (ms)	normalized sampling time
9.01	700	1.43	5.62	0.01345	0.149	0.2302	0.6073	8.49	14.53	12.08	1.59
9.11	703	1.42	5.62	0.01343	0.149	0.233	0.6044	7.97	14.21	10.56	1.42
9.04	702	1.42	5.62	0.01342	0.149	0.2336	0.6039	7.13	13.12	4.38	0.61
9.08	703	1.42	5.62	0.01343	0.149	0.2337	0.6038	8.06	14.05	9.22	1.19
8.98	700	1.43	5.62	0.01343	0.149	0.2334	0.604	8.34	14.33	12.11	1.63
8.96	701	1.43	5.62	0.01342	0.149	0.2335	0.6039	7.64	13.86	8.02	1.06
9.09	704	1.42	5.62	0.01345	0.149	0.233	0.6043	7.67	13.82	6.54	0.85
8.92	699	1.43	5.62	0.01344	0.149	0.2334	0.604	8.87	15	9.08	1.03
9.14	704	1.42	5.62	0.01343	0.149	0.2339	0.6034	8.06	13.59	10.12	1.37
8.97	699	1.43	5.62	0.01344	0.149	0.2333	0.6041	8.47	14.73	9.99	1.24
9.03	701	1.43	5.62	0.01342	0.149	0.2337	0.6039	7.57	13.94	11.95	1.69
9.09	702	1.42	5.60	0.01341	0.1494	0.2345	0.6026	7.34	13.43	10.44	1.51
9.03	701	1.43	5.61	0.01344	0.1492	0.2335	0.6037	7.4	13.14	9.13	1.42
$P_{\text{eff}}$ (atm)	$T_{\text{eff}}$ (K)	$1000/T_{\text{eff}}$ (1/K)	$I/O_2$	$\chi(n\text{-C}_7\text{H}_{16})$	$\chi(O_2)$	$\chi(N_2)$	$\chi(CO_2)$	$\tau_1$ (ms)	$\tau_{\text{ign}}$ (ms)		
9.33	707	1.41	5.63	0.0134	0.1489	0.2211	0.6165	7.13	12.72		
9.53	660	1.51	5.63	0.013444	0.1489	0	0.8388	21.92	30.06		
9.44	686	1.46	5.62	0.013433	0.1491	0.1337	0.7037	11.65	18.32		

## Chapter 3

# Ignition and speciation studies of the chemical kinetics of *n*-butanol

*This chapter was published as Karwat, D. M. A; Wagnon S. W.; Teini, P. D.; Wooldridge, M. S. "On the chemical kinetics of n-butanol: ignition and speciation studies", Journal of Physical Chemistry A, 2011, 115, 4909-21*

### Introduction

Bio-ethanol is at present the most widely produced biofuel and is used both as an additive to petrol/gasoline and as a fuel in its own right in specially-modified vehicles. There are significant concerns, ethical and environmental, about ethanol production from food stocks. Interest in butanol has therefore increased, due to the variety of potential feed stock sources. Butanol has a higher lower heating value than ethanol and reduced miscibility in water as compared to ethanol.<sup>43</sup> Consequently, butanol is more attractive for application to aviation, transport and storage as compared to ethanol, although toxic pollutants such as aldehydes and ketones, which are harmful to health, are formed as combustion byproducts from both ethanol and butanol.<sup>44</sup>

There has been much recent work studying the combustion chemistry of butanol (all four isomers), including studies of flame characteristics and propagation,<sup>45–48</sup> ignition,<sup>49–53</sup> decomposition,<sup>54</sup> pyrolysis<sup>55,56</sup> and elementary reaction rates.<sup>57,58</sup> Most work has been performed in the high temperature regime ( $T > 900$  K); however, an early pyrolysis study investigated *n*-butanol (*n*-C<sub>4</sub>H<sub>9</sub>OH) pyrolysis at low temperatures ( $T < 800$  K).<sup>56</sup> Recent decomposition studies have further investigated the effects of adding *n*-C<sub>4</sub>H<sub>9</sub>OH to well-studied *n*-alkanes.<sup>59,60</sup>

McEnally and Pfefferle<sup>45</sup> compared the kinetics of the four isomers of butanol in co-flowing methane/air flames. The authors state that although oxygenates are

regarded as clean-burning fuels, the alkenes formed from the butanols can participate in hydrocarbon growth processes that lead to aromatics and soot, and during their experiments they observed the butanol-doped flames to be much more luminous than the undoped methane flame. Further, the branched isomers of butanol produced more soot precursors and benzene than did the linear isomers. They concluded that the branched nature of the fuels play a more important role in soot formation than the presence or absence of oxygen bound in the fuel.

Several reaction mechanisms have also been developed in conjunction with these experimental studies. To date, ignition studies of butanol isomers have been studied predominantly in high and low pressure shock tubes. Heufer *et al.*<sup>52</sup> measured ignition delay times in the range of 10–42 atm and 770–1250 K using stoichiometric fuel/oxidizer/diluent mixtures. Moss *et al.*<sup>49</sup> conducted an experimental and kinetic modeling study of the oxidation of the four isomers of butanol for  $\phi = 0.25, 0.5, \text{ and } 1$ , at temperatures between 1196 K and 1823 K and pressures near one atm, with varying dilution levels. The chemical kinetic mechanism developed did not include low-temperature alkylperoxy chemical pathways. They found that *n*-C<sub>4</sub>H<sub>9</sub>OH is the most reactive isomer, followed by *iso*-butanol, 2-butanol, and finally *tert*-butanol. Black *et al.*<sup>50</sup> conducted a similar study, in which *n*-C<sub>4</sub>H<sub>9</sub>OH ignition experiments were performed at  $\phi = 0.5, 1 \text{ and } 2$ , with pressures between 1 atm and 8 atm, over a range of temperatures from 1100 to 1800 K. Most of the data were obtained at a dilution level of ~95% (argon), with one series at a dilution of 77%. The authors also developed a chemical kinetic mechanism for *n*-C<sub>4</sub>H<sub>9</sub>OH, based on *n*-butane chemistry<sup>61</sup> for a wide temperature (740-1660 K) and pressure range (1-34 atm). Included were simple  $\beta$ -scission reactions, as well as complex scission, in particular the four-centered elimination of water to form 1-butene:



Reaction path analysis carried out for  $\phi = 1$ ,  $T = 1450$  K, showed H-atom abstraction to be the principal route of consumption of *n*-C<sub>4</sub>H<sub>9</sub>OH, in accordance with previous modeling results.<sup>62</sup> Abstraction from the  $\alpha$  position dominates, followed by the  $\beta$ ,  $\gamma$  and  $\delta$  positions, while abstraction from the hydroxyl group is of



lesser importance. At high temperatures, sensitivity analysis for  $\phi = 2$  showed that small radical reactions (such as  $\text{H}+\text{O}_2$ ) have the greatest influence on ignition delay time. The most sensitive fuel reaction is scission of the  $\text{C}_\alpha\text{-C}_\beta$  bond, which increases the overall reactivity of the system. While these works have led to major developments in the detailed reaction mechanisms for  $n\text{-C}_4\text{H}_9\text{OH}$  combustion, the effects of lower temperatures on  $n\text{-C}_4\text{H}_9\text{OH}$  reactivity are much less well known.

Understanding  $n\text{-C}_4\text{H}_9\text{OH}$  combustion chemistry is vital to the successful development of renewable fuel strategies. Experiments which provide quantitative data on the reactivity and key reaction pathways of  $n\text{-C}_4\text{H}_9\text{OH}$  are important for understanding the fundamental chemistry of this oxygenated fuel. Measurements of intermediate species concentrations during the ignition delay time provide experimental evidence of reaction pathways of fuel consumption and pollutant formation. However, quantifying these intermediates is difficult, due to the sampling and analytical methods required. To our knowledge, only two speciation studies of  $n\text{-C}_4\text{H}_9\text{OH}$  oxidation and ignition exist in the literature. Sarathy *et al.*<sup>54</sup> studied  $n\text{-C}_4\text{H}_9\text{OH}$  decomposition and combustion through experimental studies in a jet-stirred reactor at a mean residence time of 0.07 s, a constant pressure of one atmosphere, and over a temperature range of 800-1300 K. Their studies included measurements of the parent fuel, methane, ethane, ethene, acetylene, propene, formaldehyde, acetaldehyde,  $n$ -butyraldehyde, 1-butene, carbon dioxide and carbon monoxide as a function of different reactor temperatures. They found, at  $T = 1160$  K and  $\phi = 1$ , the leading consumption pathways of  $n\text{-C}_4\text{H}_9\text{OH}$  to be complex fission resulting in the formation of 1-butene and  $\text{H}_2\text{O}$  (25%), and H-atom abstraction (60%), with H atoms (29%) and OH (57%) radicals being the main contributors to H-atom abstraction.

Oßwald *et al.*<sup>47</sup> studied fuel-rich ( $\phi = 1.7$ ), low-pressure flames of the four isomers of butanol using molecular beam mass spectrometry. The authors were able to identify fifty-seven chemical species, including radical and isomeric species, at various heights above their porous plug burners using a combination of electron ionization and photoionization mass spectrometry. The authors were able to characterize pollutant emissions and soot precursors from the flames of the four isomers, with fuel structure significantly influencing the concentrations of these

products; high concentrations of formaldehyde and acetaldehyde were detected in *n*-C<sub>4</sub>H<sub>9</sub>OH flames, and while *tert*-butanol flames produced low concentrations of oxygenated intermediates, they did produce higher concentrations of propargyl and benzene, both of which are soot precursors.

The objective of this chapter is to provide new insights into low-temperature combustion chemistry of *n*-C<sub>4</sub>H<sub>9</sub>OH through ignition and speciation studies. The experimental measurements of *n*-C<sub>4</sub>H<sub>9</sub>OH ignition delay times and intermediate species measurements are targeted to provide new data and metrics that extend our quantitative understanding of *n*-C<sub>4</sub>H<sub>9</sub>OH combustion chemistry at conditions relevant to modern jet and internal combustion engines.

## Experimental Setup

### *The University of Michigan Rapid Compression Facility*

The same experimental setup as described in Chapter 3 was used for these studies.

For this study, mixtures were prepared external to the UM RCF to ensure good reactant mixing and uniform composition for each experiment. Stoichiometric *n*-C<sub>4</sub>H<sub>9</sub>OH/O<sub>2</sub> (*n*-C<sub>4</sub>H<sub>9</sub>OH—Sigma-Aldrich, purum, >99% GC grade; O<sub>2</sub>—Cryogenic Gases, Purity Plus 4.3, 99.993%, <40 ppm Ar, <3 ppm moisture, <10 ppm N<sub>2</sub>, <0.5 ppm hydrocarbons) mixtures, with an inert/O<sub>2</sub> ratio of 5.64, were prepared manometrically using a mixing manifold and mixing tank that are connected to the UM RCF. Mixture compositions were determined using partial pressures measured with a capacitance diaphragm gauge (Varian CeramiCel VCMT12TFA, with an accuracy of ±0.01 torr). All mixtures were allowed to mix diffusively for over 12 hours. The partial pressure of *n*-C<sub>4</sub>H<sub>9</sub>OH used in the mixtures was maintained at less than half the saturation vapor pressure of *n*-C<sub>4</sub>H<sub>9</sub>OH at room temperature (8.81×10<sup>-3</sup> atm or 6.69 torr at 25°C) in order to avoid concerns of fuel condensation. The concentration of inert gases in the mixture – Ar (Cryogenic Gases, Purity Plus 5.0, 99.999%, <2 ppm O<sub>2</sub>, <2 ppm moisture, <0.5 ppm hydrocarbons) and N<sub>2</sub> (Cryogenic Gases, Purity Plus 5.0, 99.999%, <2 ppm O<sub>2</sub>, <3 ppm moisture, <0.5 ppm hydrocarbons) – was varied to control the ratio of specific heats of the reactant mixture and thereby the EOC state conditions. Total mixture pressures in the

mixing tank were 0.11-0.13 atm, and each mixture was typically used for two ignition experiments with initial fill pressures ( $P_0$ ) in the RCF of  $P_0 = 3.2 \times 10^{-2}$ - $3.7 \times 10^{-2}$  atm.

The test section is instrumented with several diagnostics to interrogate the test gas mixture during ignition studies. The pressure in the test section is monitored using a piezoelectric transducer (Kistler 6041AX4) and charge amplifier (Kistler 5010B) with a combined accuracy of 0.01 atm and 0.015 ms. All electronic signals are acquired using a data acquisition system (National Instruments (NI) cDAQ 9172 chassis coupled with NI 9215 cards) recording at 100 kHz. High-speed imaging of the combustion phenomena in the test section can be obtained either by viewing along the axis of the test section (end-view) using a transparent end wall, or orthogonal to the axis of the test section (side-view) using a transparent cylindrical section. For this study, a high-speed CMOS camera (Vision Research, Phantom v7.1, SR-CMOS 48-bit color array, maximum resolution of  $800 \times 600$  pixels, capable of 160 kHz at reduced spatial resolution,  $22 \mu\text{m}$  pixels with  $0.34 \mu\text{m}$  spacing) was used to record end-view images during ignition. Side-view imaging was not used. The chemiluminescence from the test volume was captured with a fast 50 mm lens ( $f/0.95$ , Navitar) and c-mount extension tube. For these experiments, a setting of 26,000 frames per second (fps) with an image exposure time of  $38 \mu\text{s}$  and a spatial resolution of  $256 \times 256$  pixels was used. The imaging data provide qualitative and quantitative indications of the ignition homogeneity. The camera array records color signals using red ( $\sim 95\%$  transmission above 615 nm), blue ( $\sim 86\%$  peak transmission at 460 nm) and green ( $\sim 82\%$  peak transmission at 530 nm) spectral filters. No additional spectral filtering was used.

### ***High-speed gas sampling and gas chromatography***

The experimental setup for the gas sampling experiments was the same as described in Chapter 2. However, instead of acquiring one sample per experiment, two samples were acquired by triggering the valves in the northeast and southwest corners of the sampling endwall. Experiments were also performed in which the two sampling valves were triggered at the same time such that the two gas samples had the same time-history, but were obtained from two different locations in the test

section. The samples yielded nearly identical concentrations (less than 4% difference) for the species measured.

As alluded to in Chapter 2, a primary source of uncertainty in the gas-sampling measurements is the dilution of the gas samples with unreacted gases present in dead volume of the gas sampling system. Specifically, the cold unreacted gases (essentially unreacted test gas mixture) initially present in the sampling probes are also acquired in the sampling chamber when the sampling valves are opened. The unreacted test gases dilute the concentration of the gases taken from the hot core region of the test section, and the reactant mixture can cause interference in the chromatograms. In order to quantify these effects, pyrolysis experiments were performed using EOC conditions that would consume all of the fuel in the reactive core before the gas samples were acquired. Any measured fuel would then be from the dead volume, and quantifying the fuel yields an accurate estimate of the dilution of the gases sampled from the core of the test section. For this work, pyrolysis experiments using *n*-C<sub>4</sub>H<sub>9</sub>OH were used and compared to results obtained from previous characterization work for pyrolysis of C<sub>2</sub> hydrocarbons on the UM RCF.<sup>29</sup> Model predictions show that less than 0.3% of *n*-C<sub>4</sub>H<sub>9</sub>OH would remain in the core region of the test section at 11.2 ms after EOC conditions of  $T = 1400$  K and  $P = 3.25$  atm. The *n*-C<sub>4</sub>H<sub>9</sub>OH and C<sub>2</sub> pyrolysis experiments show that the dilution ranges between 5-16%, depending on the temperature conditions in the test section. The data for this study were analyzed using 16% dilution by the unreacted test gas mixture.

The gas chromatograph (GC) was calibrated for quantitative measurements of the species of interest, namely *n*-C<sub>4</sub>H<sub>9</sub>OH, methane (CH<sub>4</sub>), carbon monoxide (CO), ethene (C<sub>2</sub>H<sub>4</sub>), propene (C<sub>3</sub>H<sub>6</sub>), acetaldehyde (CH<sub>3</sub>CHO), 1-butene (1-C<sub>4</sub>H<sub>8</sub>), and *n*-butyraldehyde (*n*-C<sub>3</sub>H<sub>7</sub>CHO). The GC system (PerkinElmer Autosystem) was equipped with a flame ionization detector (FID, air/hydrogen flame) and a thermal conductivity detector (TCD). A Restek RTX-1 capillary column was used to measure both pure hydrocarbons as well as oxygenated hydrocarbons (using the FID detector), and a Restek ShinCarbon ST packed column was used to measure CO (using the TCD detector). The columns were maintained in the GC oven at 50°C with ultra-high purity helium (Cryogenic Gases, Purity Plus, 99.999%) as the carrier gas. The helium, air, and hydrogen were further purified before use in the GC using

adsorbents to remove water, hydrocarbons, and oxygen. The FID detector was maintained at 300°C, with an attenuation of 1 and a range of 1. The TCD detector was maintained at 50°C with an attenuation of 1 and a current of +160 mA. Splitless injection was used to introduce the analytes into the columns. High-purity reference chemicals were characterized for the GC temperature programs used in the study, and the chromatograms were used to establish the calibrations for absolute concentration. Calibration gases were used for CH<sub>4</sub> (Cryogenic Gases, chemically pure, 99%), CO (Matheson, ultra-high purity, 99.9%), C<sub>2</sub>H<sub>4</sub> (Matheson, chemically pure, 99.5%), C<sub>3</sub>H<sub>6</sub> (Cryogenic Gases, polymer grade, 99.5%), and 1-C<sub>4</sub>H<sub>8</sub> (Cryogenic Gases, 99%). CH<sub>3</sub>CHO was calibrated using the vapor of liquid CH<sub>3</sub>CHO (Fluka, puriss. p.a., anhydrous, >99.5% GC grade, ≤0.5% free acid CH<sub>3</sub>COOH) and *n*-C<sub>3</sub>H<sub>7</sub>CHO was calibrated using the vapor of liquid *n*-C<sub>3</sub>H<sub>7</sub>CHO (Fluka, puriss., ≥99% GC grade, ≤1% butyric acid, <0.1% BHT as a stabilizer, <1% H<sub>2</sub>O as a stabilizer). Calibration mixtures were made in a mixing tank with the upper limit of concentrations calibrated for being greater than the maximum concentrations predicted by the Black *et al.*<sup>50</sup> mechanism for the ignition delay of a mixture with  $\chi(n\text{-but}) = 0.025$ ,  $\chi(\text{O}_2) = 0.147$ ,  $\chi(\text{N}_2) = 0.541$ ,  $\chi(\text{Ar}) = 0.288$  at  $P = 3.25$  atm and  $T = 975$  K. Calibration curves were linear in all cases. Measurements of *n*-C<sub>4</sub>H<sub>9</sub>OH were of interest for this work, and *n*-C<sub>4</sub>H<sub>9</sub>OH was well isolated in the chromatograms. However, calibration experiments showed the *n*-C<sub>4</sub>H<sub>9</sub>OH (Sigma-Aldrich, purum, >99% GC grade, <0.1% H<sub>2</sub>O) features were a non-linear function of the GC-FID detector, and the *n*-C<sub>4</sub>H<sub>9</sub>OH saturated the FID detector for mole fractions of 0.5% and higher. Consequently, potential *n*-C<sub>4</sub>H<sub>9</sub>OH measurements were limited to levels below 0.5% for this study. Signals from the GC detectors were recorded using a high-resolution data acquisition system (NI PXI 4472) with a sampling rate of 8 Hz. A temperature-controlled 10-port valve was used to direct the samples into the GC.

## Experimental Results and Discussion

### *Ignition experiments*

Figure 3.1 presents typical results from a UM RCF *n*-C<sub>4</sub>H<sub>9</sub>OH ignition experiment. The time-histories of the pressure ( $P$ ) and rate of pressure rise ( $dP/dt$ )

in the test section are shown in the lower panel. High-frequency ( $>2.5$  kHz) disturbances generated by the impact of the sabot near the EOC are filtered from the pressure time-histories using a fast Fourier transform. The pressure data show the compression process is smooth with no indications of disturbances or abrupt fluctuations. The pressure reaches the first maximum due to compression by the sabot, and the EOC is set to time  $t = 0$ , after which the volume in the test section is constant. After a period of time where the pressure remains nearly constant, the pressure increases rapidly to a second maximum due to ignition of the fuel/oxidizer/diluent mixture.

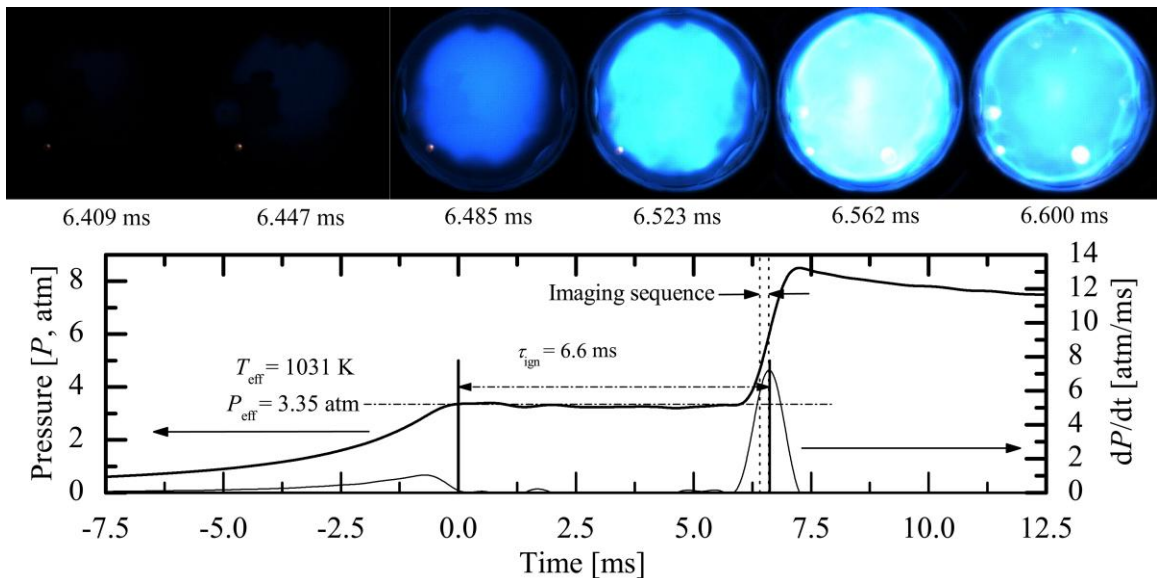


Figure 3.1 Results for a typical  $n$ -C<sub>4</sub>H<sub>9</sub>OH ignition experiment with  $P_{\text{eff}} = 3.35$  atm,  $T_{\text{eff}} = 1031$  K,  $\phi = 1$ , inert/O<sub>2</sub> = 5.64 and  $\tau_{\text{ign}} = 6.6$  ms. The lower panel shows the pressure ( $P$ ) and the rate of pressure rise ( $dP/dt$ ) in the test section. End of compression is set as time  $t = 0$  ms. The upper panel shows the corresponding still images (end view), acquired at 26,000 fps, of the chemiluminescence during ignition (no color adjustment).

The upper panel of Figure 3.1 shows stills from the image sequence of the chemiluminescence emitted during ignition. The chemiluminescence is only observed during the high rates of pressure rise that occur during ignition. The emission is attributed to CH and C<sub>2</sub> radicals due to the strong spectroscopic features of these species in the blue (CH: 431.2 nm; C<sub>2</sub>: 473.7 nm, 516.5 nm, 563.5 nm), and because CH and C<sub>2</sub> are generated through the decomposition of intermediate hydrocarbons present in the fuel/oxidizer/diluent mixture. Note the intense blue

emission occurs throughout the test section with uniform intensity, indicating good homogeneity of the reactant mixture and of thermal conditions in the test section.

For each experiment, the effective test conditions are determined using the same methods as in previous UM RCF experiments<sup>28</sup> and are based on the pressure time-history from each experiment. The effective pressure ( $P_{\text{eff}}$ ) is defined by Equation 3.1 as the time-integrated average pressure from the maximum pressure ( $P_{\text{max}}$ ) at EOC to the maximum of rate of pressure rise ( $dP/dt_{\text{max}}$ ),

$$P_{\text{eff}} = \frac{1}{t_{dP/dt_{\text{max}}} - t_{P_{\text{max}}}} \int_{t_{P_{\text{max}}}}^{t_{dP/dt_{\text{max}}}} P \cdot dt . \quad (3.1)$$

The effective temperature for each experiment is determined using  $P_{\text{eff}}$  and numerical integration of the isentropic relation (Equation 3.2),

$$\int_{T_0}^{T_{\text{eff}}} \frac{\gamma}{\gamma-1} d \ln T = \ln \left( \frac{P_{\text{eff}}}{P_0} \right) , \quad (3.2)$$

where  $P_0$  is the initial charge pressure,  $T_0$  is the initial temperature, and  $\gamma$  is the temperature-dependent ratio of the specific heats of the unreacted test gas mixture (determined using the NASA thermodynamic data base<sup>41</sup>). The ignition delay time,  $\tau_{\text{ign}}$ , for each experiment is defined as the time between EOC ( $t = 0$  ms, defined by the first maximum in  $P$ ) and  $dP/dt_{\text{max}}$ .

$n$ -C<sub>4</sub>H<sub>9</sub>OH ignition experiments were performed in a narrow pressure range (2.9-3.4 atm) between temperatures of 920 K and 1040 K. The equivalence ratio ( $\phi$ , defined as the ratio of  $[\chi(\text{fuel})/\chi(\text{O}_2)]_{\text{actual}}/[\chi(\text{fuel})/\chi(\text{O}_2)]_{\text{stoichiometric}}$ ) was  $\phi = 1$ , and the dilution (with N<sub>2</sub> and Ar being the sole diluents for all experiments) was inert/O<sub>2</sub> = 5.64 for all experiments. The  $n$ -C<sub>4</sub>H<sub>9</sub>OH concentration for the experiments was 2.4-2.5%. Table 3.1 found at the end of this chapter is a summary of the experimental conditions and results for  $\tau_{\text{ign}}$ , and Figure 3.2 shows  $\tau_{\text{ign}}$  as a function of temperature for  $n$ -C<sub>4</sub>H<sub>9</sub>OH on an Arrhenius diagram. The open symbols are the results of experiments where the transparent end wall was used. The filled symbols are the results of gas-sampling experiments. The ignition data for both sets of experiments follow typical Arrhenius behavior (with no negative temperature coefficient region

expected or observed) and are in excellent quantitative agreement with each other. Hence, as noted earlier, the effects of sampling on the ignition behavior of the test gas mixtures are negligible.

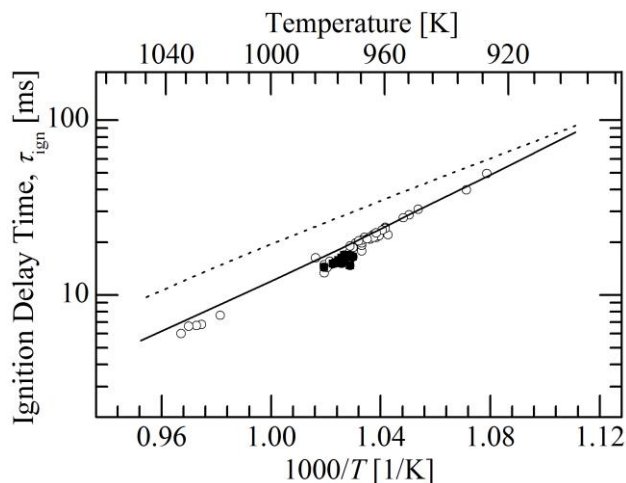


Figure 3.2 Comparison of experimental results for  $n$ -C<sub>4</sub>H<sub>9</sub>OH ignition delay time measured in the current work with model predictions ( $P = 3.25$  atm) based on the reaction mechanisms developed by Black *et al.*<sup>50</sup> (solid line) and Veloo *et al.*<sup>46</sup> (dotted line). All results presented are for  $\phi = 1$ , inert/O<sub>2</sub> = 5.64.  $\circ$ —Current work,  $P = 2.9$ -3.4 atm,  $\blacksquare$ —Current work, gas-sampling experiments,  $P = 3.22$ -3.34 atm.

The uncertainty in the measured  $\tau_{\text{ign}}$  is primarily due to the uncertainty in the effective temperature, which is calculated using the measured pressure and Equation 3.2. The accuracy of the pressure transducer is  $\pm 0.5\%$ . This translates to approximately  $\pm 0.2\%$  variation in  $T_{\text{eff}}$ . The random error in the measured  $\tau_{\text{ign}}$  is estimated using the standard deviation of the data for the temperature range 972-978 K which is 1.3 ms or  $\pm 8\%$ . A conservative estimate for the overall uncertainty for  $\tau_{\text{ign}}$  for the entire temperature range is  $\pm 15\%$ , which is the maximum scatter in the data at any of the temperatures investigated.

The experimental results for  $\tau_{\text{ign}}$  are also compared in Figure 3.2 to model predictions from two recently published  $n$ -C<sub>4</sub>H<sub>9</sub>OH reaction mechanisms. Veloo *et al.*<sup>46</sup> developed a mechanism specifically for atmospheric pressure flames, with 266 species and 1639 reactions. Black *et al.*<sup>50</sup> developed a mechanism based on C<sub>4</sub> chemistry<sup>61</sup> with an  $n$ -C<sub>4</sub>H<sub>9</sub>OH sub-mechanism, for a wide temperature (740-1660 K) and pressure range (1-34 atm). In total, their mechanism consists of 234 species and 1399 reactions. The two reaction mechanisms were used to predict  $\tau_{\text{ign}}$  using the CHEMKIN<sup>TM</sup> suite of programs and assuming a zero dimensional, spatially-



homogeneous, adiabatic constant volume system. For the simulations,  $\tau_{\text{ign}}$  was defined as the time from the start of the simulation to the maximum rate of pressure rise. The input conditions for the model simulations were mixture compositions and the effective temperatures and pressures listed in Table 3.1. As seen in Figure 3.2, *n*-C<sub>4</sub>H<sub>9</sub>OH ignition delay is quite linear on an Arrhenius scale with no negative temperature coefficient region expected or observed. In addition, there is excellent agreement between the results based on the reaction mechanism developed by Black *et al.*<sup>50</sup> and the experimental data. Specifically, the reaction mechanism by Black *et al.*<sup>50</sup> predicts  $\tau_{\text{ign}}$  to within 20% for temperatures higher than approximately 960 K and to within 10% for temperatures below 960 K. The model results using the reaction mechanism by Veloo *et al.*<sup>46</sup> are also in good agreement with the experimental data; well within a factor of two for most temperatures.

A concern for experiments conducted in rapid compression facilities is the possible reaction of the fuel/oxidizer/diluent mixture during compression, which impacts the assumptions used to define the effective temperature and pressure of the experiments, and therefore the input conditions to the CHEMKIN<sup>TM</sup> simulations. Experimentally, such concerns can be investigated by performing non-igniting experiments, where the O<sub>2</sub> is replaced by N<sub>2</sub> in the original fuel/oxidizer/diluent mixture. Such experiments were conducted as part of this study and are presented and discussed with the gas sampling data below. Briefly, the experimental data show negligible deviation in the pressure time history for the non-igniting and the igniting experiments (<1% difference in the effective pressures or pressure time-histories to the time of ignition). To further investigate these concerns, the compression process was simulated. Specifically, CHEMKIN<sup>TM</sup> simulations were performed representing the compression stroke of the UM RCF for the targeted EOC conditions of  $T = 975$  K and  $P = 3.25$  atm using the Black *et al.*<sup>50</sup> reaction mechanism, with initial mole fractions of  $\chi(n\text{-but}) = 0.025$ ,  $\chi(\text{O}_2) = 0.147$ ,  $\chi(\text{N}_2) = 0.541$ , and  $\chi(\text{Ar}) = 0.288$ . The results of the simulation for  $\tau_{\text{ign}}$  are within 10% of the results where the compression process was not simulated. In addition, the results show that less than 120 ppm of the *n*-C<sub>4</sub>H<sub>9</sub>OH of the test mixture is consumed by EOC, and both the pressure and temperature are within 0.1% of the non-reacting EOC values. See Figure 3.3 below depicting these results.

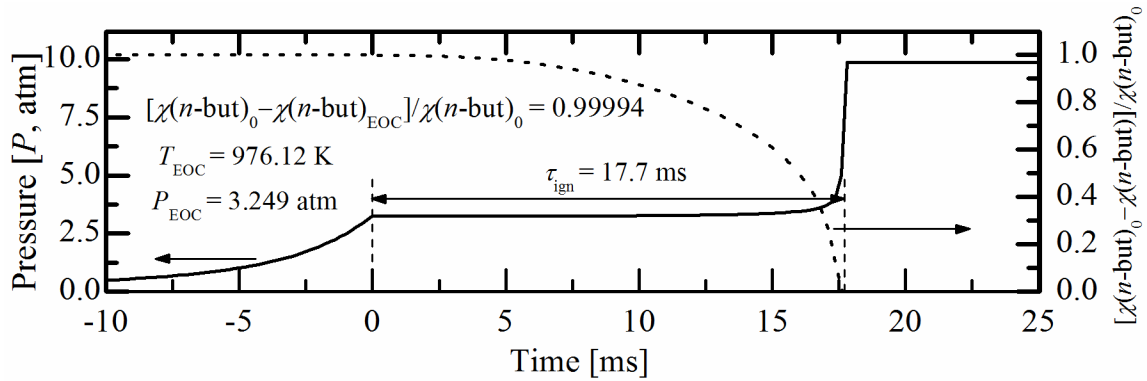


Figure 3.3 CHEMKIN™ simulation representing the compression stroke of the UM RCF for the targeted EOC conditions of  $T = 975$  K and  $P = 3.25$  atm using the Black *et al.*<sup>50</sup> reaction mechanism, with initial mole fractions of  $\chi(n\text{-but}) = 0.025$ ,  $\chi(\text{O}_2) = 0.147$ ,  $\chi(\text{N}_2) = 0.541$ , and  $\chi(\text{Ar}) = 0.288$ .

Similarly for target EOC conditions of  $T = 1025$  K and  $P = 3.25$  atm with initial mole fractions of  $\chi(n\text{-but}) = 0.025$ ,  $\chi(\text{O}_2) = 0.147$ ,  $\chi(\text{N}_2) = 0.429$ , and  $\chi(\text{Ar}) = 0.399$ ,  $\tau_{\text{ign}}$  is faster by less than 10% when the compression stroke is included in the simulation, with less than 1300 ppm of the  $n\text{-C}_4\text{H}_9\text{OH}$  in the test mixture consumed by EOC. As with the lower temperature simulation, both the pressure and temperature are within 0.1% of the non-reacting EOC values. See Figure 3.4 depicting this simulation. The results confirm that reaction during compression is of little concern for the ignition delay time experiments or the gas sampling experiments.

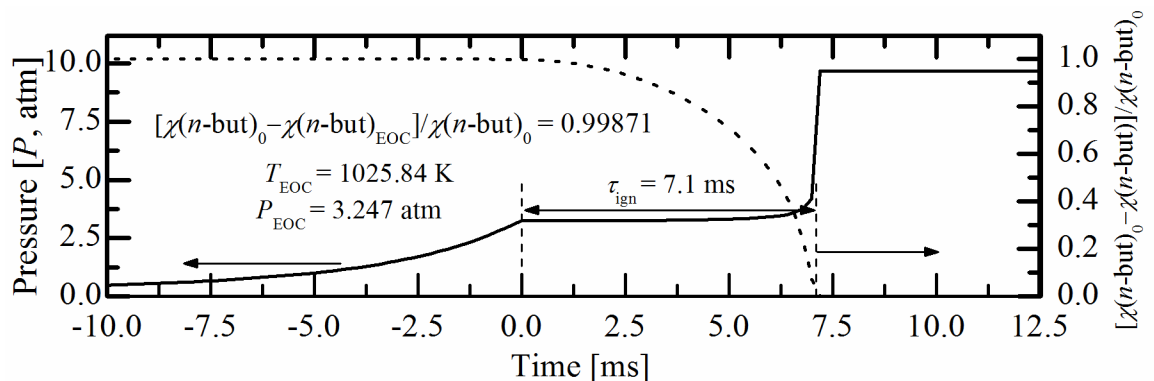


Figure 3.4 CHEMKIN™ simulation representing the compression stroke of the UM RCF for the targeted EOC conditions of  $T = 1025$  K and  $P = 3.25$  atm using the Black *et al.*<sup>50</sup> reaction mechanism, with initial mole fractions of  $\chi(n\text{-but}) = 0.025$ ,  $\chi(\text{O}_2) = 0.147$ ,  $\chi(\text{N}_2) = 0.429$ , and  $\chi(\text{Ar}) = 0.399$ .

Sensitivity analysis was used to identify the reactions having a significant effect on  $n$ -C<sub>4</sub>H<sub>9</sub>OH ignition delay time. The analysis was performed using the initial conditions of  $T = 975$  K,  $P = 3.25$  atm,  $\chi(n\text{-but}) = 0.025$ ,  $\chi(\text{O}_2) = 0.147$ ,  $\chi(\text{N}_2) = 0.541$ , and  $\chi(\text{Ar}) = 0.288$  ( $\phi = 1.0$ , inert/O<sub>2</sub> molar dilution = 5.64) using the Black *et al.*<sup>50</sup> mechanism. The OH radical concentration was used as a surrogate for ignition delay time, and the results of the OH sensitivity analysis are presented in Figure 3.5. The most important reaction is the chain-initiating decomposition of H<sub>2</sub>O<sub>2</sub> into two OH radicals. The  $n$ -C<sub>4</sub>H<sub>9</sub>OH+HO<sub>2</sub> reaction also plays a large role at these conditions as a source of H<sub>2</sub>O<sub>2</sub>. These results differ from those of Black *et al.*<sup>50</sup>, who also performed sensitivity analysis for  $n$ -C<sub>4</sub>H<sub>9</sub>OH ignition and found the chain branching H+O<sub>2</sub> reaction to be the most important. The results highlight the change in the reaction kinetics from the lower temperatures considered here (975 K) where competition between H<sub>2</sub>O<sub>2</sub> and HO<sub>2</sub> chemistry dominates the ignition chemistry, to the higher temperatures considered by Black *et al.*<sup>50</sup> (1450 K), where H, OH and O are the radical chain carriers.

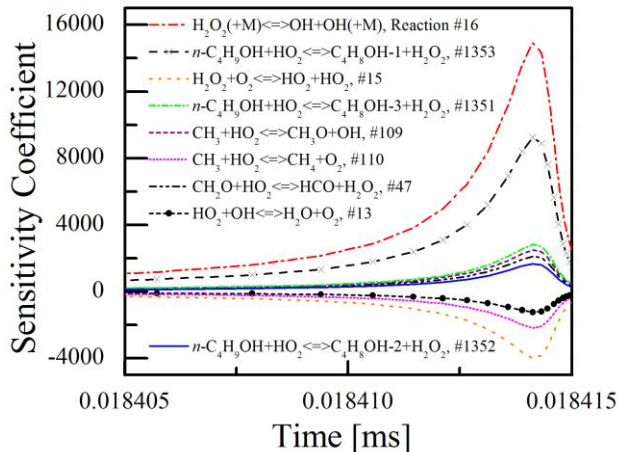


Figure 3.5 Results for OH sensitivity analysis using the mechanism of Black *et al.*<sup>50</sup> for the target gas sampling conditions of  $\phi = 1.0$ ,  $T = 975$  K,  $P = 3.25$  atm, inert/O<sub>2</sub> = 5.64.

Figure 3.6 presents the experimental data from the current work and the previous shock tube studies by Black *et al.*<sup>50</sup>, Moss *et al.*<sup>49</sup>, and Noorani *et al.*<sup>53</sup> The shock tube data were obtained at higher temperatures and dilution levels than the current study and span pressures from 1-4 atm. Zero dimensional, spatially-

homogeneous, adiabatic, constant volume model predictions based on the reaction mechanism by Black *et al.*<sup>50</sup> are also shown in the figure. Model predictions for the shock tube data (with  $\chi(n\text{-but}) = 0.008$ ,  $\chi(\text{O}_2) = 0.045$ ,  $\chi(\text{Ar}) = 0.948$ ,  $P = 1$  atm) span the dilution (composition and levels) and pressures of the experimental shock tube data for the extended temperature range  $T = 950\text{-}1650$  K. Model predictions for the UM RCF data (with  $\chi(n\text{-but}) = 0.025$ ,  $\chi(\text{O}_2) = 0.147$ ,  $\chi(\text{N}_2) = 0.541$ , and  $\chi(\text{Ar}) = 0.288$ ,  $P = 3.25$  atm) are presented for the extended temperature range  $T = 900\text{-}1650$  K. The model predictions are in excellent agreement with both data sets and they reproduce the shift to faster ignition that occurs with higher concentrations of fuel in the reacting mixtures and with slightly higher pressures.

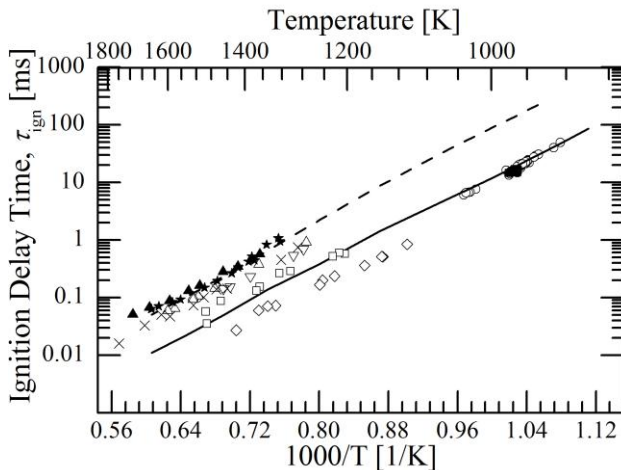


Figure 3.6 Comparison of the  $n\text{-C}_4\text{H}_9\text{OH}$  ignition delay times measured in the current work with the experimental results for shock tube studies of  $n\text{-C}_4\text{H}_9\text{OH}$  ignition by Moss *et al.*<sup>49</sup> and Black *et al.*<sup>50</sup> where  $\phi = 1$  for all data.  $\circ$ —Current work,  $P = 2.9\text{-}3.4$  atm, inert/ $\text{O}_2 = 5.64$ ,  $\blacksquare$ —Current work, gas-sampling experiments,  $P = 3.22\text{-}3.34$  atm, inert/ $\text{O}_2 = 5.64$ ,  $\triangle$ —Moss *et al.*<sup>49</sup>  $P = 1$  atm, inert/ $\text{O}_2 = 15.5$ ,  $\blacktriangle$ —Moss *et al.*<sup>49</sup>  $P = 1.3$  atm, inert/ $\text{O}_2 = 32$ ,  $\nabla$ —Moss *et al.*<sup>49</sup>  $P = 4$  atm, inert/ $\text{O}_2 = 65.7$ ,  $\star$ —Black *et al.*<sup>50</sup>  $P = 1$  atm, inert/ $\text{O}_2 = 21$ ,  $\times$ —Black *et al.*<sup>50</sup>  $P = 2.5\text{-}3.1$  atm, inert/ $\text{O}_2 = 26.6$ ,  $\square$ —Noorani *et al.*<sup>53</sup>  $P = 1.8\text{-}2.5$  atm, inert/ $\text{O}_2 = 10$ ,  $\diamond$ —Noorani *et al.*<sup>53</sup>,  $P = 1.8\text{-}2.5$  atm, inert/ $\text{O}_2 = 10$ . Model predictions based on the Black *et al.*<sup>50</sup> mechanism are presented for conditions of  $P = 1$  atm, inert/ $\text{O}_2 = 21$  (dashed line) and  $P = 3.25$  atm, inert/ $\text{O}_2 = 5.64$  (solid line).

### High-speed gas sampling experiments

The ignition delay time study provided the basis to identify thermodynamic conditions where high-speed gas sampling could be applied with good accuracy and repeatability. Based on these results, EOC temperatures of  $T_{\text{eff}} = 975$  K were

targeted for the gas-sampling experiments. Specifically, UM RCF experiments with  $T_{\text{eff}} = 975$  K yielded ignition delay times between 14 and 17 ms, allowing a sampling time resolution of approximately 10:1. Results from a typical sampling experiment are presented in Figure 3.7, where  $P_{\text{eff}} = 3.27$  atm,  $T_{\text{eff}} = 974$  K, and  $\tau_{\text{ign}} = 16.0$  ms. Figure 3.7 includes the time-histories of the pressure and pressure derivative in the test section, the two triggering signals of the gas-sampling system, and the pressures in the two sampling chambers.

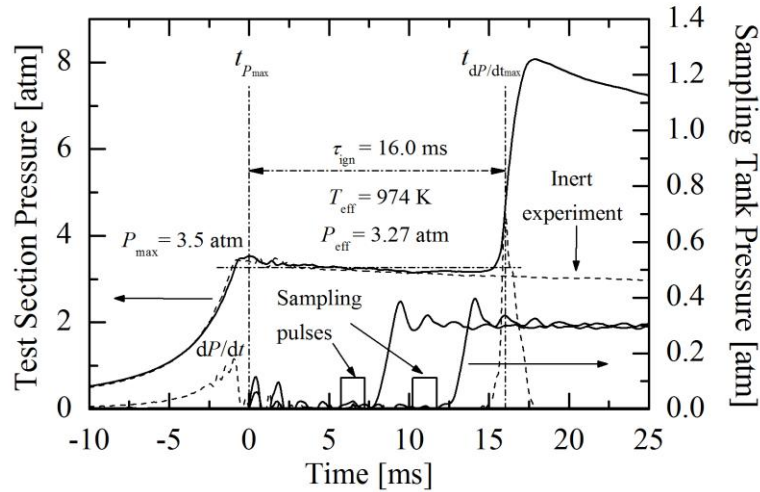


Figure 3.7 Results for a typical  $n\text{-C}_4\text{H}_9\text{OH}$  ignition experiment with gas-sampling during the ignition delay period. The pressure and pressure derivative time histories in the test section and in the two sampling chambers are presented. The triggering signals for the rapid gas sampling valves are also provided. The pressure time-history for a non-igniting (i.e. inert) experiment is included for comparison.

As seen in the figure, the pressure in the test section is unaffected by the sampling process, and the features are similar to the data of Figure 3.1, which shows ignition without gas sampling. The time-histories of the two gas samples show the rapid increase in pressure that occurs after the triggering signals and confirm the sampling times as  $< 2$  ms. Figure 3.7 also includes for comparison the pressure time-history for a non-igniting experiment (labeled “Inert experiment”) with the same thermal characteristics as an igniting  $n\text{-C}_4\text{H}_9\text{OH}/\text{oxidizer}/\text{diluent}$  mixture (where the  $\text{O}_2$  in the mixture was been replaced with  $\text{N}_2$ ). The non-igniting pressure time-history is virtually indistinguishable from the igniting pressure time-history (where  $P_{\text{eff}}$  and  $T_{\text{eff}}$  differ by less 1% and 0.5%, respectively). The comparison demonstrates

that neither the ignition chemistry nor the gas sampling affects the heat transfer physics of the experiments.

A total of 11 gas-sampling experiments were performed. A summary of the experimental conditions, the measured  $\tau_{\text{ign}}$ , and the sample times are provided in Table 3.2, found at the end of this chapter. A summary of the pressure time-histories of the gas-sampling experiments is presented in Figure 3.8. All of the sampling experiments show nearly identical, smooth compression processes. The slight decrease in pressure after EOC (due to heat losses to the test manifold walls, prior to the sampling events) is also extremely consistent between experiments. The averages and standard deviations for the effective conditions are 3.29 atm and 0.04 atm, respectively, for pressure, and 975 K and 3 K for temperature, respectively. The average and standard deviation for the measured  $\tau_{\text{ign}}$  are 15.7 ms and 0.8 ms, respectively. The standard deviations of the EOC pressures,  $P_{\text{eff}}$  and  $\tau_{\text{ign}}$  for the sample experiments are 0.06 atm, 0.04 atm and 0.84 ms, respectively.

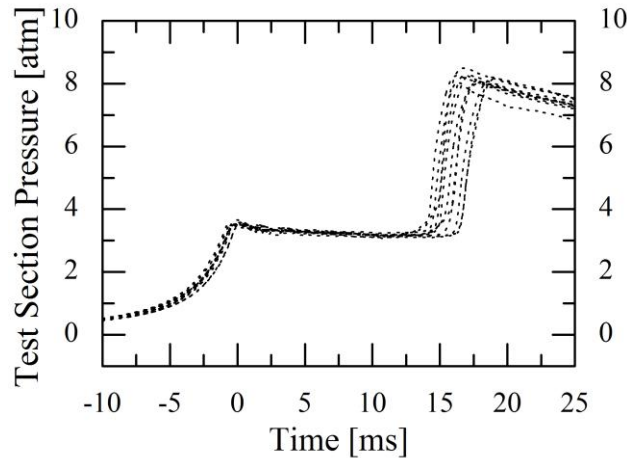


Figure 3.8 Comparison of the pressure time-histories for the high-speed gas-sampling experiments of  $n\text{-C}_4\text{H}_9\text{OH}$  ignition. Note the nearly identical compression processes for all experiments.

While the data of Figure 3.8 and Table 3.2 demonstrate the excellent level of repeatability of the sampling experiments, there are slight differences in the EOC conditions and ignition delay times. To compensate for these slight differences in the experimental pressure time-histories, the sampling data are reported using a time domain that is normalized by the actual  $\tau_{\text{ign}}$  for each experiment. EOC is

defined as  $t/\tau_{\text{ign}} = 0$ , and  $t/\tau_{\text{ign}} = 1$  is the time of ignition. Figure 3.9 presents the pressure time histories of Figure 3.8 after normalizing by the  $\tau_{\text{ign}}$  for each experiment. The normalized times when each gas sample was taken during the ignition delay period are labeled in Figure 3.9. Note that due to the low levels of intermediate species at early times, the sampling data were preferentially acquired closer to the time of ignition.

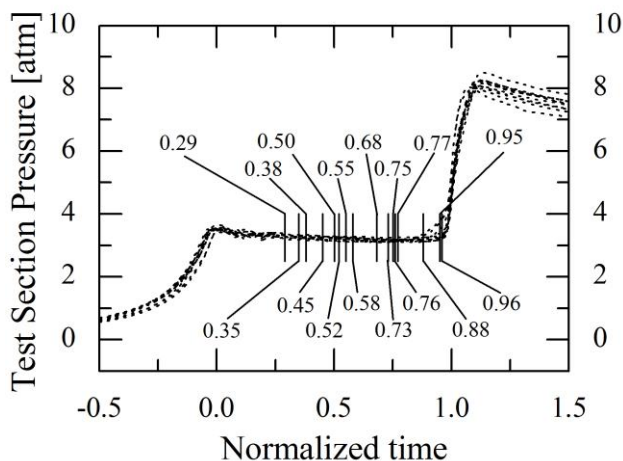


Figure 3.9 Comparison of the pressure time-histories of the sampling experiments on a time scale normalized to  $\tau_{\text{ign}}$  for each experiment. The normalized time for each gas-sample measurement is labeled in the figure.

Figure 3.10 shows a typical GC-FID chromatogram from an  $n\text{-C}_4\text{H}_9\text{OH}$  ignition experiment for conditions of  $P_{\text{eff}} = 3.27$  atm,  $T_{\text{eff}} = 974$  K,  $\tau_{\text{ign}} = 16.0$  ms and a sampling time of 7.2 ms. Peaks from  $\text{CH}_4$ ,  $\text{C}_2\text{H}_4$ ,  $\text{C}_3\text{H}_6$ ,  $\text{CH}_3\text{CHO}$ ,  $1\text{-C}_4\text{H}_8$ ,  $n\text{-C}_3\text{H}_7\text{CHO}$  and  $n\text{-C}_4\text{H}_9\text{OH}$  are identified in the figure. CO measurements were made using chromatograms from the GC-TCD detector and are not shown here. All major features on the chromatograms were identified. Using the calibration data for each species and the measured dilution levels of the gas samples, the chromatograms were converted into discrete measurements for each sampling time. Figure 3.11 presents the results for the eight intermediate species as a function of the normalized ignition delay time for the nominal experimental conditions of  $P_{\text{eff,average}} = 3.29$  atm and  $T_{\text{eff,average}} = 975$  K. In Figure 3.11, the error bars are the uncertainty in the experimental data. As described above, the uncertainty in the sampling times is  $\pm 0.75$  ms, or approximately  $\pm 0.05$  when normalized by the average ignition delay

time. The uncertainty in the measured mole fractions was  $\pm 16\%$  as determined by the uncertainty in the species calibration and dilution percentage, as discussed earlier. The calibration and dilution were considered independent sources of uncertainty, and the overall uncertainty for each species was determined using the square root of the sum of the squares for each source of uncertainty. Note that only two measurements were above the detectable limit for CO, and none of the  $n$ - $C_4H_9OH$  measurements were both below the limit that saturated the GC detector and above the detectable limit for  $n$ - $C_4H_9OH$ , given the uncertainty due to dilution.

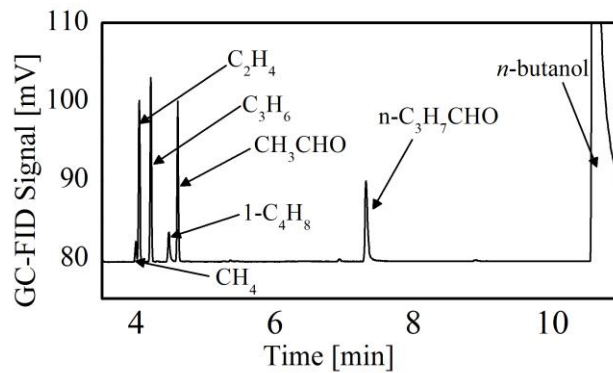
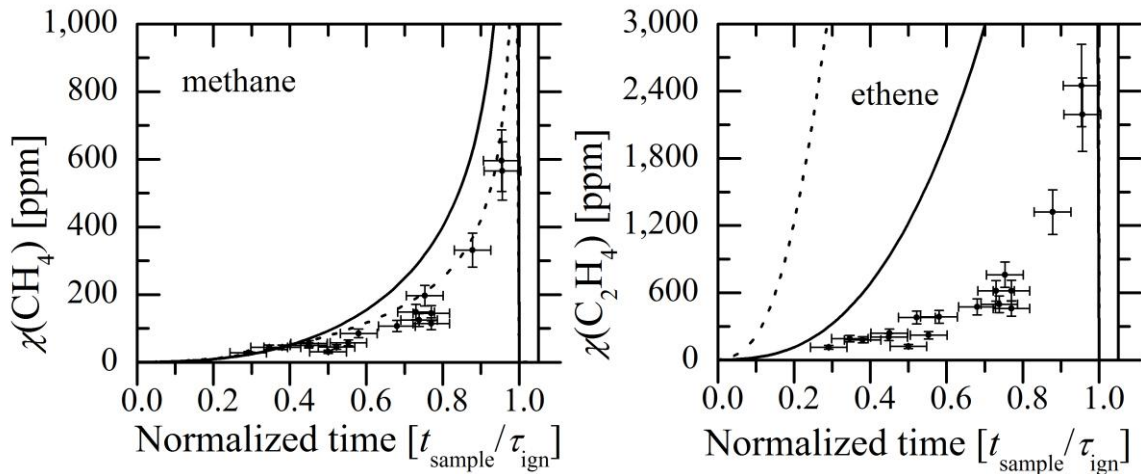


Figure 3.10 Typical GC-FID chromatogram results of a gas sample acquired at  $t = 7.2$  ms,  $t/\tau_{ign} = 0.45$ , for experimental conditions of  $P_{eff} = 3.27$  atm,  $T_{eff} = 974$  K,  $\tau_{ign} = 16.0$  ms.



(caption on next page)



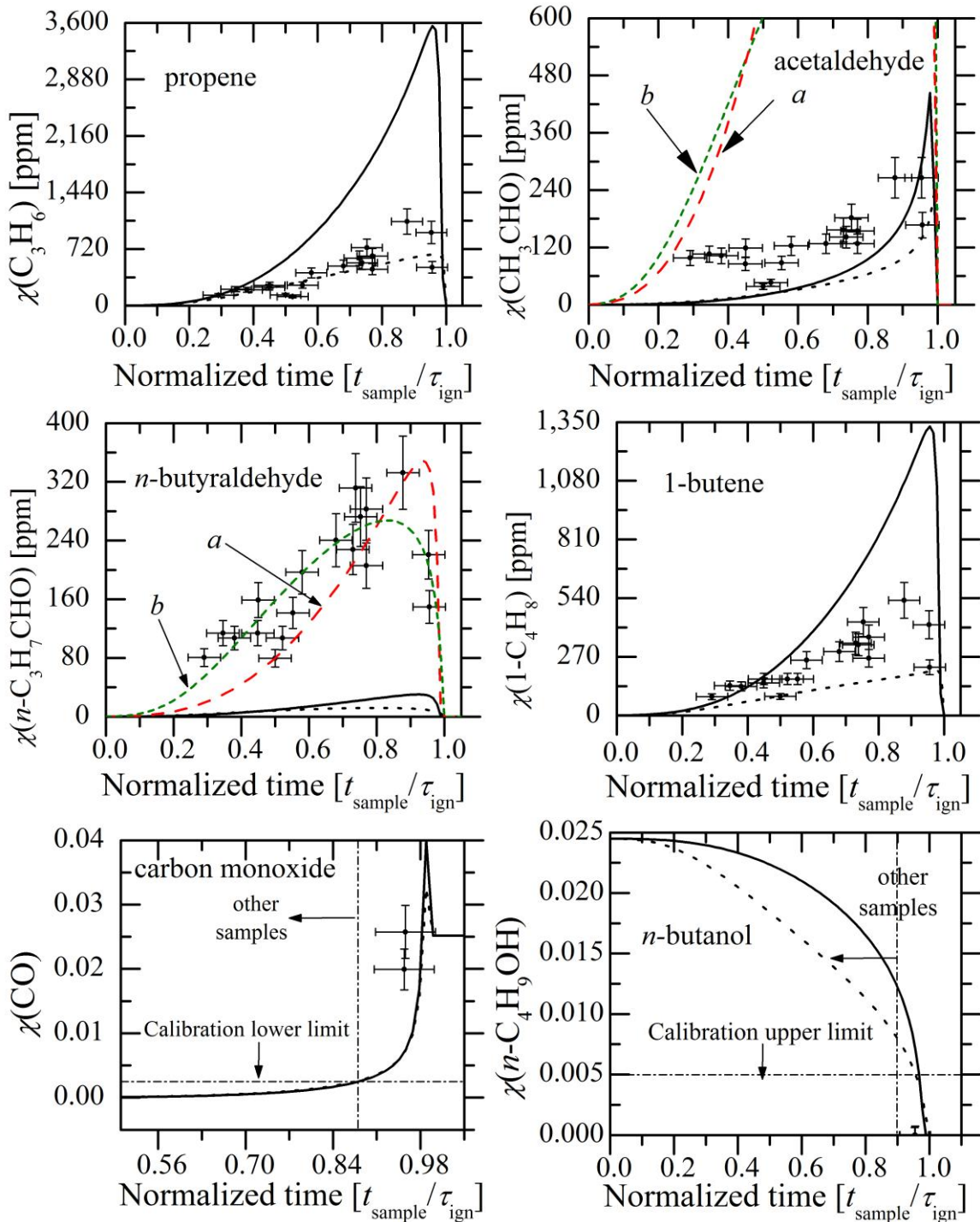


Figure 3.11 Comparison between measured intermediate species and model predictions using the reaction mechanism of Black *et al.*<sup>50</sup> and the initial conditions of  $P = 3.25$  atm,  $T = 975$  K, inert/ $\text{O}_2 = 5.64$ , and  $n\text{-C}_4\text{H}_9\text{OH} = 2.45\%$  ( $\tau_{\text{ign, predicted}} = 18.6$  ms). The unmodified mechanism predictions are shown with solid lines, and the modified mechanism predictions are shown with dotted black lines. The average experimental conditions are  $P_{\text{eff}} = 3.29$  atm,  $T_{\text{eff}} = 975$  K, inert/ $\text{O}_2 = 5.63$ , and  $n\text{-C}_4\text{H}_9\text{OH} = 2.44\%$  ( $\tau_{\text{ign, average}} = 15.7$  ms). The error bars represent the experimental uncertainties. The time domain has been normalized from  $t = 0$  (end of compression) to the time of ignition,  $t/\tau_{\text{ign}} = 1$ .

Results for the model predictions using the reaction mechanism by Black *et al.*<sup>50</sup> for the initial condition of  $P = 3.25$  atm,  $T = 975$  K,  $\text{inert}/\text{O}_2 = 5.64$ , and  $n\text{-C}_4\text{H}_9\text{OH} = 2.45\%$  are presented as the solid lines in Figure 3.11. The predicted ignition delay time is  $\tau_{\text{ign}} = 18.6$  ms, which is within 18% of the average of the experimental data ( $\tau_{\text{ign, average}} = 15.7$  ms). The model predictions show good qualitative agreement with the experimental data for all species. The quantitative agreement is very good (within a factor of 2 for the duration of the ignition delay period) for  $\text{CH}_4$ . However, the model significantly over-predicts  $\text{C}_2\text{H}_4$  (by a factor of 4-8 over the entire ignition delay period) and  $\text{C}_3\text{H}_6$  (by a factor of 2-3 over the ignition delay period).  $1\text{-C}_4\text{H}_8$  shows good quantitative agreement, with differences less than a factor of 2 over most of the ignition delay period. CO was measured at detectable levels in the GC-TCD chromatograms only closer to ignition, as predicted by the model. Note that the model predictions show a narrow peak for CO, where it is formed rapidly and consumed rapidly very close to ignition. The model predictions for CO are within the experimental uncertainties when the temporal resolution of the experimental data is considered. Similarly, the model predictions for  $n\text{-C}_4\text{H}_9\text{OH}$  are consistent with expectations based on the limiting factors for the measurements. Specifically, for times less than  $t/\tau_{\text{ign}} \sim 0.95$  the experimental data for  $n\text{-C}_4\text{H}_9\text{OH}$  are limited by the 0.5% threshold for the GC-FID detector. Quantitative measurements of  $\text{CO}_2$  can be made using the GC configuration used in the current work. However, no  $\text{CO}_2$  peaks were observed at any sampling conditions. The absence of  $\text{CO}_2$  is consistent with the predictions which indicate  $\text{CO}_2$  levels will not exceed the minimum detectable limit of 0.25% until times after  $t/\tau_{\text{ign}} > 0.98$ . The aldehydes calibrated for and measured,  $\text{CH}_3\text{CHO}$  and  $n\text{-C}_3\text{H}_7\text{CHO}$ , warrant a more detailed discussion, particularly with reference to enol-keto isomerization (tautomerization) as described by Black *et al.*<sup>50</sup> and Harper *et al.*<sup>63</sup> This discussion is presented later.

The experimental data capture a reasonable fraction of the carbon in the system. By comparison with the model predictions for the concentrations of carbon-containing species, the GC measurements account for 54-75% of the carbon not present in  $n\text{-C}_4\text{H}_9\text{OH}$  at early sampling times ( $t/\tau_{\text{ign}} < 0.4$ ), and 15-48% of this carbon at sampling times closer to ignition ( $t/\tau_{\text{ign}} > 0.7$ ). When CO was measureable ( $t/\tau_{\text{ign}} >$

0.9), the GC measurements capture 31-35% of the total carbon present in the system.

During gas sampling, radicals present in the test section are quenched and can be a source of interference with the gas sampling measurements. For example, radicals such as O, H, OH, and CH<sub>3</sub> can recombine to form water vapor and small hydrocarbons. Radical recombination has potential to affect the GC results by systematically biasing the data by introducing unexpected stable species into the samples or by increasing the concentration of species beyond the levels present before quenching. However, radical recombination is not expected to be a source of error in the current work due to the low levels of radicals present prior to ignition. For example, the predicted time histories for OH, O, H and CH<sub>3</sub> based on the Black *et al.*<sup>50</sup> mechanism and the initial conditions  $P = 3.25$  atm,  $T = 975$  K, inert/O<sub>2</sub> = 5.64, and  $n\text{-C}_4\text{H}_9\text{OH} = 2.45\%$  are shown in Figure 3.12. Negligible levels of these radicals (< 30 ppm) are predicted for nearly the entire ignition delay time period i.e.  $t/\tau_{\text{ign}} < 0.96$ .

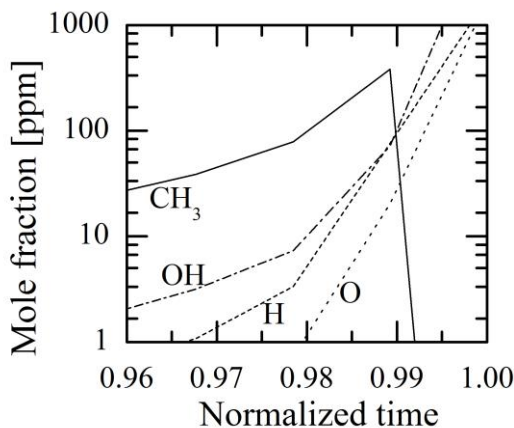


Figure 3.12 Species time histories of radicals predicted using the reaction mechanism of Black *et al.*<sup>50</sup> for initial conditions of  $P = 3.25$  atm,  $T = 975$  K, inert/O<sub>2</sub> = 5.64, and  $n\text{-C}_4\text{H}_9\text{OH} = 2.45\%$ .

Rate of production analysis was used to identify the reaction pathways important for the species measured. The analysis was conducted at 75% of  $\tau_{\text{ign}}$  using the Black *et al.*<sup>50</sup> mechanism (at the same conditions described above). Figures 3.14-3.21 show the primary reaction pathways for the major species ( $n\text{-C}_4\text{H}_9\text{OH}$  and CO) and the intermediates. The percentages listed in the figures quantify the specific reaction pathway relative to the overall consumption of the individual species. The results

for  $n\text{-C}_4\text{H}_9\text{OH}$  (Figure 3.13) show that H-atom abstraction via OH is the key decomposition pathway for  $n\text{-C}_4\text{H}_9\text{OH}$  at these conditions, followed by  $\beta$ -scission to form alkyl radicals and alkenes. Figure 3.14 shows that CO is ultimately formed via pressure-dependent decomposition of  $\text{CH}_3\text{CO}$ , as well as via HCO reacting with  $\text{O}_2$ . Figure 3.15 shows that  $\text{CH}_4$  is formed by addition of H-atoms to  $\text{CH}_3$  radicals, while  $\text{C}_2\text{H}_4$  is formed primarily through the decomposition of  $\text{PC}_2\text{H}_4\text{OH}$  and  $\text{C}_2\text{H}_5$  reacting with  $\text{O}_2$ . Recall, the model predictions for  $\text{C}_2\text{H}_4$  were significantly higher than the levels measured experimentally. As seen in Figure 3.15, increasing the removal of  $\text{C}_2\text{H}_4$  with radical species like O and  $\text{CH}_3$  would increase the  $\text{CH}_4$  levels, both directly and indirectly, where predicted  $\text{CH}_4$  levels were already in good agreement with the experimental data. A lower decomposition rate for  $\text{PC}_2\text{H}_4\text{OH}$  appears more appropriate.

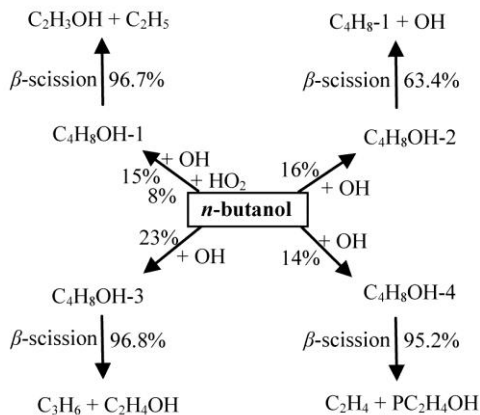


Figure 3.13 Reaction path diagram of the primary decomposition reactions for  $n\text{-C}_4\text{H}_9\text{OH}$  for  $t/\tau_{\text{ign}} = 0.75$  and the initial conditions of  $P = 3.25$  atm,  $T = 975$  K,  $\text{inert}/\text{O}_2 = 5.64$ , and  $n\text{-C}_4\text{H}_9\text{OH} = 2.45\%$ .

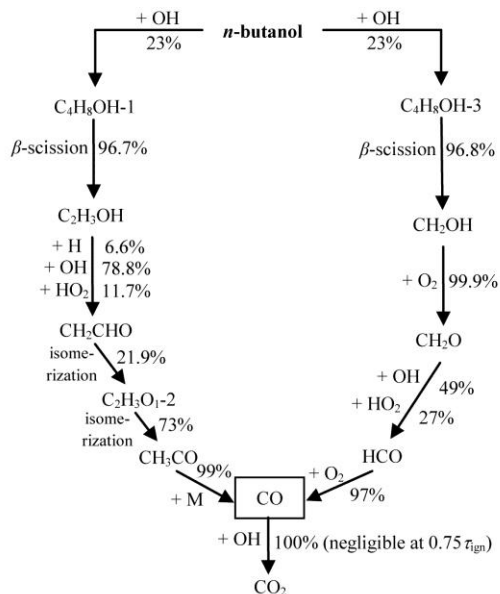


Figure 3.14 Reaction path diagram of the primary formation pathways for carbon monoxide. Same model conditions as Figure 14.

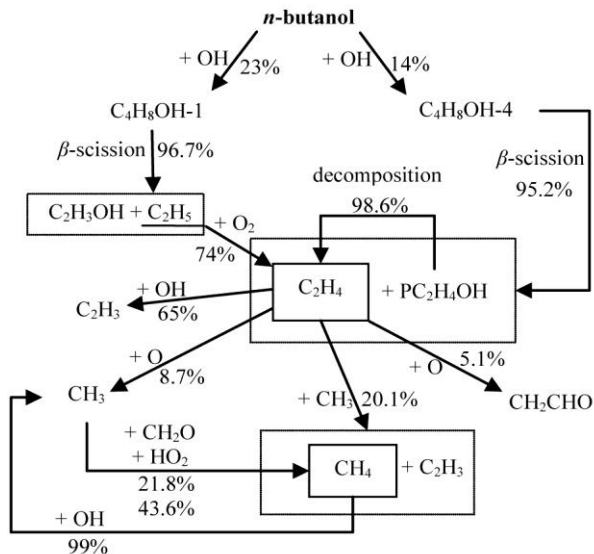


Figure 3.15 Reaction path diagram of the primary formation and removal pathways for ethene and methane. Same model conditions as Figure 14.

Figure 3.16 shows that  $C_3H_6$  is predominantly formed via  $\beta$ -scission of  $C_4H_8OH-3$ , which itself is formed through H-atom abstraction from  $n-C_4H_9OH$ .  $C_3H_6$  is predominantly consumed by reactions with H-atoms. Because the model overpredicts  $C_3H_6$ , the rate of production analysis indicates the branching fraction for the  $C_4H_8OH-3$  channel of  $n-C_4H_9OH$  decomposition may be slightly too high for

the conditions studied here. 1-C<sub>4</sub>H<sub>8</sub> (Figure 3.17) is primarily formed via  $\beta$ -scission of C<sub>4</sub>H<sub>8</sub>OH-2, which itself is formed via H-atom abstraction from *n*-C<sub>4</sub>H<sub>9</sub>OH. 1-C<sub>4</sub>H<sub>8</sub> is consumed by radical abstraction of H-atoms.

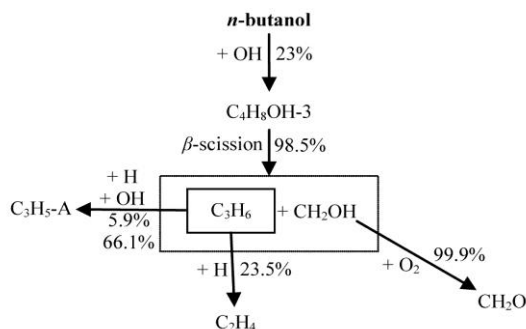


Figure 3.16 Reaction path diagram of the primary formation and removal pathways for propene. Same model conditions as Figure 14.

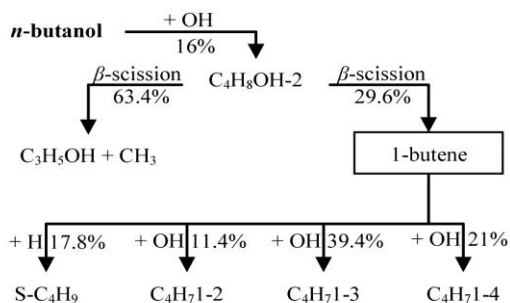


Figure 3.17 Reaction path diagram of the primary formation and removal pathways for 1-butene. Same model conditions as Figure 14.

Black *et al.*<sup>50</sup> and Harper *et al.*<sup>55</sup> provide detailed descriptions of the tautomerizing of enols to ketones which is relevant to this study. In particular, tautomerization can affect the aldehyde measurements. Black *et al.*<sup>50</sup> note that the conversion from enol to ketone cannot be easily catalyzed in the gas phase. It is therefore possible that the enol is the preferred low energy state, as the barrier height for isomerization is approximately 243 kJ/mol. Furthermore, Black *et al.*<sup>50</sup> point out that these isomers cannot be distinguished by gas chromatographic techniques. Therefore, chromatograms depicting concentrations of aldehydes are likely also influenced by the presence of enols. Figure 3.18 shows that CH<sub>3</sub>CHO is formed via multiple simultaneous pathways resulting from the breakdown of

radicals formed via H-atom abstraction from  $n$ -C<sub>4</sub>H<sub>9</sub>OH. Rate of production analysis for CH<sub>3</sub>CHO shows that at the conditions studied, tautomerization of ethenol is not an important pathway for CH<sub>3</sub>CHO production. Furthermore, as seen in Figure 3.11, CH<sub>3</sub>CHO shows good agreement, qualitatively and quantitatively, over the entire ignition delay period. However, non-negligible amounts (~100 ppm) were observed early in the experiments ( $t/\tau_{ign} < 0.6$ ), which was not predicted by the model. Plotted in Figure 3.11 as the red/long dashed line, marked  $\alpha$ , is also the sum of the isomers of C<sub>2</sub>H<sub>4</sub>O, namely CH<sub>3</sub>CHO and ethenol. Ethenol is predicted to be present in high concentrations (>3000 ppm), from the  $\beta$ -scission of C<sub>4</sub>H<sub>8</sub>OH-1, for  $t/\tau_{ign} > 0.9$ . The Black *et al.*<sup>50</sup> mechanism also predicts non-negligible amounts of ethenol for  $t/\tau_{ign} < 0.4$ . It was observed that even though ethenol may co-elute with CH<sub>3</sub>CHO, high concentrations of C<sub>2</sub>H<sub>4</sub>O isomers were not detected in the gas chromatograms. While the C<sub>4</sub>H<sub>8</sub>OH-3 channel for  $n$ -C<sub>4</sub>H<sub>9</sub>OH decomposition is a source of CH<sub>3</sub>CHO, decreasing the branching fraction of the C<sub>4</sub>H<sub>8</sub>OH-3 channel, as suggested earlier, should not significantly impact the CH<sub>3</sub>CHO time history as the C<sub>4</sub>H<sub>8</sub>OH-3 channel is small relative to the other sources of CH<sub>3</sub>CHO.

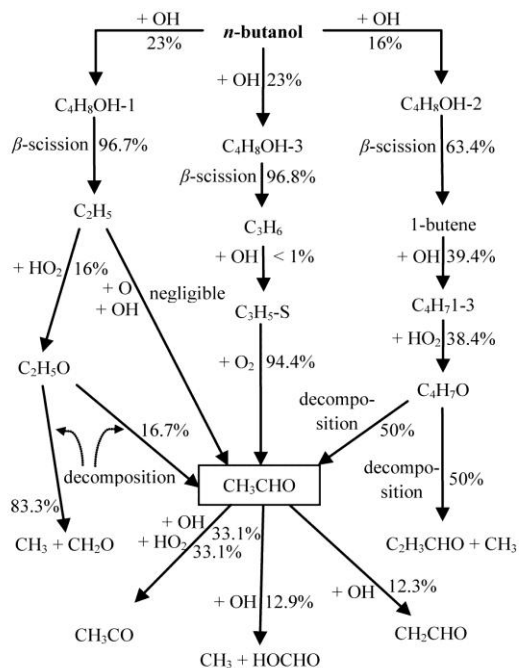


Figure 3.18 Reaction path diagram of the primary formation and removal pathways for acetaldehyde. Same model conditions as Figure 14.

$n$ -C<sub>3</sub>H<sub>7</sub>CHO shows the largest discrepancies (Figure 3.11) between the model predictions and measurements, where the model under-predicts  $n$ -C<sub>3</sub>H<sub>7</sub>CHO by an order of magnitude (by a factor of 10-20 for the duration of the ignition delay period). Figure 3.19 shows that  $n$ -C<sub>3</sub>H<sub>7</sub>CHO is formed solely via H-atom abstraction of one of the decomposition products of  $n$ -C<sub>4</sub>H<sub>9</sub>OH (C<sub>4</sub>H<sub>8</sub>OH-1) and is consumed by H-atom abstraction. Tautomerization reactions for the conversion of  $n$ -C<sub>3</sub>H<sub>7</sub>CHO to butenols are not included in the Black *et al.*<sup>50</sup> mechanism. However, just like the case with the C<sub>2</sub>H<sub>4</sub>O isomers, the C<sub>4</sub>H<sub>8</sub>O isomers, namely  $n$ -C<sub>3</sub>H<sub>7</sub>CHO, 1-buten-1-ol, 2-buten-1-ol, and 3-buten-1-ol, may co-elute and be measured simultaneously with  $n$ -butyraldehyde. When the sum of the concentrations of all the C<sub>4</sub>H<sub>8</sub>O isomers is plotted in Figure 3.11 (red/long dashed line, marked *a*), the measured and predicted trends are in very good agreement (generally within the uncertainty limits of the measured data).

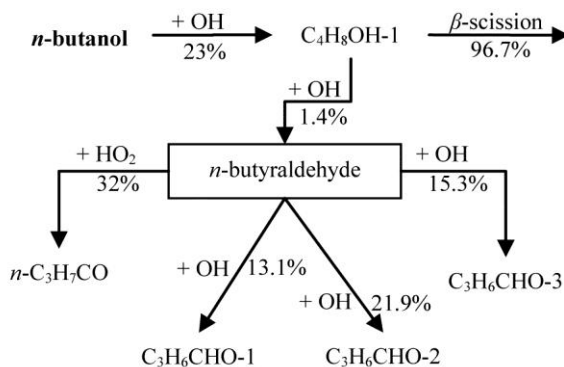


Figure 3.19 Reaction path diagram of the primary formation and removal pathways for  $n$ -butyraldehyde. Same model conditions as Figure 14.

The rate coefficient for the reaction of  $n$ -C<sub>4</sub>H<sub>9</sub>OH with OH has been the subject of recent experimental and theoretical studies.<sup>57,58</sup> Vasu *et al.*<sup>57</sup> measured the rate constant of the overall reaction of  $n$ -C<sub>4</sub>H<sub>9</sub>OH+OH  $\rightarrow$  products in a shock tube study at pressures of 2.25 atm for temperatures between 973 K and 1428 K. They developed an expression for the overall rate coefficient of this reaction, of  $k_{n\text{-butanol}+\text{OH}} = 4.118 \times 10^3 T^{2.944} \exp(1852/T)$  [cm<sup>3</sup>mol<sup>-1</sup>s<sup>-1</sup>]. The shock tube data are in good agreement with recent theoretical calculations performed by Zhou *et al.*,<sup>58</sup> who used both CCSD(T)/cc-pVQZ//MP2/6-311 g(d,p) and G3 methods to determine overall rate constant expressions for  $n$ -C<sub>4</sub>H<sub>9</sub>OH+OH. Specifically, Zhou *et al.*<sup>58</sup> determined an



overall rate coefficient of  $k_{n\text{-butanol}+\text{OH}} = 40.3T^{3.57}\exp(2128/T)$  [ $\text{cm}^3\text{mol}^{-1}\text{s}^{-1}$ ] based on the G3 method. As seen in Figure 3.20, these overall rate constants of Vasu *et al.*<sup>57</sup> and Zhou *et al.*<sup>58</sup> are a factor of two higher than the rate constant used in the Black *et al.*<sup>50</sup> mechanism for the range of temperatures considered in the current work. For Figure 3.20, the data for the Black *et al.*<sup>50</sup> mechanism are the sum of the rate constants for H-atom abstraction by OH from the  $\alpha$ ,  $\beta$ ,  $\gamma$ , and  $\delta$  carbon sites and from the alcohol group of  $n\text{-C}_4\text{H}_9\text{OH}$ .

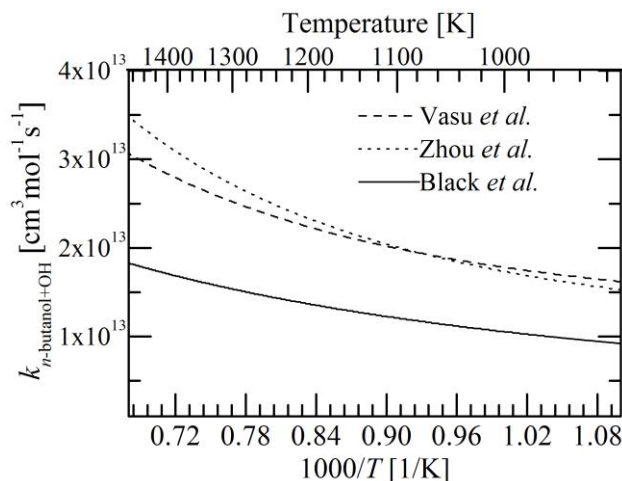


Figure 3.20 Rate constants for the overall  $n\text{-C}_4\text{H}_9\text{OH}+\text{OH}$  reaction from Vasu *et al.*,<sup>57</sup> Zhou *et al.*,<sup>58</sup> and Black *et al.*<sup>50</sup>

In order to quantify the effects of changing the overall rate coefficient and the branching fractions for the  $n\text{-C}_4\text{H}_9\text{OH}+\text{OH}$  reaction, the recommendations from Zhou *et al.*<sup>58</sup> (based on their G3 calculations) were substituted into the reaction mechanism by Black *et al.*<sup>50</sup> As expected based on the sensitivity analysis presented earlier, the modified reaction mechanism had a minor effect on the ignition delay time, at  $P = 3.25$  atm,  $T = 975$  K, inert/ $\text{O}_2 = 5.64$ , and  $n\text{-C}_4\text{H}_9\text{OH} = 2.45\%$ . Specifically,  $\tau_{\text{ign}}$  increased from 18.6 ms to 21.8 ms. However, the modified reaction mechanism resulted in much higher endothermicity during the ignition delay period compared to the unmodified mechanism, with the temperature decreasing by 15 K (to 960 K) before ignition. The unmodified Black *et al.*<sup>50</sup> mechanism predicts weak endothermicity, with a decrease of only 0.5 K before ignition. There are also several significant changes in the intermediate species, and the model predictions from the modified reaction mechanism are presented as the dashed lines in Figure 3.11.

Although there is an improvement in the prediction of CH<sub>4</sub>, C<sub>2</sub>H<sub>4</sub> is significantly overproduced, with peak concentrations almost a factor of three higher than the unmodified Black *et al.*<sup>50</sup> mechanism. The modified mechanism dramatically improves the quantitative agreement between the model predictions for C<sub>3</sub>H<sub>6</sub> and 1-C<sub>4</sub>H<sub>8</sub> and the experimental data. *n*-C<sub>3</sub>H<sub>7</sub>CHO concentrations are further underpredicted compared to the unmodified Black *et al.*<sup>50</sup> mechanism; however, the sum of the concentrations of the C<sub>4</sub>H<sub>8</sub>O isomers predicted by the modified mechanism reproduces extremely well the measured values for *n*-C<sub>3</sub>H<sub>7</sub>CHO concentrations, as is seen in Figure 3.11 with the green/short dashed line, marked b. The modified mechanism predicts the non-negligible amounts of these isomers for  $t/\tau_{\text{ign}} < 0.4$ . It is noted in Figure 3.11 with the green/short dashed line, marked b, that for CH<sub>3</sub>CHO, peak concentrations (off of scale) of the sum of the C<sub>2</sub>H<sub>4</sub>O isomers is around 1200 ppm, as compared to 3400 ppm for the unmodified mechanism.

The modified mechanism also changes the trend in *n*-C<sub>4</sub>H<sub>9</sub>OH removal, where *n*-C<sub>4</sub>H<sub>9</sub>OH is consumed almost linearly over the ignition delay time, rather than almost exponentially, as with the unmodified Black *et al.*<sup>50</sup> mechanism. These changes are consistent with expectations based on the changes in the branching fractions and the reaction path analysis presented earlier. For example, decreasing the  $\beta/\text{C}_4\text{H}_8\text{OH}-2$  and  $\gamma/\text{C}_4\text{H}_8\text{OH}-3$  channels directly decrease the production of 1-C<sub>4</sub>H<sub>8</sub> and C<sub>3</sub>H<sub>6</sub>, respectively; while increasing the  $\delta/\text{C}_4\text{H}_8\text{OH}-4$  channel increases a reaction path to form C<sub>2</sub>H<sub>4</sub>. Overall, the performance of the reaction mechanism improved with the revisions to the *n*-C<sub>4</sub>H<sub>9</sub>OH+OH reactions, with the key exceptions of *n*-C<sub>3</sub>H<sub>7</sub>CHO and C<sub>2</sub>H<sub>4</sub>, which were not captured well quantitatively with either the modified or unmodified reaction mechanism.

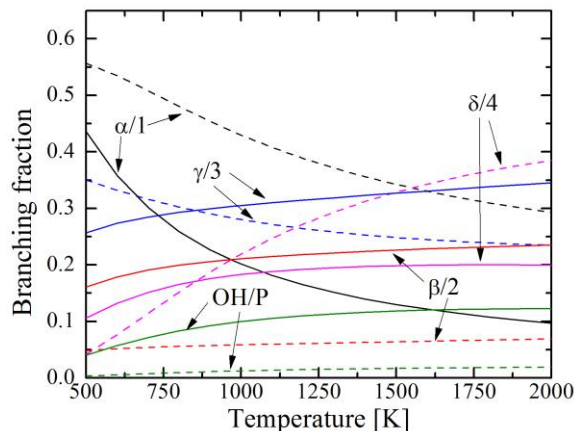


Figure 3.21 Branching fractions for the five H-atom abstraction channels by OH from the  $\alpha$ ,  $\beta$ ,  $\gamma$ , and  $\delta$  carbon sites and from the alcohol group of  $n$ -C<sub>4</sub>H<sub>9</sub>OH. The legend includes the site of the H-atom abstraction and the designation of the corresponding C<sub>4</sub>H<sub>8</sub>OH isomer produced. The solid lines are the values used in the Black *et al.*<sup>50</sup> mechanism, and the dashed lines are the values recommended by Zhou *et al.*<sup>58</sup> based on their G3 calculations.

## Conclusions

The current work presents new experimental data on the ignition characteristics of  $n$ -butanol ( $n$ -C<sub>4</sub>H<sub>9</sub>OH) and species time-histories of important intermediates formed during ignition delay time of  $n$ -C<sub>4</sub>H<sub>9</sub>OH. The experimental data are the first of their kind at the moderate temperatures (920–1040 K) and pressures (~3 atm) studied, and the data verify some expected trends, specifically Arrhenius behavior with no negative temperature dependence. Similar to hydrocarbons at comparable conditions, HO<sub>2</sub> and H<sub>2</sub>O<sub>2</sub> kinetics dominate the reactivity of the  $n$ -C<sub>4</sub>H<sub>9</sub>OH/air mixtures, and the data are in excellent agreement with model predictions based on recently developed reaction mechanisms for  $n$ -C<sub>4</sub>H<sub>9</sub>OH. Further, the reaction mechanism by Black *et al.*<sup>50</sup> yields excellent quantitative agreement with experimental ignition data from the current work and previous shock tube studies over a broad range of temperatures (900–1800 K). Many of the reaction pathways important to predicting the intermediates are well represented in the chemical kinetic mechanism of Black *et al.*<sup>50</sup> A key exception identified in this study is C<sub>2</sub>H<sub>4</sub>. The speciation data from the current study show high levels (100s of ppm and higher) of aldehydes (and related isomers) and alkenes are produced as intermediate species during  $n$ -C<sub>4</sub>H<sub>9</sub>OH ignition. C<sub>2</sub>H<sub>4</sub> and  $n$ -C<sub>3</sub>H<sub>7</sub>CHO are expected to play a role in pollutant emissions, namely soot and aldehydes; an understanding of their

formation is essential for the successful implementation of  $n$ -C<sub>4</sub>H<sub>9</sub>OH in the fuel infrastructure. Recent studies, like the important works by Vasu *et al.*<sup>57</sup> and Zhou *et al.*<sup>58</sup> on the overall reaction rate and specific branching channels of the  $n$ -C<sub>4</sub>H<sub>9</sub>OH+OH reaction, have improved the understanding of the reaction pathways important to  $n$ -C<sub>4</sub>H<sub>9</sub>OH combustion. However, more experimental and theoretical work is needed to improve the fidelity of our predictive understanding of  $n$ -C<sub>4</sub>H<sub>9</sub>OH combustion chemistry.

Table 3.1 A summary of ignition and sampling (in italics) experiments for *n*-butanol. Predicted ignition delay times from Black *et al.*<sup>50</sup> mechanism.

$\phi$	inert/O <sub>2</sub>	$\chi_{\text{but}}$	$\chi_{\text{O}_2}$	$\chi_{\text{N}_2}$	$\chi_{\text{Ar}}$	$P_{\text{eff}}$ (atm)	$T_{\text{eff}}$ (K)	$\tau_{\text{ign}}$ (ms) measured	$\tau_{\text{ign}}$ (ms) predicted
1.00	5.62	0.025	0.147	0.672	0.156	3.04	927	49.6	50.7
1.00	5.65	0.024	0.147	0.658	0.171	3.04	934	39.9	44.5
1.00	5.64	0.025	0.147	0.568	0.260	2.86	949	31	32.9
1.00	5.64	0.025	0.147	0.568	0.260	2.92	952	28.7	31.0
1.01	5.65	0.025	0.147	0.541	0.288	2.99	954	27.6	29.9
1.00	5.64	0.024	0.147	0.557	0.271	3.00	959	22.1	27.2
1.00	5.64	0.024	0.147	0.540	0.288	3.07	960	24.4	26.7
1.00	5.64	0.024	0.147	0.541	0.287	3.07	960	24	26.7
1.00	5.61	0.024	0.147	0.540	0.288	3.08	961	23.5	26.2
1.01	5.65	0.025	0.147	0.541	0.288	3.09	962	21.8	25.7
0.99	5.57	0.024	0.148	0.539	0.288	3.1	963	21.4	25.2
1.00	5.64	0.024	0.147	0.541	0.287	3.1	963	22.6	25.2
1.00	5.64	0.024	0.147	0.541	0.288	3.12	964	22.2	24.8
1.00	5.64	0.024	0.147	0.541	0.288	3.13	964	21.4	24.8
1.00	5.61	0.024	0.147	0.540	0.288	3.11	965	21.5	24.3
1.00	5.64	0.025	0.147	0.541	0.288	3.12	965	21.6	24.3
1.01	5.63	0.025	0.147	0.594	0.234	3.1	965	20.8	24.2
1.00	5.64	0.025	0.147	0.541	0.288	3.08	966	20.9	23.9
0.99	5.61	0.024	0.148	0.540	0.288	3.16	967	21.3	23.4
1.00	5.64	0.024	0.147	0.541	0.288	3.17	968	17.9	23.0
0.99	5.57	0.024	0.148	0.539	0.288	3.18	968	19.2	23.0
1.00	5.65	0.024	0.147	0.541	0.288	3.15	968	19.2	23.0
1.00	5.62	0.024	0.147	0.541	0.288	3.14	968	19.8	23.0
1.00	5.63	0.025	0.147	0.541	0.288	3.15	968	20.6	23.0
1.00	5.63	0.025	0.147	0.541	0.288	3.19	969	19	22.6
1.00	5.66	0.024	0.147	0.540	0.289	3.19	969	19.6	22.6
1.00	5.62	0.025	0.147	0.541	0.288	3.21	970	19.9	22.2
<i>1.00</i>	<i>5.64</i>	<i>0.024</i>	<i>0.147</i>	<i>0.541</i>	<i>0.288</i>	<i>3.24</i>	<i>971</i>	<i>16.5</i>	<i>21.8</i>
1.00	5.65	0.024	0.147	0.541	0.288	3.18	971	18.6	21.8
1.01	5.63	0.025	0.147	0.594	0.234	3.17	972	17.8	21.4
<i>1.00</i>	<i>5.63</i>	<i>0.025</i>	<i>0.147</i>	<i>0.541</i>	<i>0.288</i>	<i>3.34</i>	<i>972</i>	<i>14.7</i>	<i>21.4</i>
<i>0.99</i>	<i>5.61</i>	<i>0.024</i>	<i>0.148</i>	<i>0.540</i>	<i>0.288</i>	<i>3.22</i>	<i>972</i>	<i>16.8</i>	<i>21.4</i>
1.00	5.64	0.025	0.147	0.541	0.288	3.23	972	19	21.4
<i>1.00</i>	<i>5.64</i>	<i>0.024</i>	<i>0.147</i>	<i>0.541</i>	<i>0.288</i>	<i>3.27</i>	<i>974</i>	<i>16</i>	<i>20.6</i>
<i>1.00</i>	<i>5.63</i>	<i>0.024</i>	<i>0.147</i>	<i>0.540</i>	<i>0.288</i>	<i>3.26</i>	<i>974</i>	<i>16.9</i>	<i>20.6</i>

$\phi$	inert/O <sub>2</sub>	$\chi_{\text{but}}$	$\chi_{\text{O}_2}$	$\chi_{\text{N}_2}$	$\chi_{\text{Ar}}$	$P_{\text{eff}}$	$T_{\text{eff}}$	$\tau_{\text{ign}}$ (ms)	$\tau_{\text{ign}}$ (ms)
						(atm)	(K)	measured	predicted
1.00	5.64	0.024	0.147	0.541	0.288	3.28	975	15.2	20.2
1.00	5.64	0.024	0.147	0.541	0.288	3.32	975	16.3	20.2
1.00	5.62	0.025	0.147	0.541	0.288	3.29	976	15.8	19.9
1.00	5.64	0.025	0.147	0.541	0.288	3.28	977	15.3	19.5
1.00	5.61	0.024	0.148	0.540	0.287	3.31	978	15.1	19.1
1.00	5.64	0.024	0.147	0.541	0.288	3.32	979	14.9	18.9
1.00	5.64	0.024	0.147	0.579	0.249	3.33	979	15.6	18.8
1.01	5.65	0.025	0.147	0.541	0.287	3.35	980	14.4	18.5
1.00	5.63	0.025	0.147	0.579	0.250	3.25	981	14.9	18.1
1.00	5.62	0.025	0.147	0.541	0.288	3.37	981	13.3	18.1
1.00	5.64	0.024	0.147	0.541	0.288	3.34	981	14.4	18.1
1.00	5.63	0.025	0.147	0.579	0.250	3.28	984	16.3	17.2
1.00	5.62	0.025	0.147	0.479	0.349	3.25	1019	7.66	9.40
1.00	5.64	0.025	0.147	0.480	0.349	3.35	1026	6.77	8.37
1.00	5.64	0.025	0.147	0.480	0.349	3.32	1028	6.67	8.10
1.00	5.64	0.025	0.147	0.480	0.349	3.35	1031	6.62	7.72
1.00	5.64	0.025	0.147	0.480	0.349	3.4	1034	6.02	7.35

Table 3.2 A summary of sampling experiments for *n*-butanol.

$P_{\text{eff}}$ (atm)	$T_{\text{eff}}$ (K)	$\tau_{\text{ign}}$ (ms)	Nominal	Nominal	Normalized sampling time 1 ( $t_1/\tau_{\text{ign}}$ )	Normalized sampling time 2 ( $t_2/\tau_{\text{ign}}$ )
			sampling time for gas sample 1, $t_1$ (ms)	sampling time for gas sample 2, $t_2$ (ms)		
3.24	971	16.5	N/A	14.5	N/A	0.88
3.34	972	14.7	11.1	14.1	0.75	0.96
3.22	972	16.8	4.9	6.4	0.29	0.38
3.27	974	16.0	7.2	11.7	0.45	0.73
3.26	974	16.9	8.5	11.5	0.50	0.68
3.28	975	15.2	11.5	14.5	0.76	0.95
3.32	975	16.3	9	N/A	0.55	N/A
3.29	976	15.8	12.2	12.2	0.77	0.77
3.28	977	15.3	8.8	N/A	0.58	N/A
3.31	978	15.1	7.9	N/A	0.52	N/A
3.34	981	14.4	5	6.5	0.35	0.45

## Chapter 4

### On the combustion chemistry of *n*-heptane and *n*-butanol blends

*This chapter has been submitted to the Journal of the American Chemical Society as, Karwat, D. M. A.; Wagnon, S. W.; Wooldridge, M. S.; Westbrook, C. K. "On the combustion chemistry of n-heptane and n-butanol blends".*

#### Introduction

While there has been significant interest over the past few years in using biofuels in practical combustion systems for transportation, it is likely that they will be blended with traditional fuels in varying amounts based on application. Variation is also likely to exist in whether or not the biofuels blended with traditional fuels will be single component fuels (such as ethanol or butanol), or multi-component fuels (such as rapeseed methyl esters). Regardless of application or fuel type, there is a need to understand how biofuels change the chemistry of traditional fuels to understand both global reactivity effects as well as effects on air pollutant, particulate, and greenhouse gas emissions. Significant effort has been put into studying large *n*-alkanes (such as *n*-heptane, *n*-C<sub>7</sub>H<sub>16</sub>, discussed in Chapter 2), which comprise a significant fraction of complex fuel mixtures such as kerosene. Just like *n*-C<sub>7</sub>H<sub>16</sub>, *n*-butanol (*n*-C<sub>4</sub>H<sub>9</sub>OH) has garnered much interest in the recent combustion chemistry literature, as described in Chapter 3.

While it is apparent that speciation studies are capable of providing insights into the chemical kinetic effects of blending oxygenated biofuels with largely pure hydrocarbon fuels, there exist only two studies of the chemical kinetic effects of adding *n*-C<sub>4</sub>H<sub>9</sub>OH to a large *n*-alkane, both were jet stirred reactor studies.<sup>59,64</sup> Dagaut and Togbé<sup>59</sup> studied the oxidation kinetics of *n*-C<sub>7</sub>H<sub>16</sub>/*n*-C<sub>4</sub>H<sub>9</sub>OH blends at two blend ratios (80%-20% and 50%-50% by volume) at a residence time of 0.7

seconds, over a wide temperature range (500-1100 K) and constant pressure (10 atm), in highly diluted mixtures with initial fuel concentrations of 750 ppm at two fuel-to-O<sub>2</sub> equivalence ratios (0.5 and 1). They observed that fuel consumption decreased as temperature was increased between 620 K and 770 K, signifying the presence of the NTC region of *n*-C<sub>7</sub>H<sub>16</sub> oxidation, and that *n*-C<sub>4</sub>H<sub>9</sub>OH was consumed at temperatures much lower than it would be consumed at by itself. The *n*-C<sub>7</sub>H<sub>16</sub> oxidation at low temperatures thus coaxed *n*-C<sub>4</sub>H<sub>9</sub>OH to react. Furthermore, the rates of consumption of each of the components reflected the blend ratio—when *n*-C<sub>7</sub>H<sub>16</sub> was present in concentrations four times higher than *n*-C<sub>4</sub>H<sub>9</sub>OH, the rate of *n*-C<sub>7</sub>H<sub>16</sub> consumption was four times higher than that of *n*-C<sub>4</sub>H<sub>9</sub>OH, whereas in equimolar mixtures of *n*-C<sub>7</sub>H<sub>16</sub> and *n*-C<sub>4</sub>H<sub>9</sub>OH, the two components were consumed at the same rate. Dagaut and Togbé<sup>59</sup> produced two chemical kinetic mechanisms for the study—one detailed, and one reduced—and found that the reduced mechanism, which omitted reactions that left ignition predictions unaffected, predicted fast formation of CO, CO<sub>2</sub>, and H<sub>2</sub>O above 800 K.

In the study by Saisirirat *et al.*,<sup>64</sup> similar measurements to the Dagaut and Togbé<sup>59</sup> study were made (along with measurements of *n*-C<sub>7</sub>H<sub>16</sub>/*n*-C<sub>4</sub>H<sub>9</sub>OH blends in a homogeneous charge compression ignition engine), but at an equivalence ratio of 0.3 and a 50%-50% blend of *n*-C<sub>7</sub>H<sub>16</sub> and *n*-C<sub>4</sub>H<sub>9</sub>OH. The authors' analyses, using a chemical kinetic mechanism generated by merging separate mechanisms for *n*-C<sub>4</sub>H<sub>9</sub>OH and *n*-C<sub>7</sub>H<sub>16</sub><sup>59,65</sup>, showed the presence of *n*-C<sub>4</sub>H<sub>9</sub>OH tempered the NTC behavior of *n*-C<sub>7</sub>H<sub>16</sub> because the overall rate of production of OH radicals that consumed fuel molecules decreased due to the presence of *n*-C<sub>4</sub>H<sub>9</sub>OH, and the overall production of OH radicals itself decreased with the presence of *n*-C<sub>4</sub>H<sub>9</sub>OH.

The work presented in this chapter uses the unique features of the University of Michigan Rapid Compression Facility as a chemical reactor and builds on previous speciation work to present the first measurements of species time-histories of *n*-C<sub>7</sub>H<sub>16</sub>/*n*-C<sub>4</sub>H<sub>9</sub>OH blends under ignition conditions. The goal of the work is to provide insights into changes in reaction pathways and product formation in the combustion of traditional fuels when in the presence of oxygenated alternative fuels.



## Experimental Setup

The same experimental setup and procedure as described in Chapter 2 was used in this study.

## Model Description

For simulating the combustion chemistry of  $n\text{-C}_7\text{H}_{16}/n\text{-C}_4\text{H}_9\text{OH}$  blends, the chemical kinetic mechanism described in Chapter 2 was combined with the most updated chemical kinetic mechanism for  $n\text{-C}_4\text{H}_9\text{OH}$  developed by Sarathy *et al.*<sup>66</sup> This mechanism was validated against atmospheric pressure premixed laminar flame speed data, premixed laminar low pressure flame species profiles, low-to-intermediate temperature ignition data, intermediate-to-high temperature shock tube data, as well as species profiles obtained from low pressure flame studies and JSR studies.

## Results and Discussion

### *Ignition experiments and modeling*

Ignition experiments were conducted to understand the dependence of ignition delay time ( $\tau_{\text{ign}}$ ) on blend ratio at a fixed temperature (700 K) and pressure (9 atm). The studies in Chapter 2 provided baseline  $\tau_{\text{ign}}$  data against which the influence of the presence of  $n\text{-C}_4\text{H}_9\text{OH}$  was compared. It was expected that increasing the amount of  $n\text{-C}_4\text{H}_9\text{OH}$  would increase the ignition delay time, given the much faster reactivity of  $n\text{-C}_7\text{H}_{16}$  as was observed in comparing the  $\tau_{\text{ign}}$  data of Chapter 2 and Chapter 3.<sup>34</sup> Since the chemical kinetics of  $n\text{-C}_7\text{H}_{16}$  were studied at thermodynamic conditions (a temperature of 700 K and a pressure of 9 atm) that yielded a  $\tau_{\text{ign}}$  on the order of 15 ms in the baseline study described in Chapter 2, the presence of  $n\text{-C}_4\text{H}_9\text{OH}$  would allow for several discrete sampling events (each lasting 1.5 ms, as described earlier) during the ignition delay period.

For each experiment, the effective test conditions are determined based on the pressure time-history from each experiment. Since the 80-20 and 50-50 blends studied exhibited two-stage ignition for all experiments, Equation 2.1 was used to determine the effective pressure ( $P_{\text{eff}}$ ), which was used to determine the effective

temperature ( $T_{\text{eff}}$ ) for each experiment using numerical integration of the isentropic relation (Equation 2.2).

The ignition delay time ( $\tau_{\text{ign}}$ ) for each experiment was defined as the time between EOC ( $t = 0$  ms, defined by the first maximum in  $P$ ) and the maximum rate of pressure rise corresponding to autoignition ( $dP/dt_{\text{max, 2nd stage}}$ ). The time for the first stage of ignition was defined as the time between EOC ( $t = 0$  ms, defined by the first maximum in  $P$ ) and the pressure rise corresponding to the first stage of ignition ( $\tau_1$ ). All mixtures had an equivalence ratio ( $\phi$ ) of 1, and a dilution (with  $\text{N}_2$  and  $\text{CO}_2$  being the sole diluents for all experiments) of  $\text{inert}/\text{O}_2 = 5.62\text{-}5.64$ . Table 4.2 found at the end of this chapter is a summary of the experimental conditions and results for all of the UM RCF data presented in this chapter.

Figure 4.1 presents typical results from a UM RCF ignition experiment for the 80-20 blend for which imaging data were acquired. The lower panel depicts the time-histories of the pressure and rate of pressure rise in the test section. A fast Fourier transform has been applied to filter high-frequency disturbances greater than 2.5 kHz generated by the impact of the sabot near EOC. The motion of the sabot compresses the test gas mixture into the test section to the first maximum. The EOC time is set to time  $t = 0$ , after which the volume in the test section is constant. The first stage of ignition occurs at  $\tau_1 = 12.37$  ms, corresponding to a local maximum in  $dP/dt$  (circled in the lower panel of Figure 2). The pressure time-history from EOC to  $\tau_1$  defines  $P_{\text{eff}}$  and  $T_{\text{eff}}$  as 9.05 atm and 703 K, respectively. After another time interval, the pressure rises abruptly again to its maximum value. The second pressure rise corresponds to autoignition of the test mixture at 19.70 ms.

The upper panel of Figure 4.1 shows stills from the image sequence corresponding to the pressure data of the lower panel. Intense chemiluminescence occurs only during the 2<sup>nd</sup> stage of ignition. The chemiluminescence is attributed to CH and  $\text{C}_2$  radicals, which have strong spectroscopic features in the blue part of the visible spectrum (CH: 431.2 nm;  $\text{C}_2$ : 473.7 nm, 516.5 nm, 563.5 nm) and are generated only through the decomposition of intermediate hydrocarbons present in the test mixture. Note the uniformity of the blue emission throughout the test section, attesting to the homogeneity of the reactant mixture and the state

conditions in the test section. Such uniformity gives confidence in localized sampling.

Figure 4.2 shows similar imaging and pressure data for a 50-50 blend. The general features of the pressure time-history are the same as observed for the 80-20 blend. However, both  $\tau_1$  and  $\tau_{\text{ign}}$  increase to 21.77 ms and 32.39 ms, respectively, compared to the 80-20 blend.

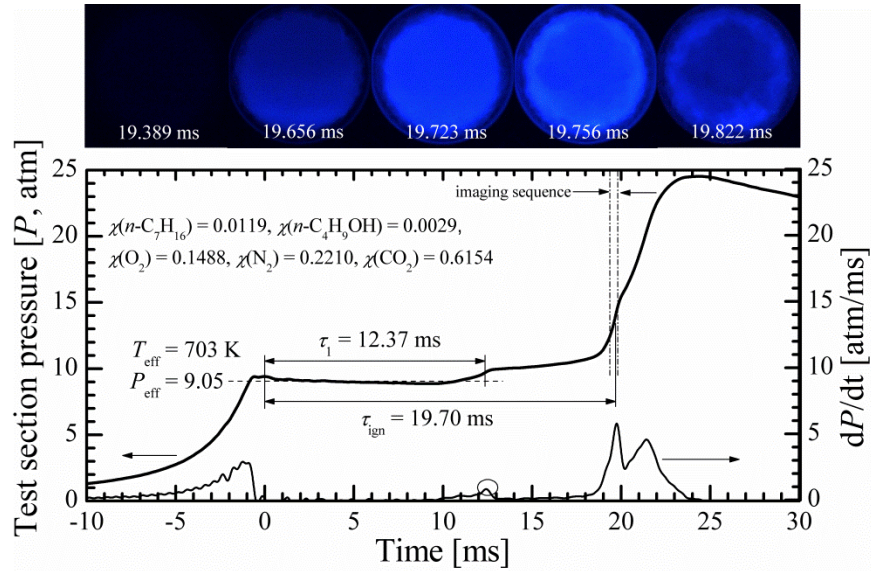


Figure 4.1 Results from a typical UM RCF 80-20 ignition experiment. The lower panel depicts the pressure time-history in the test section and the rate of pressure rise, which are used to define  $\tau_{\text{ign}}$  and the effective pressure and temperature conditions. The upper panel shows still images taken at 30,000 fps via end-view imaging. Note the homogeneity of the ignition event. The color of the images has been adjusted for clarity.

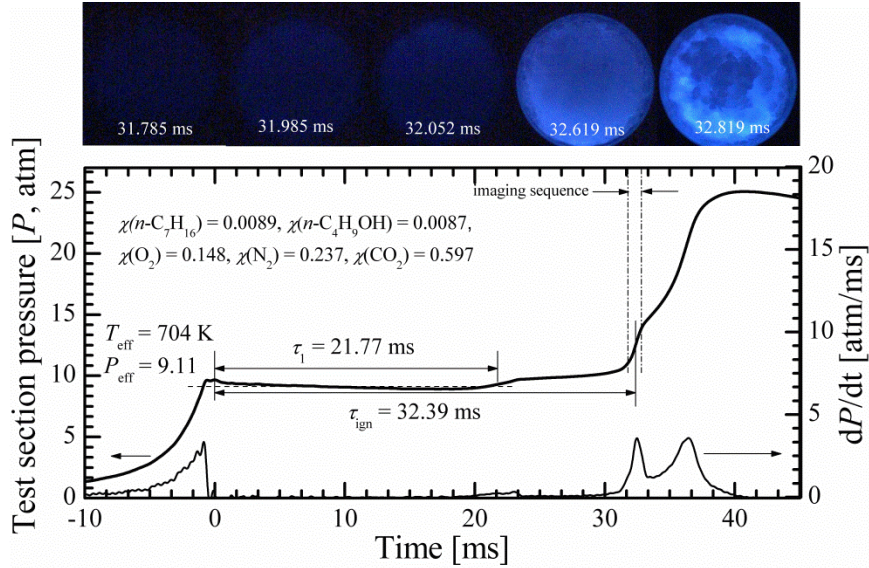


Figure 4.2 Results from a typical UM RCF 50-50 ignition experiment. Additional details described in the caption of Figure 4.1.

As is seen in Figure 4.1 and Figure 4.2, the addition of  $n\text{-C}_4\text{H}_9\text{OH}$  slows the ignition process. A clearer representation of the influence of  $n\text{-C}_4\text{H}_9\text{OH}$  can be seen in Figure 4.3, which compares the pressure time-histories obtained experimentally for the blends with the baseline (100-0) case. Also shown in Figure 4.3 are zero-dimensional, constant volume, adiabatic CHEMKIN<sup>TM</sup> simulations of the ignition delay times using the respective mixture compositions for the 80-20 and 50-50 experiments using the current mechanism described earlier. Initial pressure and temperature conditions used in these simulations corresponded to effective pressure and temperature conditions obtained experimentally. As described in Chapter 2 and Chapter 3, the effective pressure and temperature definitions adequately account for the heat transfer physics occurring in the test section of the UM RCF during these ignition experiments. As the amount of  $n\text{-C}_4\text{H}_9\text{OH}$  increases in the blend, the model correctly predicts the trends in increase of the first stage and second stage of ignition; however, differences between the model predictions and the experimental results also increase. While experiments show that  $\tau_1$  and  $\tau_{\text{ign}}$  increase by a factor of approximately three from the 100-0 to the 50-50 case, the model predicts an increase by a factor of approximately two (see also Table 1). Also, it is observed experimentally that the rise in pressure seen after the first stage of ignition decreases with increasing concentrations of  $n\text{-C}_4\text{H}_9\text{OH}$ . This is not the case with the model predictions, for even though the heat release of the first stage of ignition

occurs over a slightly longer period of time with increasing concentrations of  $n$ -C<sub>4</sub>H<sub>9</sub>OH, the nominal pressure reached at the end of the first stage of ignition is fairly consistent for the 100-0, 80-20, and 50-50 conditions. To understand the influence of  $n$ -C<sub>4</sub>H<sub>9</sub>OH on  $n$ -C<sub>7</sub>H<sub>16</sub> ignition, simulations were performed with 80-0 and 50-0 mixtures. Interestingly, the first stage of ignition in the 80-0 and 50-0 cases occurs at the same time as the 100-0 case. Therefore,  $n$ -C<sub>4</sub>H<sub>9</sub>OH serves to lengthen  $\tau_1$ . When comparing predicted  $\tau_{\text{ign}}$  values between the 80-20 and 80-0, and 50-50 and 50-0 cases, it is also observed that  $\tau_{\text{ign}}$  decreases when  $n$ -C<sub>4</sub>H<sub>9</sub>OH is present in the mixture; this is likely an overall  $\phi$  effect.

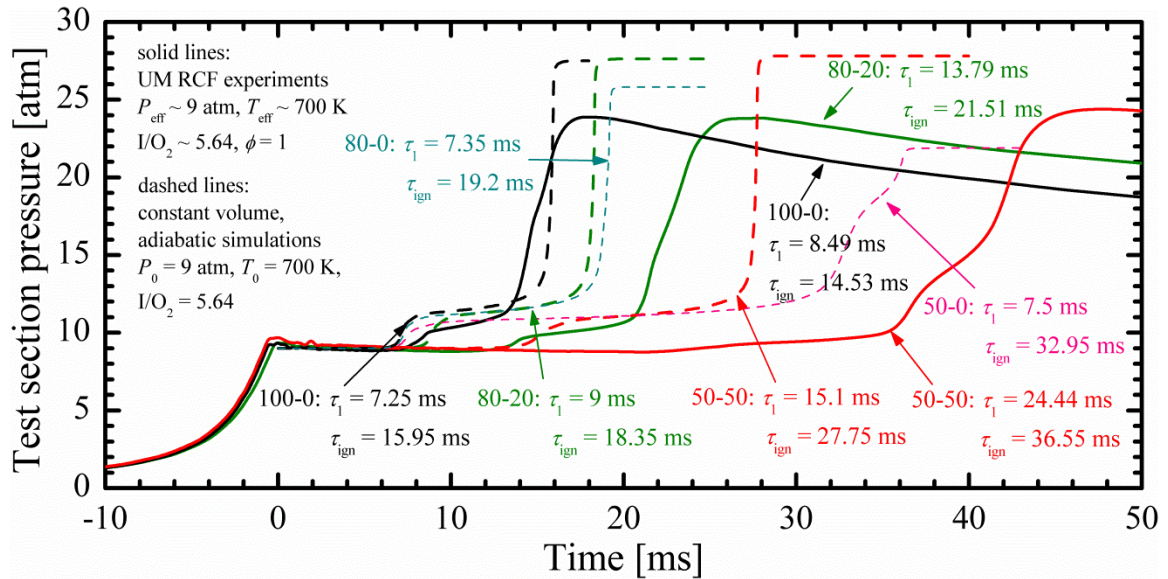


Figure 4.3 Comparison of experimental (solid lines) and modeling (dashed lines) pressure time-histories for the 100-0, 80-20, and 50-50 blend cases. While the model and the experimental data agree adequately for the 100-0 case, differences increase with increasing concentrations of  $n$ -C<sub>4</sub>H<sub>9</sub>OH in the mixture. Shown also are time-histories for simulations in which  $n$ -C<sub>4</sub>H<sub>9</sub>OH was removed from the 80-20 and 50-50 mixtures, thus simulating lean 80-0 (dark cyan) and 50-0 (pink)  $n$ -C<sub>7</sub>H<sub>16</sub> mixtures.

In order to understand why ignition slows as a function of blend ratio and to compare important features of the pressure time-histories, the ignition times were normalized, and the results are presented in Figure 4.4. Specifically, the period of time between the EOC and the first stage of ignition of each experiment was normalized by  $\tau_1$  (resulting in a normalized time domain of 0 to 1), and the period of time between the first stage of ignition and autoignition ( $\tau_{\text{ign}} - \tau_1$ ) was normalized by

$\tau_{\text{ign}} - \tau_1$  and added to the first normalized time domain. Experimentally, it is observed that as the amount of  $n\text{-C}_4\text{H}_9\text{OH}$  in the blend increases, the first stage of ignition becomes less pronounced. Based on understanding of  $n\text{-C}_7\text{H}_{16}$  ignition chemistry from Chapter 2, we can conjecture that the differences in blend behavior are due to the intermediate hydrogen peroxide. Autoignition is associated with the decomposition at approximately 900-1000 K of  $\text{H}_2\text{O}_2$ , which accumulates after the first stage of ignition. The decreasing heat release with increasing blend fraction of  $n\text{-C}_4\text{H}_9\text{OH}$  lengthens the time for the reactive mixture to reach  $\text{H}_2\text{O}_2$  decomposition temperatures, thus lengthening  $\tau_{\text{ign}}$ . Recent work by Saisirirat *et al.*<sup>64</sup> reflect similar trends. In that work, the authors studied  $n\text{-C}_7\text{H}_{16}/n\text{-C}_4\text{H}_9\text{OH}$  blends in a homogeneous charge compression ignition engine setup, and found that the presence of  $n\text{-C}_4\text{H}_9\text{OH}$  both reduced the amount of cool flame behavior and retarded autoignition and phasing. They concluded that since the fuel mixtures were oxidized primarily by OH radicals formed from decomposition of alkylperoxy and ketoperoxy radicals, the presence of  $n\text{-C}_4\text{H}_9\text{OH}$ , which decreased the rate of production of OH radicals, slowed overall reactivity.

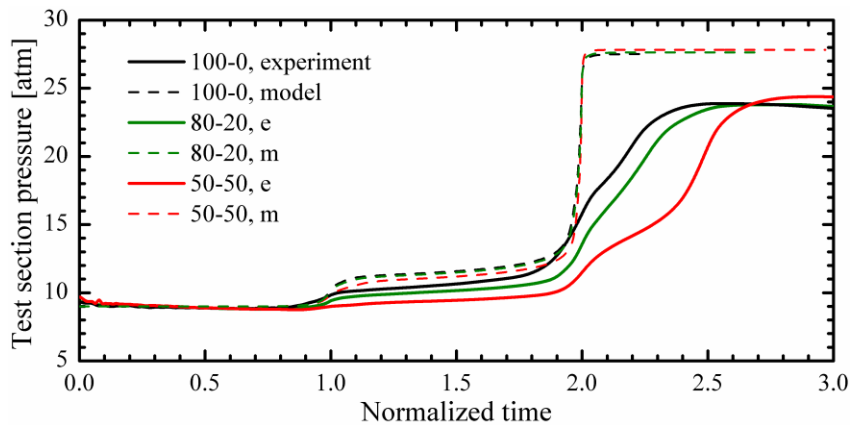


Figure 4.4 Comparison of experimental and modeling pressure time-histories for the 100-0, 80-20, and 50-50 blend cases using a normalized time domain, where 0 corresponds to EOC, 1 corresponds to the first stage of ignition, and 2 corresponds to overall ignition.

We thus observe from Table 4.1 and Figure 4.5 a nonlinear increase in  $\tau_1$  and  $\tau_{\text{ign}}$  as the amount of  $n\text{-C}_4\text{H}_9\text{OH}$  increases in the blend ratio. While the model adequately captures the increase in  $\tau_1$  and  $\tau_{\text{ign}}$  as a function of blend ratio, the model predicts smaller increases than observed experimentally. Shown also in Figure 4.5

with the thinner lines are modeling results using the Saisirirat *et al.*<sup>64</sup> mechanism, which predicts faster  $\tau_1$  and  $\tau_{\text{ign}}$  compared to the current mechanism as long as  $n\text{-C}_7\text{H}_{16}$  is present in the mixture. This mechanism will be explored in greater detail later.

Table 4.1 A comparison of experimental and predicted ignition results based on the current mechanism for first stage ignition and autoignition features.

Blend	Experiment		Current model		Saisirirat <sup>64</sup> model	
	$\tau_1$ (ms)	$\tau_{\text{ign}}$ (ms)	$\tau_1$ (ms)	$\tau_{\text{ign}}$ (ms)	$\tau_1$ (ms)	$\tau_{\text{ign}}$ (ms)
100-0	7.94	14.09	7.25	15.95	9.55	14.85
80-20	13.45	20.86	9.00	18.35	9.9	16.3
50-50	23.16	35.16	15.10	27.75	12.25	22.4
20-80	-	-	37.50	67.25	25.5	64.05
0-100	-	-	-	268		>400
% increase 80-20/100-0	69	48	24	15	4	10
% increase 50-50/100-0	190	150	110	74	28	51
% increase 20-80/100-0			420	320	170	330
% increase 0-100/100-0				1600		>2600

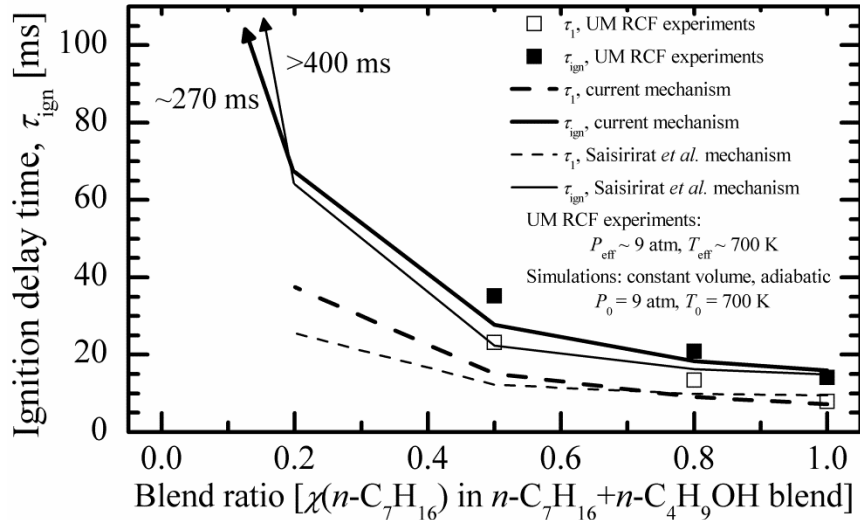


Figure 4.5 Ignition delay times as a function of blend ratio, and a comparison of the current model and a model developed by Saisirirat *et al.*<sup>64</sup>



While part of the differences between the experimental results and computational results from the current mechanism can stem from the  $n\text{-C}_7\text{H}_{16}$  submechanism, the other part potentially stems from the  $n\text{-C}_4\text{H}_9\text{OH}$  submechanism. The  $n\text{-C}_4\text{H}_9\text{OH}$  submechanism used in the current model was generated by Sarathy *et al.*<sup>66</sup>, and was validated against premixed laminar flame velocity data, speciation data from laminar flames and a jet-stirred reactor study, rapid compression machine data, and shock tube data. This submechanism, when used to simulate 100%  $n\text{-C}_4\text{H}_9\text{OH}$  ignition at  $P = 3.25$  atm,  $\phi = 1$ , and a dilution of 5.64, shows in Figure 4.6 a lower activation energy and faster  $\tau_{\text{ign}}$  when compared to previous experimental results obtained in the UM RCF<sup>34</sup>.

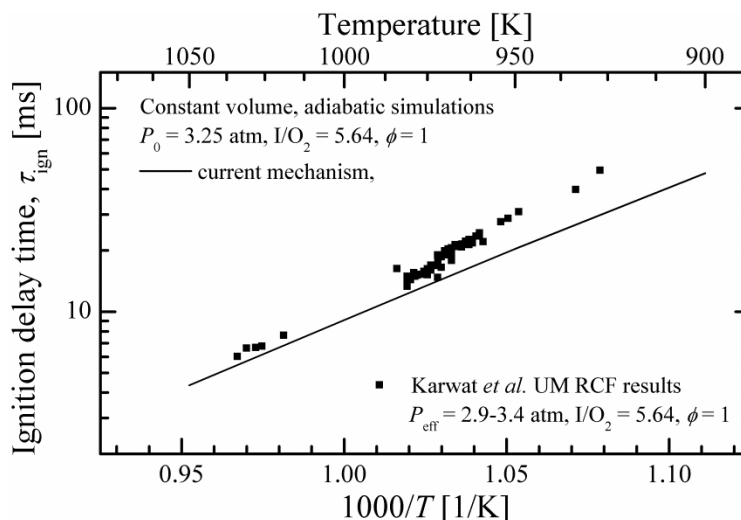


Figure 4.6 Comparison of  $n\text{-C}_4\text{H}_9\text{OH}$  submechanism performance against previous UM RCF data from Karwat *et al.*<sup>34</sup> Simulations performed with zero-dimensional, constant volume, adiabatic assumptions.

It is clear that  $n\text{-C}_7\text{H}_{16}$  reacts much more quickly than  $n\text{-C}_4\text{H}_9\text{OH}$ ; at a temperature of 700 K and a pressure of 9 atm,  $n\text{-C}_7\text{H}_{16}$  reacts almost an order of magnitude faster than  $n\text{-C}_4\text{H}_9\text{OH}$ . However, when  $n\text{-C}_4\text{H}_9\text{OH}$  is blended with  $n\text{-C}_7\text{H}_{16}$ , the low-temperature reactivity of  $n\text{-C}_7\text{H}_{16}$  forms a radical pool that stimulates  $n\text{-C}_4\text{H}_9\text{OH}$  to react at temperatures where it normally would not react. These results are similar to the conclusions observed in the JSR study by Dagaut and Togbé,<sup>59</sup> who showed the consumption of  $n\text{-C}_4\text{H}_9\text{OH}$  in the presence of  $n\text{-C}_7\text{H}_{16}$  at NTC conditions; conditions where  $n\text{-C}_4\text{H}_9\text{OH}$  would not normally react.



Furthermore, the amount of  $n\text{-C}_4\text{H}_9\text{OH}$  consumed was proportional to the amount of it present in the blend. For example, in an 80-20 molar blend, when the concentration of  $n\text{-C}_7\text{H}_{16}$  was four times higher than that of  $n\text{-C}_4\text{H}_9\text{OH}$ , four times more  $n\text{-C}_7\text{H}_{16}$  was consumed than  $n\text{-C}_4\text{H}_9\text{OH}$ .

The influence of  $n\text{-C}_4\text{H}_9\text{OH}$  on the chemical kinetics of blends is complicated and nuanced. In order to show the influence of the presence of  $n\text{-C}_4\text{H}_9\text{OH}$ , simulations were performed in which the  $n\text{-C}_4\text{H}_9\text{OH}$  was removed from the blends, thus leaving lean reactive mixtures of only  $n\text{-C}_7\text{H}_{16}$ . The simulation results are shown in Figure 4.3 as the 80-0 ( $\phi = 0.88$ , dark cyan dashed line) and 50-0 ( $\phi = 0.64$ , pink dashed line) mixtures. The  $\tau_1$  values for these mixtures are approximately the same, while the  $\tau_{\text{gn}}$  values increase with decreasing concentrations of  $n\text{-C}_7\text{H}_{16}$ . Interestingly, however, when compared to the respective 80-20 and 50-50 blends, the model predicts that  $n\text{-C}_4\text{H}_9\text{OH}$  not only *lengthens*  $\tau_1$ , but it also *shortens*  $\tau_{\text{gn}}$ .

Such changes in ignition behavior can arise due to the less reactive component of the fuel scavenging radicals that would otherwise act on the more reactive fuel and its fuel fragments. Mehl *et al.*<sup>24</sup> and Vanhove *et al.*<sup>67</sup> in their studies of binary blends of  $n\text{-C}_7\text{H}_{16}$  and toluene have discussed at length the radical scavenging properties of a compound like toluene that reacts on much longer timescales than  $n\text{-C}_7\text{H}_{16}$ . Like  $n\text{-C}_4\text{H}_9\text{OH}$ , toluene is a single stage fuel, and easily abstractable H-atoms on the methyl group of toluene act as a radical scavenger; suppressing the reactivity of the system. Just as has been observed experimentally in this work, when  $n\text{-C}_7\text{H}_{16}$  was mixed with toluene to create a 50-50 blend, Mehl *et al.*<sup>24</sup> observed that the two-stage behavior was maintained, with the first stage and second stages of ignition being lengthened, and a lower amount of heat released during the first stage of ignition. From their chemical kinetic mechanism, they observed that lower concentrations of  $\text{H}_2\text{O}_2$  were produced by the first stage of ignition. Since  $\text{H}_2\text{O}_2$  decomposition drives the second stage of ignition, lower concentrations of  $\text{H}_2\text{O}_2$  served to lengthen the second stage. A counteracting reaction, note Mehl *et al.*,<sup>24</sup> is the one between the less reactive benzyl and  $\text{HO}_2$  radicals, which produces more reactive benzyloxy and OH radicals. The overall effect, however, is a lengthening of the two ignition stages. Vanhove *et al.*<sup>67</sup> make similar conclusions, but note that the effect of the presence of a slowly reacting compound like toluene is more significant on other slowly reacting

compounds, such as *iso*-octane, given that toluene actually increases the activation energy of *iso*-octane ignition. In the case of toluene being blended with  $n\text{-C}_7\text{H}_{16}$ , the mixture reactivity is still driven by  $n\text{-C}_7\text{H}_{16}$ .

The chemical kinetic mechanism generated for this work, however, shows in Figure 4.7 very similar peak concentrations of key species—OH, HO<sub>2</sub>, and H<sub>2</sub>O<sub>2</sub>—for all blend ratios—100-0, 80-20, 50-50. Therefore, the consumption of radicals by  $n\text{-C}_4\text{H}_9\text{OH}$  to potentially slow the reactivity of the blend may be being balanced by radical production *through*  $n\text{-C}_4\text{H}_9\text{OH}$  consumption. This is in contrast to simulation findings of Saisirirat *et al.*,<sup>64</sup> who concluded that OH concentration *decreased* with the addition of  $n\text{-C}_4\text{H}_9\text{OH}$  to  $n\text{-C}_7\text{H}_{16}$  as compared to pure  $n\text{-C}_7\text{H}_{16}$ . They noted, however, that at low temperatures,  $n\text{-C}_4\text{H}_9\text{OH}$  did have the capacity to produce OH radicals through the decomposition of O<sub>2</sub>C<sub>4</sub>H<sub>8</sub>OH (formed by the addition of O<sub>2</sub> to the radical formed from  $n\text{-C}_4\text{H}_9\text{OH}$  through H-atom abstraction). When used to simulate the experiments of the current work, the Saisirirat *et al.*<sup>64</sup> mechanism indeed shows very similar predictions to the current mechanism. To further investigate the potential influences of  $n\text{-C}_4\text{H}_9\text{OH}$  on  $n\text{-C}_7\text{H}_{16}$  reactivity, simulations were performed for which  $n\text{-C}_4\text{H}_9\text{OH}$  was removed from the 80-20 and 50-50 blends, leaving lean  $n\text{-C}_7\text{H}_{16}$  mixtures (80-0 and 50-0, respectively) behind. The current mechanism does predict lower concentrations and slower formation before the first stage of ignition for all OH, HO<sub>2</sub> and H<sub>2</sub>O<sub>2</sub>. Speciation results for the 100-0, 80-20, and 50-50 blends shed more light on the kinetic effects of  $n\text{-C}_4\text{H}_9\text{OH}$  on  $n\text{-C}_7\text{H}_{16}$ .

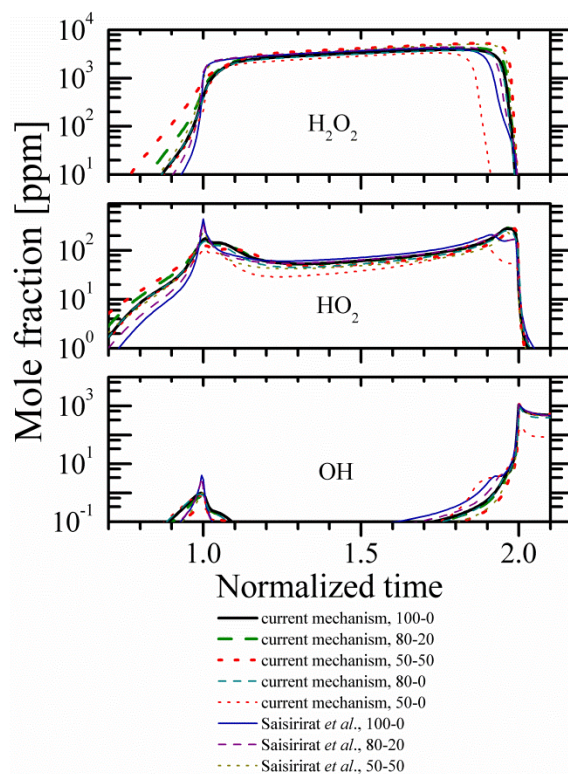


Figure 4.7 Simulation predictions of key intermediate and radical species using the current mechanism and that of Saisirirat *et al.*<sup>64</sup> for the 100-0, 80-20, and 50-50 cases.

### ***High-speed gas sampling experiments***

While the ignition studies provide an understanding of the global kinetics of ignition of  $n\text{-C}_7\text{H}_{16}$  and  $n\text{-C}_4\text{H}_9\text{OH}$  blends, speciation measurements provide more detailed understanding of the dominant chemical pathways in the reacting test gas mixture. Sampling experiments were performed to identify intermediates formed during the ignition delay time. Figure 4.8 presents results from a typical sampling experiment for an 80-20 blend, in which  $P_{\text{eff}} = 9.1$  atm,  $T_{\text{eff}} = 703$  K,  $\tau_1 = 11.98$  ms and  $\tau_{\text{ign}} = 18.44$  ms. Shown are the pressure and pressure derivative time-histories in the test section, the sampling pulse used to trigger the high-speed gas sampling system, and the pressure in the sampling chamber. Since only a very small amount of sample is removed from the reacting mixture in the test section, the pressure in the test section remains unaffected by the sampling process. All the general features seen in Figure 4.1, an ignition experiment without sampling, are identical to those seen in Figure 4.8. As indicated by the pressure rise in the sampling volume, the sample is collected within 2 ms after the falling edge of the trigger signal.

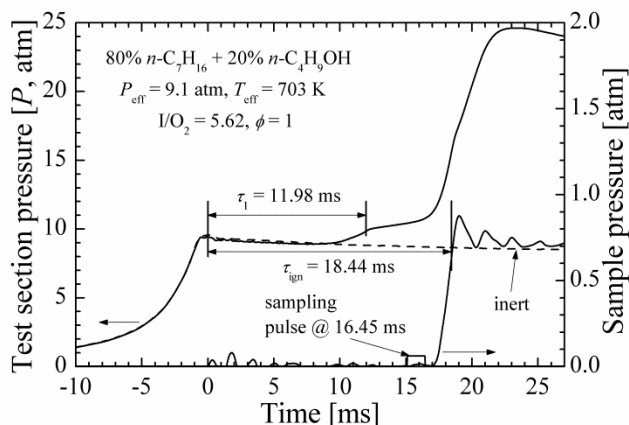


Figure 4.8 Typical results for the pressure time-histories in the test section and the sampling volume for an 80-20 sampling experiment (solid lines). The pressure time-history from a non-igniting (labeled inert) experiment is presented as the dashed line. The agreement until the first stage of ignition between the non-igniting pressure trace and the igniting pressure trace indicates the heat transfer physics of the sampling experiments are unaffected by the sampling event.

Also shown in Figure 4.8 is the time-history of a non-igniting experiment, in which the  $O_2$  of an igniting mixture is instead made with  $N_2$ . The almost identical thermal characteristics of  $O_2$  and  $N_2$  allows for direct comparison of the pressure time-histories. As seen in Figure 4.8, the bulk of the compression process in the UM RCF occurs during the last ten milliseconds before the EOC. There is always concern about possible reaction of the test gas mixture during compression, which affects the assumptions used to define the effective thermodynamic conditions (Equations 2.1 and 2.2) of the experiment. The non-igniting experiment, however, shows a nearly identical compression process to the igniting experiment, and is almost indistinguishable from the igniting experiment ( $P_{\text{eff}}$  and  $T_{\text{eff}}$  differ by less 0.3% and 0.1%, respectively) until the first stage of ignition. We conclude the heat transfer physics of the experiments remain unaffected by both the ignition events in the test section and the sampling events. Similar results are observed for the sampling experiments of 50-50 blends. Details on all of the gas-sampling experiments, including mixture compositions, can be found in Table 4.2 at the end of the chapter.

The left panels of Figure 4.9 and Figure 4.10 show the pressure time-histories for the sampling experiments for the 80-20 and 50-50 blends, respectively. All of the

experiments showed nearly identical, compression processes, and very similar pressure time-histories after EOC. The experiments showed excellent repeatability; for the 80-20 blend, the average  $P_{\text{eff}}$ ,  $T_{\text{eff}}$ ,  $\tau_1$ , and  $\tau_{\text{ign}}$  were 9.05 atm, 701 K, 13 ms, and 20.21 ms, respectively, with the corresponding standard deviations of 0.12 atm, 2 K, 0.88 ms, and 1.11 ms, respectively. For the 50-50 blend, the average  $P_{\text{eff}}$ ,  $T_{\text{eff}}$ ,  $\tau_1$ , and  $\tau_{\text{ign}}$  were 9.04 atm, 701 K, 23.28 ms, and 35.32 ms, respectively, with the corresponding standard deviations being 0.04 atm, 1 K, 1.11 ms, and 0.88 ms, respectively. The slight differences that remained in these sampling data were compensated for by plotting the pressure time-histories against a time domain that was normalized by both the first stage of ignition and the second stage of ignition, as described earlier. These results can be seen in the right panels of Figure 4.9 and Figure 4.10 for the 80-20 and 50-50 blends, respectively. The normalized pressure time-histories are virtually identical, allowing for meaningful comparisons between UM RCF experiments.

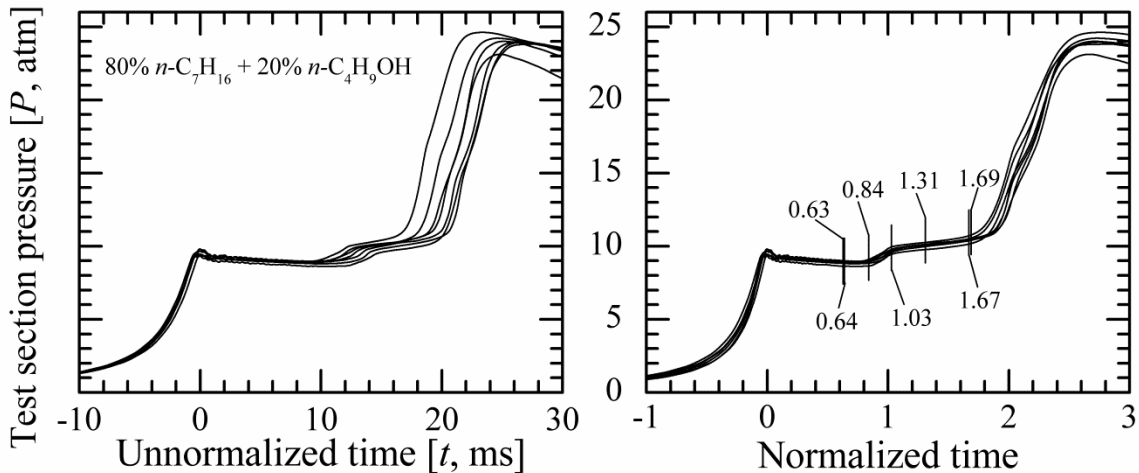


Figure 4.9 The left panel depicts the unnormalized experimental pressure time-histories of the sampling experiments for the 80-20 blend; note the level of repeatability of the compression process, as well as the first and second stages of ignition and heat release. The right panel presents the normalized data where 0 represents EOC, 1 represents the first stage of ignition, and 2 represents the second stage of ignition. Shown also are the normalized times when samples were taken from the test section.

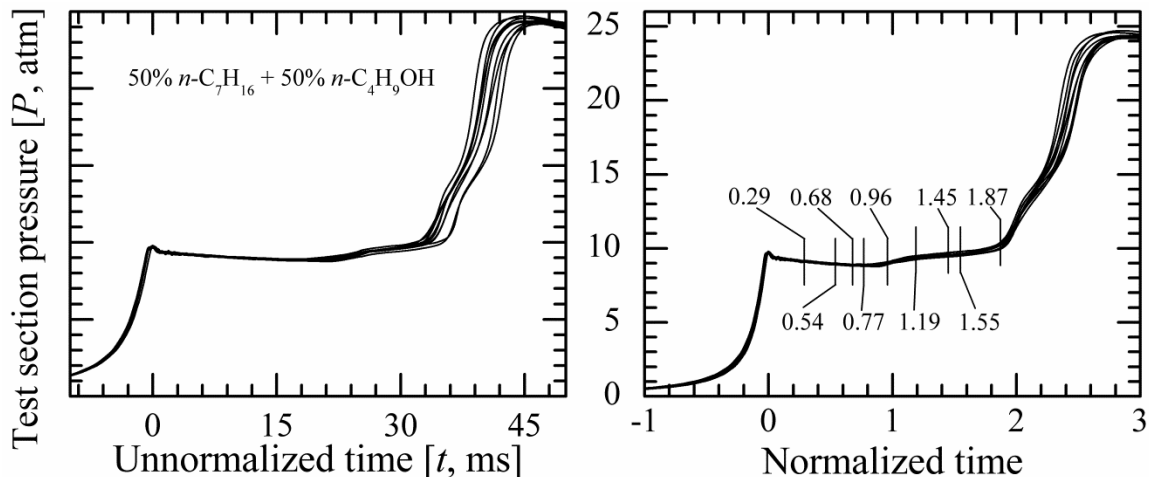


Figure 4.10 The left panel depicts the unnormalized experimental pressure time-histories of the sampling experiments for the 50-50 blend; note the level of repeatability of the compression process, as well as the first and second stages of ignition and heat release. The right panel presents the normalized data where 0 represents EOC, 1 represents the first stage of ignition, and 2 represents the second stage of ignition. Shown also are the normalized times when samples were taken from the test section.

Figure 4.11 provides an example of the chromatograms obtained from the GCs from the sampling experiment depicted in Figure 4.8. All identified species except  $C_3H_8$  and  $CO$  are identified in the chromatograms. Although several peaks remained unidentified, for the 80-20 blend, the carbon balance for the species measured was  $82 \pm 14\%$  for sampling at early times during the ignition delay period, and  $60 \pm 10\%$  for sampling closer to autoignition. The carbon balances were  $72 \pm 15\%$  and  $60 \pm 10\%$ , respectively, for the 50-50 blend. Using the calibrations for each species, the peaks were converted into discrete measurements of intermediate species for each normalized sampling time. It is worth noting that the total amount of carbon and oxygen in the system change very little as a function of blend ratio—for the 100-0 case,  $\chi(C) = 0.09401$  and  $\chi(O) = 0.2980$ ; for the 80-20 case,  $\chi(C) = 0.09455$  and  $\chi(O) = 0.3003$ ; for the 50-50 case,  $\chi(C) = 0.09526$  and  $\chi(O) = 0.3054$ .

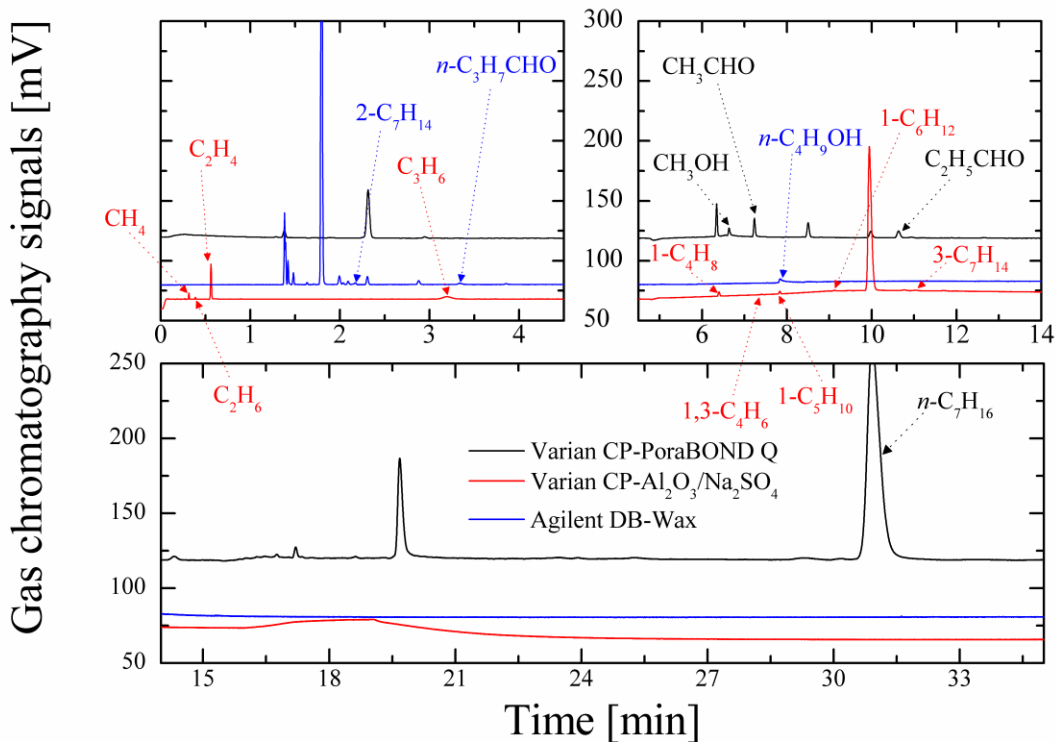


Figure 4.11 Typical gas chromatograms obtained from the three gas chromatographs. The particular data are for the experiment depicted in Figure 4.8, which was an 80-20 blend experiment with a normalized sampling time of 1.69.

Figure 4.12-Figure 4.28 present the species time-histories for the 80-20 (green squares) and 50-50 (red triangles) blends, with results for 100-0 (black circles) from Chapter 2 serving as a comparative baseline. The average experimental conditions for the 100-0 results are  $P_{\text{eff}} = 9.02$  atm,  $T_{\text{eff}} = 701$  K,  $\chi(n\text{-C}_7\text{H}_{16}) = 0.0134$ ,  $\chi(\text{O}_2) = 0.1490$ ,  $\chi(\text{N}_2) = 0.2336$ , and  $\chi(\text{CO}_2) = 0.6040$ , resulting in  $\tau_1 = 7.94$  ms and  $\tau_{\text{ign}} = 14.09$  ms with standard deviations of 0.52 ms and 0.63 ms, respectively, for the first and overall stages of ignition. The nominal conditions and ignition data for the 80-20 sampling experiments were reported above and were for an average mixture composition of  $\chi(n\text{-C}_7\text{H}_{16}) = 0.0118$ ,  $\chi(n\text{-C}_4\text{H}_9\text{OH}) = 0.0029$ ,  $\chi(\text{O}_2) = 0.1487$ ,  $\chi(\text{N}_2) = 0.2417$ , and  $\chi(\text{CO}_2) = 0.5949$ . The nominal conditions and ignition data for the 50-50 sampling experiments were also reported above and were for an average mixture composition of  $\chi(n\text{-C}_7\text{H}_{16}) = 0.0087$ ,  $\chi(n\text{-C}_4\text{H}_9\text{OH}) = 0.0087$ ,  $\chi(\text{O}_2) = 0.1484$ ,  $\chi(\text{N}_2) = 0.2580$ , and  $\chi(\text{CO}_2) = 0.5762$ . The species concentrations are plotted as a function of normalized time in which 0 represents EOC, 1 represents the first stage of ignition,

and 2 represents overall ignition. Measured concentrations for all species except  $n$ - $C_7H_{16}$  and  $n$ - $C_4H_9OH$  are plotted in two ways, each providing different information on the chemical kinetics of the mixtures. On the left-hand side, the data are plotted as absolute units of mole fraction, and on the right-hand side, the data are normalized by the initial amount of  $n$ - $C_7H_{16}$  in the mixtures. Plotted with solid black lines, dashed green lines, and dotted red lines are the corresponding zero-dimensional, constant volume, adiabatic, mechanism predictions for the average experimental conditions of the 100-0, 80-20, and 50-50 cases, respectively. The ignition results for these simulations are also included in Table 4.1.

The mechanism predictions agree well with the experimental data for some species and not for others. For all intermediate species, the model predicts an abrupt production at the first stage of ignition. While concentrations were measured to be non-zero near the time of the first stage of ignition for many species, the abruptness of the rise in concentrations was not captured experimentally. This is due at least in part to the finite amount of time required for the gas sampling valves to open and shut.

Figure 4.12 shows the data for  $n$ - $C_7H_{16}$  as a function of time. Within experimental uncertainties, each of the blend mixtures results in 30-40% of the initial  $n$ - $C_7H_{16}$  consumed during the first stage of ignition, which is approximately a factor of two less than the amount predicted computationally. (Model predictions using the Saisirirat *et al.*<sup>64</sup> mechanism, plotted in Figure 4.12, also show significant consumption at the first stage of ignition. These results will be discussed below.) The experimental and modeling results are self-consistent in that heat released during the first stage of ignition is attributed to  $n$ - $C_7H_{16}$  consumption (caused mainly due to  $n$ - $C_7H_{16}+OH$  to form  $n$ - $C_7H_{15}$  and water). Consequently, since the experiments indicate lower  $n$ - $C_7H_{16}$  consumption during the first stage of ignition, there is lower heat release during the first stage of ignition, and hence the time from first stage to autoignition increases. The converse is true of the model predictions, where more  $n$ - $C_7H_{16}$  is consumed during the first stage, yielding higher heat release and less time from first stage to autoignition. Many of the differences between the computationally predicted and experimentally measured intermediate species are due in part to the differences in consumption of  $n$ - $C_7H_{16}$  at the first stage of ignition.



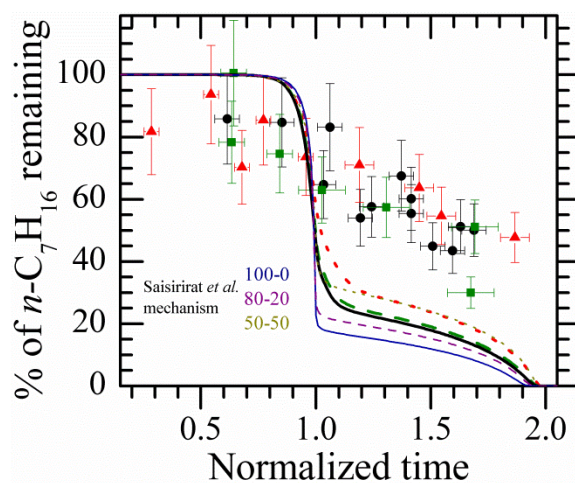


Figure 4.12 Experimental  $n\text{-C}_7\text{H}_{16}$  concentration time-histories for stoichiometric 100-0 (black circles), 80-20 (green squares), and 50-50 (red triangles) blends obtained from the UM RCF at nominal conditions of 700 K and 9 atm. Also shown are zero-dimensional, constant volume, adiabatic mechanism predictions using the current mechanism and the Saisirirat *et al.*<sup>64</sup> mechanism.

Since  $n\text{-C}_4\text{H}_9\text{OH}$  reacts only because of the presence of  $n\text{-C}_7\text{H}_{16}$  at a temperature of 700 K and a pressure of 9 atm, it follows that the amount of  $n\text{-C}_4\text{H}_9\text{OH}$  is at some level proportional to the concentration of  $n\text{-C}_7\text{H}_{16}$ . Figure 4.13 shows these trends for  $n\text{-C}_4\text{H}_9\text{OH}$ , computationally. The experimental and model results are in fairly good agreement, particularly at later times.

Also shown in Table 4.1, Figure 4.5, Figure 4.7, Figure 4.12 and Figure 4.13 are predictions using the Saisirirat *et al.*<sup>64</sup> mechanism. As observed in Table 4.1 and Figure 4.5, while the Saisirirat *et al.*<sup>64</sup> mechanism predicts slower first stages of ignition for the 100-0 and 80-20 blends, the autoignition predictions are in very good agreement (within 10-20%) with each other for cases in which  $n\text{-C}_7\text{H}_{16}$  is present in the mixture. However, key differences are observed in Figure 4.12, and Figure 4.13, which predict greater consumption of both  $n\text{-C}_7\text{H}_{16}$  and  $n\text{-C}_4\text{H}_9\text{OH}$  at the first stage of ignition. Interestingly, OH radical concentration predictions seen in Figure 4.7 show are almost identical to current mechanism predictions.

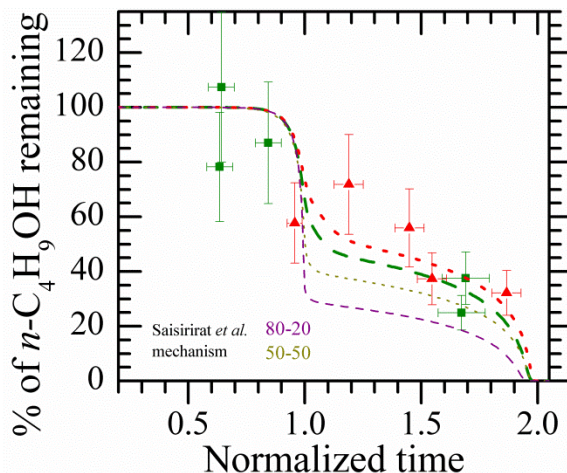


Figure 4.13 Experimental  $n\text{-C}_4\text{H}_9\text{OH}$  concentration time-histories for stoichiometric 80-20 (green squares), and 50-50 (red triangles) blends obtained from the UM RCF. Also shown are mechanism predictions using the current mechanism and the Saisirirat *et al.*<sup>64</sup> mechanism. Experimental and simulation conditions are the same as in Figure 4.12.

Figure 4.14, Figure 4.15, and Figure 4.16 show measurements and predictions for  $\text{CH}_4$ ,  $\text{C}_2\text{H}_6$ , and  $\text{C}_2\text{H}_4$ , respectively. The left-hand side (LHS) of Figure 4.14 compares the experimental and modeling data for the blends on an absolute basis. The current mechanism predicts slightly higher values for  $\text{CH}_4$  compared to the experimental data. When the data are normalized by the initial amount of  $n\text{-C}_7\text{H}_{16}$  present, as seen on the right-hand side (RHS) of Figure 4.14, it is evident that the model predictions are a function of the amount of  $n\text{-C}_7\text{H}_{16}$  in the system. Figure 4.15 shows that model predictions for  $\text{C}_2\text{H}_6$  agree well with experimental results (within less than a factor of two), and that the rate of production of  $\text{C}_2\text{H}_6$  slows as the amount of  $n\text{-C}_4\text{H}_9\text{OH}$  increases.  $\text{C}_2\text{H}_4$  concentrations are predicted within a factor of two to three of experimental results, as seen on the LHS of Figure 4.16.

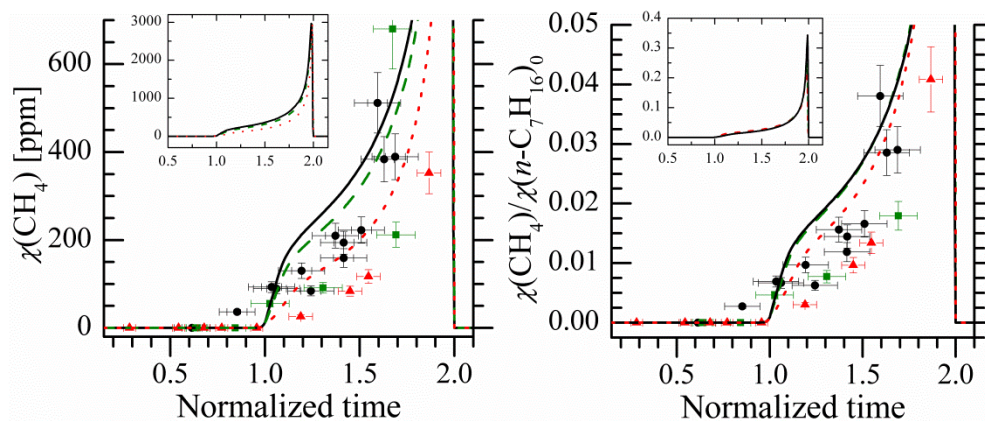


Figure 4.14 Experimental  $\text{CH}_4$  time-histories for stoichiometric 100-0 (black circles) 80-20 (green squares), and 50-50 (red triangles) blends. Also shown are predictions using the current mechanism. Experimental and simulation conditions are the same as in Figure 4.12.

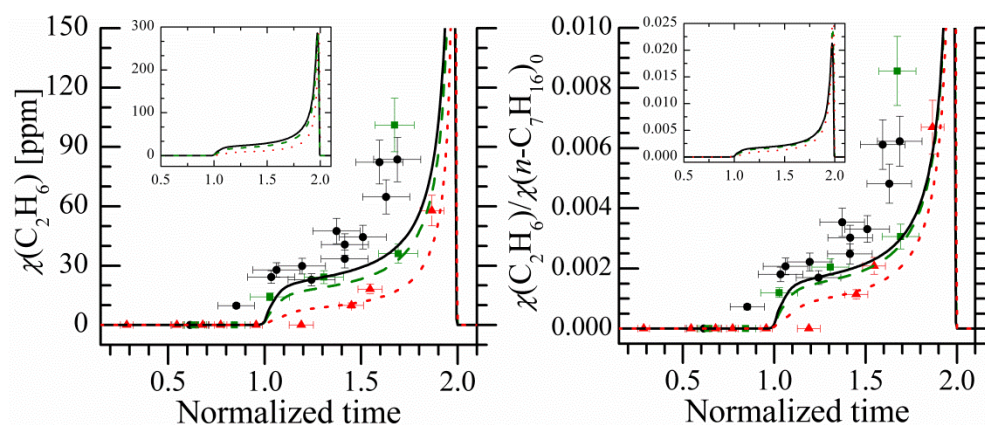


Figure 4.15 Experimental  $\text{C}_2\text{H}_6$  time-histories for stoichiometric 100-0 (black circles) 80-20 (green squares), and 50-50 (red triangles) blends. Also shown are predictions using the current mechanism. Experimental and simulation conditions are the same as in Figure 4.12.

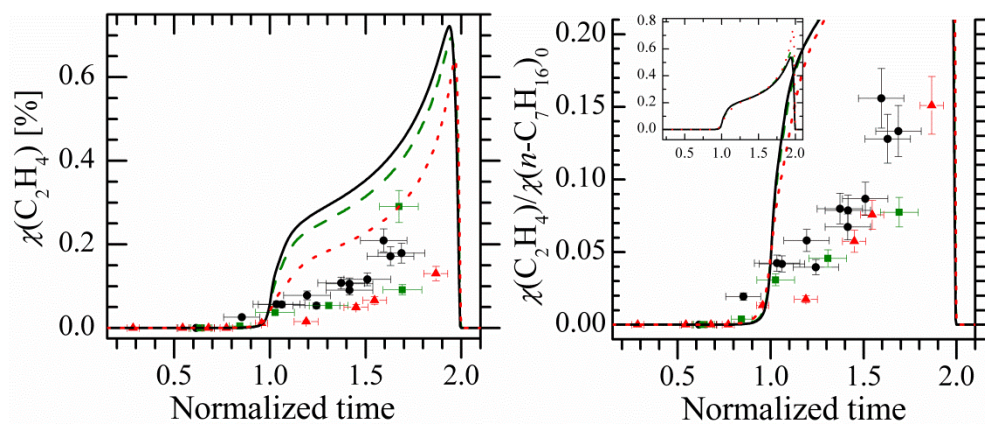


Figure 4.16 Experimental  $\text{C}_2\text{H}_4$  time-histories for stoichiometric 100-0 (black circles) 80-20 (green squares), and 50-50 (red triangles) blends. Also shown are predictions using the current mechanism. Experimental and simulation conditions are the same as in Figure 4.12.



$C_3H_8$  predictions shown in Figure 4.17 are generally in very good agreement with the experimental measurements. While the model does predict slower formation of  $C_3H_8$  with increasing  $n-C_4H_9OH$ ,  $C_3H_8$  was not observed in the experiments until much later for the 80-20 and 50-50 cases. The LHS of Figure 4.18 shows that while  $n-C_4H_9OH$  decreases the amount of  $C_3H_6$  predicted on an absolute basis,  $C_3H_6$  concentrations are predicted to increase on a per  $n-C_7H_{16}$  basis. It is observed experimentally that  $C_3H_6$  concentrations do indeed decrease with the addition of  $n-C_4H_9OH$  on an absolute basis; although the normalized experimental data do not show an increase in  $C_3H_6$  relative to the initial amount of  $n$ -heptane. The influence of  $n-C_4H_9OH$  on  $C_3H_6$  is clearer when comparing the 80-20 to the 80-0 predictions and the 50-50 to the 50-0 predictions, also presented in Figure 4.18. It is seen on the LHS of Figure 4.18, that  $n-C_4H_9OH$  not only slows the formation of  $C_3H_6$  but also slows its consumption, thereby causing an accumulation of  $C_3H_6$ . At the same time, the model predicts that  $C_3H_6$  production is enhanced relative to the amount of  $n-C_7H_{16}$  in the system.

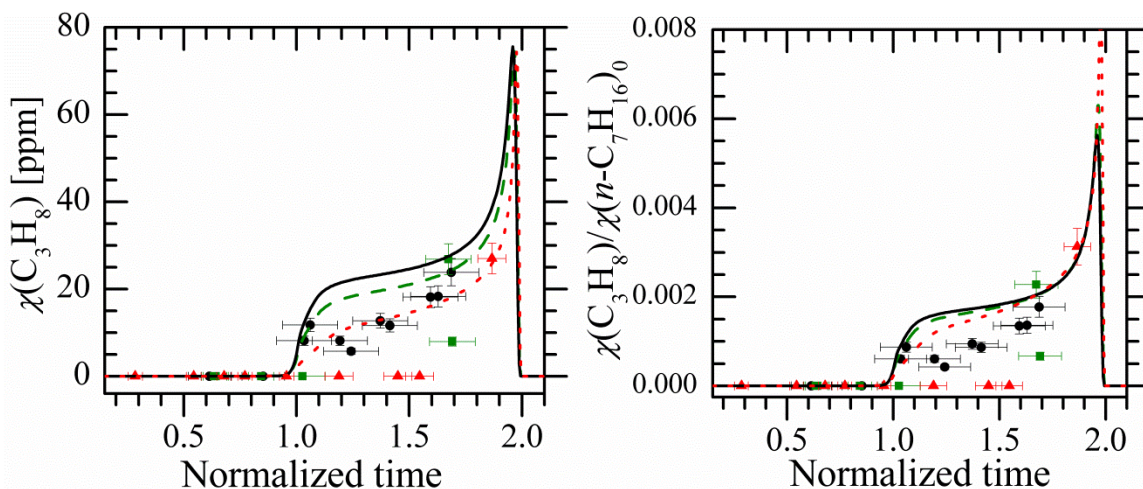


Figure 4.17 Experimental  $C_3H_8$  time-histories for stoichiometric 100-0 (black circles) 80-20 (green squares), and 50-50 (red triangles) blends. Also shown are predictions using the current mechanism. Experimental and simulation conditions are the same as in Figure 4.12.

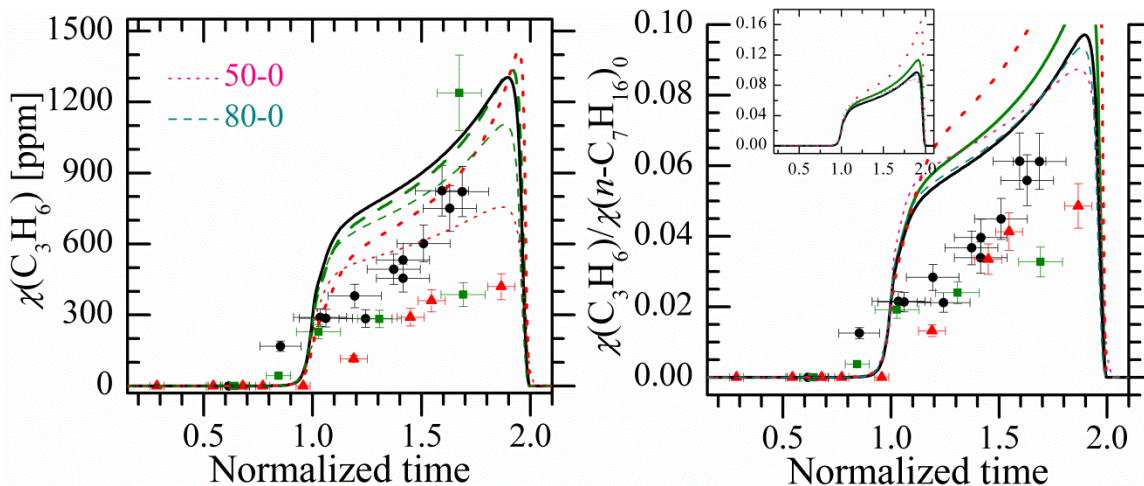


Figure 4.18 Experimental  $\text{C}_3\text{H}_6$  time-histories for stoichiometric 100-0 (black circles) 80-20 (green squares), and 50-50 (red triangles) blends. Also shown are predictions using the current mechanism, as well as mechanism predictions where the  $n\text{-C}_4\text{H}_9\text{OH}$  has been removed from the initial reactant mixture (i.e. 80-20  $\rightarrow$  80-0 and 50-50  $\rightarrow$  50-0). Experimental conditions are the same as in Figure 4.12.

Figure 4.19, which shows 1- $\text{C}_4\text{H}_8$  measurements and predictions, shows similar trends to  $\text{C}_3\text{H}_6$ . Although there are larger differences between the experimental and modeling results, the data show production of 1- $\text{C}_4\text{H}_8$  on an absolute basis decreases with the addition of  $n\text{-C}_4\text{H}_9\text{OH}$ . While it is evident that  $n\text{-C}_7\text{H}_{16}$  is the source of 1- $\text{C}_4\text{H}_8$  as seen in Figure 4.19 on the RHS, the 1- $\text{C}_4\text{H}_8$  data do not show an enhancement with the addition of  $n\text{-C}_4\text{H}_9\text{OH}$  like  $\text{C}_3\text{H}_6$ . (The 0-100 simulation, the ignition results of which are shown in Table 4.1, shows that a maximum concentration of less than 200 ppm of 1- $\text{C}_4\text{H}_8$  *right before ignition*, indicating that  $n\text{-C}_4\text{H}_9\text{OH}$  contributes very little to 1- $\text{C}_4\text{H}_8$  production during the ignition delay period.) The 1,3- $\text{C}_4\text{H}_6$  data, seen in Figure 4.20, are in good agreement with model predictions, and both experimental and modeling results show the presence of  $n\text{-C}_4\text{H}_9\text{OH}$  suppresses 1,3- $\text{C}_4\text{H}_6$  formation.

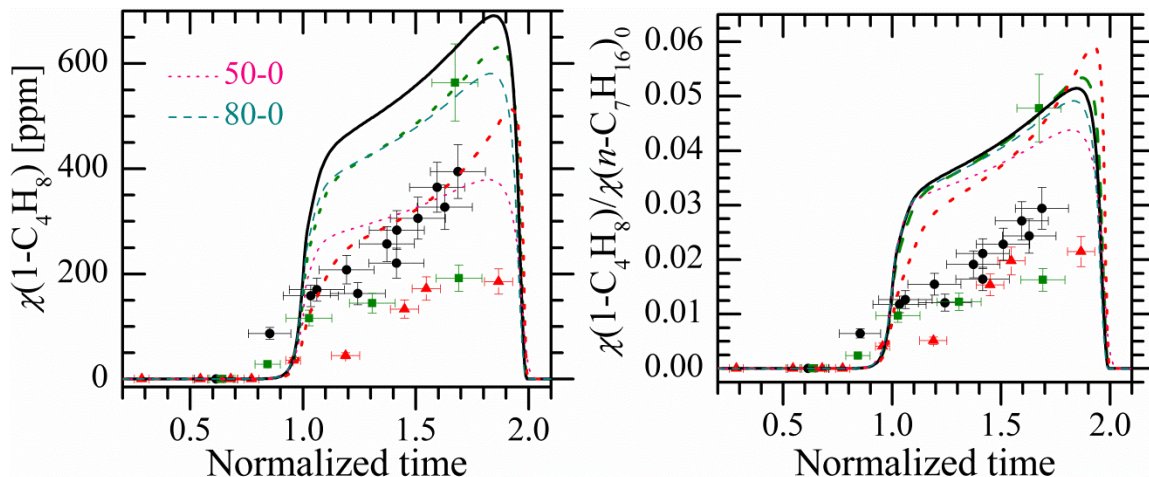


Figure 4.19 Experimental 1-C<sub>4</sub>H<sub>8</sub> time-histories for stoichiometric 100-0 (black circles) 80-20 (green squares), and 50-50 (red triangles) blends. Also shown are predictions using the current mechanism, as well as mechanism predictions where the *n*-C<sub>4</sub>H<sub>9</sub>OH has been removed from the initial reactant mixture (i.e. 80-20 → 80-0 and 50-50 → 50-0). Experimental conditions are the same as in Figure 4.12.

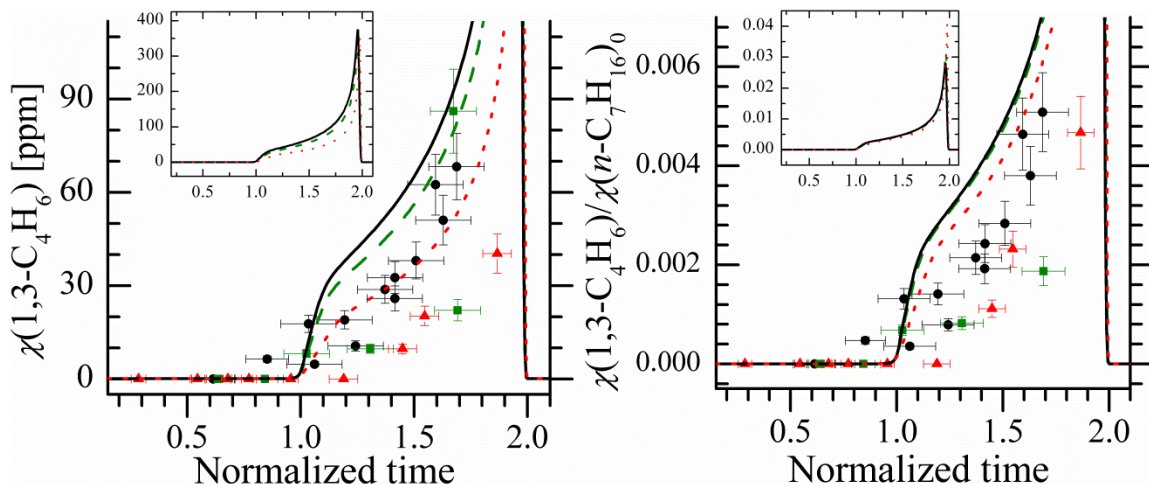


Figure 4.20 Experimental 1,3-C<sub>4</sub>H<sub>6</sub> time-histories for stoichiometric 100-0 (black circles) 80-20 (green squares), and 50-50 (red triangles) blends. Also shown are predictions using the current mechanism. Experimental and simulation conditions are the same as in Figure 4.12.

Experimental and computational results for CH<sub>3</sub>CHO are presented in Figure 22. As seen on the LHS, while the model predicts very little change in the concentration between the 100-0, 80-20, and 50-50 cases, experimental results point to a decrease in concentrations with increasing blend ratio. By comparison with the 50-0 and 80-0 simulations, the mechanism indicates the decrease in production of CH<sub>3</sub>CHO due to decreasing amounts of *n*-C<sub>7</sub>H<sub>16</sub> is offset by increasing CH<sub>3</sub>CHO



production through  $n\text{-C}_4\text{H}_9\text{OH}$  oxidation. The modeling results on the RHS of Figure 22 indicate an enhancement effect for increasing  $n\text{-C}_4\text{H}_9\text{OH}$  in the reaction mixture. However the experimental data indicate the total amount of carbon in the system dictates the concentration of  $\text{CH}_3\text{CHO}$  and  $n\text{-C}_4\text{H}_9\text{OH}$  does not enhance  $\text{CH}_3\text{CHO}$  production.

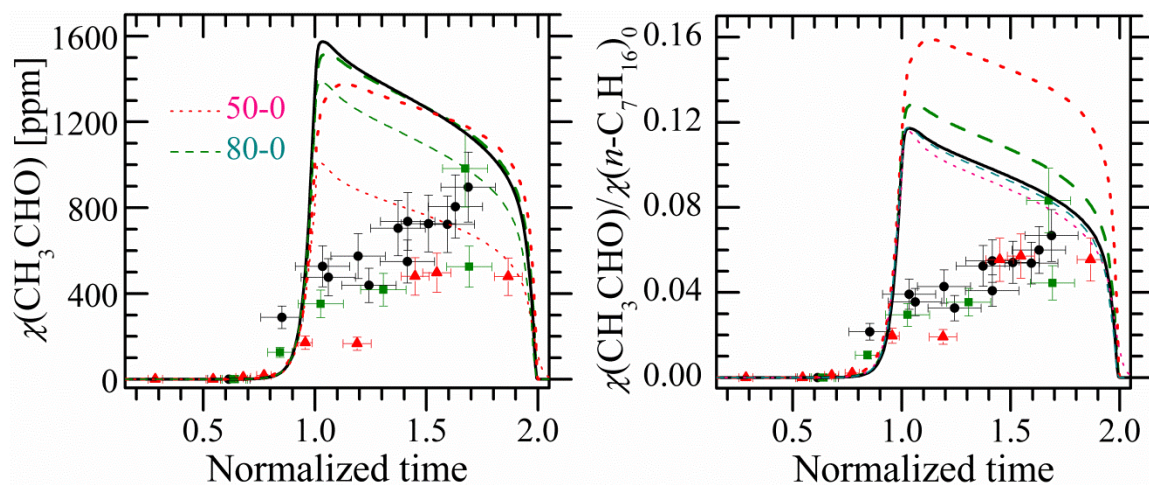


Figure 4.21 Experimental  $\text{CH}_3\text{CHO}$  time-histories for stoichiometric 100-0 (black circles) 80-20 (green squares), and 50-50 (red triangles) blends. Also shown are predictions using the current mechanism, as well as mechanism predictions where the  $n\text{-C}_4\text{H}_9\text{OH}$  has been removed from the initial reactant mixture (i.e. 80-20  $\rightarrow$  80-0 and 50-50  $\rightarrow$  50-0). Experimental conditions are the same as in Figure 4.12.

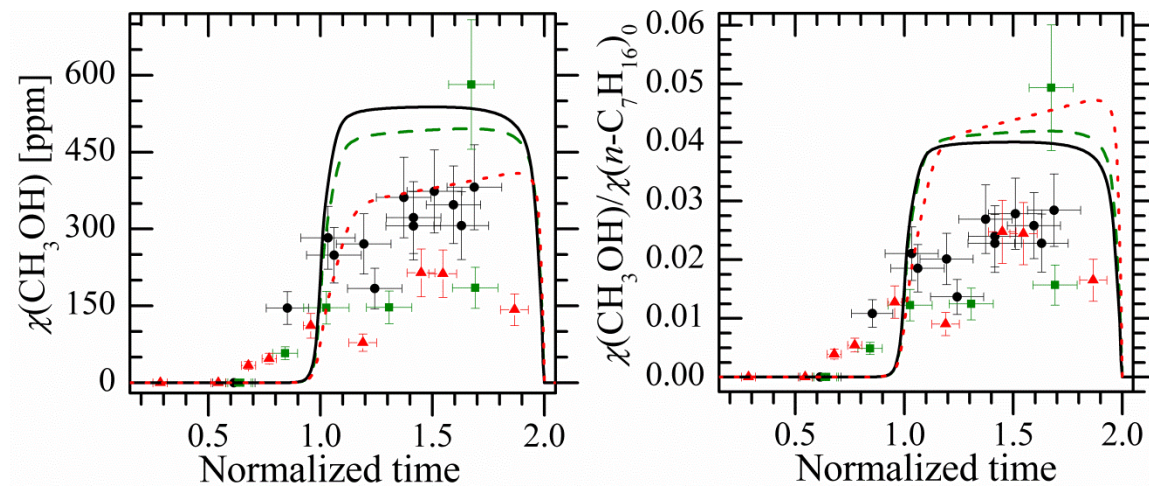


Figure 4.22 Experimental  $\text{CH}_3\text{OH}$  time-histories for stoichiometric 100-0 (black circles) 80-20 (green squares), and 50-50 (red triangles) blends. Also shown are predictions using the current mechanism. Experimental and simulation conditions are the same as in Figure 4.12

It is evident from the experimental results presented in Figure 4.22 that there is early formation of  $\text{CH}_3\text{OH}$ , prior to the first stage of ignition. The model predicts a decrease in  $\text{CH}_3\text{OH}$ , also seen experimentally, as the  $n\text{-C}_4\text{H}_9\text{OH}$  blend ratio increases. Both the experimental data and the model results in the RHS of Figure 4.22 show that  $\text{CH}_3\text{OH}$  is formed primarily from  $n\text{-C}_7\text{H}_{16}$ .

The formation of  $n\text{-C}_3\text{H}_7\text{CHO}$  is one of the key decomposition pathways of  $n\text{-C}_4\text{H}_9\text{OH}$ <sup>34</sup>. As is seen in Figure 4.23,  $n\text{-C}_3\text{H}_7\text{CHO}$  is formed earlier during the ignition delay period when  $n\text{-C}_4\text{H}_9\text{OH}$  is present in the reacting mixture. It is clear, experimentally as well as computationally, that the presence of  $n\text{-C}_4\text{H}_9\text{OH}$  increases  $n\text{-C}_3\text{H}_7\text{CHO}$  formation, as the 50-0 and 80-0 simulations show that  $n\text{-C}_3\text{H}_7\text{CHO}$  concentrations decrease compared to the 50-50 and 80-20 simulations. However, the model overpredicts  $n\text{-C}_3\text{H}_7\text{CHO}$  concentrations by an order of magnitude compared to the experimental data and indicates much larger increases in  $n\text{-C}_3\text{H}_7\text{CHO}$  with  $n\text{-C}_4\text{H}_9\text{OH}$  addition to the mixtures.

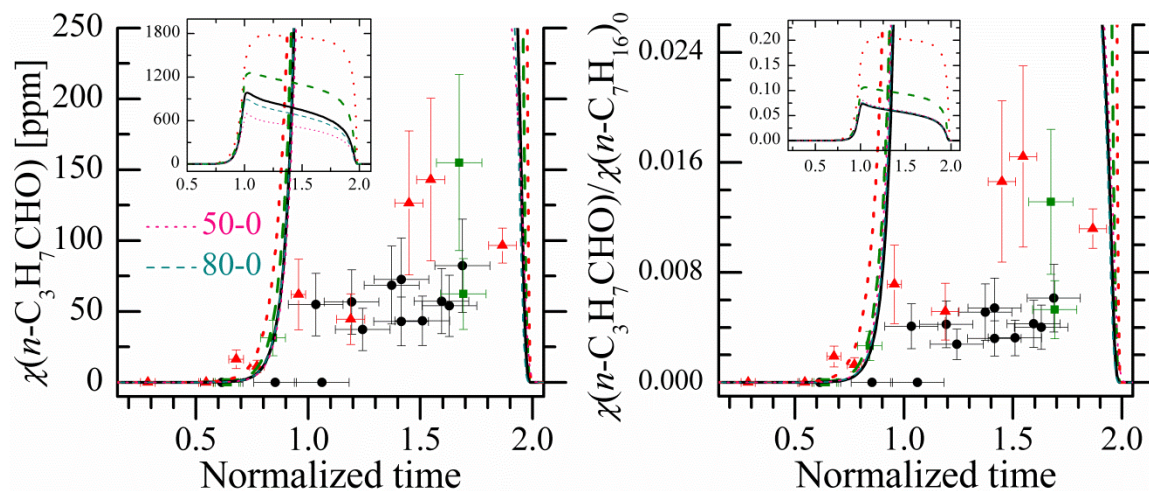


Figure 4.23 Experimental  $n\text{-C}_3\text{H}_7\text{CHO}$  time-histories for stoichiometric 100-0 (black circles) 80-20 (green squares), and 50-50 (red triangles) blends. Also shown are predictions using the current mechanism, as well as mechanism predictions where the  $n\text{-C}_4\text{H}_9\text{OH}$  has been removed from the initial reactant mixture (i.e. 80-20  $\rightarrow$  80-0 and 50-50  $\rightarrow$  50-0). Experimental conditions are the same as in Figure 4.12.

Experimental results presented in Figure 4.24 show that  $\text{CO}$  is produced at a slower rate when  $n\text{-C}_4\text{H}_9\text{OH}$  is present in the mixture. The model predicts a higher rate of production than observed experimentally; however there is good agreement



between the experimental and modeling data at later times during ignition. For CO and other species that are strongly correlated with the initial  $n\text{-C}_7\text{H}_{16}$  present in the mixture, the higher values observed from the model predictions compared to the experimental data are likely a direct result of the higher consumption rate predicted by the model for  $n\text{-C}_7\text{H}_{16}$ . As with  $n\text{-C}_7\text{H}_{16}$  consumption, the model predicts only slight differences in CO as a function of  $n\text{-C}_4\text{H}_9\text{OH}$ .

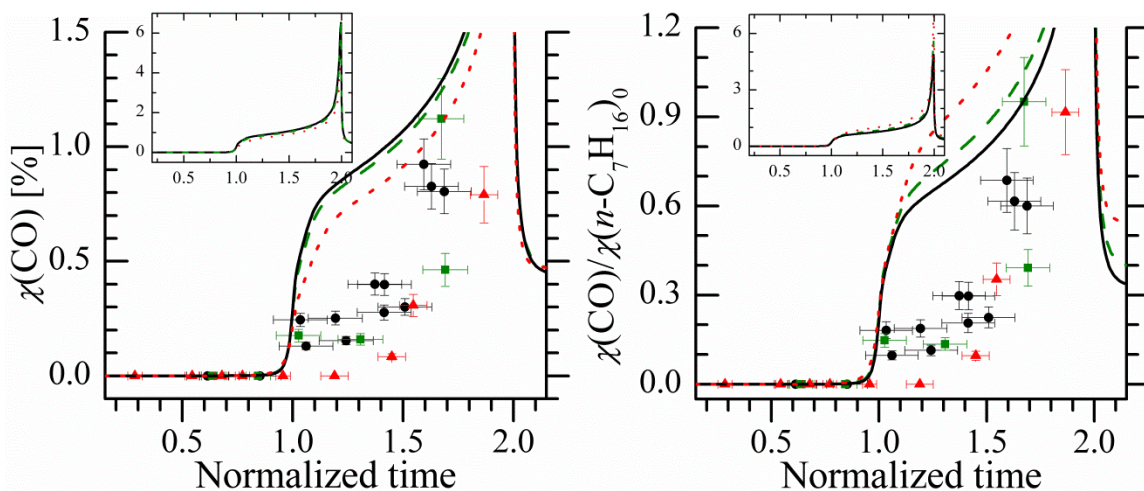


Figure 4.24 Experimental CO time-histories for stoichiometric 100-0 (black circles) 80-20 (green squares), and 50-50 (red triangles) blends. Also shown are predictions using the current mechanism. Experimental and simulation conditions are the same as in Figure 4.12.

Speciation results of smaller hydrocarbons do not provide a full understanding of how kinetics are changed with fuel blends. Indeed, the size of chemical kinetic mechanisms and the multiple and interrelated production and consumption channels of small hydrocarbons such as  $\text{CH}_4$  and  $\text{C}_2\text{H}_4$  (regardless of parent fuel) make it difficult to understand how mechanisms might be revised to more accurately represent experimental data. However, some intermediate species are only produced by one component of the fuel blend. These species shed light on how branching fractions from the parent fuel change, how global activation energies change, and how particular chemical pathways are enhanced or suppressed. The following discussion focuses on such sentinel species.

Figure 4.25 and Figure 4.26 show experimental measurements and computational predictions of the two smallest alkenes that are larger than can be

produced through  $n\text{-C}_4\text{H}_9\text{OH}$  oxidation. In Figure 4.25,  $1\text{-C}_5\text{H}_{10}$  concentrations decrease when decreased amounts of  $n\text{-C}_7\text{H}_{16}$  are present in the fuel mixture, as expected. The model predicts higher  $1\text{-C}_5\text{H}_{10}$  concentrations than the experimental data by a factor of two to three for all cases. As seen in the computational results on the LHS of Figure 4.25, comparison between the 50-0 and 50-20 simulations and the 80-0 and 80-20 simulations indicates the  $1\text{-C}_5\text{H}_{10}$  is slightly affected by the  $n\text{-C}_4\text{H}_9\text{OH}$ , even though the  $n\text{-C}_4\text{H}_9\text{OH}$  is not a direct source of  $1\text{-C}_5\text{H}_{10}$ . The RHS of Figure 4.25 interestingly highlights that even though  $n\text{-C}_4\text{H}_9\text{OH}$  does not produce  $1\text{-C}_5\text{H}_{10}$ , it reduces the amount of  $1\text{-C}_5\text{H}_{10}$  produced from the  $n\text{-C}_7\text{H}_{16}$ . Similar conclusions can be made regarding  $1\text{-C}_6\text{H}_{12}$ , the results of which are presented in Figure 4.26.

Figure 4.27 and Figure 4.28 present results for two heptane isomers. Since the  $n\text{-C}_7\text{H}_{16}$  consumption rates were much higher than observed experimentally, it is not surprising that the modeling results for  $2\text{-C}_7\text{H}_{16}$  and  $3\text{-C}_7\text{H}_{16}$  are much higher (twenty times higher for  $2\text{-C}_7\text{H}_{16}$  and a factor of 3 higher for  $3\text{-C}_7\text{H}_{16}$ ) than the experimental data. The experimental data indicate  $2\text{-C}_7\text{H}_{16}$  is suppressed by the presence of  $n\text{-C}_4\text{H}_9\text{OH}$ . Computationally, however, the opposite trends are predicted. Comparison of the 50-0 and 80-0 simulations with their 50-50 and 80-20 counterparts in Figure 4.27 shows that  $n\text{-C}_4\text{H}_9\text{OH}$  actually increases the predicted concentrations of  $2\text{-C}_7\text{H}_{16}$  from the  $n\text{-C}_7\text{H}_{16}$ . The model thus predicts a change in the branching fractions of  $n\text{-C}_7\text{H}_{16}$  decomposition with the addition of  $n\text{-C}_4\text{H}_9\text{OH}$ .

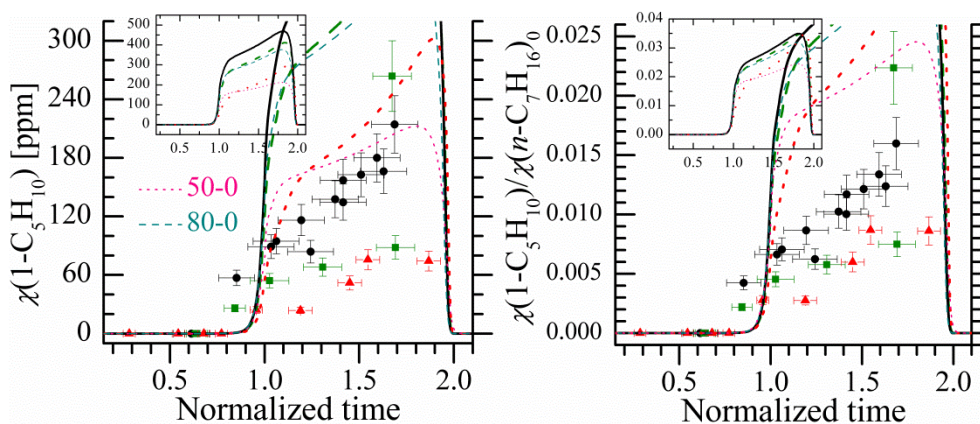


Figure 4.25 Experimental  $1\text{-C}_5\text{H}_{10}$  time-histories for stoichiometric 100-0 (black circles) 80-20 (green squares), and 50-50 (red triangles) blends. See caption of Figure 4.23 for further details.

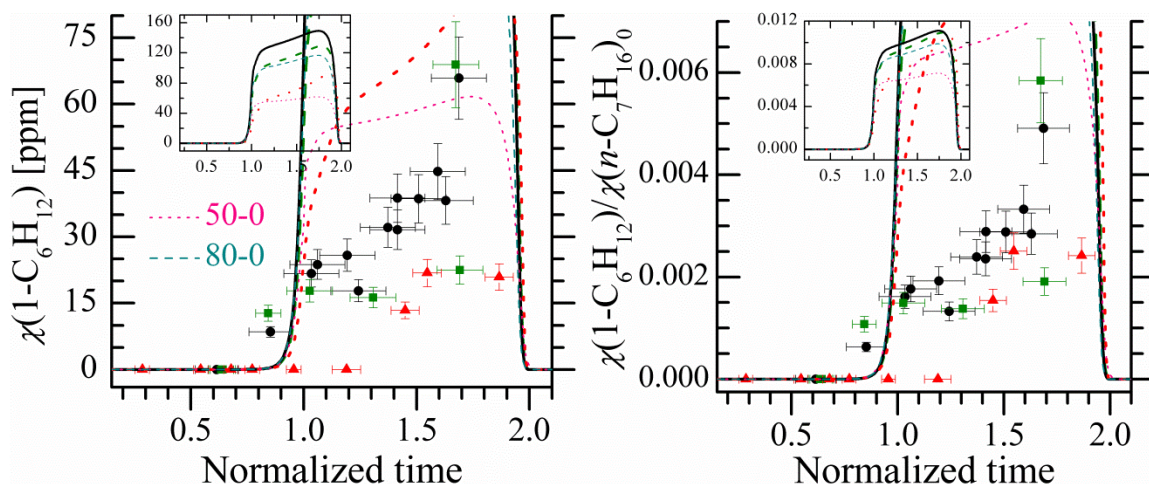


Figure 4.26 Experimental 1-C<sub>6</sub>H<sub>12</sub> time-histories for stoichiometric 100-0 (black circles) 80-20 (green squares), and 50-50 (red triangles) blends. See caption of Figure 4.23 for further details.

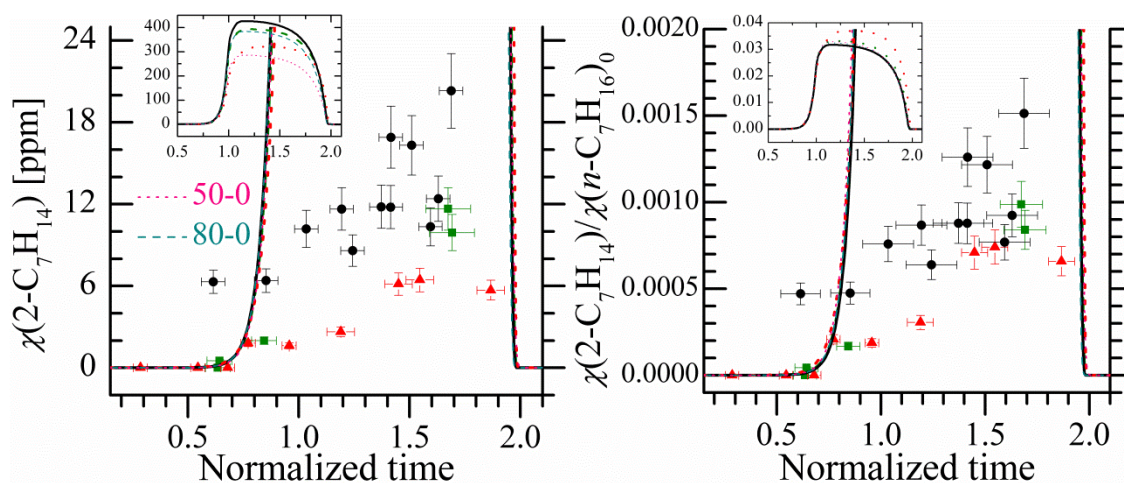


Figure 4.27 Experimental 2-C<sub>7</sub>H<sub>14</sub> time-histories for stoichiometric 100-0 (black circles) 80-20 (green squares), and 50-50 (red triangles) blends. See caption of Figure 4.23 for further details.

The experimental data for 3-C<sub>7</sub>H<sub>16</sub> were convolved with additional uncertainties compared to 2-C<sub>7</sub>H<sub>16</sub>. The 3-C<sub>7</sub>H<sub>16</sub> calibration standard was an uncertain mixture of *cis*-3-C<sub>7</sub>H<sub>16</sub> and *trans*-3-C<sub>7</sub>H<sub>16</sub> and the measured areas of these two isomers were approximately equal in the chromatograms. Consequently, 3-C<sub>7</sub>H<sub>16</sub> was quantified to within a factor of two. The upper limit of the measurements is thus represented by the open symbols in Figure 29. Predictions for 3-C<sub>7</sub>H<sub>16</sub> are on the same order of magnitude as 2-C<sub>7</sub>H<sub>16</sub> predictions.



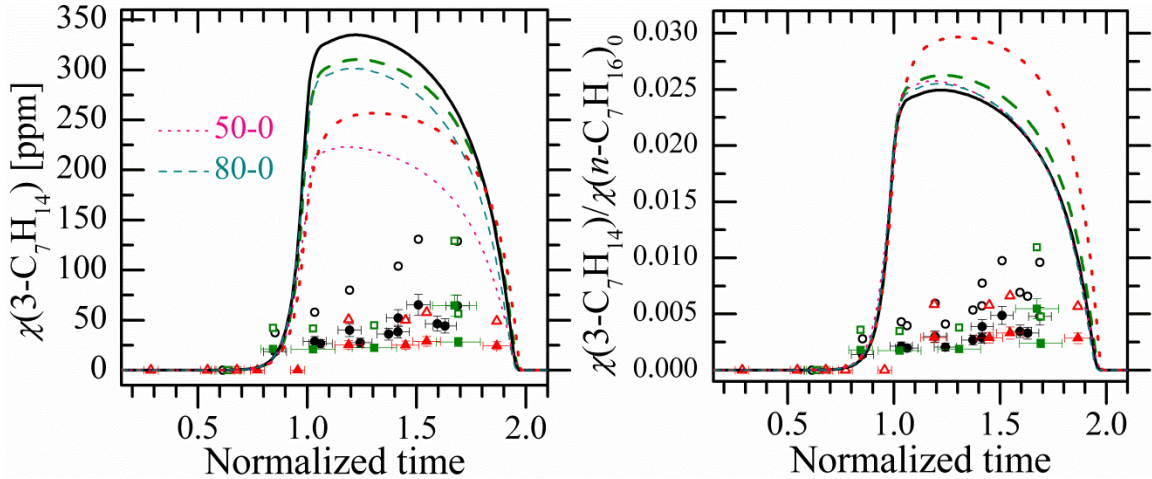


Figure 4.28 Experimental 3-C<sub>7</sub>H<sub>14</sub> time-histories for stoichiometric 100-0 (black circles) 80-20 (green squares), and 50-50 (red triangles) blends. See caption of Figure 4.23 for further details.

Radicals such as O, H, OH, and CH<sub>3</sub> can recombine when gases from the test section are sampled and quenched, potentially forming water vapor and small hydrocarbons that can interfere with species measurements by increasing the concentrations. However, predicted radical concentrations, seen in Figure 4.29, are very low (<40 ppm) until very close to autoignition. Radicals are thus not expected to be a source of error in the species concentration measurements presented in this work.

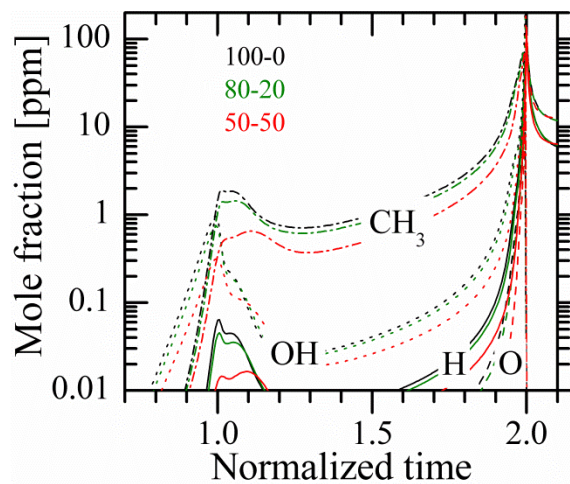


Figure 4.29 Small radical concentration predictions using the current mechanism at  $T_0 = 700$  K,  $P_0 = 9$  atm,  $\phi = 1$ , at a dilution of  $\sim 5.64$ .

## Conclusions

New speciation data have been presented on two important reference fuel compounds—*n*-heptane and *n*-butanol—at practical thermodynamic conditions of 700 K and 9 atm and at two blend ratios—80%-20% and 50%-50% by mole of *n*-heptane and *n*-butanol, respectively. When compared against 100% *n*-heptane ignition results, experimental data show that *n*-butanol slows the reactivity of *n*-heptane. Indeed, the ignition delay time of *n*-butanol is roughly an order of magnitude longer than that of *n*-heptane at 700 K and 9 atm. From a practical standpoint, this change in reactivity might require changes in jet engine design. Specifically, if the physical dimensions and pressure ratio of the compressor stages of jet engines are held constant, the flame position in the combustor will move further away from where the fuel is injected and mixed with the compressed air; and if the physical dimensions of the combustor are held constant, the pressure ratio of the compressor will need to increase to maintain the same flame location.

Speciation results of *n*-butanol concentrations show that *n*-heptane causes *n*-butanol to react at temperatures it would normally not react at under experimental conditions. Interestingly, the presence of *n*-butanol changes the measured concentrations of the large linear alkenes, particularly 1-pentene, 1-hexene, and 2-heptene. This suggests that the presence of *n*-butanol changes the fundamental chemical pathways of *n*-heptane during decomposition, for reasons unknown at this point. Smaller hydrocarbons that are formed to congruous chemical pathways regardless of parent fuel show less synergistic behavior—hydrocarbons such as ethene and propene, and smaller oxygenated hydrocarbons such as methanol and acetaldehyde, are produced at absolute levels lower than the 100% *n*-heptane case when *n*-butanol is present in the reacting mixture; however, when viewed as a function of the amount of *n*-heptane in the reacting mixture, it is observed that these small hydrocarbons are proportional to the initial amount of *n*-heptane. One may also consider the small hydrocarbon measurements to point towards a loss of memory of the parent fuel once the hydrocarbon decomposition process has reached a certain point. Yet given that the combustion environments in engines also involve the complexities of fuel mixing, turbulence, and diffusion flames, the fact that—from a chemical reaction standpoint—large alkene formation decreases with increasing

amounts of *n*-butanol suggests that *n*-butanol suppresses the production of soot precursors, thereby potentially reducing the soot formed in the inhomogeneous and fuel-rich environments of combustors. Regardless, the speciation measurements and analyses suggest that it is important to evaluate such speciation measurements in multiple ways in order to accurately assess the impact of fuel blends.

The chemical kinetic mechanism developed for this work accurately predicts trends for species such as carbon monoxide, methane, propane, 1-butene and others. However, it overpredicts the amount of *n*-heptane consumed at the first stage of ignition, and also overpredicts heptene formation during the ignition delay. It is entirely possible that changes in the reaction mechanism that both decrease the amount of *n*-heptane consumed at the first stage of ignition *and* increase the rate of consumption of heptenes would both improve the agreement of the mechanism predictions with experimental measurements for these species while maintaining the generally good agreement between ignition delay time predictions and measurements. These results inform an important part of our understanding on how bio-based and oxygenated fuels affect greenhouse gas, particulate, and toxic air pollutant formation, how the application of such fuels might require changes in practical engine design, and how to best move forward with alternative fuels policy.

## Thoughts on future work

The combustion chemistry studies of this dissertation have shed light on how the presence of *n*-butanol changes both the global reactivity of *n*-heptane and the chemical pathways taken to achieve complete combustion. However, the differences between experimental results and computational predictions raise important questions about the fundamental kinetics of such systems. One question to examine might be: Why do chemical kinetic mechanisms have the tendency to overpredict fuel consumption at the first stage of ignition of two-stage ignition fuels like *n*-heptane? This is not only a question of understanding the equilibrium between alkylperoxy formation and alkylperoxy dissociation, but also one of the temperature dependence of H-atom abstraction reactions from the parent fuel. At the same time, significant care must be taken to keep chemical kinetic mechanisms of blends at a manageable size.

*n*-Butanol *suppresses* the reactivity of *n*-heptane, but it is unclear how exactly *n*-butanol scavenges radicals produced from *n*-heptane, and to what extent. It would be interesting to better understand the makeup of the radical pool formed during the combustion of blends, and understand the influence of radical scavenging on the stable intermediate pool.

From a global reactivity standpoint, this dissertation forms the first step in understanding the influence of a bio-based fuel on the reactivity of surrogate fossil fuels. It would therefore be interesting to conduct ignition studies of chemical surrogate mixtures—made with a combination of an alkane, alkene, cycloalkane and aromatic—of complex fuel mixtures like kerosene blended with a molecule like *n*-butanol. It is important to note that the interpretation of experimental data with complex chemical kinetic mechanisms must be done in several ways to adequately understand the chemical kinetics of blends.

Studies in the UM RCF expose fuel/air mixtures to highly idealized combustion environments in which temperatures and pressures are uniform, and in which the effects of fluid mixing and stoichiometric non-uniformities are minimized. It is therefore important to study fuel blends in more applied environments, whether in automotive engines or in jet engine combustor environments.

Table 4.2 A summary of sampling experiment conditions for the 80-20 and 50-50 blend ratios. (Table 2.1 provides the same summary for the 100-0 blend.) The first row of italics for each blend ratio is the standard deviation of the column, and the second row of italics represents the standard deviation of the column

<b>Blend ratio</b>	$P_{\text{eff}}$ (atm)	$T_{\text{eff}}$ (K)	$1000/T_{\text{eff}}$ (1/K)	I/O <sub>2</sub>	$\chi(\text{C}_7)$	$\chi(n\text{-but})$	$\chi(\text{O}_2)$	$\chi(\text{N}_2)$	$\chi(\text{CO}_2)$	$\tau_1$ (ms)	$\tau_{\text{ign}}$ (ms)	sample time (ms)	normalized sampling time
80-20	8.81	698	1.43	5.62	0.01193	0.00296	0.1488	0.2372	0.5990	14.27	21.38	14.46	1.03
80-20	9.11	700	1.43	5.63	0.01180	0.00295	0.1485	0.2289	0.6077	13.50	20.89	15.77	1.31
80-20	9.17	704	1.42	5.62	0.01180	0.00295	0.1488	0.2473	0.5892	12.06	19.73	17.23	1.67
80-20	9.10	703	1.42	5.62	0.01180	0.00295	0.1488	0.2476	0.5888	11.98	18.44	16.45	1.69
80-20	9.13	701	1.43	5.62	0.01180	0.00296	0.1488	0.2470	0.5893	12.78	20.00	8.11	0.63
80-20	9.05	702	1.42	5.62	0.01185	0.00296	0.1488	0.2470	0.5894	12.61	19.54	8.1	0.64
80-20	8.97	699	1.43	5.63	0.01182	0.00295	0.1487	0.2453	0.5912	13.79	21.51	11.63	0.84
	<i>9.05</i>	<i>701</i>	<i>1.43</i>	<i>5.62</i>	<i>0.01183</i>	<i>0.00295</i>	<i>0.1487</i>	<i>0.2429</i>	<i>0.5935</i>	<i>13.00</i>	<i>20.21</i>		
	<i>0.12</i>	<i>2</i>								<i>0.88</i>	<i>1.11</i>		
50-50	9.07	700	1.43	5.62	0.00871	0.00868	0.1484	0.2570	0.5771	25.06	36.86	31.51	1.55
50-50	9.04	701	1.43	5.62	0.00870	0.00867	0.1485	0.2583	0.5758	22.38	35.07	21.41	0.96
50-50	9.04	701	1.43	5.61	0.00867	0.00867	0.1486	0.2577	0.5763	24.30	35.47	16.5	0.68
50-50	9.07	702	1.42	5.62	0.00867	0.00867	0.1485	0.2577	0.5765	22.26	34.31	12.12	0.54
50-50	9.00	699	1.43	5.62	0.00890	0.00867	0.1483	0.2577	0.5763	23.76	35.09	6.78	0.29
50-50	9.09	702	1.42	5.62	0.00863	0.00863	0.1485	0.2597	0.5745	22.47	34.47	32.87	1.87
50-50	9.04	702	1.43	5.62	0.00866	0.00863	0.1483	0.2577	0.5766	22.24	35.38	24.73	1.19
50-50	8.97	699	1.43	5.62	0.00869	0.00866	0.1484	0.2579	0.5763	24.44	36.55	18.87	0.77
50-50	9.07	702	1.42	5.62	0.00866	0.00866	0.1484	0.2582	0.5761	22.61	34.69	28.04	1.45
	<i>9.04</i>	<i>701</i>	<i>1.43</i>	<i>5.62</i>	<i>0.00867</i>	<i>0.00866</i>	<i>0.1484</i>	<i>0.2580</i>	<i>0.5762</i>	<i>23.28</i>	<i>35.32</i>		
	<i>0.04</i>	<i>1</i>								<i>1.11</i>	<i>0.88</i>		



## Chapter 5

### **“We’ve generated a lot of knowledge...but we’ve gained very little wisdom.”**

As a social and environmental activist, I wonder why we feel compelled to technologize our way out of problems—climate change is being addressed with alternative energy strategies almost exclusively; national security concerns have created an arms race; obesity caused by eating fast food can be treated with liposuction and weight-reduction pills. As I researched for this dissertation, I realized that the very stability of this economy, this society, this culture, rests on technological development, no matter what the costs to the well-being of our environment and our health. Powerful actors—state, corporate, military and university—have vested interests in promoting technological development for economic gain and maintaining national superiority, regardless of changing climates, depleting biodiversity, exacerbating poverty and weakening community resiliency. I am no anti-technologist. (I am an aerospace engineer.) But I do challenge the motives, incentives, and outcomes of technological development based on the current paradigms of thought. The goal of the remainder of the dissertation is to explore whether or not knowledge of the sociotechnical causes of large problems, such as climate change, has changed the way engineers think about what they do.

In my conversations with academics, friends, and activists about the causes of ecological degradation, climate change, and environmental injustices the usual suspects rear their heads—ignorance, perceived need, actual need, materialism, capitalism, neoliberalism, industrialism, and greed. Most people recognize (to varying degrees) the important role that technological systems play in modern societies, and their socioecological impacts. The dominant discourse around technologies, particularly among engineers, is one of technological optimism—

technologies are inherently good, the more the better—and technological determinism—technological development happens outside the sphere of human decision-making...evolutionarily, in a way. Yet, as much of the social science and humanities literature has shown, technologies are not created and do not exist in a vacuum. As historians of science and technology have demonstrated, technological development and use are guided by particular political, economic, and social motives. For example, the Accreditation Board for Engineering and Technology's guidelines for university engineering programs are set by corporations and professional organizations depending on workforce needs. The recent push to educate more students in the science, technology, engineering, and mathematics is “to make America more competitive in the global market, to create the technologies and products people will use in the 21<sup>st</sup> century”. The more technology, the better...But *why*? And to what end?

Growing up in Mumbai, I was sensitized to air pollution at a young age. I used to avoid breathing while sitting in traffic in an open air rickshaw. When I came to Michigan as an undergraduate, I learned about the politics of the environment—at the University level and the national and global levels—about the global North's (and increasingly the South's) reliance on chemicals, materials, international trade, fossil fuels, and financial engineering for agriculture, and employment. Having been exposed to and involved in the political wrangling and heated debates that issues of the environment aroused, I initially considered complementing my engineering research with non-technical research in environmental policy, law, and economics. But as the years passed, and as I conversed more and more with people of various religious, spiritual, and political backgrounds, I felt that there is something more fundamental than policy, law, and economics that is causing the problems we face. I felt that it is the very way we choose to live, as individuals, and as a collective, that is problematic.

The cognitive dissonance around us and promoted by us is striking—we envision infinite material growth on a finite planet; we want new gadgets when the old ones work fine; we promote peace through militarism in a gun-toting culture; increased waste is the first thing accompanying increased production; we hear rhetoric of democracy and justice that takes the moral high ground, while year after year international climate negotiations fail and small island nations, densely populated

coastal regions, and traditional homelands of Alaskans are quickly being lost to the rising sea. These problems are, in my mind, much deeper and more challenging than policy, law, and economic questions; they are spiritual, moral, ethical. Most policy solutions tinker with the problematic paradigm. Ethical explorations uncover unsustainable foundations with the aim to radically re-envision the paradigm.

As I conducted this experimental work over the past few years, I asked myself: Will technologies like biofuels meaningfully address climate change? Part of me thinks that biofuels do matter, for there will never be a world without combustion. But most of me thinks that it is the way we *choose* to live with these technologies and *what we do with them* matters more. A new paradigm requires deeper thought and reflexive action founded on principles of peace and harmony with ourselves and with the Earth, distributive and procedural justice for the oppressed, and long-term ecological sustainability.

We have never before had such a good understanding of human impact on the environment as we do today. Yet as my friend Graham Brown, an environmental activist and businessman, told me, “We’ve generated a lot of knowledge in the past two hundred years, but we’ve gained very little wisdom.” Have we reflected on and learned from our technological escapades so far? Or are new technologies, even “green” technologies in response to climate change, such as biofuels, just another turn of the technological crank? Do engineers think any differently about what they do given all of this knowledge of how technologies cause ecological degradation? If not, what might this mean? What ought to be done? These are normative questions, quite different from the positivist, empirical questions explored in the earlier chapters. Many technicians and scientists have so far chosen to leave these questions to the non-technicians, the non-scientists. In the next two chapters, I try to tackle these questions.

We rely on our surroundings for the materials that have built this economy and this society. Therefore, there is absolutely no way in which our economic and social fates can be disentangled from our ecological fate. It would behoove us to pause for a moment to consider the world in which we take ever greater risks—such as large-scale geoengineering projects to seed oceans with iron to generate algal blooms to absorb carbon dioxide out of the atmosphere, and massive deforestation to plant for biofuels—to solve our environmental problems. The goal of this work is to start a

culture of activist engineering—engineering that transcends the current paradigms that bind us to ecologically degrading and socially unjust outcomes.

Graham is right, but we can change.

## Chapter 6

### Is there an ecological problem that technology cannot solve?

[Engineers] are trained to be problem solvers. If you are able to describe, through interactions with other people, and frame the problem properly, generally, engineers can come up with a way to solve it.

*A senior research engineer, NASA Langley Research Center*

Engineers are good at [the] straight line. Here's the problem, here's the answer, tell me how to get there.

*Richard Altman, Commercial Aviation Alternative Fuels Initiative*

[Engineers] are very good at problem solving. Once you define a problem, they can look and see what the causes are that are creating it, and figure out ways to approach those causes to remedy [the problem]. Generally, engineers are focused on more straightforward solutions and don't get distracted with some of the social, humanistic sensitivities that are associated with the problem. They are more direct for the [technical] solution.

*Sandy Webb, Environmental Solutions, Inc.*

Problem solvers: this is the prevailing self-image of engineers. Engineers build bridges to traverse rivers, design solar panels that track the sun, and create supply chains that distribute products to where they need to be in just the right quantity. But, neither is the work of engineers solely technical, nor do engineers practice engineering in isolation—the discipline of engineering is *socially* constructed and

has social and ecological impacts. Engaging in the “people-serving profession”,<sup>1</sup> engineers work within bureaucratic contexts, be they government, corporate, or even academic. The problems engineers deal with have been framed in ways that reflect particular political motives, and social and economic goals.<sup>2</sup> According to Marx, technological development is a means to capital accumulation and the creation of a social surplus, the result of which is an ever-quickening struggle for profitable production.<sup>3</sup> In the creation of a nuclear energy dependent France, political motives and competing interests actively shaped and guided the development of different kinds of nuclear reactors, suited for the specific purposes of either electricity production or covert generation of nuclear fuel for weapons.<sup>4</sup> The division of reality into “fact” and “value”<sup>5</sup> is perpetuated in engineering education and training, with engineers trained only to deal with the former, and either actively distancing the latter or reshaping it into the former.<sup>6</sup> Furthermore, engineers are positioned within organizations and in the overall social and political order to bolster the industrial, capitalist economy. For example, recruiters from Northrup Grumman, Boeing, Schlumberger, and start-up technology companies populate the University of

---

<sup>1</sup> P. Aarne Vesilind and Alastair S. Gunn, *Engineering, Ethics, and the Environment* (Cambridge, UK: Cambridge University Press, 1998), frontmatter.

<sup>2</sup> See, for example, Langdon Winner, *Autonomous Technology* (Cambridge, MA: MIT Press, 1977). In chapter 4, Winner describes the power of scientific and technical elites and the relationship over larger masses of people that vie to make democratic claims. In chapter 6, Winner argues that in many cases, particular technologies that have *already* been developed are then applied to solve “problems” framed in ways that lend those technologies power. In this chapter, Winner also describes how and why large technical systems come to be controlled by the state. See also Lewis Mumford, *Technics and Civilization* (New York and Burlingame: Harcourt, Brace & World, Inc., 1934, 1963). In this book, Mumford describes how self-imposed limitations on Western Europe allowed the creation of “the machine” and subsequently projected it as an artifact outside of “will”.

<sup>3</sup> David Noble, *America by Design: Science, Technology, and the Rise of Corporate Capitalism* (New York, NY: Alfred A. Knopf, 1977), pp. xix, 34.

<sup>4</sup> Gabrielle Hecht, *The Radiance of France: Nuclear Power and National Identity after World War II* (Cambridge, MA: MIT Press, 1998, 2009).

<sup>5</sup> I take the definition of “fact” to be something that stems from supposedly “objective” evaluations of the world. The scientific process is, for example, a generator of facts. I take “value” to be defined as something that guides how facts are acquired, or how facts are used. The political process, the give and take among groups with competing interests, is generally believed to be guided by fact. Different groups use different facts for their own advantage, and make claims with those facts consistent with their beliefs. See, for example, Donald MacKenzie, *Inventing Accuracy: A Historical Sociology of Nuclear Missile Guidance* (Cambridge, MA: MIT Press, 1990), pp. 413-414.

<sup>6</sup> Noble, *America by Design*; also, Theodore Porter, *Trust in Numbers* (Princeton, NJ: Princeton University Press), see in particular chapters 2, 4, 5, and 7

Michigan College of Engineering Career Fair; the vast majority of young engineers are not fed to non-governmental organizations promoting social justice and peace.<sup>7</sup>

Calling engineers problem solvers paints only part of the picture. Engineers are also *socioecological experimentalists*—they invent material technologies such as computer chips that require mined minerals and metals, they build vast infrastructures such as roadways, they blow the tops off mountains to provide coal, and they do so always with limited understandings of socioecological impacts; it is practically impossible to account for all possible outcomes and effects of a technology. Technologies thus shape the world we live in, and shape our individual, social, and cultural behavior in ways expected as well as unintended.

Yet, we live in a time when information about ecological degradation—climate change, biodiversity loss, air and water pollution—caused by industrialism abounds; when the technologies and politics that cause this ecological degradation have been thoroughly researched; when we are constantly told that more information and knowledge will guide better individual choices and collective policies. As an engineer, I have therefore wondered, Has recent knowledge of ecological degradation changed the way engineers—especially those that are working on “ecological” problems, like biofuel production in response to climate change—think of ecological problems, and technology’s capacity to deal with such challenges? Are the problems engineers are given to “solve” being framed any differently than they were in the past?

I investigate these questions through two case studies, one historical and relatively localized in scope, the other contemporary and global. The first case study is a look into the past when only the scarcity of water was preventing human settlement in the untouched frontiers of the American West. This scarcity, an “environmental” problem as it was perceived at the time, allowed the federal government and engineers to embark on a mission that has left every major waterway in the West heavily dammed, with disastrous consequences. The second case study, which ties in closely with the engineering work on combustion chemistry and alternative fuels that I have studied for this dissertation, investigates

---

<sup>7</sup> Conversely, non-governmental organizations do not actively recruit new engineering graduates. Much can be said of this, but it is beyond the scope of this dissertation to detail why this is the case.

engineering responses to climate change—a spatially and temporally unbounded socioecological problem that engineering has had a major hand in creating (and at times mitigating), a problem that will cause bleaching of coral reefs, mass migrations of people living in coastal areas, and the submerging of nations such as the Maldives.

I make four conclusions in this chapter. First, engineers must view themselves as socioecological experimentalists whose actions make inherent value and political claims. For example, the decision to engineer biofuels that will cause deforestation and allow “carbon-neutral growth” of aviation values economic growth over the ecology of standing forests. Second, when in the past ecological problems were perceived as deficiencies of nature, to engineers today, ecological problems are perceived as deficiencies of technologies. In both cases, technological solutions are encouraged, and the ethics underpinning these technologies have changed very little, if at all, over the past century—ecological problems are still best resolved by technological development under the paradigms of efficiency and growth. Third, these paradigms are perpetuated in engineering education and by positioning engineers hierarchically in corporations such that problems are handed to them to solve rather than to frame. Engineers’ conceptualization of the environment makes engineers frame every problem as a technological problem requiring a technological solution. Lastly, and most importantly, these paradigms do not provide engineers with any concrete, long-term *socioecological* goals that will address the root causes of climate change, or sustainability in general. I start first with the engineering ethic towards the environment a century ago that laid the foundations of large scale damming of rivers in the United States.

### **Not wasting a drop—“conservation” through use**

The barren and arid lands of the American West presented to humans the scarcity of their most basic need—water. Thus, the human settlement and nation-building hoped for by the government in the “miserable country”<sup>8</sup> west of the Rocky Mountains required the management of water through the systematic manipulation

---

<sup>8</sup> Donald Worster, *Rivers of Empire: Water, Aridity, and the Growth of the American West* (Oxford and New York: Oxford University Press, 1985), p. 10



of the rivers. And within fifty years of the late nineteenth century, the Imperial Valley was transformed by one of the most advanced hydraulic systems in the world, which continues to be elaborately modified to this day. The technological control of water made possible not only a prosperous agriculture, but also, to a great extent, the growth of coastal cities like Los Angeles and San Francisco. Hydraulic systems made California the leading state in America, and perhaps the single most influential and powerful area in the world for its size. In the face of scarcity of water, growth and development, guised under an ethic of conservation and efficiency, were imagined and created.<sup>9</sup> Take these quotes that capture the ethic guiding the human domination of waterways:

The conquest of nature, which began with progressive control of the soil and its products, and passed to the minerals, is now extending to the waters on, above and beneath the surface. The conquest will not be complete until these waters are brought under complete control.

*W.J. McGee, Water as a Resource (1909)*<sup>10</sup>

One day, every last drop of water which drains into the whole valley of the Nile...shall be equally and amicably divided among the river people, and the Nile itself...shall perish gloriously and never reach the sea.

*Winston Churchill (1908)*<sup>11</sup>

In 1879, John Wesley Powell, an engineer and later the Director of the United State Geological Survey (USGS) from 1881-1894, published a water survey of the American West titled *Report on the Lands of the Arid Region of the United States* that made Americans aware of the possibilities and power of irrigation and damming in the American West,<sup>12</sup> and called for the planned development of water there. With the costs of building large storage dams expected to be high as well as

---

<sup>9</sup> Ibid.

<sup>10</sup> Worster, *Rivers of Empire*, p. 127

<sup>11</sup> Patrick McCully, *Silenced Rivers: The Ecology and Politics of Large Dams* (London and New York: Zed Books, enlarged and updated edition, 2001), p. 18

<sup>12</sup> David P. Billington and Donald C. Jackson, *Big Dams of the New Deal Era: A Confluence of Engineering and Politics* (Norman: University of Oklahoma Press, 2006), p. 17

technically challenging, the federal government was perceived as a savior possessing the skills and financial resources necessary to “make the desert bloom”, and to open a new era of regional growth.<sup>13</sup> In 1897, Hiram Martin Chittenden, a major in the Army Corps of Engineers, had reiterated a call for systematic development of water resources.<sup>14</sup> Empire building was the aim, said John W. Noble, the Secretary of the Interior.

I have no fear that America will grow too big. A hundred years hence these United States will be an empire, and such as the world never before saw, and such as will exist nowhere else upon the globe. In my opinion the richest portion of it, and a section fully as populous as the East, will be in the region beyond the Mississippi. All through that region, much of which is now arid and not populated, will be a population as dense as the Aztecs ever had in their palmist days in Mexico and Central America. Irrigation is the magic wand which is to bring about these great changes.

*John W. Noble, Secretary of the Interior, quoted in The Independent (1893)*<sup>15</sup>

Rivers were considered beneficial “when they yielded to humanity’s needs, whether as mechanisms of transportation or as sites for nascent towns”.<sup>16</sup> The scarcity of water was thus framed as a deficiency of nature that could be corrected through the technological development of dams. For the growth and development of the West, rivers and their tributaries had to be tamed through damming. To achieve these aims, the federal government set up the United States Reclamation Service (USRS) in 1902, which later turned into the United States Bureau of Reclamation (BuRec) in 1923. Prior to the 1920s, dams were built to control the depth of rivers to

---

<sup>13</sup> Billington and Jackson, *Big Dams of the New Deal Era*, p. 23. Also in his first message to Congress in December 1901, President Theodore Roosevelt endorsed federal support for irrigation by stressing that the construction of “great storage works...[had] been conclusively shown to be an undertaking too vast for private effort.” Roosevelt further proclaimed that “it is right for the national government to make streams and rivers of the arid region useful by engineering works for water storage as to make useful the rivers and harbors of the humid region by engineering works of a different kind”, from Roosevelt’s first annual message to Congress sent on Dec. 3, 1901, in *The Works of Theodore Roosevelt*, pp. 81-135.

<sup>14</sup> Karin Ellison, *The Making of a Multiple Purpose Dam: Engineering Culture, the U.S. Bureau of Reclamation, and Grand Coulee Dam, 1917-1942*, Ph.D. thesis, Massachusetts Institute of Technology, p. 14

<sup>15</sup> Worster, *Rivers of Empire*, introduction

<sup>16</sup> Ellison, *The Making of a Multiple Purpose Dam*, p. 41

help navigation. The chief mission of the new Bureau of Reclamation was to provide irrigation water to the arid west. The advent of long-distance electric power transmission in the late 19<sup>th</sup> and early 20<sup>th</sup> centuries brought with it another strong reason for damming—electricity generation. Around this time, citizens wanted the monopolies of private electric power providers broken, and it was believed that the government was capable of doing so. In the same period, devastating floods that periodically arose across the American landscape and across state borders instigated calls for federal dams to protect citizens and businesses from the ravages of such widespread “natural” disasters.<sup>17</sup> For these reasons, the popularity of multipurpose dams increased in the 1920s, for they could not only control flooding, but also generate hydroelectric power, provide irrigation for arid lands, and ease the navigability of rivers.

These dams had overt political purposes as well. Supporters of the USRS stipulated that it could only provide water to farms of one-hundred and sixty acres or less—the established size for homesteads under American law—to ensure that government irrigation would support small family farms. Supporters hoped that “yeoman farmers” would improve the moral fabric of the nation. Irrigated farms would provide a safety valve for the unemployed, immigrants, and other urban troublemakers, and convert them into valuable citizens for American democracy.<sup>18</sup> These political sentiments grew out of Progressive moral traditions of efficiency, improved social bonds, and anti-monopolism;<sup>19</sup> this was the Progressive “conservation” era of American politics.

When Gifford Pinchot, the Chief of the US Forest Service, named it in 1907, “conservation” was already a mainstream American ethic. Progressive conservationists, which included federal engineers and scientists,<sup>20</sup> many of whom received their degrees from the major land-grant universities and participated actively in professional societies,<sup>21</sup> made every effort to promote the ethic under the guise of national growth and strength. Time and again Pinchot pointed out that

---

<sup>17</sup> Billington and Jackson, *Big Dams of the New Deal Era*, p. 6

<sup>18</sup> Billington and Jackson, *Big Dams of the New Deal Era*, p. 8

<sup>19</sup> Ellison, *The Making of a Multiple Purpose Dam*, p. 87

<sup>20</sup> Ellison, *The Making of a Multiple Purpose Dam*, p. 103

<sup>21</sup> Ellison, *The Making of a Multiple Purpose Dam*, p. 73

conservation did not mean protecting or preserving nature.<sup>22</sup> Rather, it was overtly anthropocentric; conservation stood for the control of nature and efficient *use* of natural resources to serve the material interests of humankind with an eye to long-term needs. With the Reclamation Act of 1902, the federal government embarked on a program of irrigation development that relied on a favorite technology of conservationists—storage reservoirs. USRS engineers, especially Director Frederick Newell, promoted the idea of capturing spring floods in headwater reservoirs and putting the previously “wasted” water to constructive use.<sup>23</sup>

The Colorado River, although not large in absolute terms, flows through one of the driest regions of North America. The Colorado therefore offered possibilities for federal government-led economic development unmatched by any other water source in the arid Southwest. Control of the Colorado and its waters opened the possibilities to farm dry lands and expand the urban area of Los Angeles. Decades of political battles fought by farmers, businessmen, civic boosters, politicians, government officials, and engineers seeking to control the river revolved around the construction of large-scale storage dams to capture the flood flows of the Colorado for long-term use.<sup>24</sup>

The ambitions of the US BuRec and of the political and business interests tied to southern California were reflected in the building of the Hoover Dam, the first major storage dam on the Colorado. While the desire to protect California’s Imperial Valley from floods was the initial reason for building a large flood-control dam across the Colorado, Los Angeles civic boosters of the 1920s promoted the dam to both increase municipal water supply and feed electric power into the city’s municipally-owned electric power system.<sup>25</sup> The Hoover Dam was thus proposed as a multiple-

---

<sup>22</sup> Thus, the conservation preached by politicians and administrative officials during the Progressive Era was much different qualitatively than the environmentalism emergent in the 1960s.

<sup>23</sup> Ellison, *The Making of a Multiple Purpose Dam*, p. 110. Furthermore, in the early 20<sup>th</sup> century, people used “reclamation” to mean the process of turning desert or, much less frequently, swamp land into productive farmland, even though much of this land had never been farmland previously; there was nothing to be literally “reclaimed.” The use of the term, however, points out that Americans thought of a humid pastoral landscape as the norm and their technological interventions as an environmental return to normalcy, Ellison, *The Making of a Multiple Purpose Dam*, p. 16

<sup>24</sup> Billington and Jackson, *Big Dams of the New Deal Era*, p. 102

<sup>25</sup> Billington and Jackson, *Big Dams of the New Deal Era*, p. 107

purpose dam, which would control floods,<sup>26</sup> and provide water for irrigation, municipal uses, and the generation of electricity. The development of dams for small-scale rural settlement that was being promoted by Elwood Mead, the BuRec commissioner appointed in 1924, was supplanted by the idea of a mega dam viewed as a response to the economic conditions of the 1920s and 1930s and justified financially through the revenues from hydroelectric power generation.<sup>27</sup>

The political interests of the government, as well of federal engineers guided the design and use of the Hoover Dam. While no one disagreed on the building of Hoover Dam, there was a debate on whether a dam could serve all of its multiple purposes at once since flood control, navigation, and hydroelectric power generation rely on different capacities of a dam.<sup>28</sup> In the case of the Hoover Dam, the politics of electricity generation were pitted against those of flood control. But since electric companies were willing to pay the federal government much more money for regular electric output, engineers sought to manage water to maintain a continual hydraulic head with the potential to generate sufficient hydroelectricity. The political debates eventually ended in the 1920s by the ever-larger reservoirs that were created by larger and larger dams, allowing more flexibility for water storage—Lake Mead created by Hoover Dam was divided for its different uses. Furthermore, the development of a differential equation in 1918 demonstrated that reservoirs reduced floods, and in 1926, graphical methods were used to analyze reservoir operation.<sup>29</sup> The ability of engineers to reduce complexity to fundamental operating parameters allowed a technological “solution” to the problem of large-scale, multipurpose

---

<sup>26</sup> “to remove the *menace* (emphasis added) of flood from the Colorado River”, *Report on Problems of Imperial Valley and Vicinity* (1922), Department of the Interior, United States Reclamation Service.

<sup>27</sup> Billington and Jackson, *Big Dams of the New Deal Era*, p. 135

<sup>28</sup> See detailed descriptions of this complexity in McCully, *Silenced Rivers*; Ellison, *The Making of a Multiple Purpose Dam*; and Edward Goldsmith and Nicholas Hildyard, *The Social and Environmental Effects of Large Dams* (San Francisco: Sierra Club Books, 1984). Flood control requires empty dam reservoirs to catch all potential flood water. In contrast, for hydroelectric power generation, hydraulic head—a high column of water that stores potential energy—is necessary. Navigation and electric power generation, however, could go hand-in-hand. Navigation required uniform channel depths, and this requirement was achieved by reducing high water in the reservoir, and storing water in the reservoir during low periods – the same requirements of electric power generation. Irrigation of land adds another layer of complexity to the use of stored water. For irrigation, water is stored during spring, and then released over the course of the agricultural season.

<sup>29</sup> Robert Horton, “Determining the regulating effect of a storage reservoir,” *Engineering news-record* 81, 5 September 1918 and Melvin Casler, “Operation of river regulating reservoirs,” *Engineering news-record* 96, 20 May 1926.

damming, opening up the possibility of having full control over river water—not a drop “would be wasted”.

Politics, science, and technology formed a seamless web called “conservation”, which was founded on efficiency and growth through the correction of perceived deficiencies of nature. In addition to politicians and engineers wanting to dam rivers, advocates of conservation also influenced and guided the practices of forestry, agrostology, geology, and anthropology.<sup>30</sup> Conservation leaders were very active in professional circles in the national capital, and influenced federal “resource” policy with their ideals and practices.<sup>31</sup> Says Samuel Hays,

[l]oyalty to these professional ideals, [and] not close association with the grass-roots public, set the tone of the Theodore Roosevelt conservation movement. The idea of efficiency drew these federal scientists from resource task to another, from specific programs to comprehensive concepts. It molded the policies they proposed, their administrative techniques, and their relations with Congress and the public. It is from the vantage point of applied science, rather than of democratic protest, that one must understand the historic role of the conservation movement... The new realms of science and technology, appearing to open up unlimited opportunities for human achievement, filled conservation leaders with intense optimism. They emphasized expansion, not retrenchment; possibilities, not limitations. True, they expressed some fear that diminishing resources would create critical shortages in the future. But they were not Malthusian prophets of despair and gloom. The popular view that in a fit of pessimism they withdrew vast areas of the public lands from present use for future development does not stand examination. In fact, they bitterly opposed those who sought to withdraw resources from commercial development. They displayed that deep sense of hope which pervaded all those at the turn of the century for whom science and technology were revealing visions of an abundant future.<sup>32</sup>

---

<sup>30</sup> See, for example, Charles Wohlforth, *Conservation and Eugenics*, in *Orion*, July/August 2010.

<sup>31</sup> Samuel P. Hays, *Conservation and The Gospel of Efficiency: The Progressive Conservation Movement, 1890-1920* (Cambridge, MA: Harvard University Press, 1959), p. 2

<sup>32</sup> *Ibid.*

An engineering approach was thus applied to solve the problem of water scarcity, and those with technical expertise—foresters, hydraulic engineers, agronomists—argued that they—not politicians—would be best suited to deal with decisions about the desirable annual timber cut, the feasible extent of multiple-purpose river development and the specific location of reservoirs, the forage areas that could remain open for grazing without undue damage to water supplies.<sup>33</sup> These technologists promoted a decision-making system in which the expert would decide how everything from water to wood ought to be used. This system was considered to be objective and rational, and superior to the give-and-take of politics. The separation of the “facts” of how to use materials from the “values” undergirding that use lent federal engineers an air of authority.<sup>34</sup> Yet this technical expertise has proven to be myopic and narrow.

The Hoover Dam was closed in 1936. It was designed to store a truly massive amount of water—forty-one and a half billion tons—behind it. But while the size of Lake Mead allowed the apportioning of water for different purposes, the surface area of the “reservoir” also allowed the evaporation of twenty-five thousand gallons of water *each second*, equaling seven percent of the reservoir’s capacity over a year.<sup>35</sup> What engineers further failed to account for during the planning was how the almost stagnant weight of the water would affect the Earth’s malleable crust. At 12:44 pm on Thursday, May 4, 1939, a powerful earthquake (5.0 on the Richter scale) released its energy between Boulder City and Las Vegas, with tremors felt from Los Angeles to Phoenix and as far south as Mexico, tumbling chimneys, buckling roads, and raising eerie clouds of dust on the open range. Aftershocks and quakes of similar magnitudes continued in the following days. The region was traditionally not seismically active, and there was no anecdotal evidence of earthquakes in the area. Over the next ten years, seismographs recorded more than six hundred quakes within a few miles of the reservoir, many of them occurring along previously undetected fault lines crossing the lake bed. Engineers later

---

<sup>33</sup> Hays, *Conservation and The Gospel of Efficiency*, p. 3

<sup>34</sup> Hays, *Conservation and The Gospel of Efficiency*, preface

<sup>35</sup> Michael Hiltzik, *Colossus: Hoover Dam and the Making of the American Century* (New York: Free Press, 2010), p. 385

realized that these quakes were associated not with peak water levels, but rather with rapid changes in the lake during seasonal filling and draining. The only option left to engineers consistent with their ethic was to better moderate the flow in and out of Lake Mead...through the construction of Glen Canyon Dam and the impoundment of Lake Powell.<sup>36</sup>

The optimism that filled hydrologists by “the age of abundance”—a twenty-year wet period beginning in the mid-1960s—has left virtually every possible dam site on the Colorado occupied by a man-made structure, making it the most heavily dammed river in the Western Hemisphere. After the illusion of the abundance of water served to attract more than thirty-three million people to live in the Colorado River’s watershed, it was realized that more than sixty-two million acre-feet of storage capacity now existed on a river that produced an average of less than fourteen million acre-feet a year, with twenty percent of that water being lost each year to evaporation from storage reservoirs.<sup>37</sup> Putting these vast numbers into perspective, Michael Hiltzik notes that “[i]n the desert reservoirs of Lake Mead and Lake Powell, enough water disappear[s] into the arid skies on a single weekend to serve the domestic needs of seventeen thousand households for a year.” This evaporation increases the salinity of the water left behind; evaporation of water at Lake Mead and Lake Powell have increased the salinity of the Colorado River by 100 milligrams per liter.<sup>38</sup> With the illusion of abundance also came waste. In the US today, half of the water used in agriculture is lost to overwatering and seepage.<sup>39</sup> Further studies of multipurpose dams from around the world have shown that dams have not been able to serve all of their purposes at once.

Dam building in the Western world peaked in the 1970s and has been on the decline since, for several reasons. Of course, extensive damming has left most all rivers dammed already. Yet the visually stunning nature of dams has created a correspondingly strong anti-dam activist movement. The highly localized and immediate effects of dams—the displacement of peoples and the immediate

---

<sup>36</sup> Hiltzik, *Colossus*, p. 386

<sup>37</sup> The Colorado River is no longer “wasted”. It has been dammed so conclusively that at times, it no longer reaches the ocean.

<sup>38</sup> Hiltzik, *Colossus*, pp. 385-386

<sup>39</sup> Goldsmith and Hildyard, *The Social and Environmental Effects of Large Dams*, p. 66



destruction of ecosystems—thus provide a strong locus for rallying. Anti-dam environmentalists have argued that water impoundments and clear cuts have infringed not only on the rights of people to experience and enjoy nature, but have also infringed on the rights of nature itself.<sup>40</sup>

### **Hindsight is not 20/20**

Even in the 1970s, *after* the emergence of clear evidence showing the ill effects of large dams, vested interests glorified dams and their abilities to “perfect” nature. Gilbert G. Stamm, a former commissioner for the BuRec told a congressional committee in 1975 that,

Water resource projects have many *positive* (emphasis added) environmental effects. When water management practices regulate and augment low flows of rivers and streams, decrease erosion, prevent floods, eliminate waste of water, and in many instances change deserts into gardens where many can comfortably live and prosper, the result is betterment of environmental conditions.<sup>41</sup>

Similarly, in a 1977 publication, the US Army Corps of Engineers said that by building dams, it aimed

to preserve the unique and important ecological, aesthetic and cultural values of our national heritage; to conserve and use wisely the natural resources of our nation for the benefit of present and future generations; to restore, maintain and enhance the natural and man-made environment in terms of productivity, variety, spaciousness, beauty and other measures of quality...and to create new opportunities for the American people to enjoy the environment and the use of natural resources.<sup>42</sup>

---

<sup>40</sup> See, for example, *The San Francisco Declaration of the International Rivers Network* in McCully, *Silenced Rivers*, pp. 313-314.

<sup>41</sup> Goldsmith and Hildyard, *The Social and Environmental Effects of Large Dams*, pp. 5-6

<sup>42</sup> *Ibid.*

While dam building in the West has slowed with dams being decommissioned, dam building is surging in the “industrializing world”; it is clear that the lessons from dam building in the industrialized world have not been learned. More directly, beginning in the post-World War II period, dam construction projects have been promoted by the industrialized world in formerly colonized zones.<sup>43</sup> In addition to optimistic projections of benefits, skewed economics have been used to advocate for large dams, and large multinational corporations and international “development” banks have continually financed such dams—these organizations and elite individuals are the largest beneficiaries of dam building. “A reservoir is a man’s triumph over nature,” said S.H.C. de Silva, consultant to the Irrigation Department of Sri Lanka, “and the sight of a vast sheet of water brings an inner satisfaction to those who behold.”<sup>44</sup> Such statements nonchalantly gloss over the myriad of localized socioecological impacts—especially on the impoverished—of large infrastructural projects such as dams. Little of the food grown through the dam-irrigation schemes goes to those who need the food most. Millions of people are continually uprooted and forcefully resettled from their traditional lands to make way for dam reservoirs, with the added blows of earthquakes, increased water-borne diseases, decreased water quality, release of greenhouse gases, salinization of fertile agricultural lands, changing microclimates, loss of wildlife and estuaries, and the loss of silt and fertility downstream of dams.<sup>45</sup> Floods have also not been adequately controlled; on the contrary, the severity of flood damage has increased, just as the Hoover Dam increased flood severity on the Colorado River.

At the beginning of the 20<sup>th</sup> century, the framework of conservation, founded on efficiency and growth, morphed the scarcity of water in the American West into a deficiency of nature. This deficiency provided a reason to develop large technological infrastructures that gave the federal government experience with hydraulic engineering, and allowed the breaking of monopolies, the provision of electricity, the navigability of rivers, and the irrigation of desert and arid lands. Today, dams are

---

<sup>43</sup> See Nick Cullather, “Damming Afghanistan: Modernization in a Buffer State”, *The Journal of American History*, Vol. 89, No. 2 (September 2002), pp. 512-537; and Allen Isaacman, “Displaced People, Displaced Energy, and Displaced Memories: the Case of Cahora Bassa”, *International Journal of African Historical Studies*, Vol. 38, No. 2 (2005), pp. 201-238.

<sup>44</sup> McCully, *Silenced Rivers*, p. 11

<sup>45</sup> McCully, *Silenced Rivers*, xxxviii

disingenuously being promoted as ecologically-friendly ways of dealing with climate change, and they continue to be a harsh reality in the industrializing world.

Given all of this knowledge and understanding of the complex and global socioecological problems—such as climate change, topsoil loss, air and water pollution, *unsustainability*—of large-scale technologies, has the paradigm under which engineering and technical development is conducted changed? In what ways do contemporary engineers frame these socioecological problems? Are technologies to blame? Are they the cure? Biofuels, as a response to climate change and energy security concerns, provide a great case study to investigate contemporary engineering ecological ethics and decision-making. Biofuels are widely used today, particularly in automotive transportation in countries like the United States and Brazil. As someone studying the combustion chemistry of these fuels, I was curious to see how this technology that is being framed as a response to climate change is actually being developed.

For the status quo of large industrialism and capitalism, climate change represents a new opportunity to develop technologies that stabilize a particular technopolitical order—of the revolving doors between big oil and government, of large transportation infrastructures that guarantee economic growth. Responses to this framing might include what Princen calls “end-of-pipe”—the problem isn’t what behavior causes climate change, rather, it is carbon dioxide, and it is the carbon dioxide that must be dealt with through advanced energy solutions.<sup>46</sup> Yet in reality, climate change represents a vastly different kind of ecological problem, unbounded in space and time—“global” warming (a misleading characterization of climate change) is likely to show its full effects over the coming century and beyond.<sup>47</sup> As a fundamentally different and new kind of problem, dealing with it demands a new spirit of socio-technical interaction.<sup>48</sup> For contemporary engineers engaging in technical development, does climate change represent such a new problem? Or do

---

<sup>46</sup> See Thomas Princen, “Leave it in the Ground: The Politics and Ethics of Fossil Fuels and Global Disruption”, International Studies Association international conference, Montréal, March 16-19, 2011

<sup>47</sup> Beck, *Risk Society*, p. 2; For detailed descriptions of the nature of climate change, see also Thomas Princen, “A Sustainability Ethic” in *Handbook of Global Environmental Politics* (Cheltenham, UK: Edward Elgar, 2012), pp. 466-479; and Rob Nixon, *Slow Violence and the Environmentalism of the Poor* (Cambridge, MA: Harvard University Press, 2011), pp. 2-3, 266.

<sup>48</sup> Hans Jonas, *The Imperative of Responsibility: In Search of an Ethics for the Technological Age* (Chicago: University of Chicago Press, 1984)

engineers work in existing paradigms of thought and technopolitical regimes<sup>49</sup> to address it?

**“You know, I don’t have any data. I can’t advise a decision now.”**

Last October, I made my way to Montréal to attend the third Sustainable Alternative Fuels in Aviation Workshop at the headquarters of the International Civil Aviation Organisation (ICAO, which is the UN body that oversees international aviation), and to understand how practicing engineers think about the relationships between their work, technology, and the burgeoning challenges of climate change. The engineers I interviewed there seemed to think of engineering work as purely technical—the socioecological aspects and political implications of their work were left to be evaluated by politicians, lawyers, and business people. The seamless web of the political and technical was recast into the spheres of the *political* and the *technical* through the division of labour, and through the conceptualization of the technical as “fact” and the political as “value”.<sup>50</sup> Take, for example, this quote from Dr. Lourdes Maurice, the Chief Scientist for Energy and Environment at the Federal Aviation Administration:

[L]ast week, I was having a conversation with somebody about the [carbon dioxide] standard for [aviation], and [an] individual asked me, “Knowing what you know of the industry, do you think we can get them to cut a deal?” Cut a deal? We haven’t even figured out how to measure [how changes in the aviation infrastructure will reduce carbon dioxide emissions] yet...*we don’t have any data*. I don’t know what...[you] could even suggest that would be “cutting a deal” at this point. *I think that individual is reacting to [his] political realities*. I was disappointed that that individual does not have the inner moral compass to stand up to his management as I have a thousand

---

<sup>49</sup> Hecht, *The Radiance of France*, describes technopolitical regimes in chapters 1 and 2 as the interweaving of the technical and political aspects of engineering and nation building, the influences of which stretched beyond public discourse to influence all levels of technical development, “from the interactions between nuclear leaders and government officials to the artifacts and practices of reactor design” (p. 56).

<sup>50</sup> MacKenzie, *Inventing Accuracy*, pp. 413-414.

times and said, “You know, I don’t have any data. I can’t advise a decision now”. (emphases added)

While there was a commingling of the political and the technical, the business-y and the bureaucratic at the workshop, the participants likely retreated to “their” sphere at the end of the conference, for engineers believed that *data-driven* approaches to policy would result in the best political outcomes. Said Richard Altman of the Commercial Aviation Alternative Fuels Initiative,

MIT, [along with the] University of Chicago-Argonne and everybody we know, has looked at the life-cycle analysis in a *data-driven, critical* way. We haven’t depended on *arbitrary* views of social norms or anything of that nature. And I am convinced [of the possibilities of using biofuels in aviation] by the work of MIT, which the Department of Energy and the Air Force have both been involved in...[The work was] a peer-reviewed [study] on carbon [dioxide] life-cycle analysis that [showed] that we have a very good handle over what works and what doesn’t work. (emphases added)

The path dependency and lock-in of technologies that have caused climate change have impelled investments in greenhouse gas reducing technologies—(industrial) “risk” technologies in Ulrich Beck’s language<sup>51</sup>—not only to deal with climate change but also to further the lock-in of technologies and industries that drive a global industrial economy. Climate change is at once a problem driven by technologies, and one that is an outcome of the political and social interests embedded in technological systems and infrastructures. For example, coal- and fossil fuel-based energy generation and transportation are intimately tied to geopolitical wrangling and economic growth.<sup>52</sup> Political and social interests also manifest themselves in biofuels.

---

<sup>51</sup> Ulrich Beck, *Risk Society: Towards a New Modernity* (New Delhi: Sage Publications, 1992), translated by Mark Ritter from Beck’s *Risikogesellschaft: Auf dem Weg in eine andere Moderne* (Frankfurt am Main: Suhrkamp, 1986)

<sup>52</sup> Timothy Mitchell, *Carbon Democracy: Political Power in the Age of Oil* (Brooklyn, NY, and London: Verso Books, 2011)

## The existential pleasures of engineering

Historically, especially in the Enlightenment period, technological development and the human shaping and manipulation of nature formed the basis of a stable society—social stability rested upon the ability to move away from an imperfect past and to overcome external limits forced upon humans by nature.<sup>53</sup> For example, as was discussed earlier, dams were envisioned and built to combat the “scarcity” of water in the American West in the late 1800s, creating an illusion of abundance of water, converting the deserts of the Imperial Valley into the breadbasket of the United States, and spurring the growth of cities such as Los Angeles, San Francisco and Denver. In today’s world, writes Davison, “[t]echnological society names a particular political and moral condition in which the greatest common good is understood as the greatest possible productivity of technosystems.”<sup>54</sup> In that sense, biofuels represent not only a response to climate change, but also a response to a perceived scarcity of fossil fuels with the hope of continued technological productivity to stabilize current modes of trade and social interaction.

Modern, science-based engineering as a profession began in the mid-nineteenth century through the electrical and chemical industries. This was result of a reordering of corporate culture, the emergence of the professional engineer, scientific and industrial standardization, patent-law reform, and the alignment of industrial and university research. Educationally, newly developed engineering curricula focused on technical material, while humanistic and social science material allowing for effective management of men was included to make the engineer more suited to

---

<sup>53</sup> Aidan Davison, *Technology and the Contested Meanings of Sustainability* (Albany, NY: State University of New York Press, 2001), pp. 67-72. See in particular p. 69: “In the world Descartes and Bacon saw, external limitations are overcome, and thereby progress attained, to the extent that rational knowledge about natural machinery takes over from the inefficient meandering of evolution. A lack of rational development in existing social practices, a lack of material advance, i.e. a lack of progress, appeared as backwardness, idleness, moral decay. Yet, notions of progress and stability do not stand over and against each other so much as they inform and shape each other. The Enlightenment idea of stability was derived instrumentally from the antecedent metaphysical conviction that the purpose of social life was to develop the raw stuff of existence into a rational form, a Paradise on Earth.”

<sup>54</sup> Davison, *Technology and the Contested Meanings of Sustainability*, p. 93.

work in the corporate world.<sup>55</sup> To this day, modern engineers are thus trained to think technically for the benefit of large-scale industrialism.

Accordingly, a common view of engineering is “the art of applying science to the optimum conversion of natural resources to the benefit of man...[T]he conception and design of a structure, device, or system to meet the specified conditions in an optimum manner is engineering.”<sup>56</sup> For engineers, engineering is fundamentally about the design of technology through material construction and manipulation of artifacts.<sup>57</sup> Reductionism,<sup>58</sup> empiricism, positivism,<sup>59</sup> and dualism<sup>60</sup> form the cornerstones of modern engineering and technological development. Engineers tend to ignore or dismiss considerations for which reasons of a certain type cannot be given, thus ignoring intangibles like politics, like emotions, and other ethical concerns.<sup>61</sup> An engineer responsible for fuel purchasing in the Treasury department at Delta Airlines said that

...building [a material technology] and having it work is a success [to an engineer]. That might be a different perspective than for the person who wants to use it, for good or for bad. If [an engineer] complete[s] it, and...hit[s] on, and it works the way [he] thought it [should through testing and modeling],...that’s a success to an engineer. Whether this thing is a computer, or whether it is something used for chemical warfare, it’s a success.

---

<sup>55</sup> Noble, *America by Design*, pp. 30-32, 170-171.

<sup>56</sup> Ralph J. Smith, Blaine R. Butler, William K. LeBold, *Engineering as a Career*, 4<sup>th</sup> edition (New York: McGraw Hill, 1983), p. 9-10), pulled from page 146 of *Thinking Through Technology* by Carl Mitcham

<sup>57</sup> Carl Mitcham, *Thinking through Technology: The Path between Engineering and Philosophy* (Chicago and London: University of Chicago Press, 1994), p. 147.

<sup>58</sup> I understand reductionism as the division and discretization of complexity into well-defined parameters that can therefore be adjusted. An example of reductionism is how federal engineers converted the storage reservoir problem into a differential equation with terms that could be manipulated. Reductionism thus sets up cause-and-effect relationships. Also referred to as “atomism”—see Gloria Hauser-Kastenberg, William E. Kastenberg, David Norris, “Towards Emergent Ethical Action and the Culture of Engineering,” *Science and Engineering Ethics*, 9 (2003), 377-387.

<sup>59</sup> Positivism, which is the application of the empiricist tradition of Francis Bacon and Isaac Newton, allows the engineer to stand as a supposedly neutral observer to the forces of nature that dictate empirical outcomes. From Vesilind and Gunn, *Engineering, Ethics, and the Environment*, pp. 30-32

<sup>60</sup> Dualism is related to positivism—it is the separation of humans from the environment, the distinction, particularly in Western philosophical traditions of mind and matter.

<sup>61</sup> Vesilind and Gunn, *Engineering, Ethics, and the Environment*, pp. 30-32.

Engineering has thus been thought of as the most liberating of professions—regardless of monetary and social concerns, engineers are freed to “solve” “problems” and perform the technical task for which they were trained and which they find most pleasurable.<sup>62</sup> Yet engineers, as technical experts and managers, many times lack moral accountability for their work. Their work is fragmented, with engineers making small contributions to a project much larger; their positions in large corporate and government bureaucracies are “designed to diffuse and delimit areas of personal accountability within hierarchies of authority”; and there is pressure to move on to new projects before operating projects have been observed for long enough to observe and analyze performance and broader impacts.<sup>63</sup> Engineers have consequently “continued to serve capital, wittingly or not, their habits of thinking about problems and formulating solutions constituting for the most part but a highly refined form of capitalist reason.”<sup>64</sup>

Engineers recognize that they are not the ones that frame problems, especially ones like climate change, but are instead handed problems to solve—“[y]ou are kind of taught not to ask questions, [but rather to] just...design it,” said the Delta engineer. Sandy Webb furthered the Delta engineer’s comment by remarking that

[s]o often, engineers are employed by industry or somebody who is looking to solve a very near-term problem that can be narrowly defined, and so that’s all they are asked to do and that’s what they do. They don’t willfully try to create [unintended consequences]. But sometimes those come out of the assignment they have been given. And that’s, to a degree, what engineering is all about.

The currency of such reflections on the profession of engineering from engineers *working on climate change* makes the necessity of a radically different and morally expansive framing of ecological problems such as climate change all the more urgent.

---

<sup>62</sup> Samuel Florman, *The Existential Pleasures of Engineering* (New York: St. Martin’s Press, 1976).

<sup>63</sup> Mike W. Martin and Roland Schinzinger, *Ethics in Engineering* (New York, NY: McGraw-Hill Companies, 1996, 3<sup>rd</sup> edition), pp. 94-95

<sup>64</sup> Noble, *America by Design*, p. 323



## Biofuels, aviation, and climate change

In response to aviation's ever-increasing contributions to climate change, through carbon dioxide emissions in particular,<sup>65</sup> ICAO, corporations such as Boeing and Airbus, aviation industry trade groups such as Airlines for America and the Air Transport Action Group, government regulation agencies such as the Federal Aviation Administration, and government-industry consortia such as the Commercial Aviation Alternative Fuels Initiative, have agreed that several measures will need to be taken to reduce carbon dioxide emissions over the next fifty years—operational measures, technical improvements to aircraft, economic measures, and biofuels.<sup>66</sup> While operational measures are changing in air traffic control, for example; economic measures such as the European Union's Emissions Trading Scheme are being implemented by some governments (and vigorously fought by industry and other governments<sup>67</sup>); and technical improvements to aircraft are continually being made, the growth in overall air traffic has completely outpaced efficiency gains<sup>68</sup>. The aviation industry thus views biofuels as an essential

---

<sup>65</sup> Aviation is responsible for 2-3% of total anthropogenic carbon dioxide emissions. Aircraft also emit other greenhouse gases—such as water vapor, ozone, and methane, along with unburned hydrocarbons and particulate matter that also have radiative forcing impacts on the Earth's climate—directly into the upper troposphere and lower stratosphere, cited in J. E. Penner, D. H. Lister, D. J. Griggs, D. J. Dokken, M. McFarland (eds), *IPCC Special Report: Aviation and the Global Atmosphere*, Cambridge, UK: Cambridge University Press, 1999. In the US, aviation is responsible for approximately 13% of liquid fossil fuel use, cited in U.S. Department of Energy/Energy Information Administration, *Annual Energy Review 2005*, DOE/EIA – 0384(2005), July 2006. In light of the growing impact of aviation emissions on the climate, the International Civil Aviation Organisation was delegated responsibility to address greenhouse gas emissions from international aviation by the 1997 Kyoto Protocol.

<sup>66</sup> *Finding solutions | enviro.aero*. Available at [www.enviro.aero/whatisbeingdone.aspx](http://www.enviro.aero/whatisbeingdone.aspx). Accessed 1 April, 2012

<sup>67</sup> See for example: Karthikeyan Sundaram, Ewa Krukowska, and Liza Lin “*China, India Mount Opposition Against EU Aviation Carbon Curbs*”, Bloomberg News, 4 January 2012, retrieved 16 April 2012 from <http://www.bloomberg.com/news/2012-01-04/india-china-mount-opposition-against-eu-imposing-carbon-curbs-on-airlines.html>; “*US airlines drop legal opposition to EU ETS*”, Joint statement by Aviation Environment Federation, Center for Biological Diversity, Earthjustice, Environmental Defense Fund, Transport & Environment, WWF-UK, 28 March 2012, retrieved 16 April 2012 from <http://www.aef.org.uk/?p=1401>; Dan Hubbard, “*Aviation Groups Thank Clinton, LaHood for Strong Opposition to EU-ETS*”, National Business Aviation Association press release, 27 January 2012, retrieved 16 April 2012 from <http://www.nbaa.org/news/pr/2012/20120127-010.php>

<sup>68</sup> Models developed by the Intergovernmental Panel on Climate Change (IPCC) show that by 2050, the greenhouse gas emissions from global aviation will grow to between 1.6 and 10 times the emissions in 1992, and that the emissions increase in their reference scenario is threefold compared to 1992, equivalent to 3% of the projected total anthropogenic CO<sub>2</sub> emissions relative to the mid-range IPCC emissions scenario. Global passenger air travel has been growing steadily and quickly in recent decades, and is projected to grow by about 5% until 2015, whereas total aviation fuel use is projected to

technology that will eventually curb the industry's contribution to climate change. Intended to be “drop-in” fuels that would require little to no engine modification, biofuels would fit within the existing aviation infrastructure, bringing together technologists and engineers involved in fuel processing and standardization to make sure that the biofuels comply with safety standards and protocols; genetically engineering algae and bacteria that will convert different organic and non-organic streams into viable biofuels; and setting research agendas and regulatory frameworks to allow the adequate development of biofuels.

Technologists, engineers, and policymakers are expending vast amounts of time and effort in creating a technology, and a socially acceptable space for its viability. But do biofuels represent a fundamentally different technology being guided by a deeper concern about climate change and sustainability, or are they being guided by existing technological paradigms? What do engineers think about the capacities of technologies such as biofuels to address the ever-growing number of ecological problems? How do they reconcile infinite material growth under the paradigm of efficiency—an unquestioned tenet of industrial capitalism—with the reality of a finite planet with ecological problems unbounded in space and time? From my interviews, I concluded that contemporary engineers and the engineering profession is profoundly committed to, and has an unerring confidence in, *new* technologies that are industrial in scale, which engineers believe will repair ecological harms done by older technologies, while at the same time allowing for a stable future. “I have always believed people are smart enough to do what they want,” said Dr. Jennifer Holmgren, CEO of LanzaTech (a company that has genetically engineered microbes to convert carbon monoxide into a synthetic fuel). “As soon as we figure out that we have a problem, we usually can muster up the resources to solve it. [Technologically] is the only way you are going to solve [climate change], I think.”

---

increase by 3% per year until 2015, the difference being due largely to improved aircraft efficiency, cited in B. Metz, O.R. Davidson, P.R. Bosch, R. Dave, L.A. Meyer (eds), *Contribution of Working Group III to the Fourth Assessment Report of the Intergovernmental Panel on Climate Change*, Cambridge, UK: Cambridge University Press, 2007. Therefore, it is widely accepted that the overall emissions of greenhouse gases will *increase* for the foreseeable future, and aviation's share of overall greenhouse gas emissions from transportation *will also increase*.

Mark Rumizen, Aviation Fuels Specialist of the Federal Aviation Administration, invoked efficiency as a guiding principle in the development of biofuels:

We can [make biofuels]... that...work [in jet engines]. The challenge is the production scale of them. And...as people start looking into the problem of how to scale up production, increase feedstock productivity, solve the distribution and harvesting problems...I am confident that [through] engineering resources...we will come up with solutions to make [biofuels] work, and make [them] efficient enough such that you can make a synthetic jet fuel for basically the same price as a petroleum derived jet fuel. I am extremely confident that we will be able to solve those problems.

While many engineers would argue that biofuels represent a fundamentally different technology that has the capacity to limit ecological harm, the development of biofuels elicit the same sort of optimistic response from engineers as would any new technology, be it genetically engineered crops for trying to increase food production, or the building of dams on rivers to control floods, or the development of low-cost computers for the impoverished. In Beck's framework, the scale at which biofuels are required render biofuels a reconciliation between "risk" technology and a traditional industrial technology. While "risk [is] a systematic way of dealing with hazards and insecurities induced and introduced by modernization itself",<sup>69</sup> the risks posed by climate change for aviation are reframed to create a *demand* for biofuels, a demand that can be commoditized to elevate the production and consumption of biofuels to high status in an industrial society.<sup>70</sup> Biofuels, as many engineers and technocrats repeated at the workshop, must be produced *efficiently*, so as to allow "carbon-neutral" *growth*<sup>71</sup> of the aviation industry for the foreseeable future.<sup>72</sup> The

---

<sup>69</sup> Beck, *Risk Society*, p. 21.

<sup>70</sup> Beck, *Risk Society*, p. 56.

<sup>71</sup> See, for example, "Fact Sheet: Carbon-Neutral Growth", IATA, retrieved 19 April 2012 from [http://www.iata.org/pressroom/facts\\_figures/fact\\_sheets/pages/carbon-neutral.aspx](http://www.iata.org/pressroom/facts_figures/fact_sheets/pages/carbon-neutral.aspx)

<sup>72</sup> I take the notion of "efficiency", a common engineering design goal, and "growth"—the growth of profits, the growth of corporations, the growth of industry—at face value. For detailed explanations of "efficiency" and "growth", see Thomas Princen, *The Logic of Sufficiency* (Cambridge, MA: MIT Press,

technological fix<sup>73</sup> of biofuels is one that offers “engineering as an alternative to conservation or restraint”.<sup>74</sup>

**“It’s all fuckin’ ridiculous. You should just all ride bicycles.”**

Climate change thus is a problem that has at its root a particular socioeconomic and political order that has been shaped by technologies emitting greenhouse gases—technologies that have been subsidized and bolstered by nation states and corporations<sup>75</sup>—and responses to climate change rely on this very order. If engineers were the ones to frame ecological problems like climate change, would their framing reflect the unique nature of climate change? Cognitive bias created through education,<sup>76</sup> through the institutionalization of particular epistemologies of what constitutes “factual” knowledge,<sup>77</sup> and through organizational hierarchies would not necessarily lead to different framings or different approaches to technological development. A scientist working for an international non-governmental organization (NGO) promoting clean(er) transportation commented that

...policy questions [run] into problems when you ask scientists and engineers because you get an awful lot of cognitive bias...In general, if you ask a bunch of scientists a question, they are going to try and come up with a scientific solution. If you ask a bunch of engineers a question, they are going to want to build something...[Y]ou already know what the answer is going to be before you ask them. [So], the question is, [since] you know what the answer

---

2005), and Herman E. Daly, *Steady-State Economics: The Economics of Biophysical Equilibrium and Moral Growth* (San Francisco: W.H. Freeman and Company, 1977).

<sup>73</sup> Weinberg, Alvin. “Can Technology Replace Social Engineering?” *University of Chicago Magazine*, October 1966, 6-10. [Reprinted many times]

<sup>74</sup> James Rodger Fleming, *Fixing the Sky: The Chequered History of Weather and Climate Control* (New York, NY: Columbia University Press, 2010), p. 8.

<sup>75</sup> Mitchell, *Carbon Democracy*

<sup>76</sup> Noble, *America by Design*, chapters 8 and 9.

<sup>77</sup> See Michelle Murphy, *Sick Building Syndrome and the Problem of Uncertainty: Environmental Politics, Technoscience, and Women Workers* (Durham: Duke University Press, 2006), pp. 81-110. For example, in the case of sick-building syndrome, claims of the negative health effects of working in modern office buildings, with their plastics and ubiquitous chemicals, were countered with the epistemologies of industrial hygiene that required toxic exposures to chemicals to be both regular and specific, which rendered the effects of constant low-level exposures improvable and imperceptible. Therefore, dominant epistemologies and ontologies shape the framing of a problem for those that are trained in those dominants, rendering alternative and opposing framings powerless.

is going to be, do you think these people are the best people to ask the question to?

Fundamentally then, do engineers think that there is an ecological problem that technology *cannot* solve? An Environment Officer for ICAO claimed that

[e]very technological achievement reflects the fact that we have learned something new, and reflects the fact that you have better understanding and that understanding is matured to the point where you can create something that leverages that understanding. We're getting to the point where we understand the environment more. So, that gives me confidence that with that improved understanding, we can then come up with tools to address...[ecological] challenges.

This sentiment was echoed by Sandy Webb, who incidentally shared the 2007 Nobel Peace Prize that was awarded to the Intergovernmental Panel on Climate Change and former US Vice-President Al Gore. He felt that:

...I've never seen [an ecological problem that technology cannot solve]. Technology can't solve climate change because we don't have the political will to get started. If we do, when we do, the technology will be there. We can bring technology to bear on the problem. We are not bringing technology to bear on the problem today...Other than an unwillingness to apply technology, it is not clear to me that there are [ecological problems that technology cannot solve].

Engineers form essential nodes in the network of actors involved in technological design. They create and shape materials and the natural environment in ways that change human interaction with the world, while actively distancing the technical development from the political. But further, as those people that are handed problems to solve, they propagate the ethos of efficiency and growth—ideals that found a utilitarian, Pareto-optimality based system of politics, governance, and culture—through their techno-optimism. Framing an ecological problem as a

technological deficiency allows engineers to combine their existential pleasure of creative effort that is embodied in large infrastructural projects with the intention of “[contributing] to the well-being of his fellow man”,<sup>78</sup> while at the same time stabilizing a particular technopolitical system. The environment consequently serves as the impetus for technological development, the source of material inputs of technology, as well as the sink of outputs and fallouts of technology. The NGO scientist elaborated on this point:

How do we solve climate change? Engineers have a limited toolbox...They don't deal in behavior[al] change...People know that their job is to engineer and science-ize. [But] then if...an engineer comes back to you and says, “It's all fuckin' ridiculous. You should just all ride bicycles”, they will say, “Why are you telling me this? You are...an engineer. What do you know about getting people to ride bicycles?” Not only do you know the answer you are looking for, but you are also sort of predetermined to reject an alternative type of answer, because you don't trust those peoples' opinions on those other types of questions...

Why are we doing biofuels?...[I]gnoring for a moment [whether or not these statements are true], [biofuels] have a lifecycle analysis that says we [would achieve] a level of carbon savings [if implemented]. [But] *[n]o one has to do anything* (emphasis added). We're not going to charge anyone. We're not going to spend any public money. All of the funding will be taken from the consumer at the pump, at a level that is too late to be noticed. We can chalk it up on our renewable energy targets, we can chalk it up on our climate change targets. And we have *more* energy rather than less (emphasis in original)...We like more, and more, and more energy. We have a “more” energy solution [that looks] great. So, we love biofuels policy. And [the situation with aviation is] the same. You ask, “What do we want to do?” Well, the last thing we want to do is change anything that we do. [And] for an

---

<sup>78</sup> Mike W. Martin and Roland Schinzinger, *Ethics in Engineering* (New York, NY: McGraw-Hill Companies, 1996, 3<sup>rd</sup> edition), p. 30; Martin and Schinzinger also reference Florman, *The Existential Pleasures of Engineering*, pp. 143-147.

airline, the actual production process of the fuel is of no interest whatsoever. So, if you don't want to change, biofuels are a great way...of really not changing anything and achieving change...if you believe you are achieving change.

Michelle Murphy, in her book *Sick Building Syndrome and the Problem of Uncertainty*, describes how the framing of problems and accepted technoscientific norms dictate responses to those problems. Actions to address problems are taken only when understood by the powerful in the language they have created and under the norms they have promulgated. Murphy describes how sick building syndrome (SBS) emerged and materialized as an occupational illness in middle-aged working women, and how its existence was questioned and rendered imperceptible to industry-sponsored toxicology. In the 1960s and 1970s, modern architecture, interior design, and office supplies of the post-war era relied on new materials and plastics that off-gassed toxic chemicals such as 1,2-dichloroethane, ethyl benzene, and 4-phenylcyclohexane. At the same time, ventilation systems were designed to “optimize comfort” based off of only three variables—temperature, humidity and airflow—with testing done on white, male college students. The norms that guided what constituted a chemical exposure were laboratory-created and chemical exposures were rendered either perceptible or imperceptible based on the monitoring equipment devised for laboratory purposes. SBS, on the other hand, was a diffuse occupational hazard, with different people, particularly women, experiencing different symptoms. While claims of suffering from SBS were large in number, they were, according to scientific toxicological standards, anecdotal, uncertain, and too low to be measured. In response to this disregard from the scientific community, non-scientist women workers produced counter-knowledge by turning to popular epidemiology to gather more detailed, quantified knowledge about SBS through surveys that used bureaucratic language with the power to give scientific shape to SBS. Yet what counted as a chemical exposure in the scientific community solidified the toxicological standards given how chemical exposures manifested in women and how they were codified in legal and juridical frameworks. What was required according to toxicological standards was direct causal pathways between an occupational illness and a chemical exposure, just as asbestos caused asbestosis;

linkages between chemicals and physiological outcomes were only acceptable if detected through the use of technologies such as blood tests, X-rays, air samplers, and exposure chambers.<sup>79</sup> The case of SBS shows how problems get remorphed and reframed to fit existing paradigms.

The dominant ethic of engineering is that of efficiency to constantly feed a utilitarian, materially-based industrial system to grow (supposedly) infinitely. Engineers claim that the ecological problems we face are created through technological deficiencies that can be corrected through newer technologies, such as biofuels. However, large-scale technologies that are used to address large-scale ecological problems are created to stabilize the current technopolitical and economic order. This is done through actively shaping the way engineers think about the capacities of technology, and also by framing problems in particular ways that elicit technological solutions. In Beck's language, biofuels that will allow "carbon-neutral" growth of aviation are indeed an *industrial* technology that is a result of a skewed understanding of the risk of climate change. Lost are opportunities to define new paradigms. I speculate that this is why David Noble's introduction to *America by Design* reads:

Modern Americans confront a world in which everything changes, yet nothing moves. The perpetual rush to novelty that characterizes the modern marketplace, with its escalating promise of technological transcendence, is matched by the persistence of pre-formed patterns of life which promise merely more of the same. Each major scientific advance, while appearing to presage an entirely new society, attests rather to the vigor and resilience of the old order that produced it. Every new, seemingly bold departure ends by following an already familiar path...[T]his strange set of affairs [makes for] a remarkably dynamic society that goes nowhere.<sup>80</sup>

Unless accompanied by changes in socioeconomic behavior, technologies perpetuate particular socioeconomic outcomes. For example, in the case of irrigation

---

<sup>79</sup> See Murphy, *Sick Building Syndrome and the Problem of Uncertainty*, introduction, and chapters 1, 3, and 4.

<sup>80</sup> Noble, *America by Design*, introduction.



schemes in Sri Lanka's dry zone, the change to land-based rights access to irrigation water during British rule turned the gravity-flow irrigation system into a socioeconomic differentiation mechanism that created capitalistic class hierarchies, when in fact the previous water-based rights access had allowed equitable access to irrigation water. It was not the technology that had changed, but rather the socioeconomic and political contexts within which it existed that caused drastically unequal outcomes.<sup>81</sup> Will biofuels be accompanied by such a change in socioeconomic and political behavior? In the sense that different parts of the world, such as the rainforests of Borneo, will be further affected by land-use change through deforestation, local communities and biodiversity will feel the powerful socioeconomic forces of an industrial technology.<sup>82</sup> More fundamentally, however, framing a problem like climate change as one that requires a technological solution always unleashes a wave of capital investment, debates about government regulation and deregulation and market distortions, intellectual property and competition, just as any other technological development does. "Carbon-neutral *growth*" still remains an ambition founded on *efficiency*, both economic and physical.

It is such supposedly "neutral" claims—efficiency and growth—that form the philosophical foundations of engineering practice. Neutrality claims are not only made in engineers' thinking of the physical technology itself, but also in justifying technological interventions in the first place. For example, cost-benefit analysis (CBA) allows the separation of "fact" from "value" in the same ways that engineers separate the technical from the political.<sup>83</sup> While the utilitarianism that founds CBA is profoundly anthropocentric, monetization through CBA allows competing *political*, *social*, and *ecological* claims to be lent the air of "objectivity"; economic numbers are assigned to unquantifiables such as air quality and pollution. The resulting technologies do not make engineers question what they have done. Criticisms of utilitarianism and CBA abound, particularly those related to the reductionism that discretizes complex socioecological interactions. Engineers, as

---

<sup>81</sup> Bryan Pfaffenberger, "The Harsh Facts of Hydraulics: Technology and Society in Sri Lanka's Colonization Schemes", *Technology and Culture*, Vol. 31, No. 3 (July 1990), pp. 361-397.

<sup>82</sup> See, for example, the presentation of Dr. Chris Malins on indirect land-use changes, 20 October 2011, accessible at [http://legacy.icao.int/sustaf/Docs/20\\_Malins.pdf](http://legacy.icao.int/sustaf/Docs/20_Malins.pdf)

<sup>83</sup> See Porter, *Trust in Numbers*, chapters 3, 6, and 7. In fact, CBA was a technique developed by the US Army Corps of Engineers to justify dam building.

“experts”, have been *lent* the power to decide these discretizations, making CBA inherently value-laden.<sup>84</sup> Furthermore, reductionism in technical design results in unintended consequences, evaluative techniques are short-sighted and political, and engineers perpetuate an ethic of infinite-growth-on-a-finite-planet industrialism.

### Concluding thoughts

The goal of this work is to not focus on the deficiencies of the various ways in which efficiency is currently calculated—others have done a fantastic job at this<sup>85</sup>—but rather to show that a metric, indeed an *ethic*, such as that of growth through efficiency has persisted over time and continues to define approaches to evermore challenging socioecological problems. Problems are being framed in the same way as they were a century ago. While I draw these conclusions from two case studies that span space and time, they serve as fitting examples. One can go through most of the technical and scientific literature to see that the arguments for technical investment, be it in genetically modified foods or accuracy of missiles have the same threads that have emerged from these few short pages.

A radical change of the ethical underpinnings of the engineering profession from an anthropocentric utilitarianism to a more holistic ecological ethic that affords the ecosystems and oppressed peoples standing is absolutely necessary. A new ethic may expose the *irrationality*<sup>86</sup> of imagining infinite material growth on a finite planet. This is not to say that ethical debates have gone nonexistent in today’s society; ethical debates *within* engineering have increased multifold over time, with new ethical issues in computing, cybersecurity, biomedicine, and genetic engineering having arisen over the recent decades.<sup>87</sup> “[E]thical debates have [not] fallen silent in the technological society. Quite the opposite—they prosper,” writes Aidan Davison in *Technology and the Contested Meanings of Sustainability*. “Concerns about the

---

<sup>84</sup> For a succinct critique of CBA, see chapter 8 of Michael Huesemann and Joyce Huesemann, *Techno-fix: Why Technology Won't Save Us or the Environment* (Gabriola Island, BC, Canada: New Society Publishers, 2011).

<sup>85</sup> For a detailed discussion on the calculations of efficiency and their deficiencies, see Princen, *The Logic of Sufficiency*, chapters 3 and 4.

<sup>86</sup> From the standpoint of the conservation laws of mass and energy, engineers tend to draw their control volumes a little too small.

<sup>87</sup> Carl Mitcham, *Thinking Ethics in Technology: Hennebach Lectures and Papers, 1995-1996* (Colorado School of Mines, 1997).

conduct of journalists, accountability of corporations, treatment of domesticated animals, use of the Internet by pedophiles, and high rates of suicide amongst homosexual teenagers rightly make for passionate discussions about ethics.”<sup>88</sup>

However, an ecological ethic must inform engineering decision-making rather than be siloed within the profession that has siloed itself off from the rest of society. Davison therefore continues by saying that,

[y]et, it seems that the more we seem compelled to take a stand in ethical debates,...the less we seem able to take account of our peculiar, deformed practices and the public world they produce. Increasingly, we find expert ethicists, ethics committees, and ethical codes of practice in most areas of social debate. But...[t]he more discussion about ethics thrives, the more it seems detached from any meaningful social and practical negotiation about how our forms of life must be changed. “As it ponders social choices that involve the application of new technology, contemporary moral philosophy works [in] a vacuum...created...by the absence of widely shared understandings, reasons and perspectives that might guide societies as they confront the powers offered by new...large-scale technological systems”.<sup>89</sup>

Technologies actively shape our view of the world and our interaction in it.<sup>90</sup> Technologies and technological systems create momentum and path dependence.<sup>91</sup> They shape social, political and economic interactions, which in turn shape technologies. The fossil fuel-based economy is a telling example of how particular political motives led to the colonization of the Middle East and anthropogenic climate change. The material nature of coal and oil not only shaped the modern democracies in England and the United States, but also gave these countries reason to actively shape the politics of the Middle East after World War I, either through

---

<sup>88</sup> Davison, *Technology and the Contested Meanings of Sustainability*, pp. 142-143.

<sup>89</sup> Ibid. In this passage, Davison cites Langdon Winner, “Citizen Virtues in a Technological Order,” *Inquiry* 35, nos. 3/4 (1992): 341-361, p. 341, for, “As it ponders...technological systems.”

<sup>90</sup> Martin Heidegger, *The Question Concerning Technology, and Other Essays* (New York, NY: Harper and Row, 1977), translated by William Lovitt.

<sup>91</sup> Thomas P. Hughes, *The Evolution of Large Technical Systems* in Wiebe E. Bijker, Thomas P. Hughes, and Trevor J. Pinch (eds.), *The Social Construction of Technological Systems: New Directions in the Sociology and History of Technology* (Cambridge, MA: MIT Press, 1989), pp. 51-82.

state-sponsored colonization or through economic imperialism. Furthermore, the path dependency created by fossil fuel technologies have allowed only limited political and technical spaces in which to search for alternatives for greenhouse gas-emitting technologies today, as is evident in biofuel development.<sup>92</sup> Taking this one step further, the political and technological decisions made today will actively shape the decision-making space of future generations, either by constraining them through law, or through technology.<sup>93</sup> Engineering and technological development will play a profound role in shaping the future, not only in the techno-optimist sense of creating abundance in a world of scarcity, but also in the socioecological problems that future generations will have to deal with. Not even wind energy or solar energy—supposedly “renewable energy” technologies—or energy storage devices such as lithium batteries, will be free of problems.<sup>94</sup> From an energy consumption standpoint itself—let alone the issues of mining, pollution, dislocation, compensation—increased efficiency in energy use has time and again led to increased energy use that outpaces and undoes any efficiency gains.<sup>95</sup> Thus, the connotation of *decreasing* use that accompanies the term “efficiency” is highly misleading.

What lends engineering its power is the image of its separateness from “the social” or “the political”, and its capacity to perpetuate this image. Technologies are

---

<sup>92</sup> Mitchell, *Carbon Democracy*

<sup>93</sup> See, for example, Edward A. Parson and Darshan Karwat “Sequential Climate Change Policy” *WIREs Climate Change*, 2 (2011), pp. 744-756. doi: 10.1002/wcc/128. The technical infrastructures that the global economy is based on, that stabilises the current social order constrain the decision-making space available today to respond to climate change *if* we continue to imagine a fossil-fuel based economy that envisions infinite growth.

<sup>94</sup> Note, for example, the rising geopolitical tensions surrounding rare earth metal production. China, as a producer of 95% of the world’s supply of these metals, has the ability to affect the production of technologies such as wind turbines and batteries for hybrid cars. This is besides the ecological toxicity of these metals and their production. See “US, EU and Japan challenge China on rare earths at WTO”, British Broadcasting Corporation, 13 March 2012, retrieved 27 May 2012 from <http://www.bbc.co.uk/news/business-17348648>. See also Lawrence Wright, “Lithium Dreams: Can Bolivia become the Saudi Arabia of the electric-car era?” *The New Yorker*, 22 March 2010, retrieved 27 May 2012 from [http://www.newyorker.com/reporting/2010/03/22/100322fa\\_fact\\_wright](http://www.newyorker.com/reporting/2010/03/22/100322fa_fact_wright).

<sup>95</sup> This is Jevons Paradox, and its existence has been noted in instances from rural lighting in India and charcoal usage for stoves in Sudan to household energy consumption in Austria. John M. Polimeni, Koza Mayumi, Mario Giampietro, and Blake Alcott, *The Jevons Paradox and the Myth of Resource Efficiency Improvements* (London and Sterling, VA: Earthscan, 2008). The authors cite Eiman O. Zin-Elabdin, “Improved stoves in Sub-Saharan Africa: The case of the Sudan”, *Energy Economics*, Vol. 19, No. 4, pp. 465-475; Joyashree Roy, “The rebound effect: Some empirical evidence from India”, *Energy Policy* (2000), Vol. 28, pp. 433-438; Reinhard Haas and Peter Biermayr, “The rebound effect for space heating: Empirical evidence from Austria”, *Energy Policy* (2000), Vol 28, pp. 403-410.

allowed to unfold on the world “outside” of the sphere of technological development. I find it tremendously ironic that the interviews I conducted with engineers in Montréal required Institutional Review Board authorization, but the technologies that engineers produce and *introduce*, technologies that will shape politics and policy, that will dictate war and peace, ecological degradation and high school education, do not require any such permission or authorization other than that they comply with laws written by industry, that they guarantee profitability to an industrial economy, that they will produce abundance when scarcity seems imminent. *Engineering is not objective*. Rather, it is political, and it is socioecological. As socioecological experimentalists, engineers must understand the contexts of their work. Will current responses (like fracking and tar sands removal) to large-scale socioecological problems cause scarce fresh water reserves? Or possibly large scale disruptions of the nitrogen cycle through increased fertilizer use required by industrial agriculture?<sup>96</sup> It would not be surprising if the answer to both of these questions is in the affirmative.

---

<sup>96</sup> Peter M Vitousek, John Aber, Robert W. Howarth, Gene E. Likens, Pamela A. Matson, David W. Schindler, William H. Schlesinger, and G. David Tilman, “Human Alteration of the Global Nitrogen Cycle: Causes and Consequences” *Issues in Ecology*, 1 (Spring, 1997). Retrieved from the Ecological Society of America on 16 April, 2012, [http://www.esa.org/science\\_resources/issues/FileEnglish/issue1.pdf](http://www.esa.org/science_resources/issues/FileEnglish/issue1.pdf)

## Chapter 7

### The activist engineer

As technology developers, engineers are essential nodes in the network supporting the paradigm of infinite material growth through efficiency; of constantly technologizing our way out of problems. The political, economic and social structures that this paradigm bolsters falter if technological development cedes. Engineering is not neutral as engineers and lay people are led to believe. Instead, in the engineers' constant objective-fying of their work, they make political or value claims, as described in the previous chapter. The problem, as framed for this dissertation, then takes the shape of the nature of what is demanded of engineers—that is, the kinds of technology they develop and the ethics that guide them—and the engineers' willingness to fulfill those demands.

My observation is that a large fraction of engineering work that is supported by the federal-military-industry-university complex results in technologies that have socioecologically unjust, violent, and degrading outcomes. Metrics to evaluate these outcomes morph those that are clearly problematic into ones that have the air of positivity, or pit them against each other—for example, as we continue to pump greenhouse gases into the atmosphere, the current economy continues to grow positively. Engineers play a pivotal role in affecting these outcomes, and they continue to be educated in ways that perpetuate the interests of materialism, of consumerism, of abundance-from-scarcity, of distributed costs and highly individualized benefits, and of violence.<sup>97</sup> A truly sustainable existence has at its

---

<sup>97</sup> For example, in 1987, the World Commission on Environment and Development (WCED) noted that more than half a million of the world's scientists worked on weapons research that accounted for 50% of all research and development expenditures, from *Our Common Future*, chapter 11, p. 157, WCED (1987). Also, as boasted by an executive vice president of Lockheed Martin in 2005, "We are the largest single supplier to the U.S. Department of Defense and the largest provider of information technology services to the federal government. We also happen to be one of the nation's largest employers of engineers and scientists, with about 50,000 of our 130,000 employees around the world holding some sort of technical degree or credential. To sustain this critical mass of talent, we will hire approximately

core a social and engineering paradigm that creates a culture of peace, satisfaction, and sufficiency; that is ecologically sensitive and holistic. It is the role of the activist engineer to create a new paradigm of engineering in which the engineer is equipped with not only technical tools and knowhow, but also with the requisite *socioecological* perspectives, knowhow and ethics that allow for activist engineering.

The activist engineer faces significant barriers to change. Perhaps the most difficult barrier to overcome is engineering's historical associations with violence and empire building for overtly social purposes, including through modifying the environment. For example, the damming of rivers, as explored in the last chapter, had overt social and political goals.<sup>98</sup> Many technologies and large-scale infrastructures that were promoted under the guise of providing "freedom" have instead resulted in an unending reliance on those technologies and infrastructures—the automobile is the quintessential example of such a technology, which led to the development of highway infrastructure, suburban sprawl, decaying urban cores, and so on. In the contemporary world, I believe that technological development and investment by the American military is for the purpose of maintaining the vast empire of American neoliberal influence, just as the British used technologies such as steam engines and telecommunication to consolidate its empire in the Indian subcontinent.<sup>99</sup> How then can engineering be viewed as legitimately concerned for socioecological welfare? Engineers must critically examine and understand engineering's historical roots, as well as grapple with and question its current realities. These issues I discuss later.

Given the inextricable ties between society and technology, the current paradigm must be confronted and challenged and changed by the engineer as much as by the

---

9,000 engineers this year, including 3,700 new graduates. In fact, in any given year, Lockheed Martin hires about one of every 20 engineering baccalaureates in the United States—four to five percent of the entire nation's undergraduate output", from Donna Riley, *Engineering and Social Justice* (Morgan & Claypool, 2008), p. 64.

<sup>98</sup> See also, Richard P. Tucker, *Containing Communism by Impounding Rivers: American Strategic Interests and the Global Spread of High Dams in the Early Cold War*, in John R. McNeill and Corinna R. Unger, eds. *Environmental Histories of the Cold War* (Washington, DC: German Historical Institute; New York, NY: Cambridge University Press, 2010), pp. 139-163

<sup>99</sup> See also, Thomas Misa, *Leonardo to the Internet: Technology and Culture From the Renaissance to the Present* (Baltimore: Johns Hopkins University Press, 2<sup>nd</sup> edition, 2011), in which the author discusses how the British developed steam engines, quinine, railroads and telegraph systems to maintain control over the Indian subcontinent, pp. 98-99. See also, Caroline Baillie, *Engineers Within a Local and Global Society* (Morgan & Claypool, 2006), in which the author describes how famine in India was worsened because of the development of railroad infrastructure.

non-engineer; the outcomes of engineering are dictated not only by the type and nature of the technologies developed, but also by the ways in which society changes its behavior because of those technologies and by the ways in which those technologies change what is demanded from engineers by the organizations they work in. In the previous chapter, contemporary engineers spoke of the top-down organizational hierarchies that engineers operate in; engineers obey authority.<sup>100</sup> Many engineers claimed that the problems that engineers solve are ones that are framed and handed to them by their superiors with vested interests. These claims make it seem that engineers lack agency;<sup>101</sup> that they are subservient to the demands of their bosses and a technological culture. Part of me can see this power dynamic; however, part of me holds firmly that as socioecological experimentalists,<sup>102</sup> as those equipped with technical knowhow, engineers have the capacity to transform not only the material world, but themselves and the engineering profession as well, consequently effecting paradigmatic social change. If engineers have been essential in building and maintaining the current sociotechnical order, why can't they be the ones empowered to forge a new order?

In *The Structure of Scientific Revolutions*, Thomas Kuhn argues that “the decision to reject one paradigm is always simultaneously the decision to accept another”<sup>103</sup>. The new paradigm subscribes a field or profession to new fundamentals, and changes the methods and applications of the field or profession. These changes lead to “a decisive difference in the modes of solution,...[and] a change in view of the field...and its goals”.<sup>104</sup> Kuhn argues, rightly, that these transformations are only possible with the advantages of hindsight, and the explicit guidance attained from the outcomes of the paradigm being replaced.<sup>105</sup>

Kuhn argues that no two paradigms leave the same problems unsolved.<sup>106</sup> Indeed, the differences in goals and approaches between paradigms reshape and

---

<sup>100</sup> Riley, *Engineering and Social Justice*, pp. 116-117

<sup>101</sup> I take “agency” to mean the capacity to make decisions and choices for themselves given their knowledge.

<sup>102</sup> I describe this term in the previous chapter.

<sup>103</sup> Thomas S. Kuhn, *The Structure of Scientific Revolutions* (Chicago: University of Chicago Press, 3<sup>rd</sup> edition, 1962, 1996), p. 77

<sup>104</sup> Kuhn, *The Structure of Scientific Revolutions*, pp. 84-85

<sup>105</sup> Kuhn, *The Structure of Scientific Revolutions*, pp. 102-103

<sup>106</sup> Kuhn, *The Structure of Scientific Revolutions*, p. 110



recast problems differently, leading to fundamentally different outcomes. Furthermore, the criteria according to which the outcomes of the two paradigms are evaluated are fundamentally different; the criteria for evaluating the work of the activist engineer, I assert, lie outside the scope of the current engineering paradigm, making the activist paradigm revolutionary. If the current paradigm is focused on the quarterly profit, the activist paradigm is focused on long-term resiliency. If the current paradigm is based on extractive industry and efficient growth, the activist paradigm is based on modularity, repurposeability, and sufficiency. If the current paradigm is based on reliance on large corporations and capitalism, the activist paradigm must, in large part, be based on community-scale works based on community engagement, democracy, and equality.

To effect these revolutionary changes, the activist engineer might employ what Karl Marx and Paolo Friere call *praxis*<sup>107</sup>—the critical thinking and reflective action upon the world to transform it. Praxis is both the mode of defining the new paradigm as well as the mode to address problems under the new paradigm. According to Donna Riley, praxis draws on the understanding of how engineering work affects communities and the world, and is guided normatively through moral and ethical guidance, which in the activist paradigm focuses on social justice and ecological soundness. Importantly, praxis involves an openness to change. While technical work may be guided by traditional engineering principles and learning,

no assumptions are made about what the right process to follow is...[p]rocess and product, ends and means, thought and action, the general and the specific, the theoretical and the practical are in constant exchange and dialogue. As we think about answers or solutions or goals for change, the process for getting there may change. As we go about the process, the end

---

<sup>107</sup> See Karl Marx and Friedrich Engels, eds. *Collected Works of Karl Marx and Friedrich Engels, 1845-47, Vol. 5: Theses on Feuerbach, The German Ideology and Related Manuscripts* (New York, NY: International Publishers, [1845] 1976); Paolo Friere, *Pedagogy of the Oppressed* (New York, NY: Continuum Publishing, 30<sup>th</sup> Anniversary Edition, [1970] 2000), p. 51, translated by Myra Bergman Ramos; Riley, *Engineering and Social Justice*, p. 108.

goals may change...[Praxis] requires critical thinking and ethical judgment. It is “not merely the doing of something.”<sup>108</sup>

The “existential pleasure of engineering” (that is, not thinking about the politics of engineering decision-making)—as the engineer and writer Samuel Florman puts it<sup>109</sup>—is replaced with technical development that goes hand-in-hand with the political and social.

In this new paradigm, problems are defined not from corporate bureaucracies, lawyers, or businesspeople, but rather surface from the communities of people where problems exist, and from observing how human actions may pollute and degrade ecosystems. The process of engineering itself raises important questions about who stakeholders are, what their concerns are, and how everyone’s concerns may be adequately accounted for in any technological work. Activist engineering does not render claims of social injustice or ecological degradation through technology as illegitimate; rather, the activist paradigm allows the activist engineer a more detailed view of socioecological interactions. A constant reevaluation of process and goals tempers attempts to technologize and reformulates technological designs accordingly. Profoundly, the radical—and necessary—possibility of *not* “engineering a solution” arises. (I liken this to being a surgeon who decides not to perform an operation on a patient given the risks involved with a particular surgery.) During this process, not only are engineers learning about the actual nature of problems and acting upon that learning, but the demands of the community the technology will affect change given the community’s direct involvement in the technical design process.

The activist paradigm imbues a different sense of responsibility and accountability in engineers. In the current paradigm, most engineers that work on large problems work only on small parts of them, and many of these engineers are given information about projects only on a need-to-know basis. Final engineering products are many times physically removed from the engineers’ workplace, lessening the sense of personal accountability. The large bureaucracies that

---

<sup>108</sup> Riley, *Engineering and Social Justice*, pp. 108-109; and Mark Smith, *Praxis*, The Informal Education Web, accessed July 26, 2012 from <http://www.infed.org/biblio/b-praxis.htm>

<sup>109</sup> Samuel Florman, *The Existential Pleasures of Engineering* (New York: St. Martin’s Press, 1976).

engineers work in “diffuse and delimit areas of personal accountability within hierarchies of authority”. Since there is frequent pressure to move on to new projects before immediate projects have been operating long enough to observe outcomes carefully, the sense of accountability over the long term is lessened.<sup>110</sup> In the activist paradigm, instead, an engineer builds strong relationships with the places and people. *The activist engineer thus follows a piece of technology, from its design to its implementation, studies the outcomes and weighs them given an ethic of social justice and ecological soundness, and changes the technological design process accordingly.* This process thus transforms the relationship between the engineer and society, holding the engineer responsible and accountable for her actions, while also creating an environment in which society becomes more and more accepting of engineering with political and social purposes.

As mentioned earlier as well as in the previous chapter, engineering education does not focus on the history of engineering and technological development. Instead, technological development is *ahistorical* to engineers, and they tend to dissociate the shape and form of technologies from political and social pressures. Extending Kuhn’s observations of the scientific process to the engineering process, technological development is thus made to seem cumulative and progressive, that is, it is made to seem as if the shape and form of technologies is deterministic, always linearly forward-looking, and always capable of producing abundance when scarcity seems near. For example, new designs of solar panels or computer chips or car engines, while of course resting on knowledge gained through previous technical exercises, are to the engineer “the best we can do given what we know, *technologically.*” From my observations and conversations, from attending engineering seminars and conferences, I assert that this dynamic of the technological development process is replicated for most all technologies, and the interactions between the various government, NGO and industry groups interested in technological development sound the same. I imagine that the discussions and dialogue that I heard at the ICAO conference where I collected the interviews in the last chapter sounded like those at any conference—private industry says that

---

<sup>110</sup> Mike W. Martin and Roland Schinzinger, *Ethics in Engineering* (New York, NY: McGraw-Hill Companies, 1996, 3<sup>rd</sup> edition), pp. 94-95

government regulation is holding back the development of [insert technology here]; government, ever-reliant on economic growth, tries to allow private industry deregulated space, while also placating NGOs. (And with a global problem like climate change, governments and industry say, “We are all in this together, and we will only do something if everyone has to do something.”)

Ahistoricity also profoundly influences the notion of safety that is one of the paramount ethical concerns in engineering.<sup>111</sup> (“The bridge won’t fall down.”) In the detailed codes of ethics such as those written by the American Society of Civil Engineers<sup>112</sup> and the National Society of Professional Engineers,<sup>113</sup> significant attention is paid—particularly in a sector such as aviation—to the safety of engineering projects. Furthermore, there are countless examples of the halting or redesign of technologies because of whistle-blowing. Yet, given that the vast majority of engineers work for private corporations, the bulk of these codes of ethics focuses on professional ethics and these codes deal only superficially with guidance for engineers in thinking about the long-term socioecological outcomes of engineering work. Issues of safety therefore serve as *liability* issues for engineers and the firms they work for; projects and technologies are made safe for *now*. (It can also be argued that building unsafe projects results in reduced economic profitability while also solidifying the perception of engineering as solely for the benefit of a few people.<sup>114</sup>) Therefore, there is very little space in the current engineering paradigm for the reflective thinking that incorporates socioecological outcome, the thinking that forms the heart of praxis.

Through praxis, there is much to be learned then from other knowledges and epistemologies that have inextricable ties with technological development. John Paul Lederach, a Mennonite theologian, activist, and professor of peace-building at the Joan B. Kroc Institute of International Peace Studies at the University of Notre Dame, has said the main reason peace-building missions undertaken by the US military don't succeed is because the missions do not keep in mind the nature of the

---

<sup>111</sup> See Martin and Schinzinger, *Ethics in Engineering*, chapter 4.

<sup>112</sup> See Code of Ethics of the American Society of Civil Engineers, accessed from [http://www.asce.org/Leadership-and-Management/Ethics/Code-of-Ethics/#note\\_3](http://www.asce.org/Leadership-and-Management/Ethics/Code-of-Ethics/#note_3) on 23 August 2012.

<sup>113</sup> See Code of Ethics of the National Society of Professional Engineers, accessed from <http://www.nspe.org/Ethics/CodeofEthics/index.html> on 23 August 2012.

<sup>114</sup> Vesilind and Gunn, *Engineering, Ethics, and the Environment*, pp. 28-30.

peace wanted when waging war. Rather, the US is caught trying to end what it feels are injustices and tyranny without regard for what might come of military disruptions. This leads to protracted conflicts such as those in Iraq and Afghanistan, and the unstable places left behind when military engagements cease. Instead, argues Lederach, “[w]e must concentrate as much on the [nature of the] peace we wish to pursue as on the grievances we wish to address. [We must have] the capacity to link a specific response to what it is [we] are hoping to build, not just what it is [we] trying to end”.<sup>115</sup> This line of reasoning is counter to the reasoning (presented in the previous chapter) of René Descartes and Francis Bacon, who claimed during the Enlightenment that we must constantly move away from an imperfect past through technological development. The imperfect past and the current reality, according to the current paradigm, is that carbon dioxide emissions are causing climate change. Solutions to a problem like climate change thus take the shape of technologies that absorb carbon dioxide or do not emit it, yet are still ecologically degrading—for example, biofuels, mountaintop removal coupled with carbon capture and sequestration, seeding the oceans with iron to create algal blooms that will absorb carbon dioxide, and so on. *But these technological responses still envision infinite material growth into the future.* Indeed, many engineering approaches to solve climate change come with significant risks, risks that would not by any measure be guaranteed to address climate change, risks that fail to account for social justice and ecological outcomes.<sup>116</sup>

In a Kuhnian sense, the nature of climate change does not allow it to fit within the current paradigm of short-term thinking and technological solutions that can be uniformly applied the world over. While carbon dioxide is causing climate change—from a purely scientific perspective—through praxis, it is apparent that addressing the root causes of climate change requires an overhaul of political, economic, and social structures. Climate change represents a system destabilizing<sup>117</sup> problem, and

---

<sup>115</sup> For more of these insightful thoughts, listen to John Paul Lederach’s conversation with Krista Tippett on *Speaking of Faith* (now *On Being*) in an episode titled, “Justice and a Just War,” from 9 November 2001, available at <http://www.onbeing.org/program/justice-and-just-war/115>

<sup>116</sup> See Dale Jamieson, “Ethics and Intentional Climate Change” in *Climatic Change*, 1996: 33, 323-336

<sup>117</sup> For a detailed description of the features of system stabilization, see Thomas Hughes, *The Evolution of Large Technical Systems* in Wiebe Bijker, Thomas Hughes, and Trevor Pinch, eds. *The Social Construction of Technological Systems* (Cambridge, MA: MIT Press, 1987), pp. 51-82.

the framing of climate change as a “carbon” problem is “possibly the greatest and most dangerous reductionism of all time: a 150 year history of complex geologic, political, economic, and military security issues all reduced to one element.”<sup>118</sup> *Through praxis, however, the activist engineer couples technological solutions to climate change with requisite social changes*—such as a *reduction* in large-scale energy consumption and the promotion of locally-based lifestyles—that are as necessary if not more so than the technological solutions. I posit that the outcomes of such social changes obviate the need to take the risks of geoengineering or large scale technological solutions to climate change. Guided by social justice and ecological soundness, the goal of activist engineering is to effectively incorporate the concerns of stakeholders such as people whose lands are being lost to rising sea levels and biofuel plantations and extractive mining for rare earth metals used in alternative energy technologies. Solutions to climate change under the activist paradigm are thus not just another turn of the technological crank.

Activist engineering incorporates historical and contemporary political, technological, and social knowledge to guide responses to problems. However, since the activist paradigm frames a problem such as climate change differently than the current paradigm, the solutions stemming from the activist paradigm cannot be judged according to metrics from the current paradigm, because *the activist paradigm is solving a different problem. The goals of the activist paradigm are fundamentally different than the goals of the current paradigm.* The activist paradigm allows solutions such as “leave it in the ground”, as Thomas Princen suggests for fossil fuels<sup>119</sup> and non-technological solutions, too.

The profession of engineering has much to learn from other professional fields. For example, the profession of urban planning, which provides the templates for the design of technological infrastructures such as roads, transit systems, energy grids, and water treatment facilities that engineers design is founded on principles of social theory. A significant portion of urban planning education is dedicated to learning historical contexts of urban planning, equality, and planning for

---

<sup>118</sup> See Thomas Princen, “Leave It in the Ground: The Politics and Ethics of Fossil Fuels and Global Disruption” prepared for the International Studies Association International Conference, Montréal, March 16-19, 2011; to appear in *State of the World 2013* (forthcoming).

<sup>119</sup> Princen, *Leave It in The Ground*

organizational and community change. Since engineering actually creates and builds these infrastructures, it is absolutely essential that engineers understand social theory and are able to evaluate socioecological outcomes. At the same time, the activist engineer must work on concrete and specific projects that shed light on the complex nature of problems such as climate change, and in her work, define the activist paradigm. New models of urban gardening provide case studies of such substantive projects, for example. Given the inertia of trying to combat the ill-effects of industrial agriculture such as decreasing crop diversity, water pollution from chemical fertilizers and pesticides, and long-distance transportation, urban gardening projects have the capacity not only to provide access to fresh fruits and vegetables grown in an ecologically sound manner, but also have the capacity to remediate brownfield sites, provide opportunities for at-risk youth, and build neighborliness. Regardless of whether or not these attempts are fruitful, important questions have already been raised about why past efforts in urban planning and education have led to inequity and structural poverty. In the same way, it is essential that the socioecological outcomes of engineering and technological systems are a part of the dialogue.

In summary, the activist engineering paradigm is defined by and constantly redefined by praxis—critical thinking and reflective action; the activist paradigm is process-oriented. The activist engineer couples technological solutions to problems with requisite social changes, follows a piece of technology, from its design to its implementation, studies the outcomes and weighs them given an ethic of social justice and ecological soundness, and changes the technological design process accordingly. Indeed, the goals of the activist paradigm are fundamentally different than the goals of the current paradigm. That said, I would like to discuss how the activist engineer may approach aviation's contribution to climate change, if at all possible, and other contexts within which activist engineering may be able to provide more substantial guidance.

Aviation is a global infrastructure and is governed by domestic political regimes as well as a complex international political regime established by the Chicago

Convention of 1944.<sup>120</sup> ICAO is the United Nations body that governs international aviation, and the United Nations Framework Convention on Climate Change has given ICAO responsibility to deal with aviation's contribution to climate change. Given the nature of the aviation industry and its operating cost structures,<sup>121</sup> the industry constantly adopts more efficient operations and seeks lower fuel consumption—efficiency gains have made aircraft 70% more efficient than forty years ago, and 20% more efficient than ten years ago.<sup>122</sup> However, according to the Chicago Convention, ICAO's interests are in the *global growth* of the aviation sector, and as mentioned in the previous chapter, efficiency gains have been outpaced by overall growth in air travel. Furthermore, for reasons<sup>123</sup> that I will not discuss here, interactions of aviation in the climate change regime have led to very little leadership from the aviation industry in addressing its contributions to climate change.

Aviation can be considered the most conservative engineering sector—given the paramount importance given to safety—while at the same time one of the most technologically advanced. Praxis in aviation would involve the use of socioecological indicators apart from carbon dioxide reductions. Significant thought must be given from biofuel developers to indirect land-use changes, the effects of deforestation on biodiversity loss, and disruptions to local communities. The extent to which new technologies ought to be incorporated in aviation depends on how drastically current infrastructures would need to be changed. If little material investment in new technologies allows large strides in reducing aviation's impact on the environment, then the activist engineer must consider these technologies seriously, while also trying to ensure that these gains are not outpaced by the indefinite growth in the use of aviation and that the gains can be made in socially just and ecologically sound ways. Technologies such as biofuels in aviation must be accompanied by political

---

<sup>120</sup> ICAO, *Convention on International Civil Aviation* (1944, 2000)

<sup>121</sup> Fuel costs are approximately 30% of an airline's annual operating budget. See, for example, "InFlight Optimization Services Offers Airlines More Fuel-Efficient En-Route Operations", Boeing, retrieved 27 July 2012 from [http://www.boeing.com/commercial/aeromagazine/articles/2011\\_q2/4/](http://www.boeing.com/commercial/aeromagazine/articles/2011_q2/4/)

<sup>122</sup> See, for example, "Environment: Fuel Efficiency", International Air Transport Association, retrieved 27 July 2012 from [http://www.iata.org/whatwedo/environment/Pages/fuel\\_efficiency.aspx](http://www.iata.org/whatwedo/environment/Pages/fuel_efficiency.aspx)

<sup>123</sup> ...such as the forbiddance of unilateral actions by member parties to the Chicago Convention, and the concept of "common but differentiated responsibilities" under the Kyoto Protocol, the duopoly between Boeing and Airbus, competing interests of federal agencies such as the Federal Aviation Administration and the Environmental Protection Agency, and so on...



and social changes that reduce the very need for biofuels; however, the inroads to make these sociotechnical and technopolitical connections are beyond me at this moment. Activist engineering may find a firmer footing for radical action in other contexts.

Problems such as climate change are large and unbounded in space and time, but responses to them are decidedly specific—people may install solar panels on their home, or choose not to buy plastics given their hydrocarbon base (or, choose not to buy many things altogether); farmers may choose to use natural pest deterrents on their crops rather than petrochemical-based pesticides; companies may encourage teleconferencing rather than flying across the world for an afternoon meeting; activists may oppose the building of a pipeline meant to carry tar sands oil from Alberta to Texas. It is the collection of many small yet transformative responses, either guided by changing norms, or those with the explicit intention of changing norms, that will go a long way in changing political, economic, and social structures that perpetuate the emissions of greenhouse gases that are causing climate change. Activist engineering will play a significant role in creating these changes as well.

The post-industrial city of Detroit—*the* American city—is a context within which activist engineering may first thrive. The socially unjust and ecologically degrading outcomes of the current paradigm are nowhere clearer than in Detroit, with toxic brownfields scattered across the city, with the most polluted zip code in the State of Michigan, with technological infrastructures such as roads reminding everyone of the city's ties to fossil fuel-based transportation, and with the extreme urban poverty and lack of mobility for the people of Detroit. Given the continuing cuts to city services and the increasing restlessness of the people of Detroit to see the city turn the corner on its past, the city is ripe for radical, activist solutions to meet peoples' needs. Instead of large-scale technological solutions, the activist engineer has the ability to design technological systems to focus on smaller communities of people. Such efforts make it easier to understand the political, social, and cultural contexts where the technologies will be used and allow more community input in technological design. There are many basic requirements and services that these communities need, such as heating and cooling, lighting, clean water, and mobility, to name a few. Activist engineering can provide these needs in a socially just and ecologically sound manner, thereby building community resiliency, and radically

redefining the paradigm of the engineering profession. In doing so, the activist engineer, through praxis, can provide innovative and creative models for technological development, with the explicit aim of combating contributions to large problems like climate change. In doing so, the activist engineer can redefine her role in society and transform society itself.

## Technical references

- (1) Ciezki, H. K.; Adomeit, G. *Combustion and Flame* **1993**, *93*, 421-433.
- (2) Shen, H.-P. S.; Steinberg, J.; Vanderover, J.; Oehlschlaeger, M. A. *Energy & Fuels* **2009**, *23*, 2482-2489.
- (3) Herzler, J.; Jerig, L.; Roth, P. *Proceedings of the Combustion Institute* **2005**, *30*, 1147-1153.
- (4) Smith, J. M.; Simmie, J. M.; Curran, H. J. *International Journal of Chemical Kinetics* **2005**, *37*, 728-736.
- (5) Davidson, D. F.; Oehlschlaeger, M. A.; Hanson, R. K. *Proceedings of the Combustion Institute* **2007**, *31*, 321-328.
- (6) Akih-Kumgeh, B.; Bergthorson, J. M. *Energy & Fuels* **2010**, *24*, 2439-2448.
- (7) Davidson, D. F.; Hong, Z.; Pilla, G. L.; Farooq, A.; Cook, R. D.; Hanson, R. K. *Combustion and Flame* **2010**, *157*, 1899-1905.
- (8) Dagaut, P.; Reuillon, M.; Cathonnet, M. *Combustion and Flame* **1995**, *101*, 132-140.
- (9) Silke, E. J.; Curran, H. J.; Simmie, J. M. *Proceedings of the Combustion Institute* **2005**, *30*, 2639-2647.
- (10) Tanaka, S.; Ayala, F.; Keck, J. C.; Heywood, J. B. *Combustion and Flame* **2003**, *132*, 219-239.
- (11) Griffiths, J. F.; Halford-Maw, P. A.; Mohamed, C. *Combustion and Flame* **1997**, *111*, 327-337.
- (12) Minetti, R.; Carlier, M.; Ribaucour, M.; Therssen, E.; Sochet, L. R. *Combustion and Flame* **1995**, *102*, 298-309.
- (13) Cox, A.; Griffiths, J. F.; Mohamed, C.; Curran, H. J.; Pit, W. J.; Westbrook, C. K. *Symposium (International) on Combustion* **1996**, *26*, 2685-2692.
- (14) Ingemarsson, Å.; Pedersen, J.; Olsson, J. *The Journal of Physical Chemistry A* **1999**, *103*, 8222-8230.

- (15) Bakali, A. E.; Delfau, J. L.; Vovelle, C. *Combustion Science and Technology* **1998**, *140*, 69-91.
- (16) Doute, C.; Delfau, J. L.; Akrich, R.; Vovelle, C. *Combustion Science and Technology* **1997**, *124*, 249-276.
- (17) D'Anna, A.; Alfe, A.; Apicella, B.; Tregrossi, A.; Ciajolo, A. *Energy & Fuels* **2007**, *21*, 2655-2662.
- (18) Ji, C.; Dames, E.; Wang, Y. L.; Wang, H.; Egolfopoulos, F. N. *Combustion and Flame* **2010**, *157*, 277-287.
- (19) Warnatz, J. *Gas/surface Interactions and Damaging Mechanisms in Knocking Combustion, CEC Contract: JOUE-0028D-MB*; 1993.
- (20) Côme, G. M.; Warth, V.; Glaude, P. A.; Fournet, R.; Scacchi, G.; Battin-Leclerc, F. *Symposium (International) on Combustion* **1996**, 755-762.
- (21) Ranzi, E.; Gaffuri, P.; Faravelli, T.; Dagaut, P. *Combustion and Flame* **1995**, *103*, 91-106.
- (22) Curran, H. J.; Gaffuri, P.; Pitz, W. J.; Westbrook, C. K. *Combustion and Flame* **1998**, *114*, 149-177.
- (23) CRECK Modeling Complete mechanism (Low and High Temperature), version 1201 <http://creckmodeling.chem.polimi.it/kinetic.html>.
- (24) Mehl, M.; Pitz, W. J.; Westbrook, C. K.; Curran, H. J. *Proceedings of the Combustion Institute* **2011**, *33*, 193-200.
- (25) He, X.; Donovan, M. T.; Zigler, B. T.; Palmer, T. R.; Walton, S. M.; Wooldridge, M. S.; Atreya, A. *Combustion and Flame* **2005**, *142*, 266-275.
- (26) Walton, S. M.; He, X.; Zigler, B. T.; Wooldridge, M. S.; Atreya, A. *Combustion and Flame* **2007**, *150*, 246-262.
- (27) Walton, S. M.; He, X.; Zigler, B. T.; Wooldridge, M. S. *Proceedings of the Combustion Institute* **2007**, *31*, 3147-3154.
- (28) Walton, S. M.; Wooldridge, M. S.; Westbrook, C. K. *Proceedings of the Combustion Institute* **2009**, *32*, 255-262.
- (29) Teini, P. D.; Karwat, D. M. A.; Atreya, A. *Combustion and Flame* **2011**, *158*, 2045-2055.
- (30) Teini, P. D.; Karwat, D. M. A.; Atreya, A. *Combustion and Flame* **2012**, *159*, 1090-1099.

- (31) He, X.; Zigler, B. T.; Walton, S. M.; Wooldridge, M. S.; Atreya, A. *Combustion and Flame* **2006**, *145*, 552-570.
- (32) He, X.; Walton, S. M.; Zigler, B. T.; Wooldridge, M. S.; Atreya, A. *International Journal of Chemical Kinetics* **2007**, *39*, 498-517.
- (33) Walton, S. M.; Karwat, D. M.; Teini, P. D.; Gorny, A.; Wooldridge, M. S. *Fuel* **2011**, *90*, 1796-1804.
- (34) Karwat, D. M. A.; Wagnon, S. W.; Teini, P. D.; Wooldridge, M. S. *The Journal of Physical Chemistry. A* **2011**, *115*, 4909-21.
- (35) Donovan, M. T.; He, X.; Zigler, B. T.; Palmer, T. R.; Wooldridge, M. S.; Atreya, A. *Combustion and Flame* **2004**, *137*, 351-365.
- (36) Reaction Design CHEMKIN Release 10101 (x64) **2010**.
- (37) Metcalfe, W. K.; Burke, S. M.; Aul, C. J.; Petersen, E. L.; Curran, H. J. *Proceedings of the European Combustion Meeting* **2011**.
- (38) Villano, S. M.; Huynh, L. K.; Carstensen, H.-H.; Dean, A. M. *The journal of physical chemistry. A* **2011**, *115*, 13425-42.
- (39) Villano, S. M.; Huynh, L. K.; Carstensen, H.-H.; Dean, A. M. *The Journal of Physical Chemistry. A* **2012**, *116*, 5068-89.
- (40) Westbrook, C. K.; Pitz, W. J.; Herbinet, O.; Curran, H. J.; Silke, E. J. *Combustion and Flame* **2009**, *156*, 181-199.
- (41) McBride, B. J.; Gordon, S.; Reno, M. A. *Thermodynamic and Transport Properties of Individual Species*; 1993; Vol. NASA Techn.
- (42) Westbrook, C. K.; Warnatz, J.; Pitz, W. J. *Symposium (International) on Combustion* **1988**, *22*, 893-901.
- (43) Gu, X.; Huang, Z.; Li, Q.; Tang, C. *Energy & Fuels* **2009**, *23*, 4900-4907.
- (44) Jacobson, M. Z. *Environmental science & technology* **4AD**, *41*, 4150-4157.
- (45) McEnally, C. S.; Pfefferle, L. D. *Proceedings of the Combustion Institute* **2005**, *30*, 1363-1370.
- (46) Veloo, P. S.; Wang, Y. L.; Egolfopoulos, F. N.; Westbrook, C. K. *Combustion and Flame* **2010**, *157*, 1989-2004.
- (47) Oßwald, P.; Güdenberg, H.; Kohse-Höinghaus, K.; Yang, B.; Yuan, T.; Qi, F. *Combustion and Flame* **2011**, *158*, 2-15.

- (48) Grana, R.; Frassoldati, A.; Faravelli, T.; Niemann, U.; Ranzi, E.; Seiser, R.; Cattolica, R.; Seshadri, K. *Combustion and Flame* **2010**, *157*, 2137-2154.
- (49) Moss, J. T.; Berkowitz, A. M.; Oehlschlaeger, M. A.; Biet, J.; Warth, V.; Glaude, P.-A.; Battin-Leclerc, F. *Journal of Physical Chemistry a* **2008**, *112*, 10843-10855.
- (50) Black, G.; Curran, H. J.; Pichon, S.; Simmie, J. M.; Zhukov, V. *Combustion and Flame* **2010**, *157*, 363-373.
- (51) Liu, W.; Kelley, A. P.; Law, C. K. *Proceedings of the Combustion Institute* **2011**, *33*, 995-1002.
- (52) Heufer, K. A.; Fernandes, R. X.; Olivier, H.; Beeckmann, J.; Roehls, O.; Peters, N. *Proceedings of the Combustion Institute* **2011**, *33*, 359-366.
- (53) Noorani, K. E.; Akih-Kumgeh, B.; Bergthorson, J. M. *Energy & Fuels* **2010**, *24*, 5834-5843.
- (54) Sarathy, S. M.; Thomson, M. J.; Togbé, C.; Dagaut, P.; Halter, F.; Mounaim-Rousselle, C. *Combustion and Flame* **2009**, *156*, 852-864.
- (55) Harper, M. R.; Van Geem, K. M.; Pyl, S. P.; Marin, G. B.; Green, W. H. *Combustion and Flame* **2011**, *158*, 16-41.
- (56) Barnard, J. A. *Transactions of the Faraday Society* **1957**, *53*, 1423-1430.
- (57) Vasu, S. S.; Davidson, D. F.; Hanson, R. K.; Golden, D. M. *Chemical Physics Letters* **2010**, *497*, 26-29.
- (58) Zhou, C.-W.; Simmie, J. M.; Curran, H. J. *Combustion and Flame* **2011**, *158*, 726-731.
- (59) Dagaut, P.; Togbé, C. *Energy & Fuels* **2009**, *23*, 3527-3535.
- (60) Dagaut, P.; Togbé, C. *Fuel* **2008**, *87*, 3313-3321.
- (61) Bourque, G.; Healy, D.; Curran, H.; Zinner, C.; Kalitan, D.; de Vries, J.; Aul, C.; Petersen, E. *ASME Conference Proceedings* **2008**, *2008*, 1051-1066.
- (62) Dagaut, P.; Sarathy, S. M.; Thomson, M. J. *Proceedings of the Combustion Institute* **2009**, *32*, 229-237.
- (63) Hansen, N.; Harper, M. R.; Green, W. H. *Physical Chemistry Chemical Physics* **2011**, *13*, 20262-20274.
- (64) Saisirirat, P.; Togbé, C.; Chanchaona, S.; Foucher, F.; Mounaim-Rousselle, C.; Dagaut, P. *Proceedings of the Combustion Institute* **2011**, *33*, 3007-3014.

- (65) Dagaut, P.; Togbé, C. *Fuel* **2010**, *89*, 280-286.
- (66) Sarathy, S. M.; Vranckx, S.; Yasunaga, K.; Mehl, M.; Oßwald, P.; Metcalfe, W. K.; Westbrook, C. K.; Pitz, W. J.; Kohse-Höinghaus, K.; Fernandes, R. X.; Curran, H. J. *Combustion and Flame* **2012**, *159*, 2028-2055.
- (67) Vanhove, G.; Petit, G.; Minetti, R. *Combustion and Flame* **2006**, *145*, 521-532.